The Pennsylvania State University
The Graduate School

MULTI-SENSOR BASED CONDITION ASSESSMENT SYSTEM FOR BURIED CONCRETE PIPE

A Thesis in
Civil Engineering
by
Shivprakash Iyer

Submitted in Partial Fulfillment
of the Requirements
for the Degree of

Doctor of Philosophy

May 2007

The thesis of Shivprakash Iyer was reviewed and approved* by the following:

Sunil K. Sinha
Assistant Professor of Civil and Environmental Engineering
Thesis Advisor, Chair of Committee

Mian C. Wang
Professor of Civil and Environmental Engineering

Andrew Scanlon
Professor of Civil and Environmental Engineering

Bernhardt Tittmann
Professor of Engineering Science and Mechanics

Chao-Hsien Chu
Professor of Information Science and Technology

Peggy Johnson
Professor of Civil and Environmental Engineering
Head of the Department of Civil Engineering

*Signatures are on file in the Graduate School.

Abstract

The American Society of Civil Engineers' 2005 Report Card for America's Infrastructure gave a $D-$ grade to water/wastewater infrastructure . It has been estimated that up to 40% of the United States' underground infrastructure will have failed or will be on the brink of failure within 20 years, unless efforts are initiated to renew it. But system renewal requires adequate funding. According to an April 2000 report by the Water Infrastructure Network (WIN) Agency, "America's water and wastewater systems face an estimated funding gap of $23 billion a year between current investments in infrastructure and the investments that will be needed annually over the next 20 years to replace aging and failing pipes and meet mandates of the Clean Water Act and Safe Drinking Water Act". This necessitates the need to monitor, detect and prevent any unforeseen failures in the working of underground pipelines that are complex in nature. A reliable pipeline assessment system is necessary so that pipeline operators can develop cost-effective maintenance, repair, and rehabilitation programs. This research proposes an automated ultrasound-immersion-based inspection system that can add complementary pipe information (depth perception) to existing surface image assessments done on concrete pipes commonly used as gravity stormwater and sewer pipes. Most municipal pipeline systems in North America are inspected visually by mobile Closed Circuit Television (CCTV) systems to access the in-situ condition of buried pipes. The video images are examined visually and classified into grades according to extent of damage against documented criteria by human operators prone to fatigue, subjectivity and ambiguity. Additionally, current imaging systems like Sewer Scanning & Evaluation Technology (SSET) and CCTV are able to provide information from within the pipe regarding surface cracks in 2-D only and do not have the capability to provide depth perception.

This thesis provides a proof-of-concept of an automated ultrasound-immersion-

based inspection system to detect defects in buried concrete pipes. The inspection system is proposed as a two step approach. The first step is called a reconnaissance mission that uses the ultrasound transducer to scan a region of interest. A signal interpretation and classification scheme coupled with a post processing algorithm is proposed that classifies the region of interest into a clean or defect region. If the scanned region of interest belongs to a defect, the second step characterizes the region of interest with a C-scan imaging process that provides depth perception. Results have shown that the feature extraction, classification and post processing schemes proposed in this thesis provide a sound proof-of-concept for developing this inspection system into a field applicable tool. Such a tool can aid asset managers to quickly evaluate the status of their buried infrastructure, ultimately leading to a sustainable asset management system.

Table of Contents

List of Figures

List of Tables

Acknowledgments

I wish to acknowledge and thank those people who contributed to this thesis in particular, and my life, in general:

Dr. Sunil Sinha, for his never-ending enthusiasm and advice in the area of underground pipeline inspection. His constant encouragement, support and willingness to sit down together for a casual chat appealed to me the most. I am thankful to him for agreeing to serve as my PhD Adviser. I look forward to continued association with him through collaborative work in the coming years.

Dr. Andrew Scanlon, for having graced me with his consent to serve on my doctoral committee. His presentation on a Graduate Student's progress curve imitating the stress-strain curve for steel has left a significant impression on my visions as a graduate student. The two courses I took with him have given me the gist of how brilliant individuals perceive their ideas. I am impressed by his practical approach to research problems and the sharpness of his intellect. His presence on my doctoral committee has ensured that I cover a lot of ground in my area of research.

Dr. Mark Wang, for his boyish chuckles that remind me of always being young at heart, a.k.a research! Conversations that I had in his office at times on technical or other matters have always proven to be insightful and full of experience. I will always treasure those short talks in his office.

Dr. Bernie Tittman, for having provided the much needed encouragement, expertise and advise on working in the area of ultrasound acoustics. His brilliant mind would always come up with an out-of-the-box idea that would uncannily tend to solve my research problem. I will always remember him for the countless hours of brain storming done in the Ultrasonics lab to get a tiny signal in and out

of concrete. His contribution in my thesis research is duly appreciated.

Dr. Chao-Hsein Chu, for serving on my doctoral committee and religiously attending all my doctoral exams with enthusiasm and fervor.

Dr. Andrea Schokker, my M.S. thesis advisor for her invaluable guidance and encouragement during my first two years of stay at Penn State. I believe that she is a wonderful human being and a dedicated teacher par excellence.

Judy Early, Mary Miller, T. Reed, Ruth Weber, Amy, Bobbi, Laurinda, Heather, Bob White, Peg, Dave Faulds, Dan Fura and many other beautiful human beings whose names have not been stated here and that have graced this department with their amiable nature and unending dynamic energy to help out in all possible ways during my stay at Penn State. Words cannot show my gratitude towards them, it can only describe to the best possible extent.

Prof. S.Suryanarayan (IIT-Bombay, India) and Prof. N.T.Desai (REC-Surat, India), for having initiated me into the golden purpose of life beyond professional pursuits.

Hiral and Anurag, for their perennial reservoir of love and benevolence. Nigam and Prachi; Nigam was my first roommate in the US who has become a part of my family over the time we spent together for a year and half. His methodical approach and planning has impressed me a lot and taught me that proper planning coupled with a deep, meaningful and productive mind can channel the strong currents of intelligence.

I would like to thank all my current and former colleagues in the Construction Engineering and Management Group: Patrick Dunn, Devani Varuni Perera, George Joseph, Venkatesh Ganesan, Ahmed Bassiouni, Tanmay Kumar, Adam Platt, Shrimant Jaruhar, Seyed Safa Eslambolchi, Rashi Bhushan, Sungho Kim. It has been a pleasure to be among very bright and friendly people. Thanks also to many other fellow graduate students for their help and support: Subash Jayaraman, Michael Pedrick, Gautam Wagle, Dave Tepke, Dhruv Desai, Edwin Salcedo, Brian Swartz, Eric Musselman, and Sumanth Chejarla.

Special thanks to my 'old' friends, Kaushal Solanki, Ojas Gandhi, Anand Nanavati, Vishwa Ved, John Gabharani, and Viral Rathod for their lifelong friendship, and the fun we had. They have always been with me in my good and bad times alike. Also, friends that I made at Penn State: Sanjiv, Narasimhan, Mohit, Sid-

dharth, Jagdish, the entire Penn State Cricket Club, and many more that could not make it to this list, have given me a flavor of life with their interesting personalities.

Chandrika, my wife, I give my deepest thanks for her patience, understanding, encouragement and pure love. I pray that we continue this journey of togetherness and take our relationship to the deepest levels.

My parents have been the pillars of my existence and have supported me to the utmost in everything that I have done. I would have been nothing but a heap of dust without the grace and blessings of my beloved parents. I owe every part of my existence to them. It is their firm conviction and dream that I am in a position to write this acknowledgement for my research that culminates into this doctoral thesis. May God bless all. Love and light to everybody.

Last but not least, I would like to thank The Technology Collaborative (TTC) for supporting the work presented in this dissertation.

Shivprakash Iyer
The Pennsylvania State University
March 2007

To Baba,
for accepting this soul into His divine fold.

To my parents,
for their daring to dream big, love, encouragement and blessings.

To my lovely wife,
for her million dollar smile that inspires me to go on forever.

Chapter 1

Introduction

Beneath North America's roads lie 1.6 million miles of pipelines that bring purified water to homes and carry away waste water (sewage and storm water). Aging wastewater management systems discharge billions of gallons of untreated sewage into U.S. surface waters each year. The Environmental Protection Agency (EPA) estimates that the nation must invest $390 billion over the next 20 years to replace existing systems and build new ones to meet increasing demands. These buried infrastructure systems have been functioning longer than their intended design life with little or no repair. They are aging and in a progressive state of deterioration. Maintenance and rehabilitation of pipeline systems pose a major challenge for most municipalities in North America given their budgetary constraints, demand on providing quality service, and the need for preserving their pipeline infrastructure. Neglecting regular maintenance and rehabilitation (M&R) of these buried pipelines adds to life-cycle costs and liabilities, and in extreme cases causes stoppage or reduction of vital services. Unsurprisingly, as shown in figure 1.1, the American Society of Civil Engineers' 2005 Report Card for America's Infrastructure gave a $D-$ grade to water/wastewater infrastructure . It has been estimated that upwards to 40% of the United States' underground infrastructure will have failed or will be on the brink of failure within 20 years, unless efforts are initiated to renew it (Technical Report (WIN), 2001, 2002). But system renewal requires adequate funding. According to an April 2000 report by the Water Infrastructure Network (WIN) Agency, "America's water and wastewater systems face an estimated funding gap of $23 billion a year between current investments in

infrastructure and the investments that will be needed annually over the next 20 years to replace aging and failing pipes and meet mandates of the Clean Water Act and Safe Drinking Water Act" (Technical Report (WIN), 2001). This necessitates the need to monitor, detect and prevent any unforeseen failures in underground pipelines.

Accurate pipeline condition assessment is vital to developing a cost effective and efficient pipeline M&R program. At present, the assessed condition of buried pipes is based on the subjective visual inspection of closed circuit television (CCTV) surveys (Gokhale et al., 1997). CCTV surveys are conducted using remotely controlled vehicle carrying a television camera through a buried pipe. The data acquired from this process consist of videotape, photographs of specific defects, and a record produced by the technician. Typical scanned image of CCTV surveys is shown in figure 1.2. It is a well known fact that the diagnosis of defects depends on experience, capability and concentration of the operator thus making the detection of defects error prone.

Large number of new technologies such as Sewer Scanner and Evaluation Technology (SSET), laser based scanning systems, etc. have made it possible to obtain high quality images of buried pipes. SSET is an innovative technology for obtaining unfolded images of the interior of buried pipes (Iseley, 1999). This is achieved by utilizing scanner and gyroscope technology. Typical scanned images of SSET surveys are shown in figure 1.3. Inspite of buried imaging technologies making giant strides in recent years, the basic means of analysis remain unchanged: a qualified technician is still required to identify defects on a television monitor. One of the objectives of this thesis will be to address the above limitation.

Additionally, a defect that appears on the surface to be insignificant (less than 5 mm mouth opening) might actually exist throughout the thickness of the pipe. An operator would usually classify such a defect as a 'minor defect' and shift attention to those that may appear critical on the surface but do not extend into the depth of the pipe. This may prove to be catastrophic because of the defect being classified as 'minor' due to lack of enough information. It may well be the case that the so called 'minor' defect will lead to a pipe collapse much earlier than the other cracks that were classified to be critical based on surface analysis only. Hence, any crack (or defect) classification system that primarily depends on

surface characteristics is incomplete and needs to be complemented with additional depth perception to provide for a reliable, accurate and effective buried pipeline asset management system. Therefore the development of an automated buried pipeline condition assessment system that can provide additional depth perception of defects is the main objective of this research study. Main efforts are placed on investigating the use of ultrasound acoustics to acquire depth perception and complement 2-D crack features available from the SSET camera. Additionally, improving the interpretation of surface scanned images and ultrasound signals by implementing new algorithms and techniques from image processing, feature extraction and pattern classification are also within the scope of this study.

As mentioned before, the main focus of this thesis is on developing proof-of-concept of an intelligent automated ultrasound inspection system that can inspect concrete pipes and provide depth perception. In particular, this thesis explores the use of various signal and image processing concepts, nonlinear filtering, ultrasound acoustics, feature extraction and pattern classification techniques that are combined to provide a two step inspection system. The proposed inspection system can lead to overcoming many limitations of the current manual inspection practice and can provide a more accurate assessment of buried pipe conditions.

The next sections outline motivation for this research, followed by contributions and a description of the organization of this thesis.

1.1 Motivations

Visual inspection based on closed circuit television surveys is widely used in North America to assess the condition of buried pipes (Wirahadikusumah et al., 2001). The human eye is extremely effective at recognition and classification, but it is not suitable for assessing pipe defects in thousand of mile of pipeline due to fatigue, subjectivity and cost. This drawback of the present method of visual inspection is one of the main motivations behind this research study in developing a sophisticated condition assessment system.

The present state of technology only affords a 2-D view of pipe surface characteristics using the SSET scanning method and there are justifiable reasons to know the depth (3^{rd} dimension) information of defects (e.g., cracks). Hence, acquiring

depth perception of defects that are presently visible only at the surface (in 2-D) through the current inspection technology, is of considerable interest to the buried asset management community. This additional data source has the potential to solve problems of fatigue, subjectivity, and ambiguity by the very fact that defects can now be interpreted based on their depth in pipe thickness.

Most of the literature concerning the detection/classification of defects based on imaging in civil structures deals with the analysis of pavements and concrete/steel distresses(Cheng, 1996, Cheng and Miyogim, 1998, Haas and Hendrickson, 1990, Walker and Harris, 1991). In the past few years, research on assessing the condition of buried pipes has gained recognition in the buried infrastructure asset management community through the efforts of Isley et al (1997), Isley (1999), Wirahadikusumah et al (1998), and Feiguth and Sinha (1999). In analyzing scanned buried pipe images, one needs to consider complications due to the inherent noise in the scanning process, irregularly shaped cracks, as well as the wide range of pipe background patterns. One of the major problems is detecting defects (especially cracks) that are camouflaged in the background of corroded areas, debris, patches of repair work, and areas of poorly illuminated conditions. But, most of the available methods of detection and classification are strictly based on 2-D information provided by the SSET scanned images. Approaches that can provide a complete description of the defects based on 3-D features do not exist and hence provide for an interesting research problem.

In light of the above discussion, there is sufficient motivation for the development of computationally viable, efficient and robust methods for image preprocessing, segmentation, and detection of surface defects from SSET images. However, the main focus is on acquiring depth perception through ultrasound acoustics based methods. Many researchers have been working on characterizing concrete using ultrasound acoustics. Concrete has always been a difficult material to deal with from an ultrasonic point of view owing to its heterogeneity and high attenuating properties (Malhotra and Carino, 2004). These aspects also motivated the development of an ultrasound-based inspection system that is capable of detecting defects and then characterizing them with respect to depth perception in

representative concrete pipe specimens.

1.2 Objective & Scope

The primary objective of this research is to develop an automated buried concrete pipe inspection system based on scanned images obtained from SSET camera and signal/image data from the ultrasound sensor. Specifically, the scope of this thesis begins with researching new techniques to improve the detection of cracks under varying background, pipe color and complicated defect patterns from surface scanned images. This step provides accurate two dimensional data about various kinds of cracks on the internal surface of the concrete pipe. The second and most important objective of this study is to propose an ultrasound acoustics-based methodology to acquire depth perception about surface cracks outlined in the previous step. The scope of this study concludes with the implementation of an ultrasound inspection system consisting of a two step approach. At the point in time when this thesis research had commenced, the following work had been accomplished (Sinha, 2000, Fieguth and Sinha, 1999, Sinha et al., 1999, Sinha and Fieguth, 2001):

- Automatic segmentation of buried pipe images
- Detection of cracks in segmented pipe images
- Feature extraction of image features for defect classification

The contributions of this thesis that builds upon the above accomplishment are listed below.

1.3 Contributions

CCTV Image Processing & Segmentation

Contrast enhancement is a pre processing step before segmentation. Contrast enhancement can be defined as a radiometric enhancement technique used to improve the visual contrast of an image. In the analysis of the objects in images, it is essential to distinguish between the objects of interest and "the rest." This latter group is also referred to as the "background." The techniques that are used to find the objects of interest are usually referred to as segmentation techniques and the process is known as segmentation - segmenting the foreground from background. In this thesis, two approaches for enchancing the contrast of CCTV images for better interpretation have been developed. The first approach uses a modified version of unsharp masking through non-linear quadratic filtering to enhance the crack features and suppress the background characteristics in an image. This is accomplished in the first proposed method using non-linear quadratic filtering. The second approach increases the contrast of the dark pixels from the estimated "background" image by comparing the intensity of each pixel in the original color image with that of the background image. If the difference in intensities is higher than a given threshold, it darkens the dark pixels and lightens the background pixels thus enhancing the contrast between crack and background.

To determine the efficiency of both the proposed methods, a simple, robust and efficient algorithm for detecting crack patterns in pipeline images is developed. The algorithm consists of three steps, contrast enhancement, morphological treatment and curvature evaluation in the cross direction, and finally the alternating filters that produce the final segmented binary crack map. The proposed approach can be completely automated and experimental results demonstrate that algorithm is effective for segmenting CCTV images with varying background, color, and crack patterns.

Development of Ultrasound-based Inspection System

In this thesis, various ultrasound-based inspection techniques that may be employed to acquire depth perception data for defects in buried concrete pipes are evaluated. Two methods, guided wave and impact echo, are experimentally examined for suitability with concrete inspection. Both these techniques have their own limitations in terms of their suitability for concrete pipe inspection. The guided

wave technique is successful with a transducer configuration that cannot be implemented in a buried pipe inspection scenario. The frequency range of operation in concrete pipe with 60 mm thickness proves to be fairly high for typical impact-echo applications.

A significant contribution of this thesis is the development of an ultrasound immersion based technique that uses water couplant as a suitable approach for inspecting concrete pipes. Experimental results, in an amplitude time series signal (A-scan) and image format (C-scan), of several concrete samples with defects of interest to the water/wastewater pipe community show that it is possible to make interpretations about the presence of defect and provide depth perception by this method. The results prove that this methodology is successful in providing additional insight into the condition of concrete samples under investigation.

Development of Feature Extraction & Classification Schemes

In buried concrete pipe defect analysis, the main objective is to identify and classify regions of the pipe as "clean" or "defective". Further classification of defects into various sub-classes like hole, fracture, crack and hairline crack is possible based on data provided by the proposed ultrasonic inspection system.

Classification is a statistical procedure in which individual items are placed into groups based on quantitative information on one or more characteristics inherent in the items (referred to as traits, variables, characters, etc) and based on a training set of previously labeled items.In this thesis, a multi-layer perceptron (MLP) neural network classifier that uses discriminatory features from the ultrasonic signal is developed. The proposed approach uses wavelet analysis to decompose the signal into its useful information components and then employs an unsupervised clustering scheme to extract feature vectors that represent the class of the signal. Wavelet analysis refers to the representation of a signal in terms of a finite length or fast decaying oscillating waveform (known as the mother wavelet). This waveform is scaled and translated to match the input signal. The MLP classifier classifies the signal into its appropriate class based on extracted features of interest from the wavelet filtered signal.

Development of Inspection Approach

An overall contribution of this thesis is in developing a framework for the inspection system. It is proposed that the inspection system be envisioned as a two step approach consisting of the reconnaissance mode and characterization mode. In the reconnaissance mode, the ultrasound transducer is used to scan a region of interest (ROI) and acquire A-scan signals. The ROI A-scan signals are passed through the classifier and identified as belonging to defect or clean class. If the scanned ROI belongs to a defect of interest, the second step of the approach is to characterize the ROI with a C-scan imaging process for depth perception. A relevant contribution of this thesis is in developing a post processing scheme that provides a high confidence that C-scan imaging will only be '*triggered*' when a defect of interest is detected. The feature extraction, classification and post processing schemes proposed in this thesis provide a sound proof-of-concept for developing this inspection system into a field applicable tool.

1.4 Thesis Organization

Chapter 2 presents the background relevant for understanding the automated buried pipe inspection system. It begins with a broad overview of various pipeline assessment techniques in general. It then briefly introduces the methodology for automated image-based inspection. The next two sections discuss image segmentation and feature extraction methods. Next, we review ultrasound nondestructive testing and discuss various approaches applicable to concrete. Finally, a brief review of pattern recognitions tasks is provided at the end of this chapter.

Chapter 3 presents two approaches for enchancing the contrast of CCTV images for better interpretation. A modified version of unsharp masking which computes the enhancement map for thresholding ,so that crack features are enhanced and background is suppressed, is discussed. The chapter also discussed the second approach which increases the contrast of the dark pixels from the estimated "background" image by comparing the intensity of each pixel in the original color image

with that of the background image. Next, the chapter discusses the efficiency of both these methods by developing a crack detection filter and applying an adaptive algorithm to contrast enhanced images.

In Chapter 4, a simple algorithm for detecting crack patterns in pipeline images is adapted and implemented. This chapter begins by presenting mathematical foundations of the morphological operations used in the proposed algorithm. Next, it discusses the implementation strategy, followed by performance evaluation of the proposed method with other conventional detection techniques.

Chapter 5 describes the ultrasound-based inspection techniques that may be employed to acquire depth perception data for defects in buried concrete pipes. First, it presents the challenges in developing an inspection methodology for buried concrete pipes. Next, several techniques like guided wave and impact echo are examined for suitability with concrete inspection. The chapter proposes ultrasound immersion technique as a suitable approach for inspecting concrete pipes. This chapter also presents experimental results of several concrete samples with defects of interest to the water/waster water pipe community. A-scan signal and C-scan image representations from a region of interest (ROI) are presented to make interpretations about the presence of defect and provide depth perception.

Chapter 6 describes the feature extraction methods and pattern recognition strategies for the classification of ultrasound inspection data. A formulation of the multilayer perceptron neural network with input and output parameters is presented in this chapter. This chapter also discusses a feature extraction scheme based on discrete wavelet transform and unsupervised clustering to extract signal features for classification. A post processing scheme to interpret the classifier outputs and finally classify the signals into an appropriate class taking into consideration some *apriori* knowledge of the problem is discussed towards the end of this chapter. Chapter 6 also provides a framework for the inspection system consisting of two steps, a reconnaissance mode and a characterization mode.

Chapter 7 briefly presents the concept, implementation, and results from a wa-

ter bubbler system that emulates the immersion environment discussed in chapters 5 and 6 in a real-world scenario on an actual concrete pipe specimen with defect.

Chapter 8 summarizes the outcome of this thesis, lists major contributions of this work, details future directions for research, and provides concluding remarks.

Figure 1.1. ASCE's 2005 report card on America's infrastructure. *Image courtesy www.asce.org/reportcard/2005.*

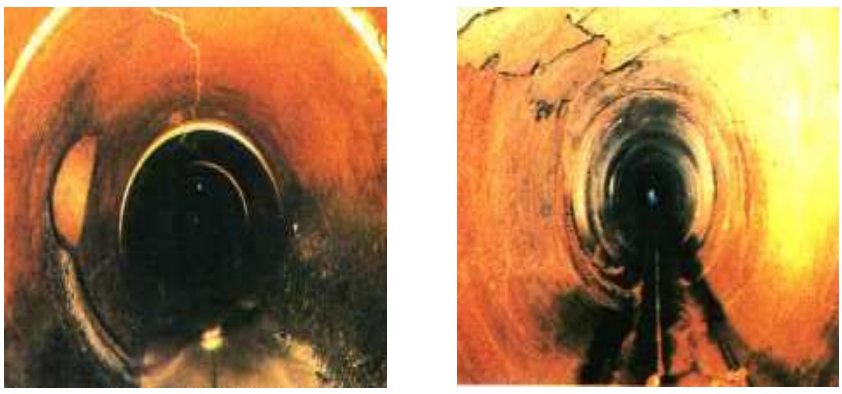

(a) (b)

Figure 1.2. (a) and (b) forward vision (FV) image from CCTV camera

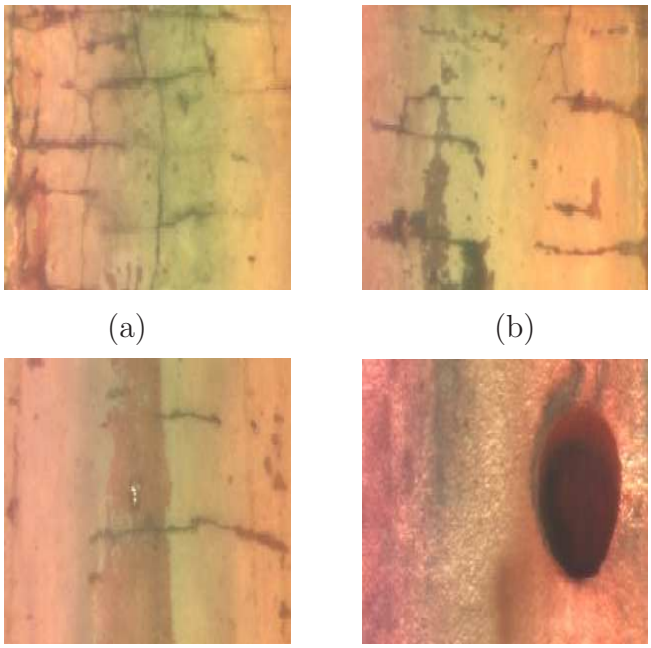

(a) (b)

(c) (d)

Figure 1.3. Typical images of buried pipe scanned by Sewer Scanner and Evaluation Technology (SSET) camera

Chapter 2

Background

2.1 Introduction

The main objective of this chapter is to introduce the background knowledge required for developing a sophisticated buried pipeline inspection system that can provide additional information about the pipe condition through depth perception. Section 2.2 presents an overview of buried pipeline inspection techniques while Section 2.3 discusses the methodology for the development of an automatic image-based inspection system. Section 2.4 introduces the concept of image processing and segmentation. An introduction to ultrasound acoustics and work related to its applications in the present context finds mention in section 2.5. Sections 2.6 and 2.7 briefly mention the feature extraction and analysis techniques available for use in this research.

2.2 Overview of Pipeline Assessment Techniques

Pipelines are now an integral part of the worlds' economic structure and literally billions of dollars worth of products are now moved annually in pipelines (Stewart, 1993). Both economic and environmental factors are influential in pipeline operation, and therefore integrity monitoring is vitally important in the control and operation of complex systems. Pipeline defect detection systems range from simple visual to complex inspection systems. No one method is universally applicable

and operating requirements dictate which method is the most cost effective. The aim of this section is to review the basic techniques of defect detection that are currently in use. The advantages and disadvantages of each method are discussed and some indications of applicability are outlined.

2.2.1 Destructive Testing Methods for Defect Assessment

Destructive testing methods consist of testing a product beyond its design load until a brittle failure develops. Often these tests are specified at the construction stage to ensure that the pipe material meets or exceeds design specifications. Common destructive test methods are discussed below.

Tension. Tension testing consists of placing coupons of pipe material in a testing apparatus and pulling the coupon apart until failure occurs (American National Standards Institute, 1995a). During a test, the coupon load and deflection are measured. This test ensures that the pipe material meets or exceeds tensile strength design requirements and is useful for determining the load bearing capabilities of the material and its ductility under load.

Hardness. Hardness is usually defined as resistance to penetration. Other tests are also used, such as amount of rebound of a weight and scratch tests. Hardness tests include Rockwell, Scleroscope, Brinell and Vickers (Davis et al., 1982). Good correlation exists between hardness and strength. Thus, the hardness test can give a quick estimate of the pipe strength and/or wear resistance.

Impact. The pendulum impact test, also known as the Charpy test, gives an indication of the amount of energy that can be absorbed by the material (American National Standards Institute, 1995b). The test procedure consists of cutting a notch in a sample and then hitting the sample with a drop hammer. The difference in energy that the hammer has after striking the material is the material impact strength.

Flexural. The three-edge-bearing flexural test is a severe pipe loading condition. This test allows for no lateral pipe support (unconfined) and applies forces that

are point loads (Davis et al., 1982).

The Parallel Plate. The parallel plate test is an accepted method for measuring pipe stiffness. This test consists of placing the pipe between two parallel plates located at the top p and bottom of the pipe. The pipe stiffness is determined from the load required to displace the top plate to a specified deflection.

2.2.2 Non-Destructive Testing Methods for Defect Assessment

Non-destructive testing (NDT) is the branch of engineering concerned with all methods of detecting and evaluating defects in materials without causing physical damage to the material or active intervention (Davies and Mamlouk, 1985). Defects can affect the serviceability of the material or structure, so NDT is important in guaranteeing safe operation as well as in quality control and assessing pipe life. The defect may be cracks or inclusions in welds and castings, or variations in structural properties that can lead to loss of strength or failure in service. Non-destructive testing is used for in-service inspection and for condition monitoring (Van Cauwelaert et al., 1989). It is also used for measurement of components and for the measurement of physical properties such as hardness and internal stress. The essential feature of NDT is that the test process itself produces no deleterious effects on the material or structure under test. The subject of NDT has no clearly defined boundaries as it ranges from simple techniques such as visual examination of surfaces, through well established methods of radiography, ultrasonic testing, magnetic particle crack detection, to new an very specialized methods. NDT methods can be adapted to automate production processes as well as to the inspection of localized problem areas. All NDT techniques have the ability to measure only specific types of defects, material properties, and/or material response. Therefore, the best choice of an NDT method in a specific pipeline application will depend on the pipeline physical properties and defects. Thus, before the selection of an appropriate NDT method, a thorough knowledge of each NDT method, its application, and limitations is required along with a good understanding of the buried pipeline infrastructure.

2.2.2.1 Non-Visual NDT Methods

Ultrasonic Inspection (Sonar). Ultrasonic inspection is performed using a beam of very high frequency coherent sound energy wherein the frequency in magnitude is much higher than what a human being can hear (Birks and Green, 1991). The high frequency sound wave travels into the object being inspected and reflects whenever there is change in the density of the material, with some of the energy in the wave returning to the surface and some passing on through the new material at interface. Ultrasonic beams can be used to image the human body, inspect aircraft, or examine oil pipelines. The technique is capable of detecting puts, voids, and cracks, although certain crack orientations are much more difficult to detect than others. The ultrasonic wave reflects most easily when it crosses an interface between two materials that are perpendicular to the wave. As an example, cracks that lie perpendicular to the wave are easily detected, but cracks that lie parallel to the beam are usually not identified by an ultrasonic examination. Evaluation is often difficult.

Eddy current testing. Eddy current testing is an electromagnetic technique that can detect surface and subsurface discontinuities in tube walls up to about 3/8" (10mm) thick on conductive materials (Joynson et al., 1986). Applications range from crack detection to rapid sorting of small components for defects, size variations, or material variation. When an energized coil is brought near to the surface of a metal component, eddy currents are induced into the specimen. These currents set-up a magnetic field that tends to oppose the original magnetic field. The impedance of coil in close proximity to the specimen is influenced by the presence of the induced eddy currents in the specimen. When the eddy currents in the specimen are distorted by the presence of a defect or a material variation, the impedance in the coil is altered. This change is measured and displayed in a manner that indicates the type of defect or material condition. This method is commonly performed on heat exchanger tubing by inserting a probe down the full length of each tube to be inspected as shown in Figure 2.1. The probe contains a coil arrangement, energized by alternating currents operating at one or more frequencies. The electrical impedance of the test coil arrangement is modified by the proximity of the tube, tube dimensions, electrical conductivity, magnetic per-

meability of the tube material, and metallurgical and mechanical discontinuities. Wear on the tube surface under a support is also detectable. The electromagnetic response caused by passing these variables produces electrical signals, which are processed electronically to produce a visual response characteristic of change encountered. Visual responses, often called "Signatures" are displayed on the test instrument monitor for evaluation by the field technician.

Acoustic emission monitoring. This method involves listening to the sounds (which are usually inaudible to the human ear) emitted by a material, structure or machine in use or under load (Bassim and Houssny-Emam, 1983). The technique involves attaching one or more ultrasonic microphones to the object and analyzing the sounds using computer-based instruments. Acoustic emission inspection methodology is shown in Figure 2.2. The noises may arise from friction (including bearing wear), crack growth, turbulence (including leakage) and material changes such as corrosion. Applications include testing pipelines and storage tanks (above and below ground), fiberglass structures, rotating machinery, weld monitoring, biological and chemical changes in environment.

2.2.2.2 Visual NDT Methods

Visual inspection is a NDT method used extensively to evaluate the condition or the quality of a component (Krstulovic et al., 1996). It is easy to perform, inexpensive and usually does not require special equipments. It is most effective for the inspection of welds where quick detection and thee correction of defects or process-related problems can result in significant cost savings. It is the primary evaluation method of many quality control programs. The method requires good vision, good lighting and operator knowledge. Most municipal pipeline systems are inspected visually by mobile Closed Circuit Television (CCTV) systems or human inspectors (Gokhale et al., 1997). CCTV examination using a mobile camera system is the typical approach to this type of examination. However, there are several CCTV variants that may reduce the cost of the inspection or provide improved results. There are also alternative techniques that will work where CCTV will not or that will give direct measurements of pipe condition as opposed to the estimates produced by CCTV inspection. Each inspection technique is discussed below.

CCTV Inspection. There are two basic types of the CCTV system. Each uses a television camera in conjunction with a video monitor, videocassette recorders, and possibly other recording devices. In one of the type, inspection is performed using a stationary zoom camera mounted at a manhole so that it looks into the pipe, whereas in the other type, a mobile, robotic system is placed within the pipe itself. The camera provides images to an operator who is trained to detect, classify and rate the severity of defects against documented criteria (Wirahadikusumah et al., 2001). The typical CCTV camera and scanning process of buried pipes are shown in Figure 2.3. Either form of CCTV inspection may miss certain types of defects, especially those that are hidden from the camera by obstructions as it looks down the pipe. This method is also vulnerable to lapses in operator concentration, inexperience, and the inability of the image to reveal important defects. Thus, the results are widely agreed to lack reliability and consistency in tracking deterioration so that preventive maintenance can be undertaken with confidence. Nonetheless, it provides useful information on gross defects.

Sewer Scanner and Evaluation Technology. Sewer Scanner and Evaluation Technology (SSET) is an innovative technology for obtaining images of the interior of pipe (Iseley, 1999). SSET is developed by TOA Grout, CORE Corp., California, and the Tokyo Metropolitan Government's Services (TGS) Company. SSET is a system that offers a new inspection method minimizing some of the shortcomings of the traditional inspection equipments that relies on a CCTV inspection. This is accomplished by utilizing scanning and gyroscopic technology. The mechanics of inspecting the pipes by SSET camera are similar to the CCTV inspection. The SSET is designed to operate from a tractor platform to propel the tool through the pipe. Since the SSET utilizes state-of-the-art scanner technology, it can travel through the pipe at a uniform speed. The SSET camera and digitized images of buried pipe with various defects are shown in Figure 2.4. The major benefit of the SSET system over the current CCTV technology is that the engineer will have higher quality image data to make critical rehabilitation decisions.

Laser-Based Scanning Systems. In addition to the simple light line system

described above, lasers have been used in the past to evaluate both, the shape of pipelines and the type of defects they contain (Hibino et al., 1994). These systems are restricted to the part of the pipe above the waterline, but they can, in theory, provide extremely accurate inspections of pipe condition. An additional advantage to this approach is that the information from the laser scans is readily recorded and analyzed by a computer thus substantially reducing operator errors. Although the initial equipment may be more expensive than a CCTV system, the reduced operator time necessary to use the technique may also mean that its operation will be more economical. The technology is still in the development stage.

2.3 Automatic Image-based Inspection

Industry is increasingly using machine vision systems to aid in the manufacturing and quality-control processes (Newman and Jain, 1995). The goal of machine vision is to create a model of the real world from images (Chin and Harlow, 1982). A machine vision system recovers useful information about a scene from its two-dimensional projections. Since images are two-dimensional projections of the three-dimensional world, the information is not directly available and must be recovered. To recover the information, knowledge about the objects in the scene is required. The emphasis in machine vision systems is on maximizing automatic operation at each stage and these systems should use knowledge to accomplish its objectives. Machine vision emulates human vision in that it attempts to interpret images. Human vision deals with the global information available in a scene, resolves ambiguities due to perspective, lighting, and attribute, and can perform navigation through unfamiliar territories. Inspite of all this, human vision has been shown to be incapable of performing reliable inspection (Agin, 1980). The human vision process is prone to subjective considerations, fatigue, and boredom, which interfere with consistent evaluations. Also, the human vision is limited to the visible spectrum while machine vision system exploit a much larger range of the electromagnetic spectrum, including infrared radiation, X-rays, and ultrasound, thereby making it suitable for a wide range of nondestructive testing and inspection process related tasks (Ballard and Brown, 1982).

An automated image-based inspection means to extract information from an

image on the conditions of objects represented on the image. Usually it is impossible to extract this information concerning the dimensions of objects or their defect properties directly from the image. For this purpose, all machine vision systems involve image acquisition, image pre-processing, segmentation and extracting relevant features for classification of the type, severity and extent of defects present in the pipe image scanned.

2.4 Image Processing And Segmentation

Vision allows humans to perceive and understand the world surrounding them. Computer vision aims to duplicate the effect of human vision by electronically perceiving and understanding an image. Giving computers the ability to see is not an easy task - we live in a three-dimensional (3D) world, and when computers try to analyze objects in 3D space, the visual sensors available (e.g. TV cameras) usually give two-dimensional (2D) images, and this projection to a lesser dimension incurs an enormous loss of information.

The term digital image processing generally refers to processing of a two-dimensional picture by a digital computer. In a broader context, it implies digital processing of any 2D data. The first step in the process is image acquisition - that is, to acquire a digital image. After a digital image has been obtained, the next step is to process that image. This sequence of operations-image capture, processing, region segmentation, extraction, high-level identification, qualitative/quantitative conclusion-is characteristic of image understanding and computer vision problems. Most computer vision techniques use the results and methods of mathematics, pattern recognition, artificial intelligence, psychophysiology, computer science, electronics and other scientific disciplines (Besl et al., 1985). In order to simplify the task of computer vision understanding, two levels are usually distinguished: low-level image processing and high-level image understanding (Haralick and Shapiro, 2000). Low-level methods usually use very little knowledge about the content of images. In the case of the computer-knowing image content, it is usually provided by high-level algorithms or directly by a human who knows the problem domain. Low-level methods often include image pre-processing methods for noise filtering, contrast enhancement, and edge extraction.

Image pre-processing and segmentation is the initial stage for any recognition process, whereby the acquired image is 'broken up' into meaningful regions or segments. The segmentation process is not primarily concerned with what the regions represent, but only with the process of partitioning the image. In the simplest case (binary images) there are only two regions: a foreground (object) and a background region. In gray level images, there may be many types of region or classes within the image; for example, in a natural scene to be segmented, there may be regions of sky, clouds, ground, building and trees. Broadly speaking, there are two approaches to image segmentation, namely thresholding and region or edge-based methods (Pratt, 1978).

2.4.1 Image Pre-processing

The principle objective of enhancement techniques is to process an image so that the result is more suitable than the original image for specific applications. The word "specific" is important, because it establishes at the outset that the techniques discussed in this section are very much problem-oriented. Thus, for example, a method that is quite useful for enhancing x-ray images may not necessarily be the best approach for enhancing images of buried pipes.

2.4.1.1 Gray Scale Transformation

Gray scale transformations do not depend on the position of the pixel in the image. A transformation of the original brightness p from scale [p_o,p_k] into brightness q from a new scale [q_o,q_k] is given by

$$p = \boldsymbol{\lambda} q \tag{2.1}$$

p_o, p_k and q_o,q_k are the minimum and maximum brightness values on a scales 'p' and 'q'. The most common gray scale transformations are shown in Figure 2.5; the straight line 'a' denotes the negative transformation; the piecewise linear function 'b' enhances the image contrast between brightness values p_1 and p_2. The function 'c' is called brightness thresholding and results in a black-and-white image. A gray scale transformation for contrast enhancement is usually found automatically using the histogram equalization technique (Rosenfeld and Kak, 1982). The aim

is to create an image with equally distributed brightness levels over the whole brightness values as shown in Figure 2.6. Histogram equalization enhances contrast for brightness values close to histogram maxima, and decreases contrast near the minima.

2.4.1.2 Image Smoothing

Image smoothing is the set of local pre-processing methods whose predominant use is the suppression of image noise. Calculation of new value is based on the averaging of brightness values in some neighborhood. Smoothing poses the problem of blurring sharp edges in the image, and so those methods which are edge preserving is of interest to this study. They are based on the general idea that the average is computed only from those points in the neighborhood that have similar properties in comparison to the point being processed. Assume that the noise value v (measured in decibels) at each pixel is an independent random variable with zero mean and standard deviation σ. We can obtain such an image by capturing the same static scene several times. The result of smoothing (I_s) is an average of the same n points in these images i_1,...i_n with noise values v_1...v_n:

$$I_s = \frac{i_1 + ... + i_n}{n} + \frac{v_1 + ... + v_n}{n} \tag{2.2}$$

Median filtering is a non-linear smoothing method that reduces the blurring of edges (McDonnell, 1981). In this method, the current pixel in the image being processed is replaced by the median of the brightness values in its neighborhood. The median of the brightness in the neighborhood is not affected by individual noise spikes and so median smoothing eliminates impulse noise quite well. Moreover, as median filtering does not blur edges significantly, it can be applied iteratively for desired results.

2.4.1.3 Color Image Processing

The use of color in image processing is motivated by two principal factors. First, in automated image analysis, color is a powerful descriptor that often simplifies object identification and extraction from a scene. Secondly, in image analysis performed by human beings, the motivation for color is that the human eye can discern thou-

sands of color shades and intensities, compared to about only two-dozen shades of gray (Smith, 1997). Color is connected with the ability of objects to reflect electromagnetic waves of different wavelengths; the chromatic spectrum spans the electromagnetic spectrum from approximately 400nm to 700nm. Humans detect color as combination of primary colors red, green and blue, which for the purpose of standardization have been defined having a wavelength of 700nm, 546.1nm and 435.8nm respectively (Smith, 1997). This standardization does not imply that all colors can be synthesized as combinations of these three. The purpose of a color model is to facilitate the specification of colors is some standard, generally accepted way. In essence, a color model is a specification of a 3-D coordinate system and a subspace within that system where each color is represented by a single point. The color models most often used are the RGB, the YIQ and the HIS models.

RGB Color Model. The RGB (Red, Green, Blue) specie is used most frequently in computer graphics and image processing applications (Pratt, 1978, Smith, 1997). A color in this space is represented by a triplet of values typically between 0 and 255. Each color can be broken down into its relative intensity in the three primaries corresponding to the spectral response of one of the three types of cones present in the human eye: red, green and blue. The space is easily represented as a three dimensional cube where each axis represents the strength of the color in one of the three primaries as shown in Figure 2.7.

YIQ Color Model. The YIQ model is useful in color TV broadcasting, and is a simple linear transform of an RGB representation:

$$\begin{pmatrix} Y \\ I \\ Q \end{pmatrix} = \begin{pmatrix} 0.299 & 0.587 & 0.144 \\ 0.596 & -0.275 & -0.321 \\ 0.212 & -0.523 & 0.311 \end{pmatrix} \begin{pmatrix} R \\ G \\ B \end{pmatrix} \tag{2.3}$$

This model is useful since the Y component provides all that is necessary for a monochrome display; further, it exploits advantage of properties of the human visual system, in particular our sensitivity to luminance, the perceived energy of a light source. Details of this model and its use may be found in relevant texts (Pratt, 1978, Smith, 1997).

HSI Color Model. The HIS (Hue, Saturation, and Intensity) model can be said to follow more closely the human perception of color qualities. Hue (H) is the color described by wavelength - for example, the distinction between red and blue. Hue represents the fundamental or dominant color. Saturation (S) represents the amount of color present, where pastel shades (e.g. pink) have low saturation values while pure spectral colors (e.g. red) are completely saturated. The intensity (I) represents the overall brightness or the amount of light. It is independent of color and is a linear value. It is measured as an angle on a color circle with the three primary colors spaced 120° apart. The first two values specify the chromaticity of a color point. Figure 2.8 shows the relationship between HIS and RGB color spaces. It is noted that the HSI color space is one of several spaces that can be derived from the General Hue, Luminance and Saturation (GHLS) space (Pratt, 1978). There are other slightly different interpretations of hue, luminance and saturation. By setting certain parameters in this transformation, one can specify any of the transformations from the RGB space to an HSI, HLS or HSV (Hue, Saturation and Value) representation.

$$\begin{aligned} \cos\theta &= \frac{\frac{1}{2}(R-G)+(R-B)}{[(R-G)^2+(R-B)(G-B)]^{1/2}} \\ H &= \{\boldsymbol{\theta}\ If B < G,\ 2\boldsymbol{\pi} - \boldsymbol{\theta}\ otherwise\} \\ S &= 1 - \frac{3*min(R,G,B)}{R+G+B} \\ I &= \frac{1}{3}(R+G+B) \end{aligned} \tag{2.4}$$

Ohta (I, I_2, I_3) Color Model. The linear transformations of principle components (R,G,B) can be achieved through simple conversions to other sets of components by a simple relationship of linear coefficients. Some common representations are (X,Y,Z), (U,V,W), (Y,I,Q) and (I,I_1,I_2) (Sanchez et al., 1994). The image in Figure 2.9(e) is the (I,I_1,I_2) Ohta transformed color model image with the transfer

matrix equivalent to:

$$\begin{pmatrix} I \\ I_1 \\ I_2 \end{pmatrix} = \begin{pmatrix} 0.33 & 0.33 & 0.33 \\ 1.00 & 0.00 & -1.00 \\ 0.50 & -1.00 & 0.50 \end{pmatrix} \begin{pmatrix} R \\ G \\ B \end{pmatrix} \tag{2.5}$$

A chromaticity information separation is achieved by the Ohta color space using a statistical study of the uncorrelated color components on a large population of typical images (Gevers and Smeulders, 1996). The transform is given by equation (2). In spite of the separation of the chromatic (color) and achromatic (luminance) information, the representations mentioned above are still based on triples and any dimensionality reduction can be achieved only by completely neglecting one of the components.

Fisher's Linear Discriminant Model. It is known that morphology based segmentation is the next step involved in image understanding and analysis. A grey-scale image, in which each pixel x_g is a scalar $x_g = w^T x_c$, where 'w' is some linear projection, is required to apply morphological operators. In the event that discrimination has to be made between pipe background and cracks, Fisher's Linear Discriminant can be used to determine the axis, 'w', onto which vector color data can be projected that preserves as much of the discriminating capability of the color information as possible (Duda et al., 2000). The transformations resulting 'Fisher Linear Discriminant' maximizes the separability of the two classes. A compelling aspect of this approach is that the discriminating power of the color data can be exploited, while still providing a degree of invariance to changes in illumination. Further, since the learning of the Fisher discriminant is done off-line, there is minimal additional computational load incurred and scalar feature detectors can be used on the resultant Fisher projection. Pipe images like the one shown in Figure 2.9(a) representative of those likely to be encountered during object recognition and classification phase can be used to learn the Fisher discriminant axis (Sinha, 2000). Figure 2.9(b) shows a gray-scale image obtained by taking the straightforward average of three primary color bands (red (R), green (G) and blue (B)) and 2.9(f) shows image after projection onto a Fisher axis. Although the gray-scale image shows high contrast, the crack boundary is blurred and the image is noisy. The

Fisher discriminant on the other hand, results in an image with good contrast, good visualization of the crack boundary and the image is less noisy.

2.4.2 Image Segmentation

Image segmentation is one of the most important steps leading to the analysis of processed image data and its main goal is to divide an image into parts that have a strong correlation with objects or areas of the real world contained in the image. Image data ambiguity is one of the main segmentation problems, often accompanied by information noise. Segmentation methods can be divided into three groups according to the dominant features they employ. First among them is global knowledge about an image or its part; the knowledge is usually represented by a histogram of image features. Edge-based segmentation form the second group, and region based segmentations the third in which many different characteristics may be used in edge detection or region growing, for example, brightness, texture, velocity field, etc. Because of the different natures of the various edge and region-based algorithms, they may be expected to give somewhat different results and consequently different information.

2.4.2.1 Threshold-based Segmentation

Gray level thresholding is the simplest segmentation process. Many objects or image regions are characterized by constant reflectivity or light absorption surfaces; a brightness constant or threshold can be determined to segment objects and background. Thresholding is computationally inexpensive and fast. It is also the oldest segmentation method and is still widely used in simple applications. Mathematically, a complete segmentation of an image R is a finite set of regions $R_1 ... R_s$,

$$R = \bigcup_{i=1}^{S} R_i \qquad R_i \bigcap R_j = \phi, \ i \neq j \tag{2.6}$$

Complete segmentation can result from thresholding in simple scenes. Thresholding is the transformation of an input image 'f' to an output(segmented) binary

image ‘g’ as follows:

$$g(i,j) = 1 \quad for f(i,j) \geq T; \quad 0 \quad for f(i,j) \leq T \tag{2.7}$$

where ‘T’ is the threshold, g(i,j)=1 for image elements of objects, and g(i,j)=0 for image elements of the background (or vice versa). If objects do not touch each other, and if their gray levels are clearly distinct from background gray levels, thresholding is a suitable segmentation method. It is very important to select a correct threshold for successful threshold segmentation. This selection can be determined interactively or it can be the result of some threshold detection method. Only under very unusual circumstances can thresholding be successful using a single threshold for the whole image (global thresholding) since even in very simple images, there are likely to be gray level variations in objects and background; this variation may be due to non-uniform lighting, non-uniform input device parameters or a number of other factors. Segmentation using variable thresholds (also called adaptive thresholding), in which the threshold value varies over the image as a function of local image characteristics, can produce solutions in such cases (Weszka and Rosenfeld, 1979). Methods based on approximation of the histogram of an image using a weighted sum of two or more probability densities with normal distribution represent a different approach called optimal thresholding (Chow and Kaneko, 1972). The threshold is set as the closest gray level corresponding to the minimum probability between the maxima of two or more normal distributions, which results in minimum error segmentation (Rosenfeld and Kak, 1982). The difficulty with these methods is in estimating normal distribution parameters together with the uncertainty that the distribution may be considered normal. These difficulties may be overcome if an optimal threshold is sought that maximizes the gray level variance between objects and background (Kittler and Illingworth, 1985).

2.4.2.2 Edge-based Segmentation

Edge-based segmentation represents a large group of methods based on information about edges in the image; it is one of the easiest segmentation approaches and still remains very important. Edge-based segmentations rely on edges found in an image by edge detecting operators-these edges mark image location of discontinuities in

gray level, color, texture, etc. The image resulting from edge detection cannot be used as a segmentation result; supplementary processing steps must follow to combine edges into edge chains that correspond better with borders in the image. The most common problems of edge-based segmentation, caused by image noise or unsuitable information in an image are: an edge present in locations where there is no border and no edge present where a real border exists. Clearly both these cases have a negative influence on segmentation results.

Edge detectors are a collection of very important local image segmentation methods used to locate changes in the intensity function; edges are pixels where this function (brightness) changes abruptly. Calculus describes changes of continuous functions using derivatives; an image function depends on two variable-coordinates in the image plane and so operators describing edges are expressed using partial derivatives. A change of the image function can be described by a gradient that points in the direction of the largest growth of the image function. An edge is a property attached to an individual pixel and is calculated from the image function behavior in a neighborhood of that pixel. It is a vector variable with two components, magnitude and direction. The edge magnitude is the magnitude of the gradient, and the edge direction ϕ is rotated with respect to the gradient direction Ψ by $-90°$. The gradient direction gives the direction of maximum growth of the function, e.g., from black [f(i,j)=0] to white [f(i,j)=255].

Edge detection represents an extremely important step facilitating higher-level image analysis and therefore remains an area of active research, with new approaches continually being developed. Recent examples include edge detectors using fuzzy logic, neural networks, or wavelets (Chow and Kaneko, 1972, Aydin et al., 1996, Law et al., 1996, Vrabel, 1996). It may be difficult to select the most appropriate edge detection strategy; a comparison of edge detection approaches and an assessment of their performance nay be found in (Ramesh and Haralick, 1994, Demigny et al., 1995).

2.4.2.3 Region-based Segmentation

The aim of segmentation methods described in the previous section was to find borders between regions; the methods discussed in this section construct regions directly. It is easy to construct regions from their borders, and it is easy to detect

borders of existing regions. However, segmentations resulting from edge-based methods and region-growing methods are not usually exactly the same, and a combination of results may often be a good idea. Region growing techniques are generally better in noisy images, where borders are extremely difficult to detect. Homogeneity is an important property of regions and is used as the main segmentation criterion in region growing, whose basic idea is to divide an image into zones of maximum homogeneity. The criteria for homogeneity can be based on gray level, color, texture, shape, model (using semantic information), etc. (Haralick and Shapiro, 2000, Chang and Li, 1995, Grimson and Lozano-Perez, 1987, Pal and Pal, 1987). Properties chosen to describe regions influence the form, complexity, and amount of prior information in the specific region-growing segmentation method. Methods that specifically address region-growing segmentation of color images are reported in (Gauch and Hsia, 1992, Priese and Rehrmann, 1993, Schettini, 1993).

2.4.3 Mathematical Morphology

A powerful set of image processing operations developed from a set-theoretical approach comes under the classification of mathematical morphology (Serra, 1982). Although the basic operations are simple; morphological operations along with other variants can be concatenated to produce much more complex effects. The basic morphological operations are erosion and dilation. While commonly used on binary images, this approach can be extended to gray-scale images as well (Giardina and Dougherty, 1988). Dilation, in general, causes objects to dilate or grow in size; erosion causes objects to shrink. The amount and the way that they grow or shrink depend upon the choice of the structuring element. The opening operation is somewhat like erosion in that it tends to remove some of the foreground (bright) pixels from the edges of regions of foreground pixels. However it is less destructive than erosion in general. As with other morphological operators, the exact operation is determined by a structuring element. In the general case, morphological image processing operates by passing a structuring element over the image in an activity similar to convolution (Maragos and Schafer, 1990). As in the case of a convoluting kernel, the structuring element can be of any size, and it can contain any complement of 1's and 0's. At each pixel position, a specified

logical operation is performed between the structuring element and the underlying binary image. The binary result of that logical operation is stored in the output image at that pixel position. The effect created depends upon the size and content of the structuring element and upon the nature of the logical operation.The effect of this operator is to preserve foreground regions that have a similar shape to the structuring element, or that can completely contain the structuring element, while eliminating all other regions of foreground pixels.

However, Closing is similar in some ways to dilation in that it tends to enlarge the boundaries of foreground (bright) regions in an image (and shrink background color holes in such regions), but it is less destructive of the original boundary shape. The effect of this operator is to preserve background regions that have a similar shape to this structuring element, or that can completely contain the structuring element, while eliminating all other regions of background pixels. Figure 2.10 shows an example of gray-scale opening and closing operation using a circular structuring element 'g(x)' on a representative signal 'f(x)'. As seen, when the circular structuring element traces out on top of function 'f', the regions that cannot fit the element are 'closed' (Fig. 2.10c). Similarly, when the circular element traces under function 'f', the regions cannot fit in the element are 'opened'.

Mathematical morphology is very often used in applications where shapes of objects are main consideration for example, analysis of microscopic images (in biology, material science, geology, and criminology), industrial inspection, optical character recognition and document analysis. In this thesis, mathematical morphology has been used to segment crack features from CCTV images of buried pipes.

2.5 Ultrasonic NDT

Nondestructive evaluation(NDE) has played critical role in processing, testing and structural evaluation of composite materials. Many conventional and emerging NDE tools are used for NDE of composites. Ultrasonic methods have been demonstrated as an effective tool in characterization of anisotropic composite materials

and structures. Most of the ultrasonic testing is performed on finished products and most of the conventional test device and ultrasonic transducers cannot be directly used for in-process applications. Figure 2.11 illustrates the range of ultrasonic sensors that have been adapted in the field of composite inspection. The need for robust, sensitive, and inexpensive ultrasonic inspection measurement methods is common to many NDE needs. Ultrasonic testing configurations can utilize many wave types. Types of ultrasonic stress-waves that can be present in pipe material of thickness 't' are shown in Figure 2.12. Generally, ultrasonic NDE is performed with ultrasonic wavelengths much smaller than 't' using transducer configurations generating longitudinal or shear waves. Structural and materials testing is possible using Lamb or Rayleigh (surface) waves. However, conventional contact and immersion transducers are not readily adaptable for surface or Lamb wave applications. Non-contact ultrasonic NDE sensor technologies using alternate wave types, namely laser ultrasonic and air-coupled ultrasonic have been demonstrated in the laboratory and now appear to be on the threshold of broad ranged applications. The development of non-contact sensor technologies is of special importance to process control and for defect detection in fiber placed composite structures (Djordjevic and Green, 1994, Boltz et al., 1995, Djordjevic et al., 1998).

It is widely believed that atmospheric absorption is the major obstacle to the use of air-coupled ultrasonic inspection systems which is not the fact in totality (Grandia and Fortunko, 1995). It can be readily shown that, in the frequency region of interest (around 250 KHz for buried concrete pipe inspection), the limitations are due to the very large specific acoustic impedance differences between typical solids and gases. In a system that uses air-coupled transducers for both generation and detection, the received signal amplitude is principally determined by the transmission losses at the four air/solid interfaces, as shown in Figure 2.13. Additional but significantly smaller losses can also be expected due to diffraction, loss of phase-front coherence and finite amplitude saturation effects which are sometimes experienced at very high drive levels.

Guided waves are those waves that require a boundary for propagation. Typical examples include wave propagation along a surface or in a rod, plate, tube, or multi-layer structure. Guided waves are really made up of a superposition of bulk longitudinal and shear waves, but, because of boundary conditions, wave

interference patterns are developed so that nicely formed guided wave packets can propagate in the structure. Bulk longitudinal and shear waves are those considered to propagate in either a half space or infinite space with no boundary disturbances whatsoever. Recent developments in guided wave generation, reception, and mode control show that increased penetration power and sensitivity are possible (Rose, 2000). A tone burst function generator and appropriate signal processing are generally used. Variable angle beam and comb-type transducers are key to this type of evaluation. Problems in tubing, metal piping, hidden corrosion detection in aging aircraft, adhesive and diffusion bonding, and ice detection have been tackled using the guided wave ultrasonic method (Rose, 1999).

2.5.1 Basic Types of Ultrasound Waves

Waves are generated due to induced particle vibration in the material. If the particle motion in a wave is along the line of the direction of travel of the wave, the resulting wave is called a *longitudinal wave* or a *compressional wave*. Such waves can be propagated in solids, liquids and gases. When the particle movement (or vibration) is at right angles to the direction of travel of the wave, a *shear wave* is said to have been generated (see Fig. 2.14). The shear wave velocity is approximately half of that of the longitudinal wave (Halmshaw, 1991). In air, sound travels by compression and rarefaction of air molecules in the direction of travel. However, in solids, molecules can support vibrations in other directions, hence, a number of different types (modes) of sound waves are possible. Longitudinal and shear waves are most often used in ultrasonic inspection. However, at surfaces and interfaces, various types of elliptical or complex vibrations of the particles make other waves possible. Some of these wave modes such as *Rayleigh* and *Lamb waves* are also useful for ultrasonic inspection. Surface or Rayleigh waves travel the surface of a relative thick solid material penetrating to a depth of one wavelength. Rayleigh waves are useful because they are very sensitive to surface defects and since they will follow the surface around curves, they are often used to inspect areas that other wave types might have difficulty reaching.

Lamb wave or guided wave is another type of ultrasonic wave propagation in which the wave is guided between two parallel surfaces of the test object (Rose,

1999). For an object sufficiently thin to allow penetration to the opposite surface, e.g. a plate having thickness of the order of a wavelength or so, Rayleigh waves degenerate to Lamb waves, which can propagate in a number of modes, either *symmetrical* or *antisymmetrical* (see figure 2.13) (Rose, 2000, Hayashi and Rose, 2003, Redwood, 1960). The velocity is dependent on the product of frequency and material thickness.

2.5.2 Contact And Non-contact Ultrasound Transduction

Ultrasound inspection can be carried out primarily in two ways, contact with the test material and through non-contact. Testing carried out in which the transducer face makes direct contact with the test object through a thin film of couplant is called contact ultrasound testing. Non- contact ultrasonic testing is one in which the waves are generated and transmitted into the material to be tested without direct contact with the generating source. Static capacitance, electro-magnetic acoustic transmission (EMAT) and magneto-resistive transducers are examples of non-contact ultrasonic transduction. When sound passes across an interface between two materials only a proportion of the sound is transmitted, the rest of the sound is reflected. The proportion of the sound that is transmitted depends on how close the acoustic impedance of the two materials matches. Water is a fairly good match for most commonly used materials - for example typically around half the sound energy is transmitted at the interface between water and a carbon laminate. After four solid- liquid interfaces (from the probe, to the couplant, to the test piece, and then back again) there is still a few percent of the original energy left so accurate measurement is possible. Conversely if the sound has to move between the test piece and air (which has very low acoustic impedance) only around 1% of the sound energy is transmitted. Thus, it has been a long standing challenge in the ultrasonic testing area to be able to produce high resolution data using air-coupled ultrasound.

2.5.3 Ultrasonic NDT of Concrete

In spite of the development of test techniques and equipment, the use of NDT for inspecting concrete poses many difficulties. Compared to metal and metal-based

materials, NDT of concrete is a relatively immature discipline. The heterogenous nature of concrete and unspecified code or standard of concrete NDT are two main areas where concrete inspection technology lags behind. Concrete is a multi-phase material consisting of a coarse aggregate comprising particles of more than 5 mm in diameter, a fine aggregate, sand, cement and admixtures. The coarse granular structure, such as the relative concentration of the constituent particles, degree of compaction, moisture content, and the nature of defects present gives rise to a high degree of acoustic scattering leading to attenuation. For this reason, testing in concrete is usually limited to the kilohertz frequency range.

Ultrasonic techniques that detect defects, measure the mechanical properties, or monitor the state of deterioration in concrete structures has been a topic of considerable interest to the civil infrastructure community (Malhotra and Carino, 2004, Bungey and Millard, 1996). The ultrasonic pulse velocity method uses compression waves to evaluate the conditions of materials like concrete (Olsen, 1993). The ultrasonic pulse velocity is by far the most widely accepted method for assessing the quality of concrete in structures (Popovics and Popovics, 1992). Structural changes taking place in concrete during loading has also been monitored with the ultrasonic pulse velocity method. The use of ultrasonic velocity measurements for nondestructive evaluation of Portland cement concrete was proposed in the late 1940's (Jones, 1949). Although Jones (1949) studied the behavior of concrete during loading, his work focused on the development of relationships between ultimate compressive strength and pulse velocity. Later researchers found that in addition to the time domain analysis used in earlier studies, the frequency domain can provide significant information (Wei-Du, 1992, Popovics and Popovics, 1992). Na et al. (2002) investigated the feasibility of detecting and quantifying delamination at the interface between steel bar and concrete using ultrasonic guided waves. This technique could predict and quantify the degree of separation or delamination but was unable to localize the exact location of the separation between the transducer and receiver. Na et al. (2003) also conducted another study to compare the delamination between steel/cocnrete and glass fiber reinforced polymer/concrete interfaces using guided waves.

Research in detecting defects in concrete has mainly been focussed on single surface breaking cracks (Song et al., 2003). Most efforts made use of time-of-flight (TOF) methods to determine the depth of simulated cracks (notches with well defined tips) in concrete where the velocity of wave propagation in concrete is known and a characteristic wave pulse-crack interaction is realized (Lin and Su, 1996, Sansalone et al., 1998, Wu et al., 1995). However, the TOF method is not effective when realistic concrete cracks are tested. Song et al. (2003) proposed a self-compensating surface wave transmission coefficient measurement technique to measure surface-breaking cracks and notches in concrete. But, the transmission coefficient is sensitive to changing crack depth and is reliable only in a certain range. Ramamoorthy et al. (2004) studied the determination of depth of surface-breaking cracks in concrete specimens using an ultrasound diffusion technique. Their method demonstrated feasibility for notch defects for which the two surfaces were not in contact. Results for realistic cracks with surfaces in contact were not discussed. Jung et al. (2000) investigated the feasibility of detecting defects in concrete beams using lamb waves. Artificial internal defects were simulated in a concrete beam and *V(f)* curves were plotted for various frequencies of operation.

To apply pulse-echo testing to concrete inspection, it was necessary to develop low-frequency transducers with sufficiently short impulse responses. With the introduction of such transducers and instruments in the beginning of the 1990's, recording of single (A-scan) and multiple (B/C-scan) measurements was made possible (Hillger and Neisecke, 1993). Imaging methods such as SAFT (Synthetic Aperture Focusing Technique) reconstruction have been shown to enable thickness measurement, detection of tendon ducts, and flaws, and can expose the inner structure of concrete elements (Schickert et al., 2003, Schickert, 2005). But, to adopt them in the field, additional research is required concerning the efficiency of these techniques. A large number of single measurements are necessary to limit the effect of structural noise and enhance image quality (Schickert et al., 2006). Moreover, parts of the measurement process, especially the tedious transducer coupling to concrete, still pose problems. Conventional coupling agents are difficult to apply or remove, and therefore do not seem to be adequate. On the other hand, alternative methods such as water or dry coupling are under investigation (Schickert,

2005).

It may be noted that most of the research in concrete imaging has been conducted on thick walled concrete (few hundred centimeters) wherein signal echoes are well separated in time. In this thesis, wastewater concrete pipes that are 60 mm in thickness are considered. Issues such as penetration depth versus time-of-flight resolution are key factors that need to be considered while dealing with such low thicknesses. There are various factors that govern the selection of an appropriate inspection method while dealing with concrete pipes like geometry, ease of access, etc. To put this research work in context to the current state of ultrasound NDT of concrete, this thesis explores various ultrasound-based inspection techniques and proposes an inspection system that is suitable for concrete pipes. This research builds upon previous work done individually in ultrasound immersion testing and ultrasonic imaging and develops a system that can not only detect defects in thin-walled concrete, but also characterize them through C-scan imaging to gain depth perception.

2.6 Feature Extraction

Recognition of object (ultrasonic signal, in this study) features is an important step on the way to understanding signal/image data, and requires an exact description in a form suitable for a classifier. This discussion will help understand the importance of feature generation for pattern recognition tasks.

In order to build a pattern recognition system, it is important to decide which characteristics of the objects should be measured so that descriptive parameters can be produced. These characteristics are termed as features and the resulting parameter values as feature vectors. Proper selection of the features is important as only these will be used to perform pattern recognition tasks. Feature ordering techniques compute the relative power of various features (Duda et al., 2000). In general, good features have the following four characteristics (Guyon et al., 2004):

- Discrimination: Features should take on significantly different values for ob-

jects belonging to different classes.

- Reliability: They should have similar values for all objects belonging to the same class.
- Independence: They should be uncorrelated with each other.
- Few in number: The complexity of a pattern recognition system increases rapidly with the dimensionality of the system. The number of training data required to train the classifier and to measure performance increases exponentially with the number of features (Duda and Hart, 1973). Moreover, adding more features that are either noisy or highly correlated with existing features can actually degrade the performance of the classifier (Kanal and Chandrasekaran, 1971).

Over the last past few decades, extensive research has taken place in the development of efficient and reliable methods for the selection of features (Mukherjee and Pal, 2005). As mentioned above, the quality of performance of the classifier depends upon the relevance, discriminatory information and ease of computation of various features. Many features can be used to describe an object. The most basic of all signal features is the signal amplitude in terms of its spectral component. Signal transforms provide the frequency domain information in the data. Transform coefficient based feature extractions have proved to be practical in several applications in which transform domain features are used as inputs to a pattern recognition and classification system (Polikar et al., 1998, Pittner and Kamarthi, 1999, Simone et al., 2002).

2.7 Classification

Predictive modeling is at the heart of a scientific discipline called machine learning. It refers to a branch of computer science interested in reproducing human "learning" capabilities with computer programs. Machine learning research has mostly focused on finding relationships in data and analyzing the processes for extracting such relations, rather than building truly intelligent systems (Guyon et al., 2004). Machine learning problems occur when a task is defined by a series of cases or

examples rather than by predefined rules. Such problems are found in a wide variety of application domains, ranging from engineering applications in robotics and pattern recognition (speech, handwriting, face, anomaly recognition), to Internet applications (text categorization) and medical applications (diagnosis, prognosis, drug discovery). Given a number of "training" examples (also called data points, samples, patterns or observations) associated with desired outcomes, the machine learning process consists of finding the relationship between the patterns and the outcomes using solely the training examples (Jain et al., 2000). Thus, a machine learning system "learns" the relationship between the input (training data points) and the pattern (or class) to which it belongs. It is then called upon to predict the pattern of a "new" input (test data) based on its learning of the problem inference rules. The theory of machine learning is very involved and thoroughly discussed in several references (Duda et al., 2000, Mitchell, 1997, Langley, 1995). Machine learning systems perform two main functions, *feature extraction* and *classification*. As the former has been covered in the previous section, a brief description of classification methods follows.

2.7.1 Statistical Classification

Classification has two distinct meanings. Given a set of observations, the aim may be to establish the existence of classes or clusters in the data. Or it may be known for certain that there are so many classes, and the aim is to establish a rule whereby an observation can be classified into one of the existing classes. The former type is known as *Unsupervised Learning* (or Clustering), the latter as *Supervised Learning*. In the statistical literature, Supervised Learning is usually referred to as discrimination, by which is meant the establishing of the classification rule from given correctly classified data.

There are three essential components to a classification problem:

- The relative frequency with which the classes occur in the population of interest, expressed formally as the prior probability distribution.
- An implicit or explicit criterion for separating the classes: such as an un-

derlying input/output relation that uses observed attributes to distinguish a random individual from each class.

- The cost associated with making a wrong classification.

Most techniques implicitly confound components and produce a classification rule that is derived conditional on a particular prior distribution and cannot easily be adapted to a change in class frequency. However, in theory each of these components may be individually studied and then the results formally combined into a classification rule (Michie et al., 1994). They are briefly mentioned below.

2.7.1.1 Prior probabilities and the Default rule

Let the classes be denoted by C_i, i = 1, ..., q, and let the prior probability π_i for the class C_i be:

$$\pi_i = p\,(C_i) \tag{2.8}$$

It is always possible to use the no-data rule: *classify any new observation as class C_k, irrespective of the attributes of the example.* This no-data or default rule may even be adopted in practice if the cost of gathering the data is too high. The default rule relies only on knowledge of the prior probabilities, and clearly the decision rule that has the greatest chance of success is to allocate every new observation to the most frequent class. However, if some classification errors are more serious than others, the minimum risk (least expected cost) rule is adopted, and the class k is that with the least expected cost.

2.7.1.2 Separating Classes

Suppose, it is possible to observe data x on an individual, and that the probability distribution of x within each class C_i is known to be $P(x|C_i)$. Then for any two classes C_i, C_j the likelihood ratio $P(x|C_i)/P(x|C_j)$ provides the theoretical optimal form for discriminating the classes on the basis of data x. The majority of techniques in statistical classification can be thought of as implicitly or explicitly deriving an approximate form for this likelihood ratio.

2.7.1.3 Misclassification Costs

Let the cost of misclassifying a class C_i object as class C_j be *c(i,j)*. Decisions should be based on the principle that the total cost of misclassifications should be minimized: for a new observation this means minimizing the expected cost of misclassification. Consider the expected cost of applying the default decision rule as: allocate all new observations to the class C_d, using suffix d as label for the decision class. When decision C_d is made for all new examples, a cost of *c(i,d)* is incurred for class C_i examples and these occur with probability π_i. So the expected cost $Cost_d$ of making decision C_d is:

$$Cost_d = \sum_i \pi_i c(i, d) \tag{2.9}$$

The Bayes minimum cost rule chooses the class that has the lowest expected cost. To see the relation between the minimum error and minimum cost rules, suppose the cost of misclassifications to be the same for all errors and zero when a class is correctly identified, i.e. suppose that *c(i,j)* = c for i $\neq$ j and *c(i,j)* = 0 for i = j. Then the expected cost is:

$$Cost_d = \sum_i \pi_i c(i, d) = \sum_{i \neq d} \pi_i c = c \sum_{i \neq d} \pi_i = c(1 - \pi_d) \tag{2.10}$$

and the minimum cost rule is to allocate the class with greatest prior probability.

Misclassification costs are very difficult to obtain in practice. Even in situations where it is very clear that there are very great inequalities in the sizes of the possible penalties or rewards for making the wrong or right decision, it is often very difficult to quantify them.

2.7.2 Artificial Neural Networks (ANN)

There is no precise agreed definition among researchers for a neural network, but most agree that it involves a network of simple processing elements (neurons) which can exhibit complex global behaviour, determined by the connections between the processing elements and element parameters. The original inspiration for the tech-

nique was from examination of the central nervous system and the neurons (and their axons, dendrites and synapses) which constitute one of its most significant information processing elements (Haykin, 1994). In a neural network model, simple nodes (called "neurons", "neurodes", "processing elements", or "units") are connected together to form a network of nodes hence the term "neural network." While a neural network does *not* have to be adaptive, its practical use comes with algorithms designed to alter the strength (weights) of the connections in the network to produce a desired signal flow. These networks are also similar to the biological neural networks in the sense that functions are performed collectively and in parallel by the units, rather than there being a clear delineation of subtasks to which various units are assigned. Currently, the term ANN tends to refer mostly to neural network models employed in statistics and artificial intelligence. Neural network models designed with emulation of the central nervous system (CNS) in mind are a subject of theoretical neuroscience (Hagan et al., 1996).

In modern software implementations of artificial neural networks, the approach inspired by biology has more or less been abandoned for a more practical approach based on statistics and signal processing. In some of these systems, neural networks, or parts of neural networks (such as artificial neurons) are used as components in larger systems that combine both adaptive and non-adaptive elements. While the more general approach of such adaptive systems is more suitable for real-world problem solving, it has far less to do with the traditional artificial intelligence connectionist models. However, the commonality between them is the principle of non-linear, distributed, parallel and local processing and adaptation.

2.7.2.1 Learning

Learning is accomplished in general by developing algorithms that allow the system to learn for itself from a set of input/output training data combinations. One major goal of learning algorithms is to combine the main features of a computing machine with those of human expertise to infer as many correct decisions as possible. An increasing number of systems are being designed today to have the very distinctive feature of learning. This is done by adjusting their parameters in re-

sponse to unpredictable changes in their dynamics or their operating environment without the need for an explicit knowledge of a system model or rule that guides behavior.

The aspect that has attracted the most interest in neural networks is the possibility of learning, which in practice means the following:

Given a specific task to solve, and a class of functions F, learning means using a set of observations, in order to find $f^* \in F$ which solves the task in an optimal sense. This entails defining a cost function $C : F \to \mathbb{R}$ such that, for the optimal solution f^* , $C(f^*) \leq C(f) \forall f \in F$ (no solution has a cost less than the cost of the optimal solution). The cost function C is an important concept in learning, as it is a measure of some distance from an optimal solution to the problem that is to be solved. Learning algorithms search through the solution space in order to find a function that has the smallest possible cost. For applications where the solution is dependent on some data, the cost must necessarily be a function of the observations. It is frequently defined as a statistic to which only approximations can be made. As a simple example consider the problem of finding the model f which minimizes

$$C = E\left[|f(x) - y|^2\right], \tag{2.11}$$

for data pairs (x,y) drawn from some distribution $\mathcal{D}$. In practical situations, there are N samples from $\mathcal{D}$ and thus, for the above example, the goal would be to minimize

$$\hat{C} = \frac{1}{N}\sum_{i=1}^{N} |f(x_i) - y_i|^2. \tag{2.12}$$

Thus, the cost is minimized over a sample of the data rather than the true data distribution.

When $N \to \infty$, some form of online learning must be used, where the cost is partially minimized as each new example is seen. While online learning is often used when $\mathcal{D}$ is fixed, it is most useful in the case where the distribution changes slowly over time. In neural network methods, some form of online learning is

frequently also used for finite datasets.

2.7.2.2 Learning Paradigms

There are three major learning paradigms, each corresponding to a particular abstract learning task. These are supervised learning, unsupervised learning and reinforcement learning. Usually any given type of network architecture can be employed in any of those tasks.

Supervised Learning

In supervised learning, given a set of example pairs (x, y), x ∈ X, y ∈ Y, the aim is to find a function f in the allowed class of functions that matches the examples. A commonly used cost is the mean-squared error which tries to minimize the average error between the network's output, *f(x)*, and the target value y over all the example pairs. When one tries to minimize this cost using gradient descent for the class of neural networks called Multi-Layer Perceptrons, one obtains the well-known backpropagation algorithm for training neural networks. Tasks that fall within the paradigm of supervised learning are pattern recognition (also known as classification) and regression (also known as function approximation). The supervised learning paradigm is also applicable to sequential data (e.g., for speech and gesture recognition).

Unsupervised Learning

In unsupervised learning, given some data x, the cost function to be minimized can be any function of the data x and the network's output, *f*. The cost function is dependent on the task (being modeled) and *apriori* assumptions (the implicit properties of the model, its parameters and the observed variables). For example, consider the model $f(x) = a$, where a is a constant and the cost $C = (E[x] - f(x))^2$. Minimizing this cost will give a value of a that is equal to the mean of the data. The cost function can be much more complicated. Its form depends on the application: For example in compression, it could be related to the mutual information between x and y. In statistical modeling, it could be related to the posterior probability

of the model, given the data. Tasks that fall within the paradigm of unsupervised learning are in general estimation problems; the applications include clustering, the estimation of statistical distributions, compression and filtering.

Reinforcement Learning

In reinforcement learning, data x is usually not given, but generated by an agent's interactions with the environment. At each point in time t, the agent performs an action y_t and the environment generates an observation x_t and an instantaneous cost c_t, according to some (usually unknown) dynamics. The aim is to discover a policy for selecting actions that minimizes some measure of a long-term cost, i.e. the expected cumulative cost. The environment's dynamics and the long-term cost for each policy are usually unknown, but can be estimated.

More formally, the environment is modeled as a Markov decision process (MDP) with states $s_1, ..., s_n \in S$ and actions $a_1, ..., a_n \in A$ with the following probability distributions: the instantaneous cost distribution $P(c_t|s_t)$, the observation distribution $P(x_t|s_t)$ and the transition $P(s_t+1|s_t, a_t)$. A policy is defined as conditional distribution over actions given the observations. Taken together, the two define a Markov chain (MC). The aim is to discover the policy that minimizes the cost, i.e. the MC for which the cost is minimal. Artificial Neural Networks (ANNs) are frequently used in reinforcement learning as part of the overall algorithm. Tasks that fall within the paradigm of reinforcement learning are control problems, games and other sequential decision making tasks.

2.7.2.3 Features of ANNs

As mentioned previously, an ANN is typically composed of a set of parallel and distributed processing units, called nodes or neurons. These are usually ordered into layers, appropriately interconnected by means of unidirectional (or bi-directional) weighted signal channels, called connections or synaptic weights. The internal architecture of ANN provides powerful computational capabilities, allowing for simultaneous exploration of different competing hypotheses. Neural networks gather their knowledge through detection of patterns and relationships found in the data

provided to them. There are three features that characterize an ANN: the network architecture, transfer function (or activation function), and the learning algorithm.

Neural Network Architectures

The neural network architecture refers to the ordering and organizing of the nodes from the input layer to the output layer of the network. The manner in which nodes and the interconnections are arranged within a layer and between layers of a given ANN determines the architecture. The nature of problem at hand defines the use of a particular architecture. The most common ANN architectures are feedforward and recurrent architectures (Haykin, 1994).

The feedforward architecture was the first and arguably simplest type of artificial neural networks devised. In this network, the information moves in only one direction, forward, from the input nodes, through the hidden nodes (if any) and to the output nodes. There are no cycles or loops in the network. The feedforward architecture is very popular due to its association with a quite powerful and relatively robust learning algorithm called backpropagation. The multilayer perceptron network and the radial basis function network are among the well-known networks using the feedforward architecture.

Contrary to feedforward networks, recurrent neural networks (RNs) are models with bi-directional data flow. While a feedforward network propagates data linearly from input to output, RNs also propagate data from later processing stages to earlier stages. While feedforward networks map input into output and ar static in the sense that the output of a given pattern of inputs is independent of the previous state of the network, recurrent networks map states into states and as such are very useful for modeling and identification of dynamic systems. Some of the well known neural networks designed on this architecture are Kohonen network, the Hopfield network and competitive networks.

Neural Network Activation Functions

The basic elements of the computational part of a neural network are the neurons, which take the weighted sum of their inputs from other nodes and apply to them a mapping, called the activation function, before delivering the output to the next neuron. An activation function is simply a function that is used to introduce nonlinearity to the network. The output O_m of a neuron (m)having (n) inputs is given by:

$$O_m = f\left(\sum_n w_{im}x_i + \phi_m\right) \tag{2.13}$$

where f is the node's activation function, $x_1, x_2, ..., x_m$ are the node's inputs, $w_{1m}, w_{2m}, ..., w_{nm}$ are the connection weights, and ϕ_m is the node's threshold. The processing activity within a given layer is done simultaneously hence providing the neural network with the powerful capability of parallel computing. Depending upon the problem at hand, the activation functions can take different forms: linear, sigmoid, exponential, and hyperbolic tangent. All these functions are differentiable because the backpropagation algorithm requires that activation functions have to be differentiable. A linear activation function is equivalent to having no activation function at all (i.e., the sum of the "signals" is the result sent to a node's children). A sigmoid function (also called the logistic) is an S-shaped curve that maps all input to [0,1]. It has a limit of 0 as x approaches negative infinity, and 1 as x approaches infinity. A hyperbolic tangent function is similar to a sigmoid, but it maps all of its input to [-1,1]. It has a limit of -1 as x approaches negative infinity, and 1 as x approaches infinity. An exponential function is the exponential function e^x.

Neural Network Learning Algorithms

Learning algorithms are used to update the weighting parameters at the interconnection level of the neurons during the training process of the network. Often for robustness and efficiency reasons, a combination of back propagation and conjugate gradient algorithms are used. The prediction accuracy of an ANN is measured by the mean squared difference between the actual and predicted output values. For a preselected ANN model and corresponding data set, this mean squared error depends only on the values of the connection weights. During learning, the

ANN processes training patterns consisting of input-output patterns through the network, systematically adjusting the connection weights, so that the measure of the overall goodness of the ANN model defined as the root mean squared error (RMSE) between the ANN-estimated output values and the actual values, is minimized. The minimization learning algorithm is always iterative, and each step is considered "learning".

2.8 Summary

This chapter presented the background relevant for understanding the automated buried pipe inspection system. A broad overview of various pipeline assessment techniques in general are reviewed. A methodology for automated image-based inspection is presented . The next two sections discussed image segmentation and feature extraction methods. Next, ultrasound nondestructive testing is reviewed and various approaches applicable to concrete inspection are discussed. Finally, a brief review of pattern recognitions tasks is provided at the end of this chapter.

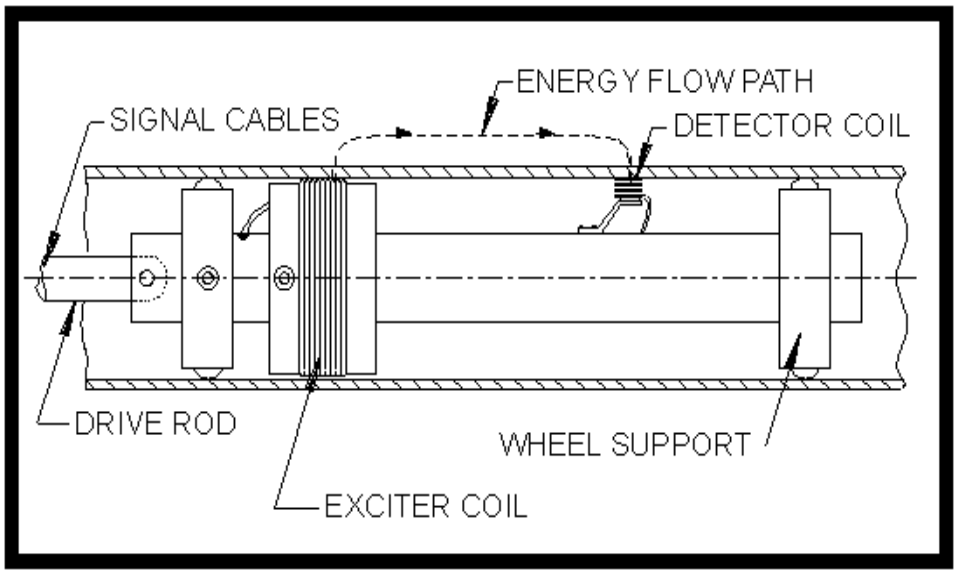

Figure 2.1. Eddy current inspection of pipes

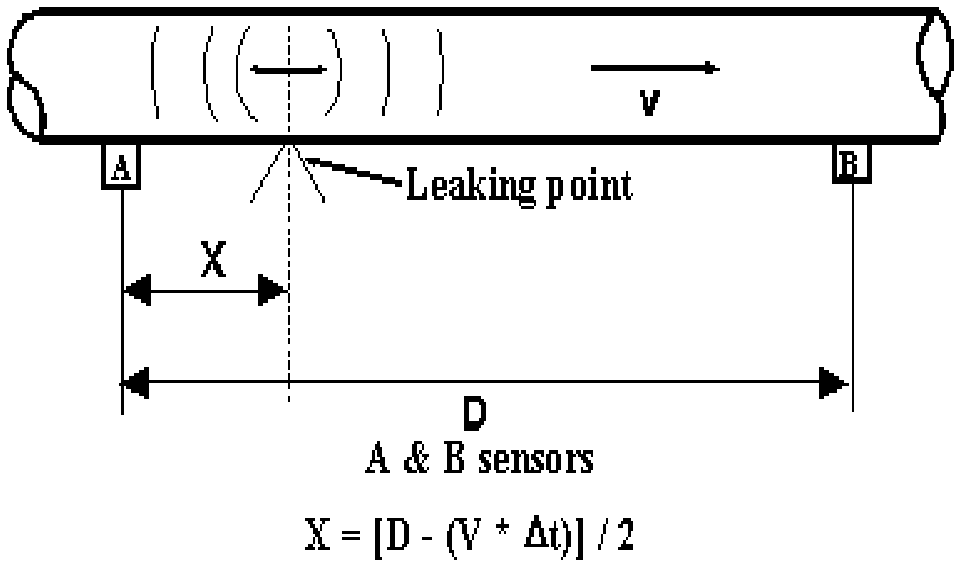

Figure 2.2. Acoustic emission based inspection of pipes

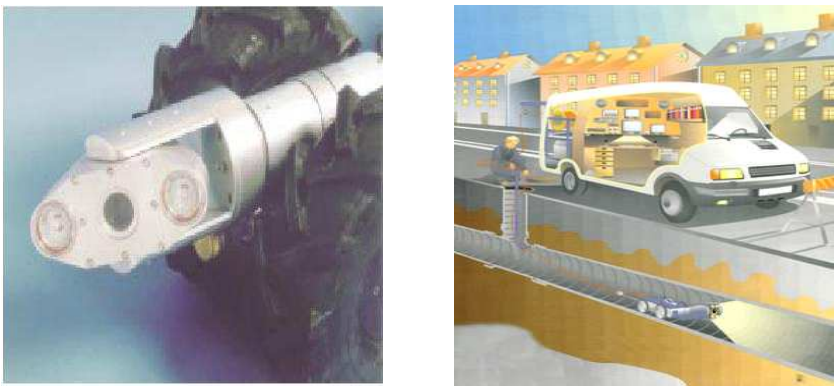

(a) (b)

Figure 2.3. (a) CCTV Camera and (b) buried inspection process

(a) (b)

Figure 2.4. (a) Digitized image of pipeline and (b) SSET inspection probe

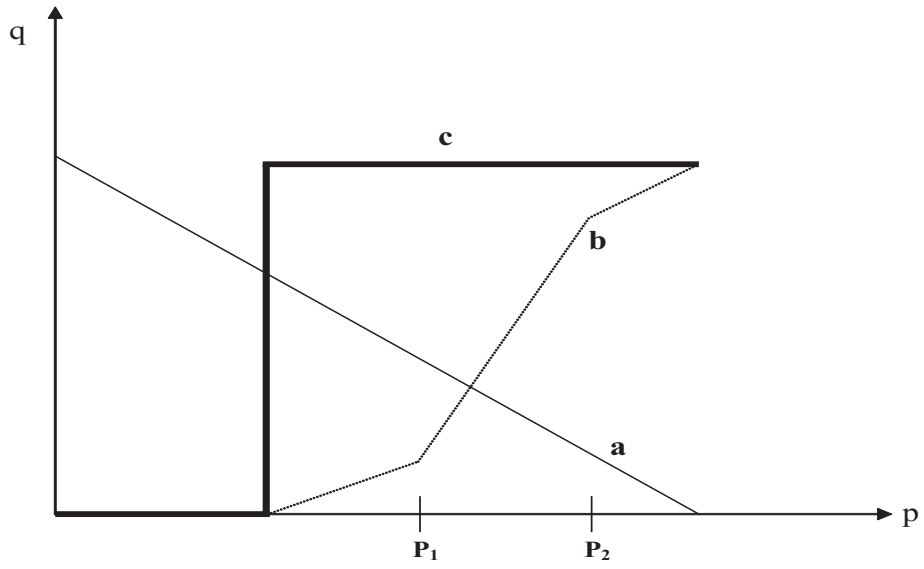

Figure 2.5. Some gray-scale transformations

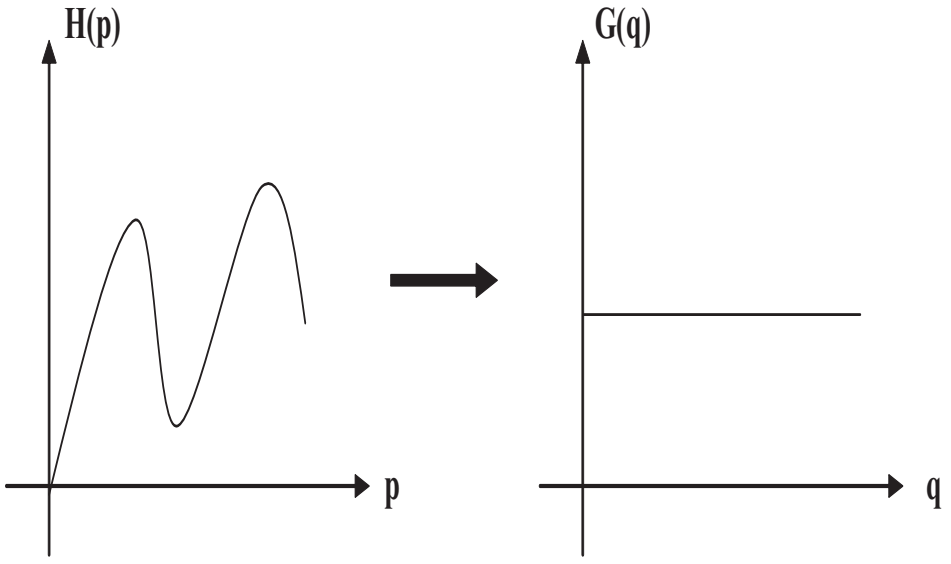

Figure 2.6. Histogram equalization

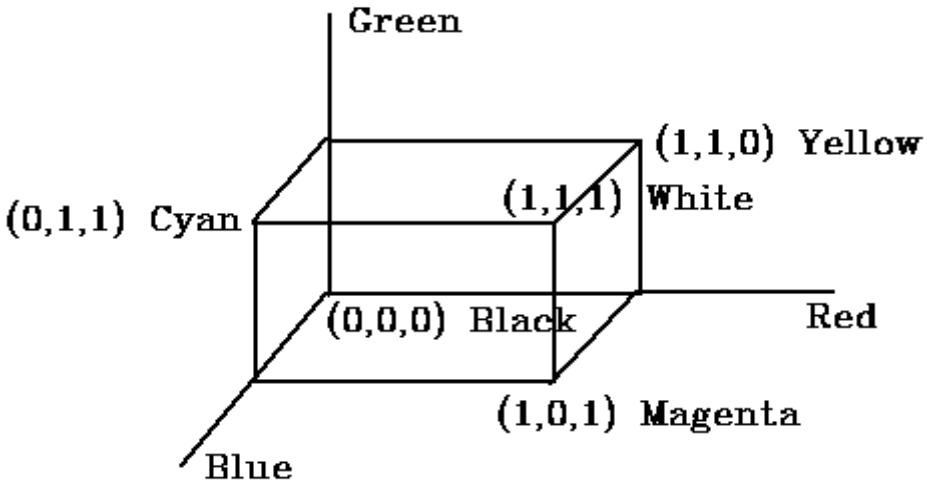

Figure 2.7. The RGB color space

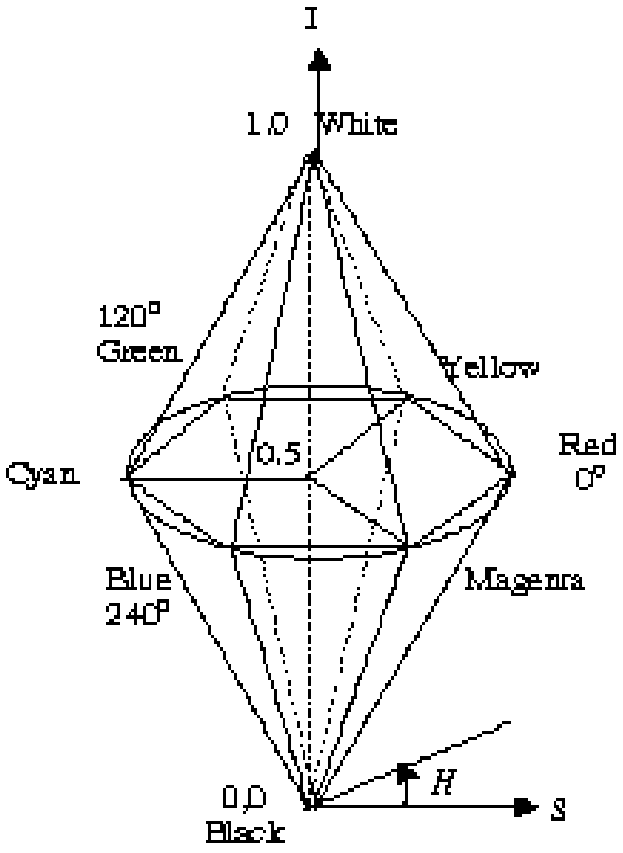

Figure 2.8. HSI Color Space

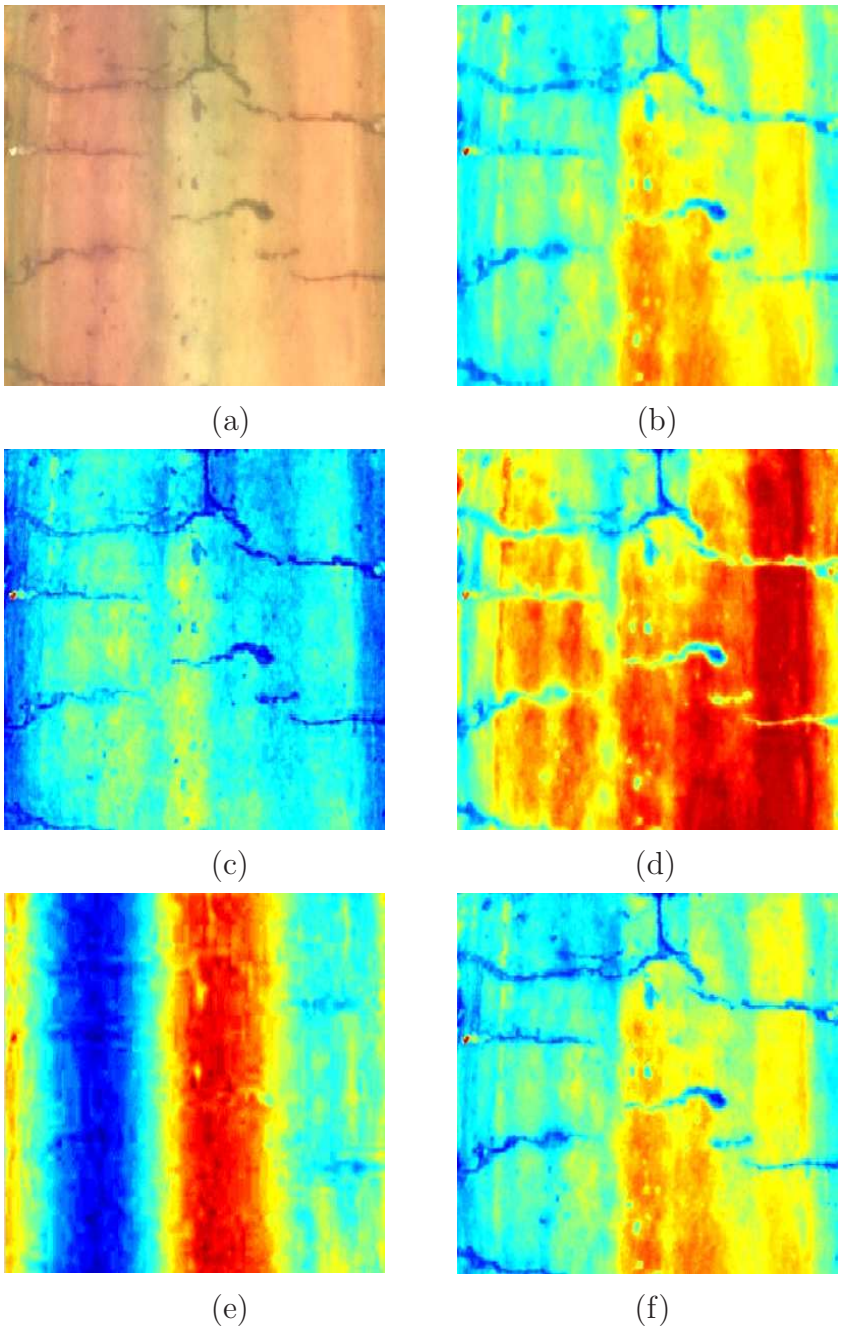

Figure 2.9. (a) Original scan image, (b) Gray-scale image, (c) HSI Color model image, (d) YIQ Color model image, (e) (I, I1, I2) Ohta Color model image and (f) Fisher Discriminant image

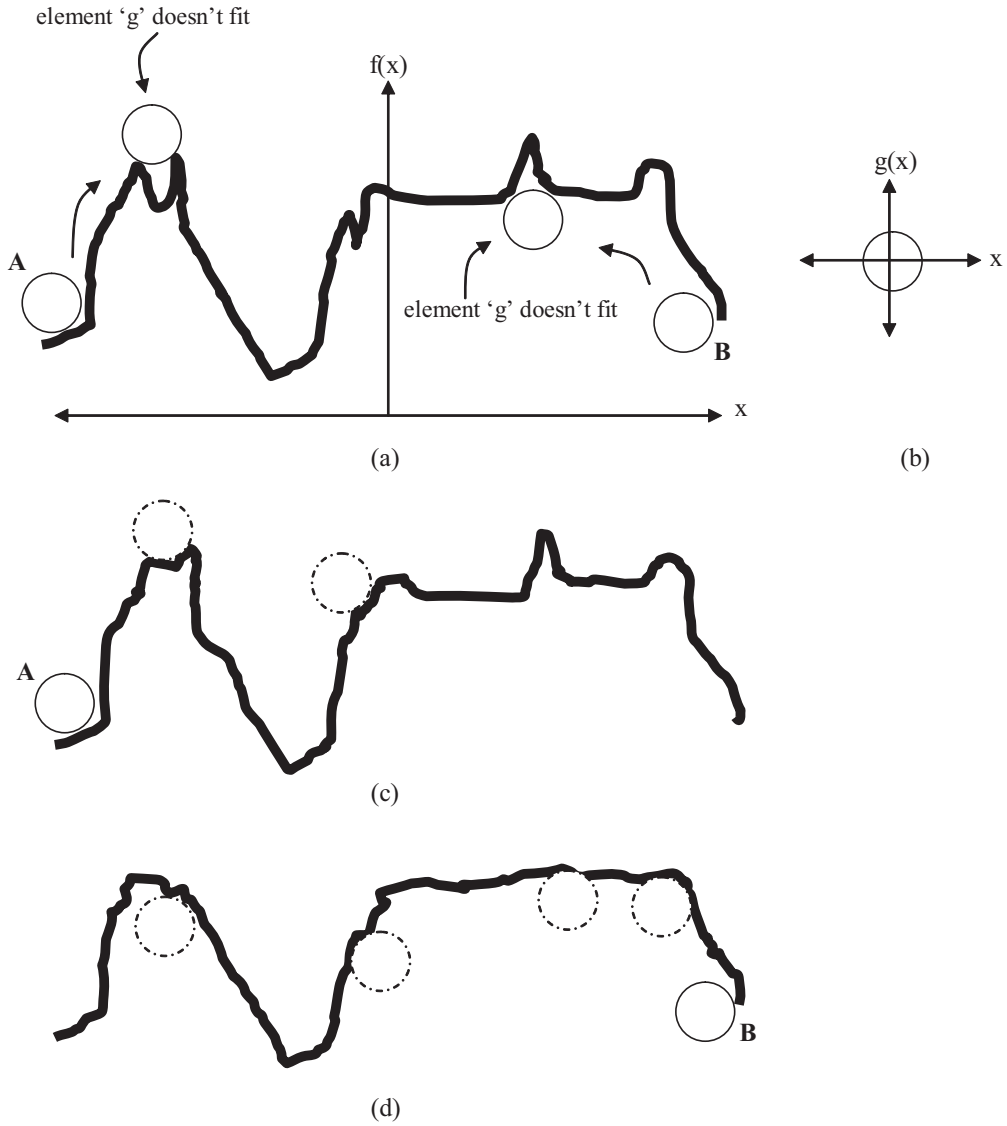

Figure 2.10. Illustration of gray-scale Opening and Closing operation. (a) A gray-scale scan line 'f(x)'; (b) circular structuring element 'g(x)'; (c) result of closing showing various locations of structuring element during operation and (d) result of opening showing various locations of structuring element during operation.

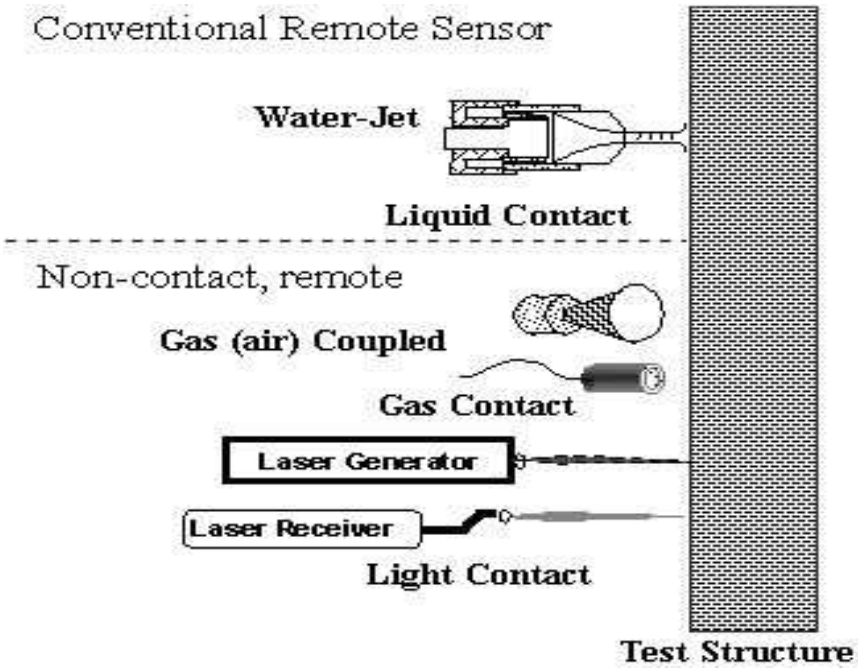

Figure 2.11. Ultrasonic sensors suitable for scanning composites

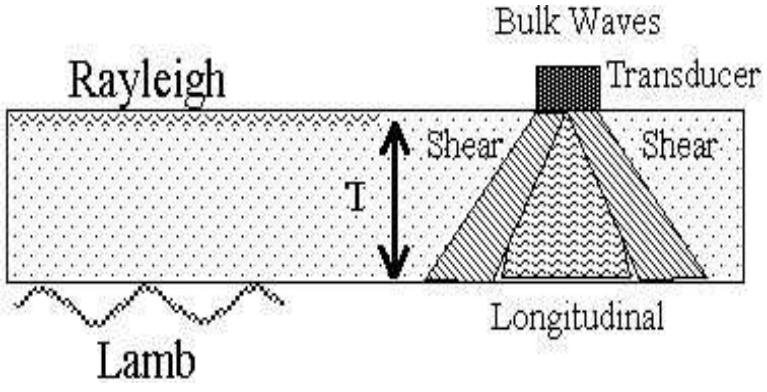

Figure 2.12. Ultrasonic stress wave types present in the plate thickness 't'

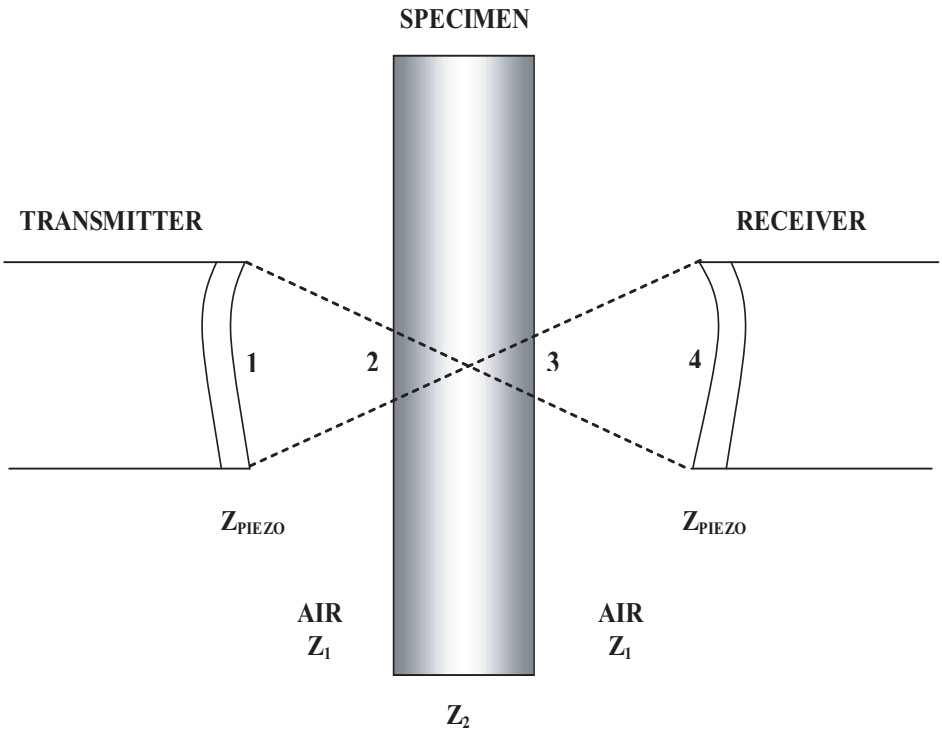

Figure 2.13. Air to solid interfaces 1,2,3,4

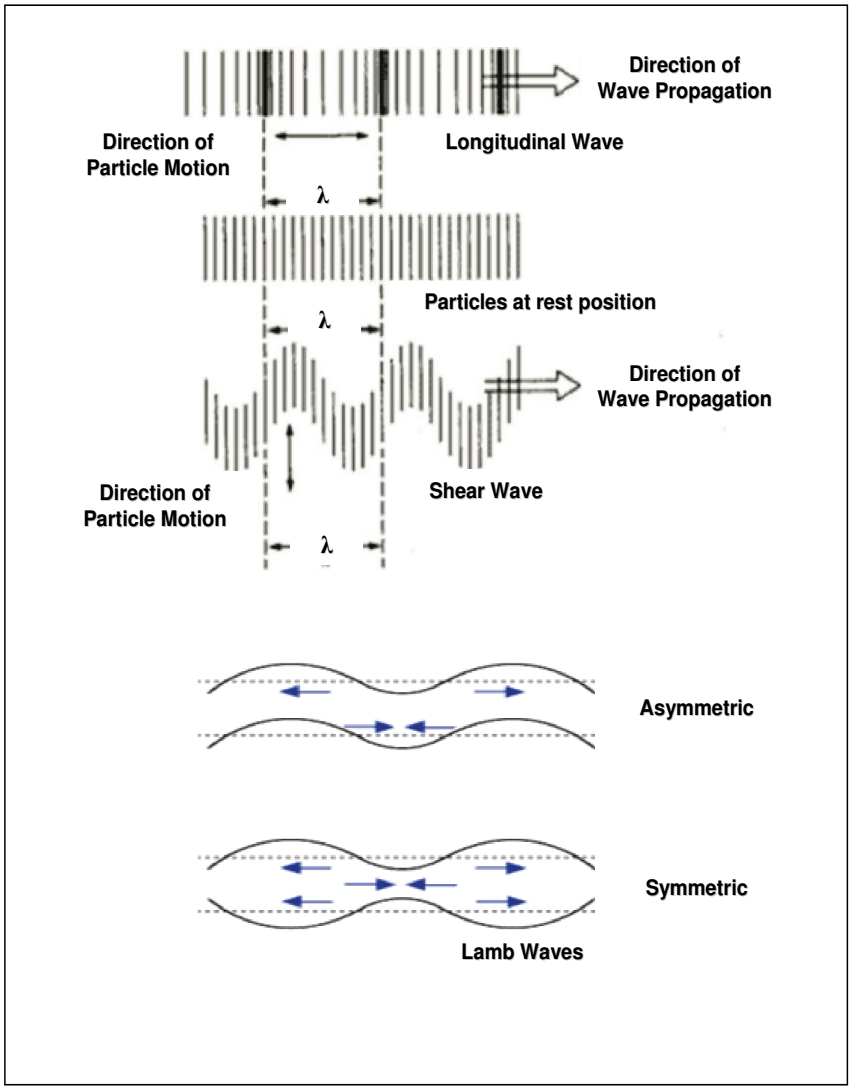

Figure 2.14. Basic types of ultrasound waves

Chapter 3

CCTV Pipeline Image Pre-processing

3.1 Introduction

The use of digital image data for a spatial database requires several preprocessing procedures. These procedures include, but are not limited to: geometric correction, image enhancement, and feature selection. The goal of digital image preprocessing is to increase both the accuracy and the interpretability of the digital data during the image processing phase. Geometric correction involves the reorientation of the image data to selected parameters. This will allow for accurate spatial assessments and measurements of crack features from the SSET or CCTV imagery. The aim of pre-processing in underground pipeline images is an improvement of the image data that suppresses unwanted distortions in background or enhances some image features (like cracks) important for further processing. Image pre-processing methods use the considerable redundancy in images. Neighboring pixels corresponding to one object in real images have essentially the same or similar brightness value. Thus, distorted pixel can often be restored as an average value of neighboring pixels. Four categories of image pre-processing methods according to the size of the pixel neighborhood that is used for the calculation of new pixel brightness are: pixel brightness transformations, geometric transformations, pre-processing methods that use a local neighborhood of the processed pixel, and image restora-

tion that requires knowledge about the entire image. Gray scale transformation and image smoothing which are image pre-processing methods belonging to the pixel brightness transformation and local pre-processing categories respectively were briefly discussed in the previous chapter. There are several color coordinate systems, each having its particular merits that are being used in color image processing. For examples, HIS, YIQ, CIELAB, and CIELUV coordinate systems are the most popular. Quantization error may exist during coordinate transformations in any one of the above systems. The effect of quantization error on color image processing is analyzed in order to minimize the artifacts created by the error in the resultant image. The chapter on background carries sufficient information on the above color image processing techniques and their relevance to the 'specific' problem that this research study intends to address.

A data set consisting of hundreds of images of underground pipes from major cities in North America has been acquired. This data set was used to explore basic characteristics of underground pipe images. Analysis of images have shown that there are two important characteristics that complicate the segmentation of pipe images, viz., the presence of a complicated background pattern due to earlier runoff, patches of repair work, corroded areas, debris, non-uniformities in illumination, and flaws in the image acquisition process; and secondly because the three main objects of interest - cracks, joints, and laterals - are all dark features that cannot be distinguished by intensity criteria alone. Although the goal of this research is to develop an automated method that detects cracks from a given pipe image, the image segmentation problem is difficult to automate because the differences between classes such as joints and cracks, although obvious to a human, can be very difficult to encode mathematically at the pixel level. This task becomes even more complex given the quality of the images and conditions under which they are obtained by PSET imagery. Thus, this necessitates an urgent need to enhance the raw digital color image in a pre-processing phase before subjecting it to segmentation operations. It is of great interest to us that the contrast between the background and crack features is enhanced to facilitate efficient segmentation and classification. Two techniques are proposed in this chapter to achieve better contrast than the originally acquired color image from the imaging sensors thus reducing the probability of loss of data in the conversion process to a simpler

format like the gray-scale image.

3.2 Method I: Non-Linear Quadratic Filtering Method

Image enhancement seeks to improve the visual quality of images. However, an inherent difficulty is to define a mathematical criterion for visual quality. As a result, many algorithms remain to a large extent empirical and a final assessment can only be performed by the human observer. In this section, image contrast enhancement based on the unsharp masking method is considered (Gonzalez and Woods, 2002). The common techniques of contrast enhancement generally fall into one of two categories (Jain, 1989). Techniques belonging to the first category, such as histogram equalization, modify the brightness of each pixel from the statistical information of an image. The techniques in the other category enhance the contrast of images by first separating the high and/or low frequency components of images, manipulating them separately and then recombining them together. The unsharp masking or high-frequency emphasis method belongs to this second category. Unsharp masking for edge enhancement, commonly used in the printing industry, is equivalent to adding back the scaled gradient magnitude to the original signal. Mathematically, unsharp masking can be formulated as

$$x_e[m,n] = x[m,n] + \gamma \nabla x[m,n] \tag{3.1}$$

where x_e[.] denotes the enhanced image; x[.] represents the original input image ('m' and 'n' denote pixel location on a 2-D grid); ∇x[.] refers to the gradient of x[.] and γ the enhancement factor. A discreet laplacian operator is commonly used as a gradient function (Gonzalez and Woods, 2002, Jain, 1989). Mitra and Strobel proposed a modification that is based on replacing the gradient operator x[.] in Eq. (3.1) by an enhancement fraction Δx[m,n] (Mitra and Strobel, 1995). This fraction is derived from quadratic filters where

$$\Delta x[m,n] = f(\frac{y[m,n]}{max(|y[m,n]|)}) \times x[m,n] \tag{3.2}$$

with y[m,n] denoting the output of the quadratic filter. An example of the quadratic filter is the type 1B quadratic filter defined by Mitra and Yu (1991) as

$$y[m,n] = 2x^2[m,n] - x[m-1,n+1]x[m+1,n-1] - x[m-1,n-1]x[m+1,n+1] \quad (3.3)$$

As the filter response y[m,n] in Eqs. (3.2) and (3.3) can take both positive and negative values, the function max(‖y[m,n]‖) selects the maximum absolute value. The (normalized) quotient y[m,n]/max(‖y[m,n]‖) is referred to as the *enhancement map*, and the overall product results in an enhancement fraction whose magnitude is bounded by the maximum intensity level of the display device. A new modified algorithm proposed by Mitra and Strobel has been applied here which can be summarized in a block diagram as shown in Figure 3.1.

In the present study, a quadratic filter derived by Thurnhofer (1994) was considered in the modified algorithm and implemented as shown in Figure 3.1:

$$\begin{aligned} y[m,n] = 3x^2[m,n] &- 0.5 \times (x[m+1,n+1]x[m-1,n-1]) \\ &- 0.5 \times (x[m+1,n-1]x[m-1,n+1]) \\ &- x[m+1,n]x[m-1,n] - x[m,n+1]x[m,n-1]) \end{aligned} \quad (3.4)$$

This algorithm was applied in a local window within the image for more prominent results. Three size of windows used were 3 x 3, 5 x 5 and 7 x 7. The enhancement factor γ was also varied from 0.25 to 1.5 for each window size. A huge database of images with all the parametric combinations yielded 180 images by applying the algorithm on five sample images exhibiting a variety of crack features and patterns and five sample images with different background characteristics. Figure 3.2 shows one representative original crack color image and the contrast enhanced images using the proposed method. The enhanced images shown are obtained by running a 3 x 3, 5 x 5 and 7 x 7 window and an enhancement factor γ of 0.5. Observations have shown that a 5 x 5 filter size with an enhancement factor γ of 0.5 gave the best result. Further validation will be possible only when the crack segmentation and detection algorithm is developed to process this enhanced image. A high percent of cracks detected from images that are enhanced using this method

will serve as a proof for accepting it to improve image pre-processing. The next phase being undertaken is of developing a crack detection algorithm as a sequential step in this research study. Figure 3.3 shows background specific color image and its enhanced images using the same filter size and enhancement factor γ as in the crack feature case in Figure 3.3.

3.3 Method II: Magnification Of Dark Image Features

Crack features are deeper than the pipe surface. This causes the deep regions to produce color pixels with lower intensity value compared to the rest of the image. A new approach to enhancement is proposed in this section by increasing the contrast of the dark pixels from the estimated "background" image. The output is a gray scale enhanced image. The background image is the image of the pipe without any small features (e.g. cracks). Given the input color image, a median filter is applied to each of the R, G, and B component images. The window size for the median filter is 15 x 15. This was determined based on the width of the crack lines. The window size experimentally selected is large enough to erode the small features and at the same time small enough to be computationally fast. This method picks the dark pixels by comparing the intensity of each pixel in the original color image with that of the background image. The algorithm can be summarized below: Let M be the original color image of the pipe and let 'BackG' be the estimated background image, computed as:

$$BackG = MedianFilterRGB(M) \tag{3.5}$$

where MedianFilterRGB(M) is a median filter applied to each of the R, G, and B bands of the color image 'M'. Let GrayM[m,n] be the gray scale value of the color pixel M[m,n] and GrayBackG[m,n] the gray scale value of color pixel BackG[m,n].The 'enhancement' is described by the following decision function:

if (GrayM[m,n] $<$ GrayBackG[m,n])
Enhanced[m,n] = GrayM[m.n] - diff-factor * $\|$M[m,n]-BackG[m.n]$\|$

else Enhanced[m,n] = GrayM[m,n]
where, Enhanced[m,n] is the gray scale value of the enhanced pixel,
diff-factor is the parameter controlling the degree of contrast,
and the operator ‖.‖ is the Euclidean norm.

The term ‖M[m,n] - BackG[m.n]‖ is the equivalent to the Euclidean distance between the two RGB color vectors M[m,n] and BackG[m,n]. The parameter diff-factor controls the contrast of the dark pixels from the background. Its value should be set large enough to provide sufficient contrast but not too large so as to darken the other gray regions. Figures 3.4 and 3.5 show a typical crack and background image enhanced using this method. It must be noted that these are representative images from the database generated by running this algorithm on 10 different images similar to the quadratic filter method.

3.4 Summary

A modified version of unsharp masking was implemented that is flexible enough to accommodate different quadratic filter types in the feed-forward loop of the algorithm presented in Figure 3.1. By computing the enhancement map and final thresholding, the crack features are enhanced and background is suppressed according to their original characteristics. This is accomplished in the first proposed method using non-linear quadratic filtering. The second method which is based on magnifying the dark components of the image which are generally cracks in pipeline images also provides encouraging results in this preliminary evaluation phase. The validity and flexibility of both the techniques will be tested only in the second phase when a segmentation or crack detection algorithm is developed and applied to these enhanced images. Finally, the images after being enhanced by the two proposed schemes are ready to be segmented and classified for which the active contour algorithm called SNAKES was considered but abandoned as it did not provide promising results. Another approach based on *mathematical morphology* and *curvature evaluation* was implemented on pipeline images enhanced by the above two methods resulting in a phenomenal improvement in the ability to detect cracks under varying conditions. In order to validate the efficiency of both

the proposed contrast enhancement methods, it is necessary to develop a crack detection filter and apply an adaptive algorithm to enhanced images. The crack map that will be generated by the crack filter will be compared against the original image and the percentage of cracks detected without loss of information from images filtered using the methods above will establish the standards for adoption of either technique in further study. The next chapter on segmentation deals with crack map generation algorithms and crack filters that need to be developed to cater to the characteristic images pertaining to underground pipelines.

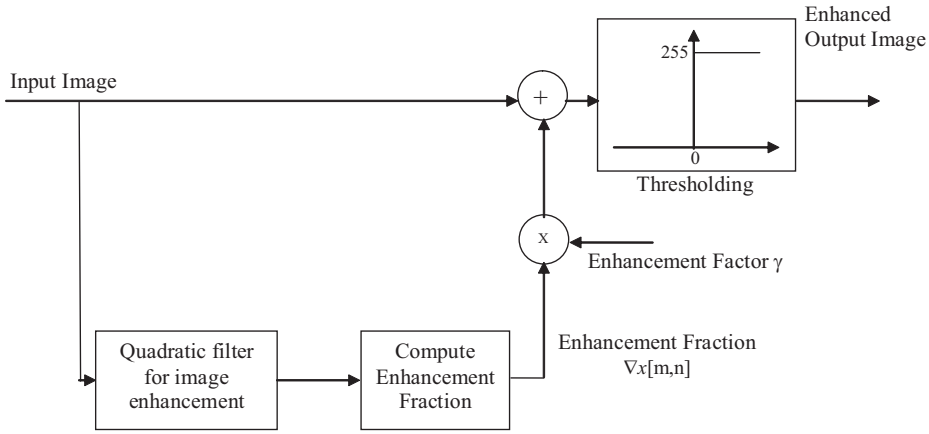

Figure 3.1. Block diagram of algorithm showing Mitra and Strobel's modified technique

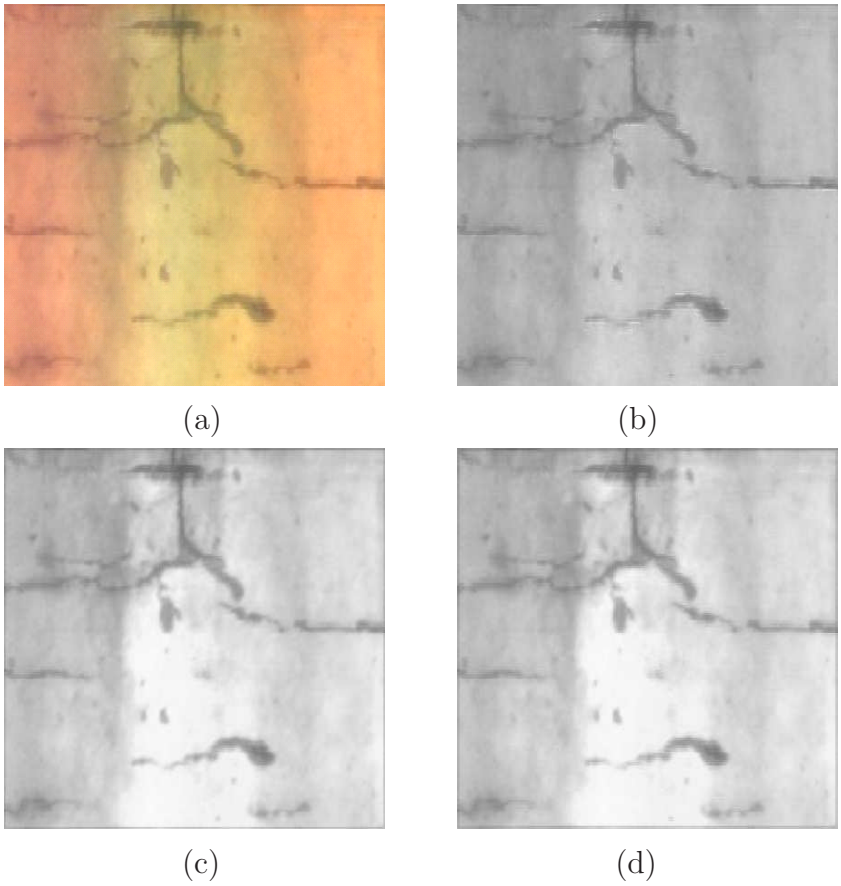

(a) (b)

(c) (d)

Figure 3.2. Non-linear quadratic filtering method (a) Original crack image, (b) 3 x 3 window, (c) 5 x 5 window and (d) 7 x 7 window enhanced image

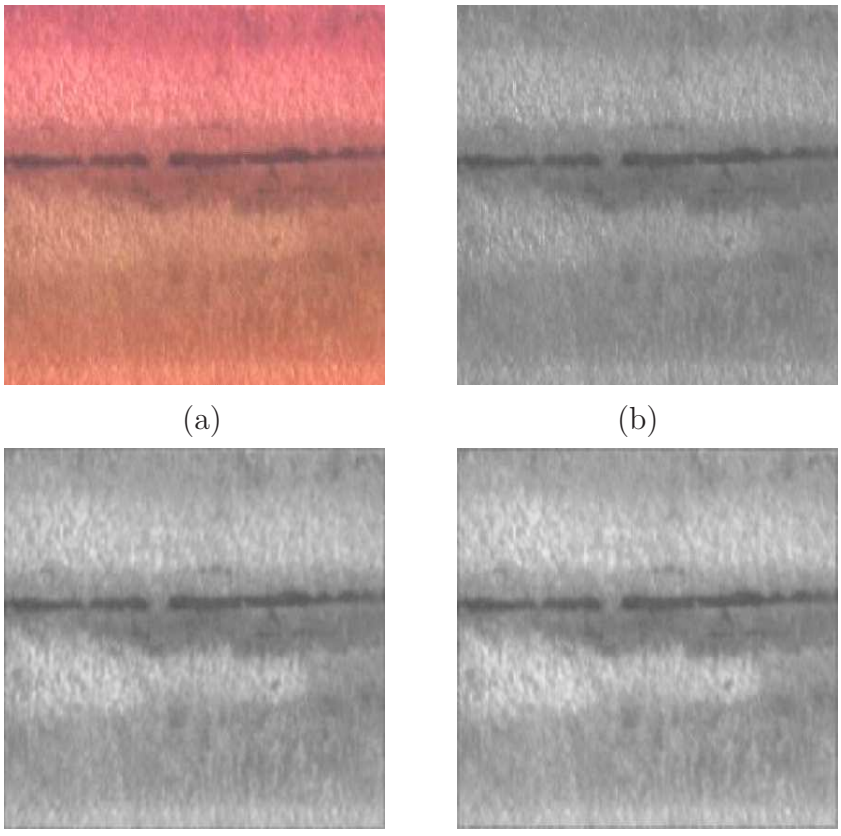

Figure 3.3. Non-linear quadratic filtering method (a) Original background image, (b) 3 x 3 window, (c) 5 x 5 window and (d) 7 x 7 window enhanced image

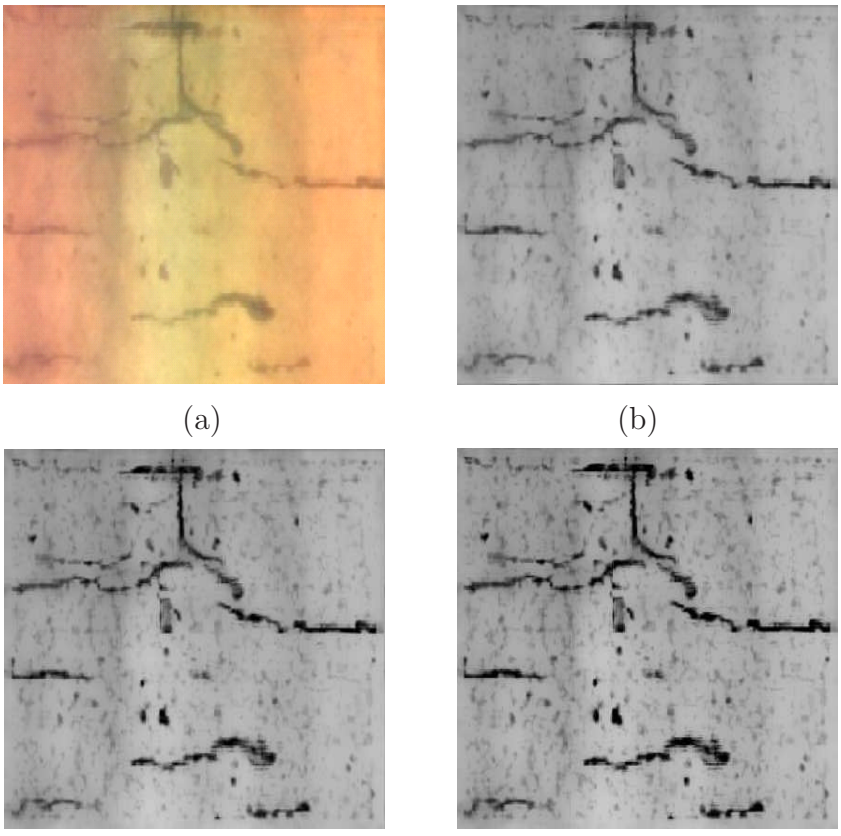

Figure 3.4. Magnification of Dark Features Method (a) Grayscale crack image, (b) diff-factor = 2, (c) diff-factor = 3 and (d) diff-factor = 4

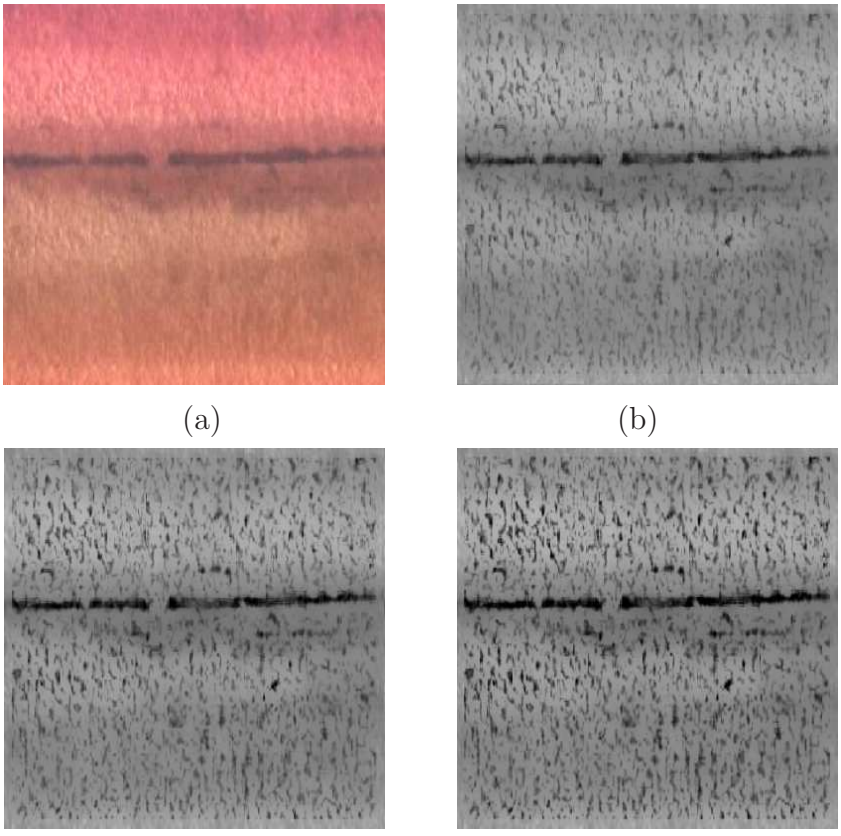

Figure 3.5. Magnification of Dark Features Method (a) Grayscale background image, (b) diff-factor = 2, (c) diff-factor = 3 and (d) diff-factor = 4

Chapter 4

CCTV Pipe Crack Segmentation

4.1 Introduction

Analysis of images has shown that there are two important characteristics that complicate the segmentation of pipe images: firstly, the presence of a complicated background pattern due to earlier runoff, patches of repair work, corroded areas, debris, non-uniformities in illumination, and flaws in the image acquisition process; secondly because the the main objects of interest - cracks,patches,etc. are all dark features that cannot be easily distinguished by implementing the intensity criteria alone. This chapter will put forth the basic idea about a simple, robust and efficient image segmentation algorithm for the automated analysis of scanned underground pipe images. As mentioned in the previous chapter, the famous SNAKE algorithm introduced in a seminal paper by Kass et al. (1987) based on active contour models did not provide promising results and was marred with modeling problems (Kass et al., 1988). The present study considered the implementation of active contour models by taking advantage of their slithering action. Unfortunately, the contour nodes failed to converge on the crack feature and alienate it from the rest of the image. Thus a new approach based on *mathematical morphology* and *curvature evaluation* was investigated and found to be successful in detecting crack-like structures in complicated pipe images. This chapter presents the theory, modeling and implementation of this new methodology in detail.

4.2 Edge Detection

Edge detection is a problem of fundamental importance in image analysis and computer vision. An edge is a jump in intensity values in the image domain. In typical images, edges characterize object boundaries and are therefore useful for segmentation, registration, and identification of objects in a scene (Heath et al., 1997). Edge detection algorithms reduce the complexity of the image allowing for more expensive (computationally) algorithms like object recognition (Liu and Srinath, 1990) object matching (Ratha et al., 1996), object registration (Brown, 1992), and surface construction from stereo images (Hoff and Ahuja, 1989, Lengagne et al., 1996) to run faster and be used more efficiently.

Crack-like patterns in underground pipeline images obtained from a Sewer Scanner Evaluation Technology (SSET) sensor seem to have a specific Gaussian profile. Detection of cracks in these images is of huge importance to the municipal authorities from several standpoints. They can help in determining residual structural strength left in the pipe based on structural analysis taking into account prevailing loading conditions. Crack information can be used to select the appropriate rehabilitation method to fix the cracked pipe and prevent any catastrophic failure. Segmented crack features can also be used as a first step before registering successive images from various depths in the thickness of pipe for the same region (Brown, 1992, Canny, 1986). Usual edge detectors and thresholding techniques based on the difference between pixel values are inefficient when applied to the underground pipe images (Sinha, 2000).

In analyzing buried pipe scanned image, it is essential to consider complications due to inherent noise in the scanning process, varied crack directions and a wide range of pipe background patterns. It is known that cracks with bright features (darkest in the image) and a tree-like geometry are very common to every pipe image that arrives as input to this stage of crack detection and classification. Hence, it is necessary to have a robust algorithm suitable for detection of cracks from images of different types that can provide reliable information useful to register images from the same region of pipe.

In this chapter, a three step method to identify and extract crack-like structure from pipe images is presented. This method combines morphological filters and

cross-curvature evaluation to segment cracks from images that have been acquired in a noisy environment. The above combination was studied and presented by Zana and Klein (2001) and modified by Fang et al. (2003) with respect to detection and reconstruction of blood vessels in retinal fundus images (Zana and Klein, 2001). The principles of these two approaches have been studied and implemented in an algorithm that can detect cracks over a wide variety of pipe images, thus extending the applicability of this combination to a unique application in the buried infrastructure industry.

Crack-like patterns are bright features defined by morphological properties: linearity, connectivity, width and by a specific Gaussian-like profile whose curvature varies smoothly along the crest line. This study employs mathematical morphology to highlight cracks and then uses cross-curvature evaluation to determine features whose curvature is linearly coherent. The proposed algorithm has been tested on images with varying background colors, changing crack patterns and background noise in order to measure its robustness and accuracy. It was found that the algorithm was sensitive to contrast in the image.

As mentioned in the previous chapter, the selection of one of the contrast enhancement approaches will depend upon the consistency and efficiency with which this crack detection algorithm detects cracks from enhanced images. Preliminary evaluation revealed that the crack detection algorithm worked very well on images that were contrast enhanced by the *Magnification of Dark Features* method. Hence this method was finally chosen over the *Non-Linear Quadratic Filtering* method as a pre-preprocessing step before the application of a crack detection filter.

4.3 Mathematical Morphology Based Operators

The techniques of mathematical morphology are based on set-theoretic concepts, on nonlinear superposition of signal, and on a class of nonlinear systems that are called morphological systems. This section is a brief review of fundamental definitions of morphological operators considered in this study. Advanced information on mathematical morphology can be found in Serra (1982) and Maragos (1990) (Serra, 1982, Maragos and Schafer, 1990).

For reference, a two-dimensional (2-D) grayscale image will be defined as having

a range of $[I_{min},\ I_{max}]$ as a functional F: $R^2 \rightarrow [I_{min},\ I_{max}]$, and a 2-D structural element as a functional B: $R^2 \rightarrow \boldsymbol{B}$ where $\boldsymbol{B}$ is the set of the neighborhoods of the origin. Structuring elements invariant by translation are considered that are identified with a subset of R^2 and will be referred to as linear structuring element when this subset is a line segment. Basic morphological operators with respect to the structuring element B, a scaling factor e, image F and a processing point P_0 $\in R^2$ can be defined as:

$$erosion: \quad \epsilon_B^e(F)(P_0) = MIN_{P \in P_0 + e \cdot B(P_0)}(F(P)); \tag{4.1}$$

$$dilation: \quad \delta_B^e(F)(P_0) = MAX_{P \in P_0 + e \cdot B(P_0)}(F(P)); \tag{4.2}$$

$$opening: \quad \gamma_B^e(F) = \delta_B^e(\epsilon_B^e(F)); \tag{4.3}$$

$$closing: \quad \phi_B^e(F) = \epsilon_B^e(\delta_B^e(F)); \tag{4.4}$$

$$top - hat: \quad TH_B^e(F) = F - \gamma_B^e(F). \tag{4.5}$$

Morphological reconstruction is most of the time presented using the notion of geodesic distance and hence the term, geodesic operators (Vincent, 1987). They are usually defined with reference to a geodesic distance and type of connectivity. In other words, they depend on a 'marker' image F_m (connectivity map) and a geodesic distance d.

The geodesic reconstruction (or opening) is defined by

$$\gamma_{F_m}^{rec}(F) = sup(\triangle_{F_m}^d(F)), d \in I \tag{4.6}$$

where $(.)$ is the geodesic dilation. The geodesic closing is defined by

$$\phi_{F_m}^{rec}(F) = I_{max} - \gamma_{(I_{max} - F_m)}^{rec}(I_{max} - F). \tag{4.7}$$

4.4 Analysis of Crack-Like Pattern

4.4.1 Crack Detection Approaches and Previous work

Most of the literature concerning the detection of defects (like cracks) in civil structures deals with the analysis of pavement and concrete/steel distress that are not directly applicable to buried pipe inspection (Cheng and Miyogim, 1998). In analyzing buried pipe scanned image data, it is imperative to consider complications due to inherent noise in the scanning process, irregularly shaped cracks, as well as the wide range of pipe background patterns. In the past two decades, many approaches have been developed to deal with the detection of linear features on retinal, satellite and most recently, buried pipe images (Merlet and Zerubia, 1996, Hellwich et al., 1992, Fieguth and Sinha, 1999). Most of them combine a local criterion evaluating the radiometry on some small neighborhood surrounding a target pixel to discriminate lines from background and a global criterion introducing some large scale *a priori* knowledge about the structures to be detected.

The techniques used for pavement distress detection in scanned images are based on conventional edge or line detectors with respect to local criterion (Mohajeri and Manning, 1991, Cheng and Miyogim, 1998). These methods evaluate differences of averages, thus indicating noisy results and inconsistent false-alarm rates. This necessitates the introduction of global constraints owing to insufficiency of local criterion in line and edge detection. As cracks in buried scanned pipe images resemble undulating curves with a generally constant width, Hough transform based approaches have also been tested for the detection of parametric curves, such as straight lines or circles (Skingley and Rye, 1987). Tracking methods and energy minimization methods, such as snakes, have been used to track roads in satellite images and heart walls in live feeds from medical ultrasound angiographies (Geman and Jedynak, 1996, Kass et al., 1988). These tracking methods find a minimum cost path in a graph by using some heuristics like an entropy criterion. Statistical methods such as those that employ Bayesian framework complemented by cross-correlation detectors have been used by Feiguth and Sinha (1999) to detect cracks to a reasonable accuracy level (Fieguth and Sinha, 1999). However, their results were noisy with high false-alarm rates when the image had dark background with multiple cracks in a tree-like geometry. Morphology based filtering

coupled with cross-curvature evaluation has not been used to detect cracks and remains an unexplored frontier till date. It will be shown that the application of some carefully selected morphological filters leads to a simplified image whose cross-curvature evaluation is easy.

4.4.2 Modeling Crack Like Pattern

The appearance of cracks in digital imagery depends on the spatial sensitivity as well as resolution of the sensor, which is the *Sewer Scanner Evaluation Technology (SSET)* camera in case of buried pipelines (Wirahadikusumah et al., 2001). In images acquired from the SSET camera, image pre-processing is necessary to improve understanding of the characteristics of sewer pipe. The presence of various features in an acquired image (see Fig. 4.1) poses considerable challenge in detecting the desired structural failure patterns such as cracks, fissures, etc. As seen in Figure 4.1, various features exist that make it complex for a recognition system to classify the desired patterns. Hence, this necessitates the application of low-level methods of image pre-processing to contrast enhance the acquired image for specific application.

"Specific" in this research applies to enhancing contrast between the background of pipe and desired crack features. It is assumed that cracks have the darkest (brightest) feature in the image and enhance the contrast of the dark pixels from the "background" image. The background image is the image of the pipe without any small features (e.g. cracks). As mentioned earlier, the literature concerning crack segmentation in the pavements and most recently the buried pipeline area does not model cracks from an image modeling perspective (Koutsopoulos et al., 1993). This study takes advantage of Zana and Klein's (2001) modeling approach and restricts the scope to contrast-enhanced grey-scale images only (Zana and Klein, 2001). It is assumed that the tree-like geometry of cracks is the only element of the buried pipe scanned image that is locally uniform and can be described by the following properties:

- intensity distribution of a cross-section looks like a specific gaussian curve (see Fig. 4.2);
- they branch like a tree;

- more or less have a constant width.

The above listed properties can be further classified into those related to morphological descriptions and those related to the calculation of curvature parameters based on linearity, connectivity, crack width, and gaussian profile.

4.5 Detection of Crack Features

4.5.1 Spectrum of SSET imagery

The SSET technology uses a high-resolution digital optical scanner to obtain a continuous, directionally-oriented, 360-degree scanned visual image so that the interior surface of the pipe is recorded.The second-generation probe also uses a CCD (Charged Coupled Device) to integrate the forward view in data capture. A fish-eye lens is used to capture the hemispherical, 360-degree side scan view. An annular segment of the image that crosses the preset scanning region is sequentially scanned in, digitally cut, flattened and concatenated to provide the unfolded picture of the entire length of a pipe. As any other image acquisition system, the SSET is prone to background noise and poor illumination during scanning. All these factors contribute to noise in pipe images.The presence of debris, vegetation and other foreign material on the surface of the pipe further complicates the detection of defects on the pipe surface from images. Figure 4.3 shows representative images from the database of unfolded images with features of interest (cracks) in presence of complicated features (background, color,vegetation, etc).

4.5.2 Geometry based recognition of crack features

In this section, the application of morphology based filters with linear structuring elements that take advantage of the linear property of crack features will be discussed. A morphological opening with a linear structuring element will remove a crack or part of it when the element cannot be included in the geometry of the crack. This is true when the structuring element is orthogonally oriented with respect to the crack and is hence longer than the crack width. However, the crack will not be affected when the structural element and the crack have parallel di-

rections. A sum of top-hats along possible directions will highlight the cracks irrespective of their inclination in the image if openings along a class of linear structuring elements is performed. But this sum of top-hats will recover a lot of noise because the openings require that the structural elements be large enough to remove unwanted features in the image that do not fall in the category of cracks. Hence, reconstruction operations are carried out using the connectivity property of the cracks before taking the sum of top-hats (Fig 4.4).

A geodesic reconstruction of the opened images into the original image F_0 will remove noise while preserving most of the cracks. Mathematically this operation can be represented as:

$$F_{op} = \gamma_{F_0}^{rec}(Max_{i=1\cdots 18}\{\gamma_{L_i}\ (F_0)\}). \tag{4.8}$$

Each of the 18 linear (width = 1 pixel) structuring elements L_i is 12 pixel wide and is oriented at every 10° from 0 to 180. The element size is based upon the range of crack widths that are of interest to the pipeline community. A more detailed discussion on this will follow in Section 4.7.3. The resulting reconstructed image F_{op} will not have any isolated round or bright zone whose diameter is less than the size of structuring element (12 pixels). This step called *linear opening by reconstruction* of size 12 removes white noise and other features that do not fit into the geometric definition of cracks. The sum of tophats on the filtered image F_{op} will enhance all cracks irrespective of their orientations including minor cracks in a low contrast image. However, the F_{op} image contains a lot of details like 1) background linear features that can be confused with cracks but do not meet all the requirements and 2) non-linear patterns like bright or dark thin irregular zones that are enhanced by the tophats operation.

4.5.3 Final segmentation based on curvature characteristics

At this stage, it is assumed that any nonzero point in the image has a potential dominant direction thus qualifying as part of some crack pattern in terms of its geometry. It is worthwhile to introduce the term *curvature* at this point as the curvature in the cross direction which is defined for every pixel under the above

assumption. Its evaluation using the Laplacian has been analytically discussed and presented in (Zana and Klein, 2001). Non-linearly correlated patterns have signals that appear as thin and irregular bright elements indicating that the curvature gets positive values on a width smaller than in the case of the cracks (see Fig. 4.5). In the case of details like 1)(Section 4.5.2), the curvature will have alternating positive and negative values in various directions owing to a low and disorganized signal. This can sometimes lead to represent a curvature trend that fits the crack description. This study does not attempt to address the above issue leading to false detection in few cases which are rare and have little bearing on the overall performance.

It has been proven that the sign of Laplacian applied to the result image of top-hats can be used as a good approximation of the sign of curvature (Zana and Klein, 2001). Further, the Laplacian of F_{op} is computed to obtain a good estimation of the curvature (see Fig. 4.5(a)). The final step in the detection process is the application of alternating filters that remove enhanced noise patterns corresponding to 1) and 2) as discussed in Section 4.5.2 thereby producing the final binary crack map. The alternating filtering operation consists of performing a linear opening by reconstruction of size 12, followed by a linear closing by reconstruction of size 12, and finally a linear opening of size 24. These sizes were chosen based on statistics generated on a database of around 225 pipe images in the database acquired from various cities in North America (rationale behind the selection of these values is discussed in section 4.7.3).

4.6 Flow Chart of The Proposed Algorithm

Pipe crack segmentation is a multi-stage and involved process as evident from the flowchart in Figure 4.6. There are various levels of segmentation that can be performed on an SSET image to detect joints, laterals, voids and other features of interest. However, this study only concerns those aspects of the detection process that deal with segmenting cracks from complicated background features and includes contrast enhancement for improved detection probabilities. The algorithm is summarized as follows:

Step I: Improve the contrast of RGB pipe image by enhancing the dark or bright pixels from the "background" image.

Step II: Perform crack enhancement described by the following equations in mathematical morphology terms:

$$F_{op} := \gamma^{rec}_{F_0}(Max_{i=1\cdots 18}\{\gamma_{L_i}(F_0)\})$$

$$F_{sum-th} := \sum_{i=0}^{18} (F_{op} - \gamma_{L_i}(F_0)).$$

The sum of top hats reduces small bright noise and improves the contrast of all linear regions in the image. At this stage, a manual threshold on F_{sum-th} could result in cracks being segmented out from the image, but in most cases the image would be noisy thus requiring further treatment through curvature computation

$$F_{lap} := \text{Laplacian } (\ Gaussian^{width=12px}_{\sigma=2}\ (F_{sum-th})\ ).$$

Step III: The third step in the detection process consists of applying a set of filters with linear structuring elements to remove the enhanced noise patterns. The set of alternating filters can be described by

$$F_1 := \gamma^{rec}_{F_{lap}}(Max_{i=1\cdots 18}\{\gamma_{L_i}(F_{lap})\})$$

$$F_2 := \phi^{rec}_{F_1}(Min_{i=1\cdots 18}\{\phi_{L_i}(F_1)\})$$

$$F_{final} := (Max_{i=1\cdots 18}\{\gamma^2_{L_i}(F_2)\} \geq 1).$$

The final opening by a larger structuring element (scaling factor of 2) removes smaller and tortuous segments of cracks that are shorter than the structure element. Cracks are readily identified as pixels whose values are larger than a small positive value such as 1.

4.7 Generalization to Pipe Images

The algorithm has been adapted to other types of pipe images: background variation and color variation based upon the geographical location and condition of pipe.

4.7.1 Background and Color Variation Images

Background variations are a result of changing illumination and maintenance conditions for a given pipeline whereas color variations depend upon the material used for the pipeline, viz., clay or concrete. Development of vegetation or algae can also add to the background color patterns (see Fig 4.3(d)). In such images, cracks are less contrasted than in images where the background is generally linear. Careful observation reveals that the crack patterns in pipe scan images show a certain extent of damage in that section of pipe. Usually, the probability that there is no crack in a section of pipe is very high as compared to the presence of crack and so an effective detection methodology must be able to filter out the images with no features of interest. Thus, crack recognition and segmentation is of utmost interest from an image registration point of view for future applications in 3-D crack visualization and feature selection for accurate pipe condition assessment.

4.7.2 Performance Evaluation

It is necessary to evaluate the performance of the proposed algorithm on images with varying crack pattern, color and background as the case may be in the field.

The evaluation is carried out by comparing automatically detected cracks with manually plotted cracks (ground truth). A set of connected pixels belonging to the cracks is manually extracted using an in-house GUI interface to replicate the process carried out by a pipe inspector in the field. The "buffer-method" for performance evaluation by matching the automatically extracted crack pixels to the reference map or ground truth image has been employed in this study (Wiedemann, 1987). This method is a simple matching procedure in which a buffer of constant predefined width is constructed around the crack data in two steps. In the first step, a buffer of constant width is constructed around the reference crack data by using a morphological dilation operation of size 5x5 (see Fig 4.7). The parts of the extracted data within the buffer are considered as matched and is denoted as *true positive* whereas the unmatched extracted data is denoted as *false positive*. In the second step, the matching is performed the other way round by constructing a buffer of the same size around the extracted crack data (see Fig 4.7) and the part of reference data lying in the buffer is considered as matched. The unmatched

reference data is denoted as *false negative*. Probability of detection is defined as the ratio of detected crack pixels to true crack pixels and probability of false-alarm is the ratio of false-alarm pixels to non-crack pixels in the image. Figure 4.7 illustrates the matching procedure to quantitatively determine the probability of detection P_d and probability of false-alarm P_{fa} (false +ve and -ve).

4.7.3 Parameter Selection

The size of structuring element and degree of rotation are two prime parameters that govern the performance of this algorithm. It is imperative to discuss the detection probabilities as a function of these two parameters. Generalization to images of all types can only be effected if the algorithm can perform very well under varying image conditions as discussed in Section 4.1. Hence, an optimum parameter combination is required that can consistently provide high detection probabilities under all conditions based on a set criteria for P_d and P_{fa} as suggested by the concerned authorities. In order to quantitatively assess the effect of structuring element size and degree of rotation on the detection rate, the probability of detection (P_d) and the probability of false-alarm (P_{fa}) for different structuring element sizes and degree of rotations are plotted. Experiments are conducted on three different classes of pipe images (crack patterns, background and color) by varying the size of structuring element (S=10, 12 and 15 pixels) and degree of rotations (D = every 5°, 10° and 15°) to determine an optimum combination of these two parameters. Given a low false +ve (7%) and false -ve (2%), the corresponding size of structural element and degree of rotation that gives the maximum P_d is selected. This is repeated for all the three classes of image and the candidate combination that satisfies the cut-off criteria throughout is finally selected as the generalized optimum parameter combination. Figure 4.8 shows the probabilities plotted against various parameter combinations for images with varying crack patterns, background and color. S12-D10 (structuring element of size 12 pixels rotated at every 10°) clearly satisfies the cut-off criteria and is selected as the optimum combination that consistently provides good detection in all types of pipe images.

4.8 Results

This algorithm has been tested on a database of around 225 images of all types taken from various cities like Los Angeles, Albuquerque, Toronto and St. Louis-Missouri in North America. All the images were acquired and unwrapped using the Sewer Scanning and Evaluation Technology (SSET) camera and its propriety software available with the system. Robustness was evaluated on noisy images with respect to changing crack patterns (Fig. 4.9), background features (Fig. 4.10) and color (Fig 4.11). Images that did not have any cracks present produced a perfect image without any detected cracks every single time the algorithm ran with the generalized optimal parameter combination.

There has been false detection in the following cases:

- extension of crack into a small rounded zone (patch) maintaining the same direction and geometry (see Fig 4.9);
- cracks are too close to each other
- bright (or dark) linear structures mistaken for cracks that appear as isolated objects in the image.
- uniform noise that would modify the connectivity of crack structure thereby disturbing the reconstruction filter and misleading curvature evaluation.

Parts of the crack were not detected mostly in very low contrast (Fig. 4.11) and sometimes in images that had shadow due to illumination issues in the pipe. However, the detection in every case was in accordance with the discussion given in Section 4.5. This algorithm works on detecting patterns with Gaussian profile bounded at the inflection point. The gaussian filter applied before the computation of the Laplacian modifies the surrounding texture leading to a shift in location of the inflection point. As a consequence, experiments show that small cracks appear wider than their real size (see Fig. 4.9). However, this is not a matter of major concern as detection is based on matching the extraction with respect to a buffer width as discussed in Section 4.7.2.

4.9 Comparison with Conventional Methods: A Qualitative and Quantitative Discussion

In order to study the performance of the proposed algorithmwith respect to other conventional filters used in the buried pipeline infrastructure industry, several detection filters are applied to an original image including the proposed algorithm. Canny's edge detector and Otsu's thresholding technique have been used to extract crack features (Canny, 1986, Otsu, 1979). Quality measures for crack extraction are discussed with the intention of comparing results from different crack detection techniques in addition to an absolute evaluation of extraction and matching results as discussed in Section 4.7.2. Quality measures are defined as follows:

- $completeness = \frac{length\ of\ matched\ reference}{length\ of\ reference}$

$$\approx \frac{number\ of\ matched\ crack\ pixels\ of\ reference}{length\ of\ crack\ pixels\ of\ reference}$$

  completeness is the percentage of reference data which is explained by the extracted data, i.e., the percentage of true cracks that could be extracted by the filters. $completeness \in [0;1]$ and its optimum value is 1.

- $correctness = \frac{length\ of\ matched\ extraction}{length\ of\ extraction}$

$$\approx \frac{no.\ of\ matched\ crack\ pixels\ of\ extraction}{length\ of\ crack\ pixels\ of\ extraction}$$

  correctness represents the percentage of correctly extracted crack data, i.e., the percentage of extraction that matches the reference crack. $correctness \in [0;1]$ and its optimum value is 1.

- $redundancy = \frac{length\ of\ matched\ extr. - length\ of\ matched\ ref.}{length\ of\ matched\ extraction}$

$$\approx \frac{\#\ matched\ pixels\ of\ extr. - \#matched\ pixels\ of\ ref.}{no.\ of\ pixels\ of\ extraction}$$

The *redundancy* represents the percentage to which the correct (matched) extraction is redundant, i.e. it overlaps itself; *redundancy* $\in$]-∞;1] and its optimum value is 0.

- $quality = \frac{length\ of\ matched\ extraction}{length\ of\ extraction + length\ of\ unmatched\ ref.}$

$$\approx \frac{compl \cdot corr}{compl - compl \cdot corr + corr}$$

The *quality* is a more general measure of the final result combining completeness and correctness into a single measure. The optimum value is 1.

The proposed approach, Canny's edge detection method, and Otsu's thresholding technique have been applied to a sample image from all three classes as shown in Figures 4.12, 4.13 and 4.14. The results of quality measures are summarized in Tables I, II and III.

The Canny edge detector produces parallel edges [Fig. 4.12, 4.13 and 4.14(c)] suggesting that the largest cracks are easily picked up by the detector at the cost of smaller cracks that appear less contrasted. Otsu's thresholding technique selects a threshold based on integration (a global property) of the gray-level histogram. Hence, in areas where the cracks and background path run into each other or low contrast dark images, false detection is inevitable as seen in figures 4.12, and 4.14(b). The proposed method produces a binary image that achieves a very small proportion of false detection. It generally produces linear structures that are clean but not always connected to each other as would be required in a complicated crack geometry. One of the limitations of this morphology based approach is that it is unable to effectively highlight bifurcation and intersection points in regions where the crack geometry is larger than the structuring element (see the two arrows in Fig. 4.12). In order to ensure the complete detection of cracks along with its bifurcations, if any, another morphological reconstruction process can be carried out based on local dynamic region growing tailored towards pipe images. This is an interesting research problem in itself and can be studied in the future.

4.10 Summary

In this chapter, an efficient algorithm for detecting crack patterns in pipeline images was adapted and implemented . The proposed method can be divided into three steps, viz., contrast enhancement, morphological treatment and curvature evaluation in the cross direction and finally the alternating filters that produce the final segmented binary crack map. The shape properties, connectivity and curvature were effectively used to select cracks in an image consisting of complex background and color features. The proposed evaluation scheme adequately estimates the performance of the algorithm in an absolute way and relative to conventional detection techniques. The robustness and weaknesses of the algorithm have been discussed in order to facilitate its use in a larger scheme for condition assessment of buried pipelines. Based upon the application and urgency, some of the quality measures such as *completeness* may outweigh others, for e.g. in an automated setup. The scope of this part of the research study was focused on improving the segmentation methodology in pipeline images. Further development of this algorithm in terms of recovering the crack structure with bifurcations in complex situations needs to be actively pursued in preparation towards an automated condition assessment tool, although, this clearly is not within the scope of this study.

Table 4.1. Quality measures for different classes of images using proposed approach

Class	Cracks	Background	Color
Completeness	0.95	0.88	0.90
Correctness	0.98	0.94	0.91
Quality	0.93	0.83	0.83
Redundancy	0.00	-0.91	0.00

Table 4.2. Quality measures for different classes of images using Otsu's thresholding technique

Class	Cracks	Background	Color
Completeness	0.98	0.61	0.62
Correctness	0.37	0.45	0.08
Quality	0.37	0.35	0.08
Redundancy	0.22	0.23	0.24

Table 4.3. Quality measures for different classes of images using Canny's edge detector

Class	Cracks	Background	Color
Completeness	0.92	0.61	0.62
Correctness	0.20	0.44	0.07
Quality	0.20	0.34	0.07
Redundancy	0.15	0.17	0.14

(a) (b) (c)

Figure 4.1. Varying background textures. (a) Image with granular background and shadow. (b) Patchy background with different colors. (c) Cracks with other linear features in the background.

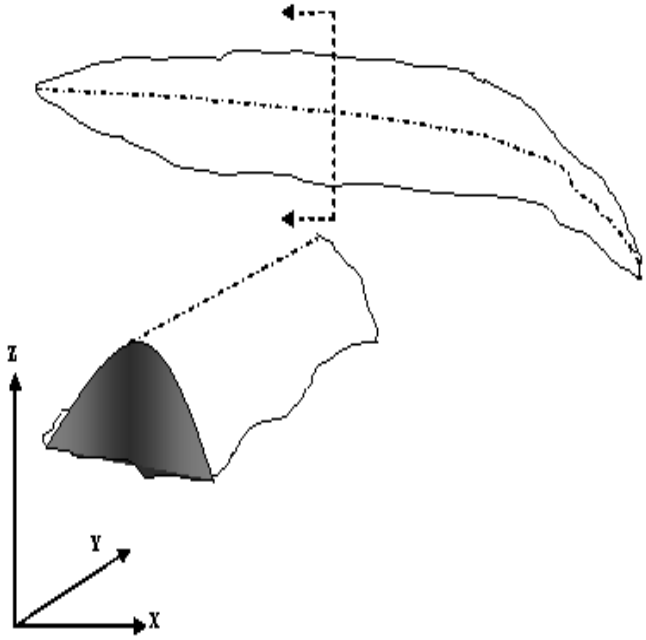

Figure 4.2. Gaussian profile based crack model.

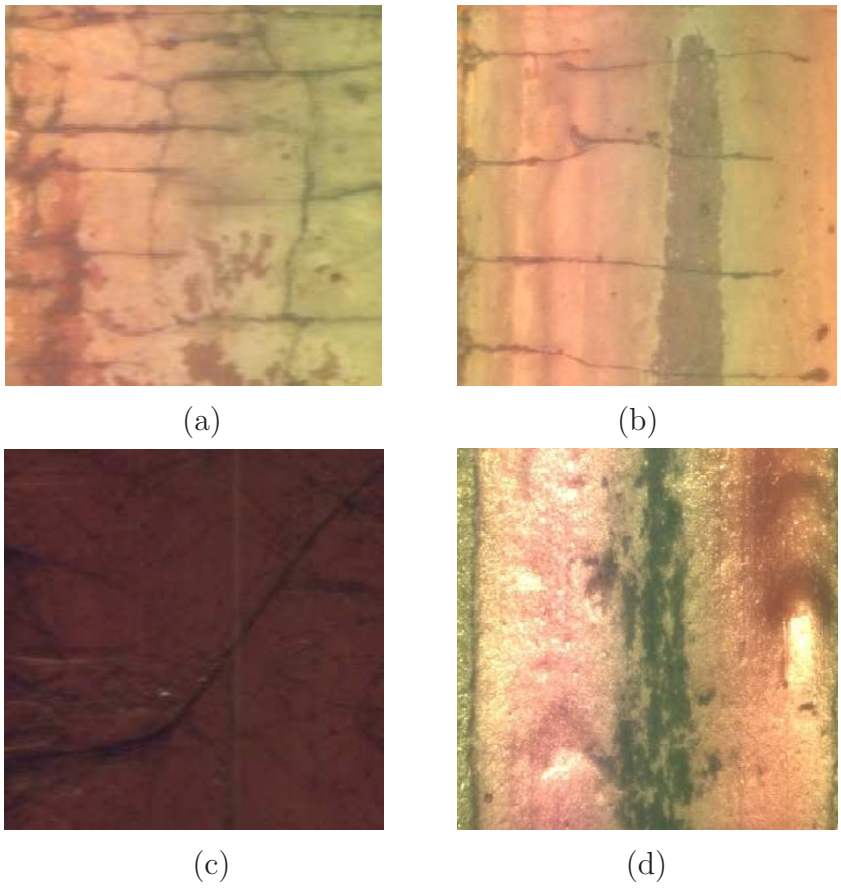

Figure 4.3. SSET Imagery. (a) and (b) different crack patterns with patchy background, (c) clay pipe with dark color background, and (d) green colored debris and vegetation in the background.

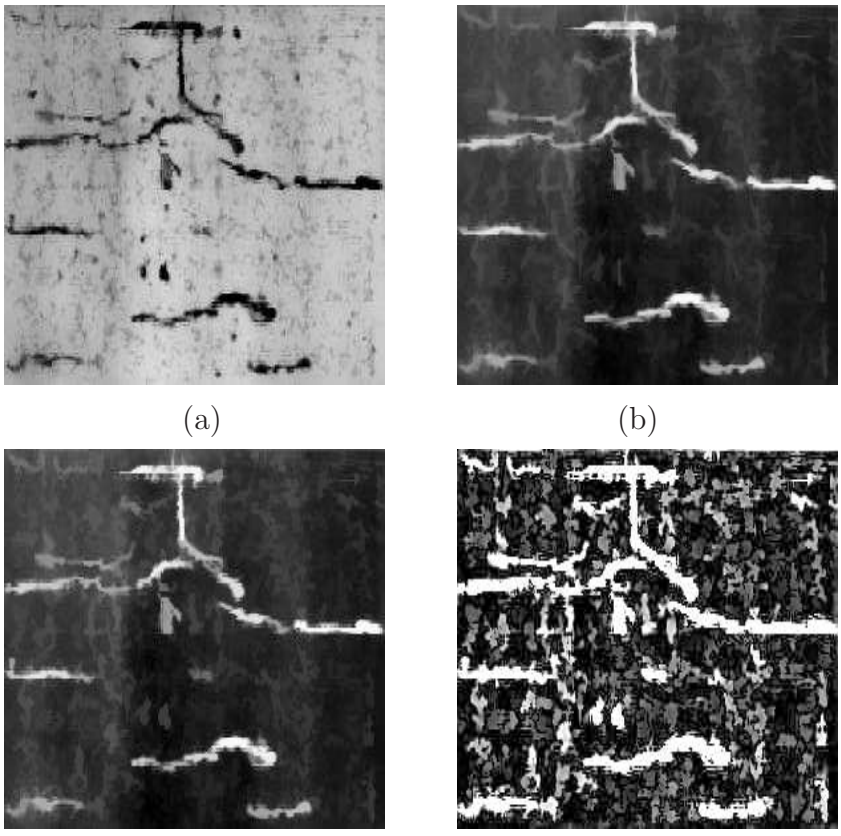

(a) (b)

(c) (d)

Figure 4.4. Steps in the morphology based recognition process: (a) original (contrast-enchanced) image, (b) supremum of opening, (c) geodesic reconstruction, and (d) sum of top-hats.

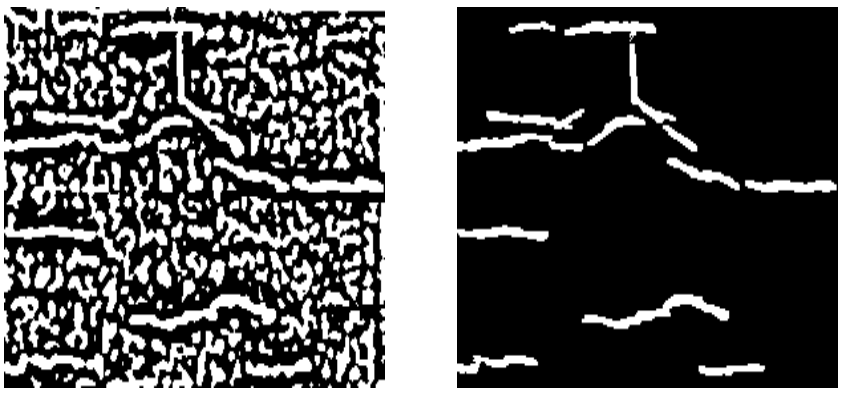

(a) (b)

Figure 4.5. Laplacian images highlighted around zero: (a) before and (b) after alternating filter.

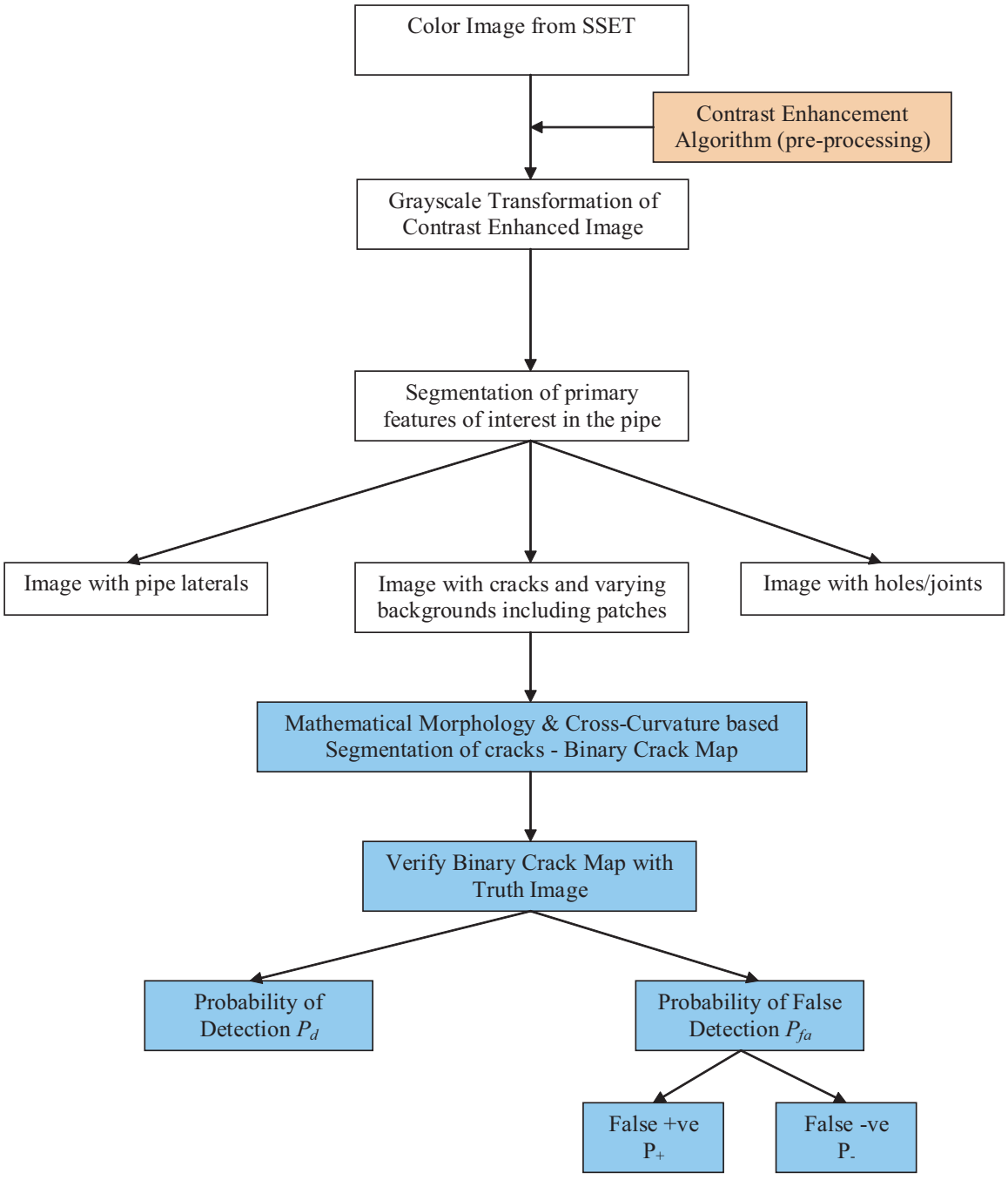

Figure 4.6. Framework for Detection of Pipe Defects. This study deals with aspects of the detection process shown in colored boxes on the flowchart.

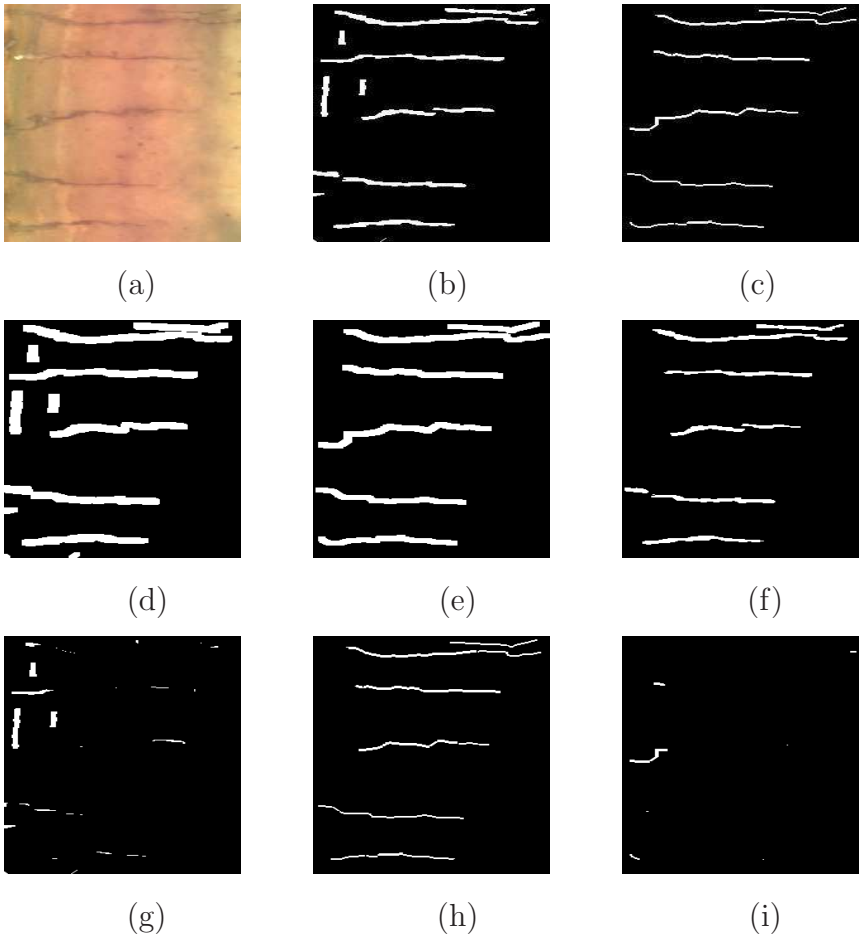

Figure 4.7. Matching procedure for detection of true and false pixels. (a) original image, (b) detected cracks, (c) ground truth, (d) and (e) detected and true cracks dilated by a 5x5 structuring element, (f) good points of the filter, (g) false +ve, (h) truly detected cracks and (i) missed cracks (false -ve).

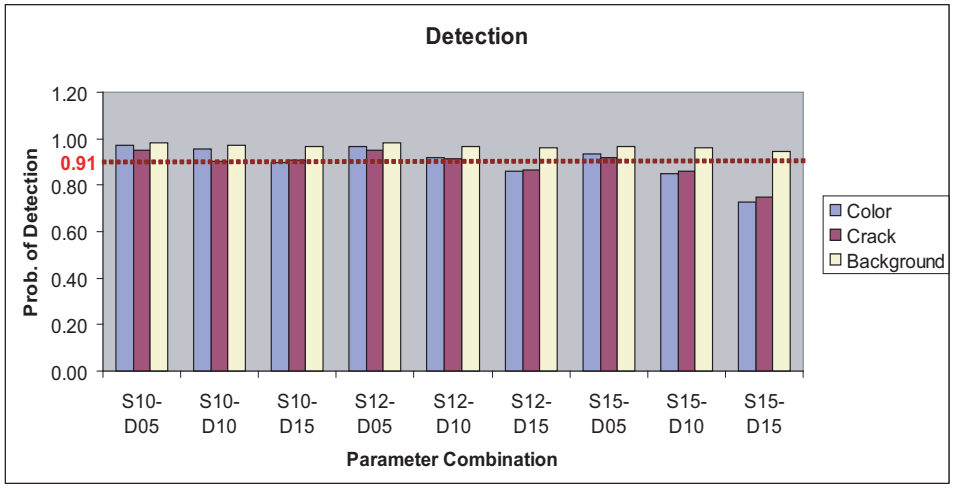

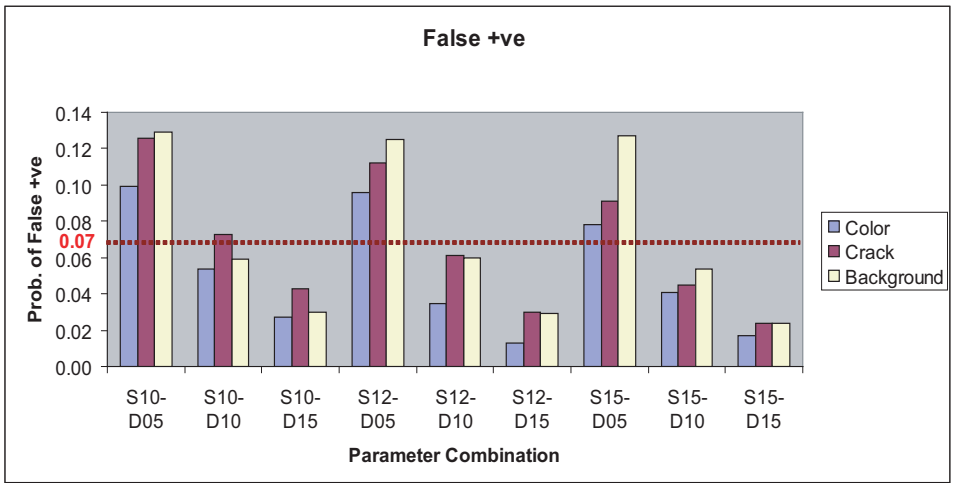

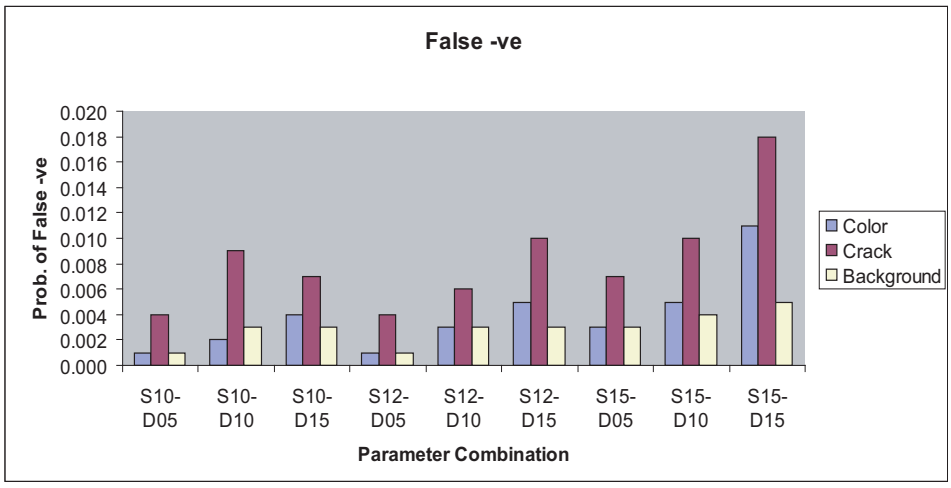

Figure 4.8. Bar chart of probabilities for different parameter combination. S12-D10 consistently meets criteria in all the three classes.

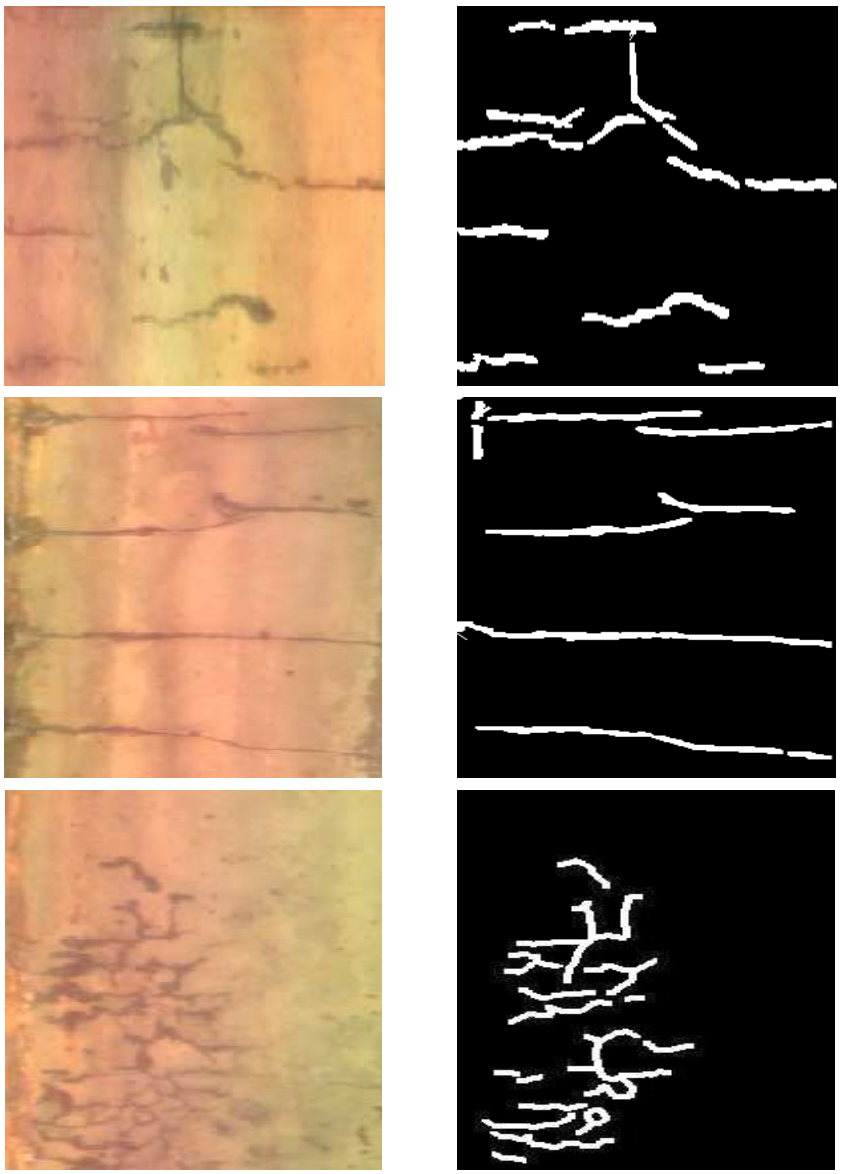

Figure 4.9. Image with different crack patterns.

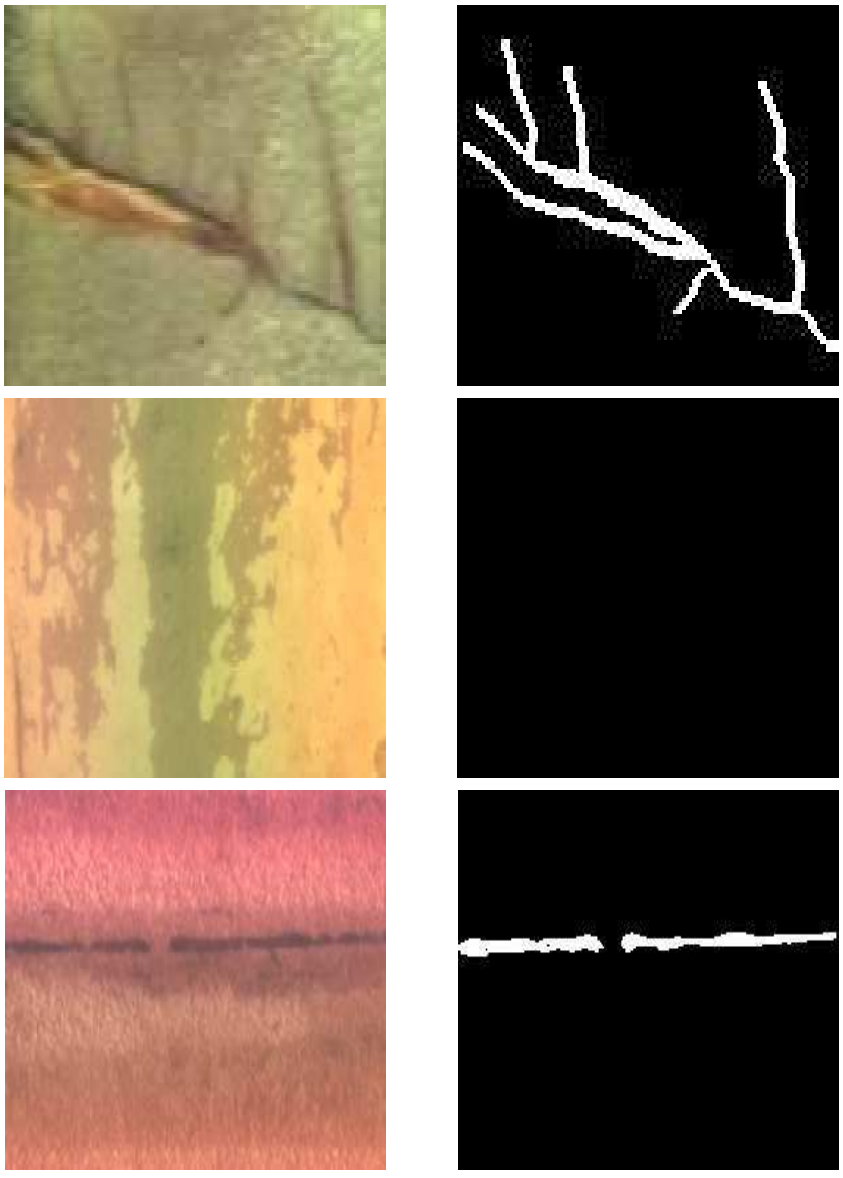

Figure 4.10. Image with different background patterns.

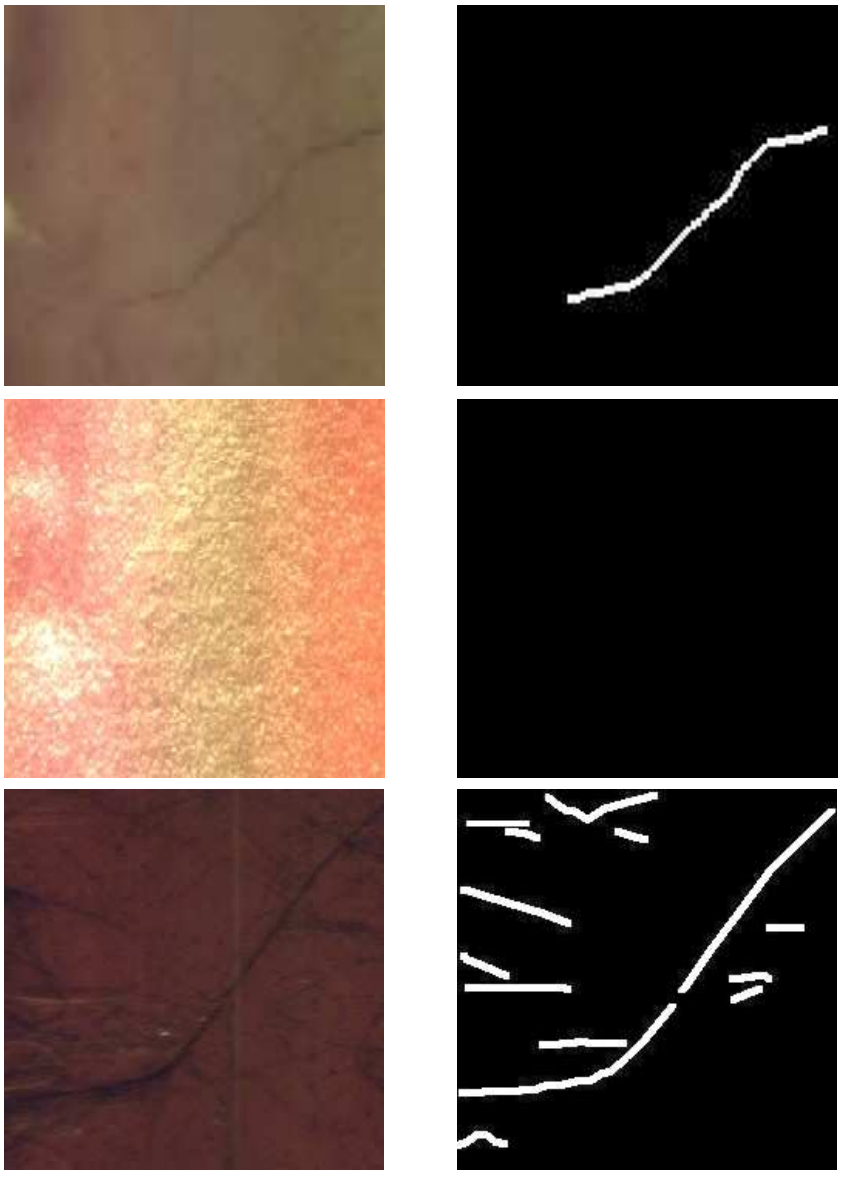

Figure 4.11. Image with different background colors.

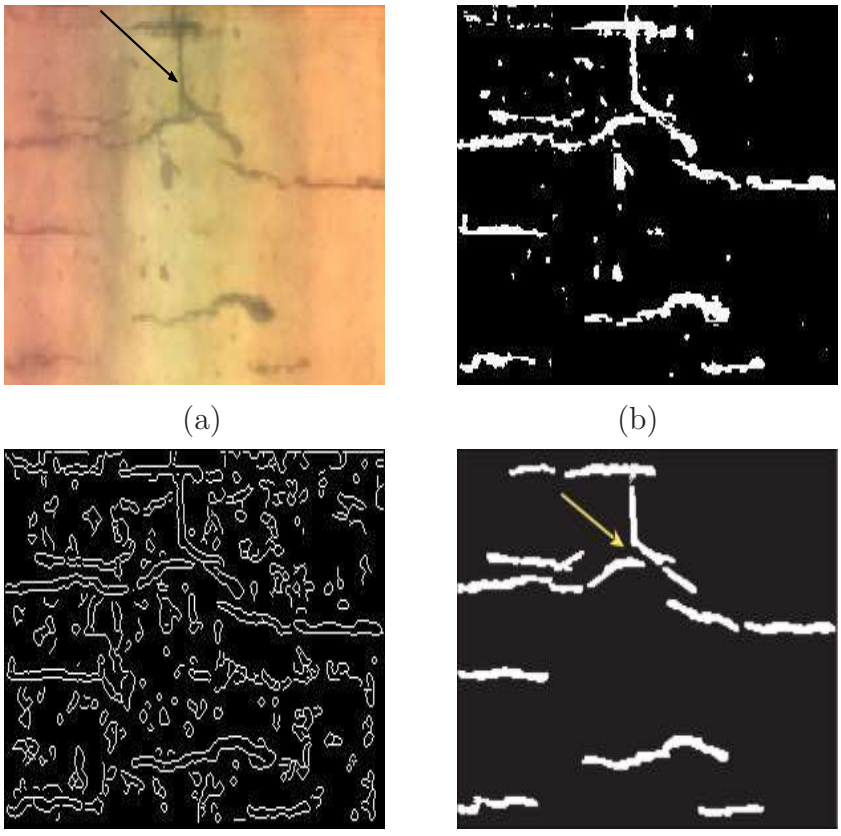

(a) (b)

(c) (d)

Figure 4.12. Edge detection algorithms on crack pattern image:(a) original image, (b) Otsu's thresholding (c) Canny's edge detector, and (d) proposed approach.

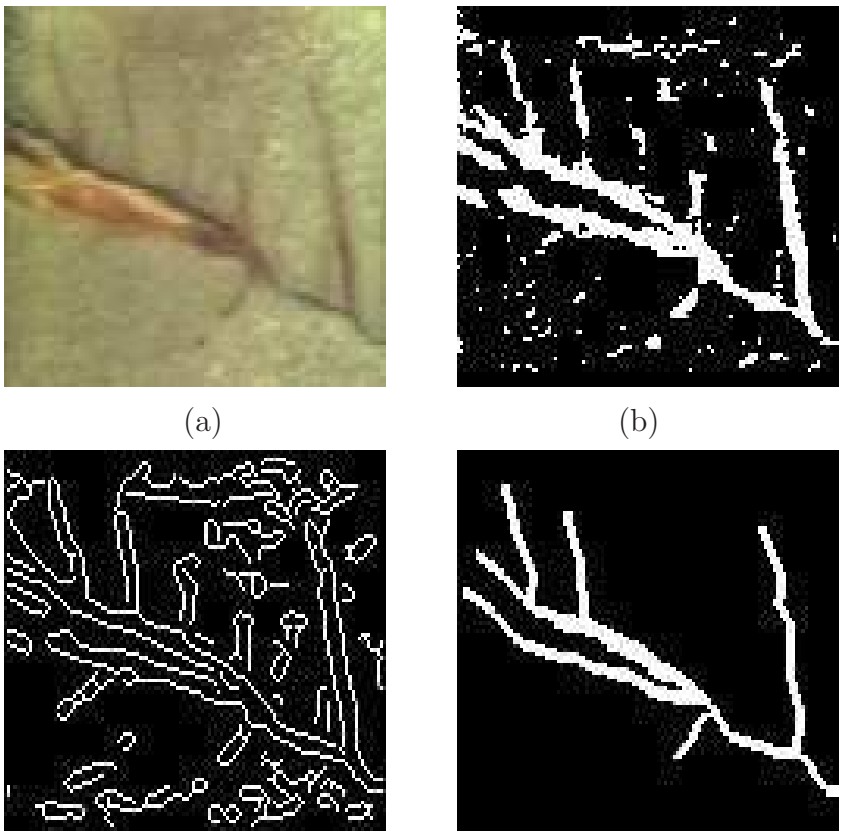

(a) (b)

(c) (d)

Figure 4.13. Edge detection algorithms on background pattern image:(a) original image, (b) Otsu's thresholding (c) Canny's edge detector, and (d) proposed approach.

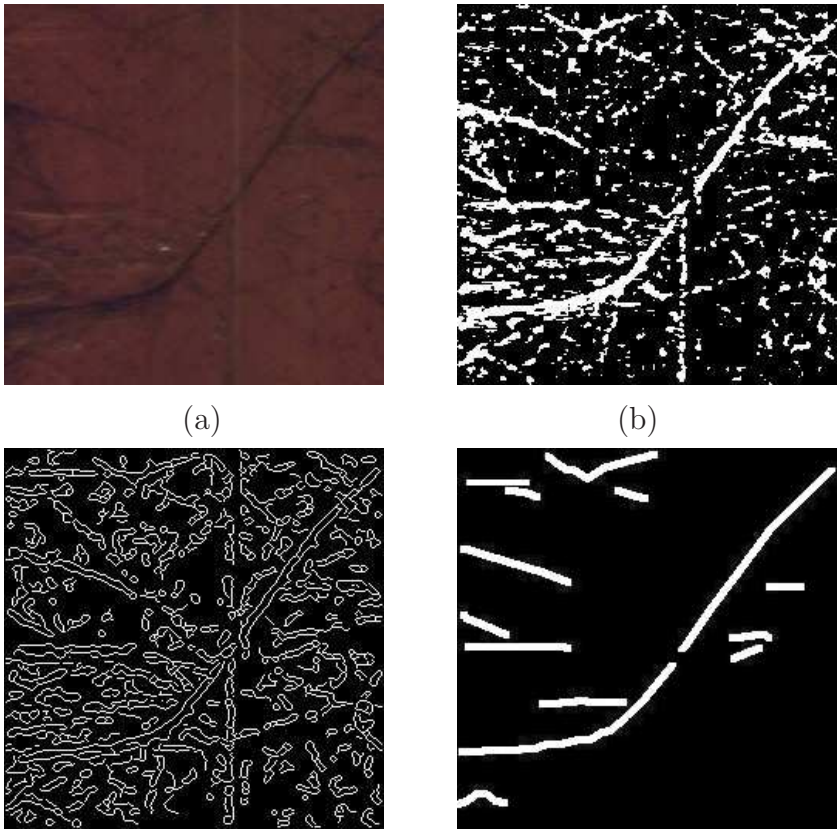

(a) (b)

(c) (d)

Figure 4.14. Edge detection algorithms on color variation image:(a) original image, (b) Otsu's thresholding (c) Canny's edge detector, and (d) proposed approach.

Chapter 5

Ultrasonic Inspection Of Wastewater Concrete Pipe

5.1 Introduction

Ultrasonics is the name given to the study and application of ultrasound, which is sound of a pitch too high to be detected by the human ear, i.e. of frequencies greater than about 18 kHz. Ultrasonic waves have a wide variety of applications over an extended range of intensity, including cutting, cleaning and destruction of tissue at the upper extremity and non-destructive testing (NDT) at the lower end (Blitz and Simpson, 1996). A non-destructive test is one in which there is no impairment of the properties and performance in future use of the object under examination. With ultrasonic non-destructive testing, which is effectively a mechanical method, periodic mechanical stresses are applied to the object. It is essential that there have been no changes in dimensions and structure of the object when the test is completed. This can only be achieved when the maximum applied stresses do not exceed the elastic limit so that the resultant strain is proportional to the applied stress. Hence it is necessary that the ultrasonic intensity is sufficiently low for the elastic limit not to be exceeded. Ultrasonic testing consists effectively of the propagation of low amplitude waves through a material to measure the time of travel and change in intensity for a given distance.

A significant part of this chapter will discuss the available approaches for de-

termining whether ultrasound can be used to inspect buried concrete pipe. The goal of this research is to develop a test method that can add complementary pipe information to existing surface image assessments. Superposing an ultrasonic image or signal (from a region with surface defects) on the optical image information in the pipe creates a visual context in three dimensions in which interpretation and analysis about the extent of defect propagation is easily achieved.

5.2 Suitable Approaches For Concrete Pipe Inspection

Although ultrasonic non-destructive evaluation has been carried out on Portland cement concrete since the 1940's, majority of the efforts have been directed towards velocity measurement and its correlation to ultimate compressive strength, modulus of rigidity, and other material properties (Jones, 1949). Recently, Song et al. (2003) have proposed a self compensating method to determine the depth of surface breaking cracks in concrete using surface wave transmission measurement (Song et al., 2003). Their study excludes cracks that might not break the surface or originate from the external (outer) surface. Therefore, approaches that can detect the depth of all types of defects in buried concrete pipes are needed. Most buried pipelines in place (especially sewer/stormwater) are made of precast concrete (PCCP) that has high impedance and large attenuation due to its heterogeneous nature. Hence, getting the energy transmission to be effective enough to reflect and come back is a challenge in air-coupled ultrasonic testing on concrete pipes. It is therefore apparent that minimization of loss at every stage is key to achieving an acceptable signal to noise ratio for the inspection if air-coupled ultrasound is the chosen method of inspection. There are a number of approaches, each of which has its own advantages and in some cases disadvantages. In some applications a particular approach may not be acceptable, or a disadvantage may not be relevant. The following section enlists issues that govern the selection of a particular ultrasonic inspection method from a practical application standpoint.

5.2.1 Practical Issues Governing Selection of Inspection Method

The issues governing the selection of an inspection method for buried utility pipes are:

- Access to pipe is difficult owing to the layer of soil above the pipe periphery.
- As the objective is to study the surface flaws from I.D. (internal diameter) and the extent of flaw in the thickness of the pipe, ideally a transmitting (T) and receiving (R) transducer in pitch-catch mode would suffice. However, it may be beneficial to detect flaws originating from the O.D. (outer diameter) towards the I.D. As the access to the outer periphery of a buried pipe is usually not possible, the T and R units need to be on the inside of pipe.
- Inspection is carried out on a mobile vehicle that moves from one manhole to another in the case of buried pipes. Hence, longer the axis points for the transducers, the more cable is required to collect data and that may prove cumbersome.
- Wrapping of transducers is not possible for external periphery scanning especially in the case of deep buried pipes owing to the porous soil medium surrounding it. Hence, ultrasonic waves that have large penetration depth and can travel to the outer diameter surface will be needed to detect anomalies originating from the outside surface inwards. In case of shallow pipes, it may be possible to generate low intensity waves to penetrate the outer periphery of the pipe from ground level but quality of data may be questionable.

All these and more factors will decide the method of ultrasonic transduction adopted to completely characterize the condition of buried public utility pipelines. In view of the above discussion, this chapter presents feasibility studies of three approaches for inspection of buried concrete pipes and finally selects one approach for detailed experimentation.

5.2.2 Ultrasonic Guided Wave Inspection

The use of ultrasonic guided waves in a pipe is beneficial due to its ability to scan large sections from a single sensor location (Cawley et al., 2002). Particular modes can be excited that will propagate with low attenuation even under water loaded conditions both on the interior and exterior of the pipe (Hayashi and Rose, 2003). The feasibility studies conducted in this study consisted mostly of concrete samples having plate-type geometry. Therefore, the discussion of guided waves in this section is limited to the plate case.

Guided waves in plates can be described by the numerical solutions of the Rayleigh-Lamb frequency equations (Rose, 1999):

$$\frac{\tan(qh)}{q} = -\frac{4k^2 p \tan(ph)}{(q^2 - k^2)^2}; \tag{5.1}$$

and

$$q\tan(qh) = -\frac{(q^2 - k^2)^2 \tan(ph)}{4k^2 p} \tag{5.2}$$

where h is the plate thickness and k is the wavenumber described in terms of the angular frequency, ω, and the phase velocity, c_p as:

$$k = \frac{\omega}{c_p}; \tag{5.3}$$

The functions p and q from equations 5.1 and 5.2 are:

$$p^2 = (\frac{\omega}{c_L})^2 - k^2; \tag{5.4}$$

and

$$q^2 = (\frac{\omega}{c_T})^2 - k^2 \tag{5.5}$$

where c_L and c_T represent longitudinal and shear wave velocities, respectively.

Equation 5.1 represents solutions for symmetric modes, which are those whose

in-plane displacements are symmetric about the center of the plate. The antisymmetric modes, represented by equation 5.2, have out-of-plane displacements that are symmetric about the center of the plate. The solution to equations 5.1 and 5.2 provide phase velocities, typically discussed as a function of the product of frequency and thickness *(fd)*. Group velocities can then be calculated from phase velocities via the following relation (Rose, 1999):

$$c_g = c_p^2 \left[c_p - (fd) \frac{dc_p}{d(fd)} \right]^{-1} \tag{5.6}$$

Figures 5.1 and 5.2 show phase and group velocity dispersion curves for concrete (c_L = 3750 m/s and c_T = 2400 m/s), respectively. All values used for dispersion curves were derived from material property data obtained from the manufacturer of the test specimens used for this study.

At 60mm in wall thickness, the samples tested in this study require relatively low frequencies for operation at feasible portions of the dispersion curve. Tests were conducted with air-coupled transducers in the two configurations shown in figure 5.3. Although successful generation of guided waves was achieved with a 50 kHz transducer, the feasibility of the technique in practical applications is questionable. Better results were achieved in the configuration shown in figure 5.3b. Given that only one-sided access from the internal pipe wall is feasible, this configuration is not applicable. With a 60mm wall thickness and a 50 kHz transducer, the *fd* product is 3. From figure 5.2, it can be seen that this represents a portion where mode isolation is difficult. Hence, this technique was not utilized for further investigations.

5.2.3 Impact Echo

The impact-echo method is a technique for flaw detection in concrete. It is based on monitoring the surface motion resulting from a short-duration mechanical impact (Malhotra and Carino, 2004). The first successful applications of impact methods occurred in geotechnical engineering to evaluate the integrity of concrete piles and caissons (Steinbach and Vey, 1975). The long length of these foundation structures allowed sufficient time separation between the generation of the impact

and the echo arrival, and determination of round-trip travel times was relatively simple. The impact response of thin concrete members, such as slabs and walls, is more complicated than that of long slender members (Sansalone and Carino, 1986, Carino, 1984, Carino et al., 1986). The easiest type of flaw to detect is a planar concrete-air interface that is parallel to the test surface, such as delaminations and voids. As the depth of a flaw increases, the smallest size that can be detected also increases. Based on analytical and laboratory studies, Sansalone and Streett (1997) suggest that if the lateral dimensions of a planar crack or void exceed 1/3 of its depth, the flaw depth can be measured (Sansalone and Streett, 1997). If the lateral dimensions exceed 1.5 times the depth, the flaw behaves as an infinite boundary and the response is that of a plate with thickness equal to the flaw depth. As with most methods for flaw detection in concrete, experience is required to interpret impact-echo test results. While the use of frequency analysis has aided in interpreting test results, experience is needed in setting up optimal testing parameters, recognizing valid recorded waveforms, and analyzing test results. Because of the varied situations that may be encountered in field-testing, a standard test method for flaw detection has yet to be developed (Malhotra and Carino, 2004).

Given concrete with 60 mm thickness, the expected through thickness resonance for a longitudinal wave is 31.25 kHz. This frequency is fairly high for typical impact-echo applications. Thus an impact source was needed to insure that frequencies in this range could be generated. This can be achieved by reducing both the impact time and the surface area of impact. For laboratory tests, impacts from a pellet gun were used as they produced sufficient frequency content. The time trace of this impact source is shown in figure 5.4. Figure 5.5 shows the general schematic used for impact-echo testing and actual setup for laboratory testing. Figure 5.6 shows the time traces for signals with and without a lateral crack between the impact source and the receiver. The effect of the defect on the signal is clear. A reduction of amplitude is seen as some of the generated stress waves are reflected from the defect decreasing amplitude of the received signal compared to the case where no defect is present. With the addition of a higher frequency impact source, this technique can be effective for defect identification in concrete

pipe applications. However, the major limitation of this technique is its inability to locate the source of the defect.

5.2.4 Ultrasound Immersion Inspection

When an ultrasound wave is directed into a sample, either the reflected or through-transmitted wave is recorded. Figure 5.7 shows a schematic flowchart of possible modes for operation of ultrasound inspection techniques. The collected data can be displayed in several ways depending on the nature of information desired about the sample. In ultrasound inspection, a couplant is needed to transfer the acoustic energy between the transducer and the sample. A convenient way of maintaining transducer coupling to the specimen surface is by using water as the couplant (Cartz, 1995). Immersion inspection is a general and useful procedure that offers the advantages of:

- Uniform sensitivity from uniform coupling
- Suitable for *automated scanning*
- Focusing of immersion transducers increases sensitivity to small reflecting surfaces. This improves the detectability of mis-oriented defects.

Immersion inspection is widely used in the industry. Water is the most common liquid for inspection in this technique. it is inexpensive, available almost everywhere, and is *not* toxic. The reflection technique in pulse-echo mode is the most commonly used method in for ultrasound immersion inspection. A single ultrasound transducer transmits and receives signals so that only single-sided access is needed. This makes it highly adaptable to buried utility pipeline inspection applications wherein access to only internal surface is possible. A pulse generator provides signal to the transmitter which generates an acoustic wave. The wave propagates from the transducer face into the sample and back using water as an impedance transition medium. During its round trip travel, the wave crosses several boundaries with different acoustic impedances that reflect the wave. The wave is first reflected at the front surface of the sample (front-wall echo). It is once again reflected when it interacts with internal surfaces of inclusions within the sample (defect echo). The last reflection takes place at the boundary of the test object and

surrounding medium (water in this case). A schematic representation is shown in Figure 5.8. For defect detection and characterization, the reflected wave (or signal) can be represented in several ways, namely, A-scan, B-scan and C-scan. A brief introduction to each of these representations follows.

5.2.5 A, B and C-scan Representations

The A-scan representation displays a time series signal showing the variations in amplitude of the ultrasound signal as it traverses a path from the transducer face to the sample back wall and back. In other words, A-scan signals capture information about the material thickness at a single point (x_0,y_0) at time t. A typical A-scan signal representation as shown in figure 5.8 is very easy to acquire and is the most commonly used one in ultrasound testing. However, it is difficult to interpret an isolated A-scan signal without a reference signal recorded from a known defect-free area. For larger samples, numerous single point A-scans would have to be collected to sufficiently inspect the area of interest. In such cases, it is beneficial to obtain a two-dimensional representation through a B-scan.

A B-scan representation is obtained by scanning across the sample and mapping several A-scans along one coordinate axis while the other is fixed. On a typical B-scan 'image', the abscissa represents position along scanning direction and the values of time of flight or distance are shown on the ordinate axis. The signal amplitude can be mapped to a colormap scheme to represent changes in amplitude owing to defects in a visual context. Figure 5.9 shows a B-scan image obtained by mapping the amplitude of reflected signal taken along a scan line in the x direction while fixing its position in the y direction. The front wall and back wall echo will usually have a higher signal amplitude than the defect echo. This is visually represented by different colors mapped to the highest signal amplitude. Due to the presence of a defect in the path of the ultrasound wave, the back-wall echo amplitude at the x-position of the potential defect is weaker and is represented by a distinct color. Thus, the B-scan image displays the length in x-direction, and the depth of a potential defect as seen in figure 5.9.

Another method of representation that is gaining popularity in material characterization is the C-scan representation. The C-scan image shows a view of the sample as seen from above and therefore shows a cross section of the sample and defect parallel to the scanning surface. The C-scan method involves a series of parallel A-scans, which are carried out over a surface, and the pulse echoes are restricted to those returning during a fixed time interval. The signal reflected from the back surface of the examined specimen is 'gated', and its peak value provides data for the C-scan image of the specimen at a given depth. To achieve such a representation, the sample is scanned in a raster pattern and the transmitted wave amplitudes within a certain time range are gated. The gated amplitude along with its x and y coordinates are mapped. A C-scan image is rendered by integrating amplitudes within the time range over the x - y plane. This type of representation provides the ability to track a defect through the thickness of the sample due to changes in amplitude. A schematic of C-scan representation is shown in figure 5.10

5.3 Experimental Program

Ultrasonic assessment techniques for concrete can be developed and implemented only if the interaction between ultrasonic waves and the material through which it propagates is well understood. Concrete is a heterogenous material made up of a weighted combination of aggregates, water, cement and admixtures. Many different concrete mix designs can be prepared with lightweight aggregates, several types of sand and gravel, different water to cement ratios, and admixtures. Concrete pipes are usually formed using zero-slump concrete or concrete with a very low water to cement ratio. It is known that the strength of wave energy (or power) propagating in concrete is influenced by several intrinsic material factors such as size of aggregate, degree of compaction, admixtures, porosity of concrete mix, etc. The experimental program discussed in the following section will outline experiments conducted on a representative concrete pipe material block using the ultrasound immersion inspection method discussed in Section 5.2.4

5.3.1 Objectives

It is evident from the discussion in the previous section (Section 5.2) that ultrasonic testing of concrete pipes for determination of defects is a complex research problem with several challenges. Hence, this research study will deal with advancing the understanding of how ultrasonic methods can be used in the determination of defects in concrete pipe material by addressing some of the issues through specific objectives mentioned below:

- To provide proof-of-concept for inspecting concrete pipes, by conducting laboratory experiments on a representative block made from the same concrete mix used to form pipes, using the ultrasound immersion technique. The aim of this step is to evaluate the technique, determine an optimum frequency range, angle sensitivity, and liftoff.
- Perform preliminary evaluation through A-scan signal processing on the sample to determine the presence of defects and
- Further characterize the defects with C-scan imaging.

It must be noted that various issues such as instrumentation and methodology for delivering, receiving and processing ultrasonic signals for actual application in buried pipe inspection is out of the scope of this research study. The technology and expertise for adopting an ultrasound-based inspection methodology into a field-application device falls in the domain of robotics and instrumentation research. Clearly, this is not the focus of the present study. Thus, this research study intends to determine in principle the methodology to localize and characterize defect information using ultrasound transduction from laboratory experiments on representative concrete pipe material samples only.

5.3.2 Specimen Description

The concrete slabs were provided by the Pennsylvania Concrete Pipe Association (PCPA) based on guidelines defined by the American Concrete Pipe Association (ACPA) for concrete mixes used in the manufacture of reinforced concrete culverts, storm drain and sewer pipes, tongue and groove joints and O-Rings (American National Standards Institute, 2002). Concrete pipes for use in buried infrastructures

like storm water and sewer pipes are available in dimensions ranging from 12 - 144 inches internal diameter (ID) with a wall thickness of $2^{1/4}$ inch as per ASTM C 76-02 (American National Standards Institute, 2002, Association, Association). Table 5.1 lists specific properties of concrete specimens used for this research. The aggregates used for the concrete specimens conform to ASTM C 33 specification with an exception that the requirement for gradation shall not be applied. The aggregates used in the zero slump concrete consisted of uniformly graded granite, basalt, limestone, and quartzite.

Several specimens were prepared exhibiting characteristic defects found in concrete sewers. Cracks of several mouth openings were generated in sample concrete slabs via three-point bending with a stress concentrating notch. Samples were also prepared with notches and boreholes to provide a more comprehensive analysis. Figure 5.11 shows photographs of the samples used for testing. Three different mouth opening were generated corresponding to levels of concern in the buried concrete pipe industry. The first mouth opening is between 0.25 and 0.5 mm constituting a hairline crack (HC). These cracks are not particularly critical to the operation of most systems and can even be found upon installation. Mouth openings between 0.5 and 1.5 mm constitute cracks (CR). The identification of a crack does not lead to replacement of the pipe section but will be monitored as it may soon lead to fracture (FR), typically on the order of 5 to 10 mm and are often completely through-wall. The borehole (H) and notch (N) defects are not typically found in water/wastewater pipe networks but may arise from inadvertent digging strikes or some types of corrosion.

5.3.3 Experimental Setup and Data Collection

An Ultran NDC 7000 system setup was used in conjunction with a plane wave Panametrics transducer having a center frequency of approximately 250 kHz. A block diagram of the set-up is shown in figure 5.12. The concrete slabs were submerged in a water tank. The Panametrics transducer, made of PZT (Lead-Zirconium-Titanate), was attached to an automated computer-controlled x-y-z stage and was excited by a Panametrics Pulser-Receiver to generate ultrasonic waves. The transducer consisting of transmitter and receiver was housed in the

same assembly thus resembling a single unit transmitter-cum-receiver in pulse-echo mode. The ultrasonic wave was reflected by the specimen and returned to the transducer, which also acted as a receiver.

The data collection scheme is shown in figure 5.13. Several concrete slabs with four classes of defects, namely, hairline crack (HC), crack (CR), fracture (FR), and hole (H) were prepared. A 50 mm x 50 mm region of interest (ROI) around the defect was identified on each sample for data collection and interpretation (see figure 5.13). The transducer was initially positioned on the bottom left corner of the region of interest for all samples. A-scan signals were collected at each predefined point in the ROI. As seen from figure 5.13, the scanning direction is x axis whereas the step direction is y axis. The data collection was automated so that the transducer collected data in the scanning direction (x axis) at points physically spaced 5 mm apart. Thus, each run in the scanning direction would produce 10 A-scan signals. The transducer would then move 5 mm in the step direction (y axis) and collect data in the scanning direction. In this manner, the entire ROI will be scanned in a raster pattern generating 100 A-scan signals.

This process is repeated for all samples keeping other parameters like scan axis and step axis increment (5 mm), liftoff distance (length of water path between the transducer face and sample surface), angle of transducer with the sample surface, and frequency constant. Two identical data sets each containing 2100 and 700 A-scan signals respectively were collected on different days to ensure reliability and consistency in the data. Set A data consisted of A-scan signals from five concrete slabs (1 clean + 4 defects) oriented at 0, 45, and 90 degrees. In real world applications, defects could be oriented in any direction in the pipe geometry. Hence, it was intended to capture this aspect in the data collection by orienting the slabs at three representative orientations. A-scan signatures were also collected from all defects in order to build an automatic signal classification system. More detailed discussions on signal processing and classification of A-scan signals are reserved for chapter 6. After the A-scan data collection was completed, all samples were subjected to C-scan imaging of the ROI as explained in section 5.2.5.

5.4 Results

Figure 5.14 shows a close up view of the ROI for each sample. A-scan signatures were collected from all defects and the clean sample in the ROI to determine if this methodology was capable of generating unique representations for each defect class. In other words, the signal characteristics would aid in building an intelligent interpretation system wherein signals that originated from a defect region would be accurately identified and classified accordingly. For any signal interpretation system to work well, the raw ultrasonic signal data from various classes has to be reliable and must possess some discriminating characteristics. Figures 5.15-18 show comparison of A-scan signatures from four defect classes with the clean class signature. It is evident by comparison that each defect class has a unique pattern in terms of back-wall echo amplitude and signal content in between the front-wall and back-wall echoes. The front-wall and back-wall echoes are 33 μ-secs apart. This is in confirmation with a simple calculation that yields the time required for ultrasound wave to travel from front surface to the back-wall, given that the thickness of slab and ultrasonic pulse velocity through concrete is known. At a longitudinal wave speed c_L of 3750 m/s and 60 mm thick concrete slab, the ultrasound wave should theoretically take 32 μ-secs for a round trip (see figures 5.15-18). This is true for the clean class but not necessarily true for other defect classes. As explained earlier, when the wave sees a defect, there are multiple reflections at the interface between the defect and its surrounding environment due to different acoustic impedances. This results in the reduction of ultrasound energy that can propagate through the defect and reach the back-wall. As a result, three effects can be observed in the A-scan signal. First, drop in back-wall signal amplitude in certain defect cases like hairline crack (see figure 5.15). Second, complete loss of back wall amplitude in defects like crack and fracture (see figures 5.15-16). Finally, the back wall echo shifts towards the front-wall echo as seen in the hole defect case (see figure 5.18).

As concrete is a highly attenuating material, there is inherent signal energy loss that also needs to be factored in while interpreting these A-scan signals. Researchers typically cite 250 kHz as the maximum operable frequency before attenu-

ation becomes too great and it is impossible to resolve the signals in terms of their front-wall and back-wall echoes. Also, it was important to determine the optimum liftoff distance and inclination angle of the transducer with respect to specimen for reliability. Data was collected on the clean sample at various inclinations and liftoff distances. The backwall signal amplitude was measured for each combination of liftoff distance-angle setting. The back-wall signal amplitude was plotted as a function of liftoff distance and angle as shown in Figure 5.19. It is clear that the back-wall signal amplitude is strong when the transducer face is oriented 4 degrees from normal incidence on either side and the liftoff distance is between 20 and 80 mm. As the liftoff distance and transducer inclination are increased beyond this range, a significant drop in back-wall amplitude is observed. This indicates that the ultrasound energy is being dissipated and does not penetrate the concrete sufficiently to reach the back surface. Hence, the optimum range of parameters for this methodology is that the frequency be around 250 kHz, liftoff be between 20-80 mm and angle of transducer be between -4 to 4 degree from normal incidence.

As mentioned in section 5.3.3, two sets of A-scan signal data were collected over a few days to compare the consistency of signal characteristics. Figures 5.20-24 shows Set A and Set B data for all classes collected at 0 degree orientation of defects. It must be noted that it is virtually impossible to replicate perfect signal characteristics over time while inspecting concrete due to the inherent variation in material, methodology and operator characteristics. However, a good system usually will be able to provide similar trends in data collected on similar samples over time. Figures 5.20-24 reinforce this point by showing that the A-scan signal characteristics are generally consistent within the same defect class between data sets A and B. Some inherent variation in scan area or digital triggering issues will cause changes such as shifting of the signal. Overall, it can be concluded that data collected using this methodology is generally consistent.

It was important to verify the signal acoustically and so the first step in C-scan imaging was to generate an A-scan in the 'clean' section of the sample to identify front-wall and back-wall echoes. This would aid in deciding gate (*time window*) locations along the signal trace representing various zones through the thickness

of the specimen. As this had already been done in the A-scan data acquisition phase, it was easy to generate the signals again for imaging. The A-scan trace was 'gated' from the front-wall to back-wall using four time windows based on available resolution on the time scale. Thus each gate approximately covered a thickness of 15 mm within the concrete sample. Figure 5.25 shows a time trace that was gated for image reconstruction. Once the gate positions had been fixed, the scan size and step size were defined for all samples and C-scan images were generated. It must be noted that the samples were scanned while keeping the defect face at the back-wall. Thus, if a defect were to be present and not running completely through the thickness of the sample , it would show up in the image slice gated nearer to the back wall (gate 4). This was done to justify worst case scenario, where the defect is not visible to the CCTV camera from within the pipe if it originates from the outside surface. It was expected that the defects would show up in the fourth or third gate in the samples used for this study, . Figures 5.26-30 show C-scan images from hole, hairline crack, crack, fracture and clean concrete samples respectively. The hole has a diameter of approximately 25 mm and is 30 mm deep at an angle of $10°$. As seen from C-scan images of gate 3 and 4, the hole is tracked in both slices but is not exactly at the same location (see figure 5.26). This is explained by the fact that the hole in concrete slab is not vertical but is at an inclination as mentioned above. Images from gate 1 and 2 show internal structure of the concrete slab. As the defect does not extend beyond 30 mm in depth, the hole is not tracked in gates 1 and 2. Figure 5.27 shows C-scan images from the hairline crack defect sample. The hairline crack is 0.25 0.5 mm wide and is less then 10 mm in depth. Gate 4 shows the hairline crack as well as the presence of another anomaly besides it. The left most anomaly in the gate 4 C-scan image is explained by a notch created by the supplier of these samples (see scanned region of interest image in Figure 5.27). As the crack does not extend beyond 10 mm, it is does not show up in gates 1, 2 and 3. Hence it can be concluded that the hairline crack originates at the farther end of the sample and is not more than 15 mm deep. Similar observations can be made for the crack (figure 5.28) and fracture (figure 5.29) samples. Although the fracture defect extends into the third gate (>15 mm deep), it is not picked up because of inherent reflections from the aggregate-cement paste interface. The ultrasonic beam is wide enough to pick

up surrounding reflections and thus the change in amplitude is not an accurate representation of the internal state of the slab at that particular location.

5.5 Saturation Issues

It is a well known fact that quite a few properties of a hardened concrete are influenced by its moisture content (Popovics, 2005). They include:

- the compressive strength of a concrete is higher if the specimen is dry when tested than the strength of the same specimen when tested in a saturated condition, and
- the ultrasonic pulse velocity which, however, is higher in the concrete when it is wet than when it is drier.

It is expected that the pulse velocity in wet hardened concrete sewer pipes buried several feet under the ground is greater. Initial trials with the dry concrete slabs in the laboratory were unsuccessful in generating acceptable signals that could be used for investigation. It was found that once the samples were saturated for around 24 hrs, the concrete would gain sufficient moisture content to facilitate the propagation of ultrasonic energy that produced strong backwall echoes. Hence, a laboratory experiment was designed to check if partial saturation of the concrete slab would raise the moisture content of the slab sufficiently so as to produce acceptable ultrasonic signals. As shown in figure 5.31, a concrete slab was partially submerged in an immersion tank with the water level at half the thickness of the slab. After 24 hrs of saturation, the slab was tested using a 250 kHz panametrics transducer in pulse echo mode. Two signals, one from the clean portion, and the other from crack region were acquired for comparison (see figure 5.32). Clearly, the back wall echo amplitude drops down when the transducer is on the crack which is supported by the increase in echo amplitude between the front and back wall echoes. Thus, it can be concluded from this short experiment that partial saturation of the hardened concrete pipe material raises the moisture content to a sufficient level wherein ultrasonic inspection is possible. It must be noted that the proposed technique has been validated on specimens that had a high moisture content. It is anticipated that this technique will be applicable in scenarios wherein

concrete sewer pipes will have been buried deep in the ground for longer periods of time. In other words, it will have been sufficiently saturated from the flowing sewer inside it and moisture ingress from the surrounding soil over several years thus maintaining a conducive moisture content level in the concrete pipes.

5.6 Summary

Various ultrasound-based inspection techniques that may be employed to acquire depth perception data for defects in buried concrete pipes were explored. In the guided wave technique, tests were conducted with air-coupled transducers in two configurations, through transmission with transducer on same side and transducer on opposite sides. Although successful generation of guided waves was achieved with transducers on opposite sides, the feasibility of the technique in practical applications is questionable because only one-sided access from the internal pipe wall is available. The expected through thickness resonance for a longitudinal wave through 60 mm concrete is 31.25 kHz. This frequency is fairly high for typical impact-echo applications. With the addition of a higher frequency impact source, this technique can be effective for defect identification in buried concrete pipes. However, the major limitation of this technique is its inability to locate the source of the defect. Moreover, because of the varied situations that may be encountered in field-testing, a standard test method for flaw detection has yet to be developed.

Ultrasound immersion inspection that uses water as a couplant is widely used in the industry owing to its adaptability to automation. A single ultrasound transducer transmits and receives signals so that only single-sided access is needed. This makes it highly adaptable to buried utility pipeline inspection applications wherein access to only internal surface is possible. For defect detection and characterization, the reflected wave (or signal) can be represented in several ways, namely, A-scan, B-scan and C-scan. This chapter presented experiments that were conducted on several concrete samples with defects of interest to the water/waster water pipe community. The experimental setup consisted of a Panametrics plane wave transducer with a central frequency of 250 kHz, Panametrics pulser-receiver, Labview automation software, three axis stage for scanning, a liftoff distance be-

tween 20 80 mm and zero degree inclination of the transducer with the vertical. Samples were scanned in a 50 mm x 50 mm region of interest and A-scan and C-scan representations were generated to make interpretations about the presence of defect and track them through the slab thickness. The experiments conducted on representative concrete pipe material specimens will only bring out the understanding of ultrasound transduction methodologies based on laboratory experiments. Although several issues related to its direct application in the field need to be resolved, it will not be addressed by this study as it is beyond the defined scope.

Table 5.1. Properties of zero slump concrete used for pipe specimens

Material Parameters	Value	
Poisson's Ratio	0.25	
Density	149.9 pcf	
Compressive strength	4000 psi	
Concrete Mix Specifications:		
	Cement	432 lbs
	Flyash	48 lbs
	Sand	252 lbs
	Stone	530 lbs

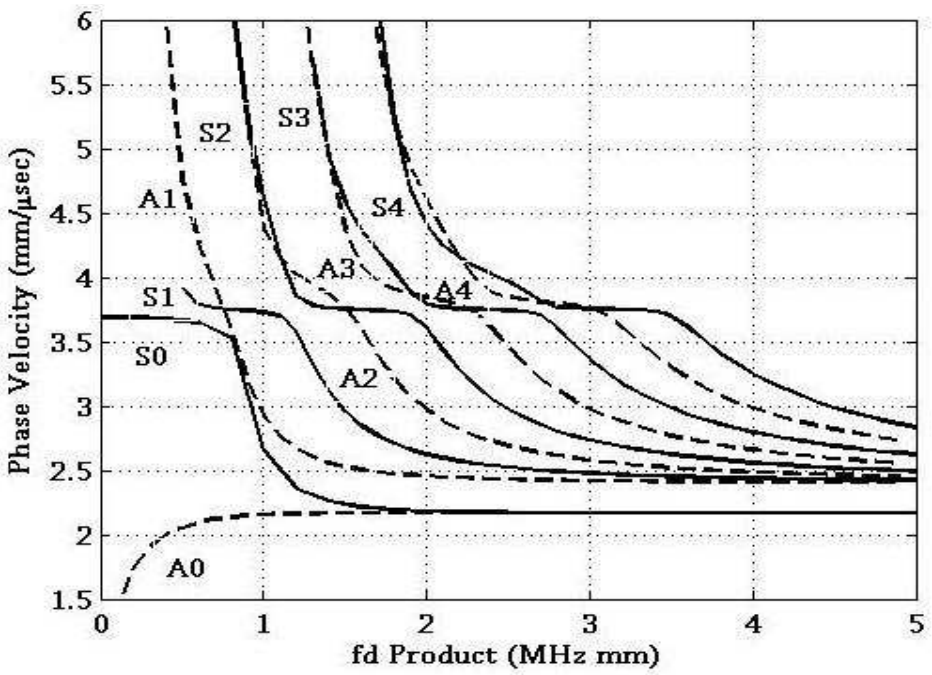

Figure 5.1. Phase velocity dispersion curves for a concrete plate (c_L = 3750 m/s, c_T = 2400 m/s

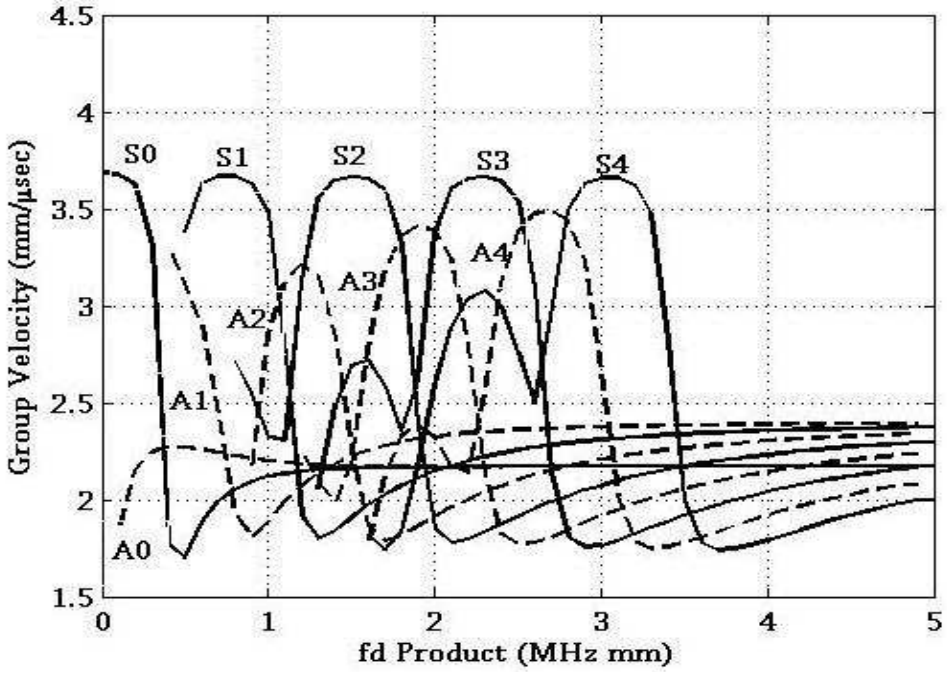

Figure 5.2. Group velocity dispersion curves for the concrete plate described in figure 5.1

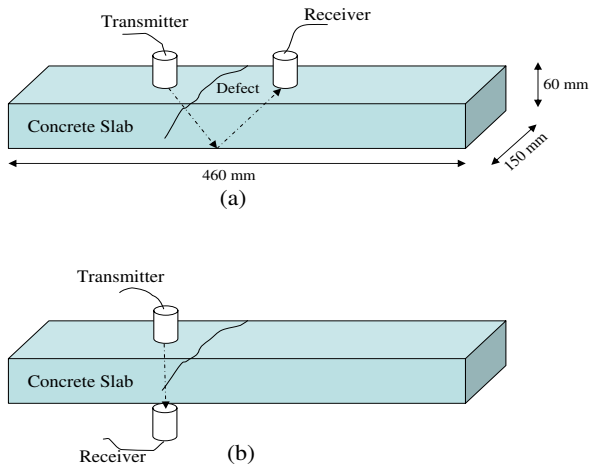

Figure 5.3. Schematic of through transmission setup for transmitting and receiving guided waves in an air-coupled system for (a) same sided transmission/reception and (b) opposite sided transmission/reception

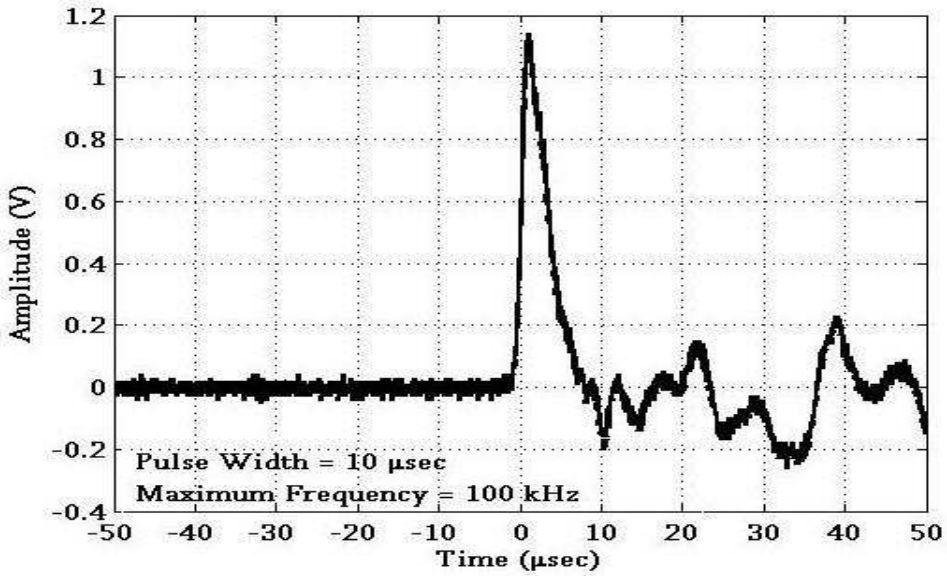

Figure 5.4. Time trace of the impact echo source signal used for generating higher frequency resonances

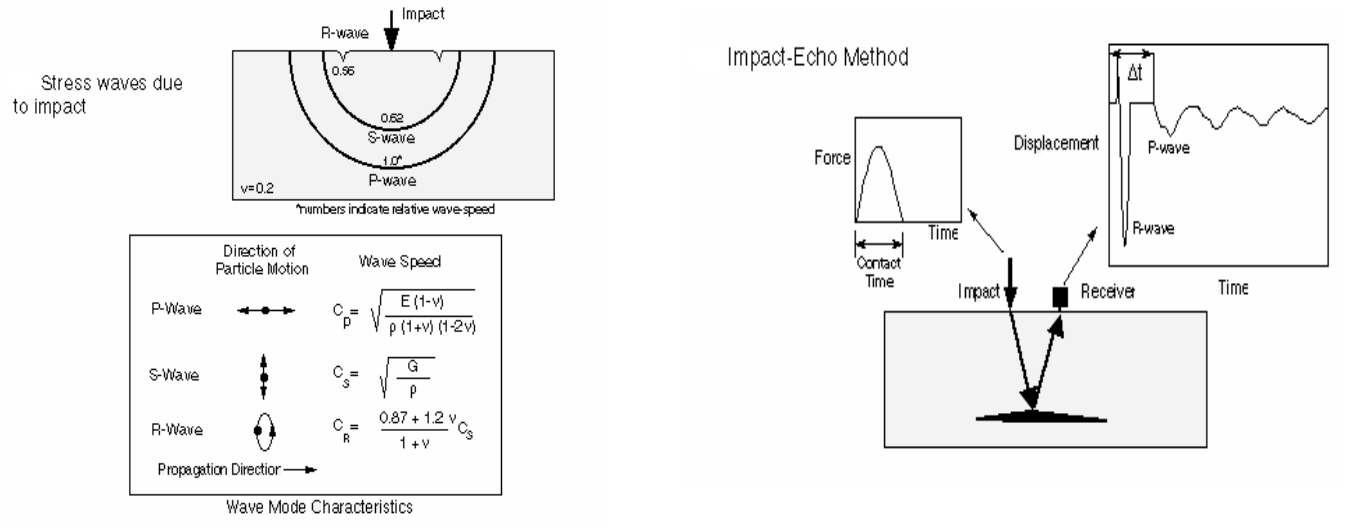

(a)

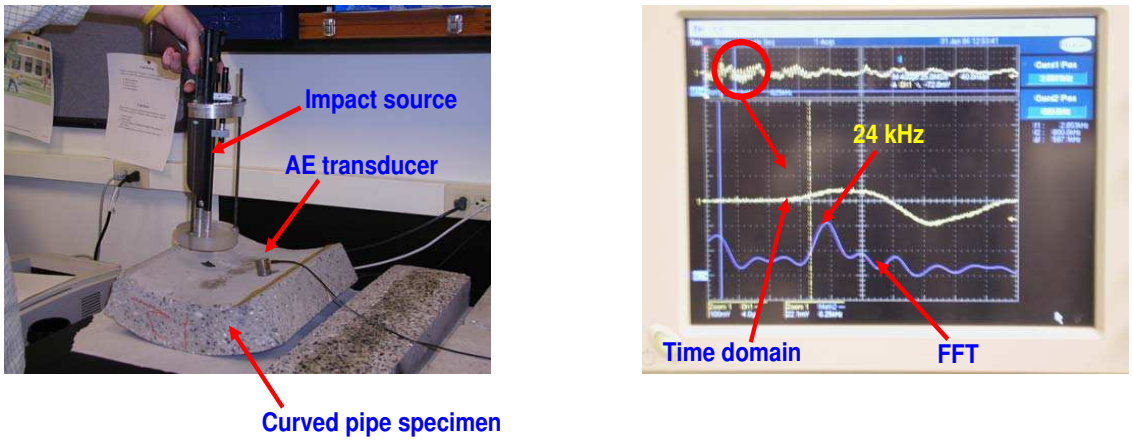

(b)

Figure 5.5. Impact Echo schematic (a) Basic principle (Image Courtesy www.nist.gov), (b) Laboratory setup with time trace

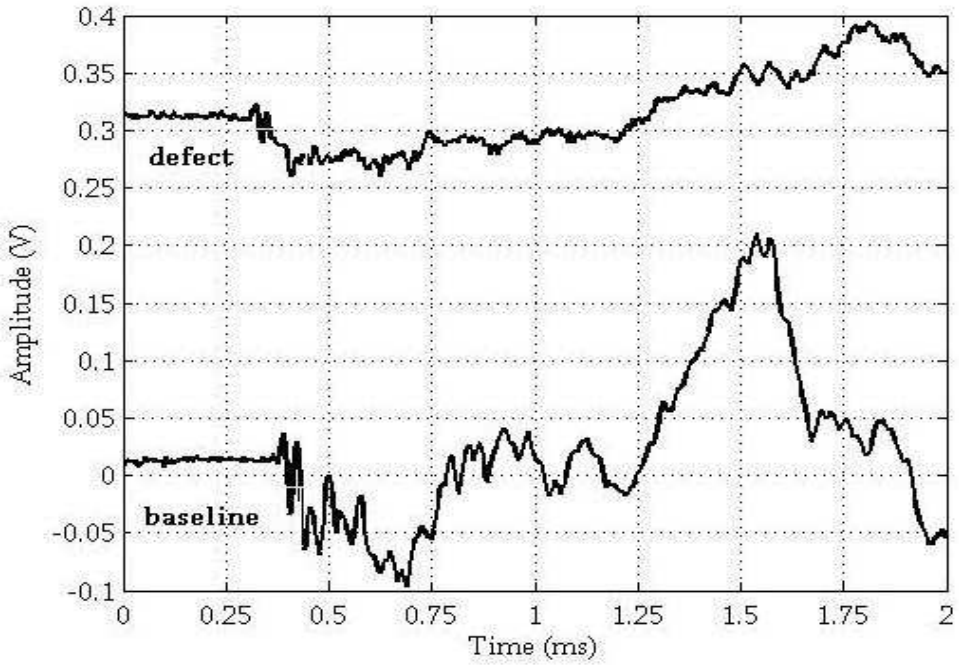

Figure 5.6. Time traces from a clean sample and defect sample of concrete

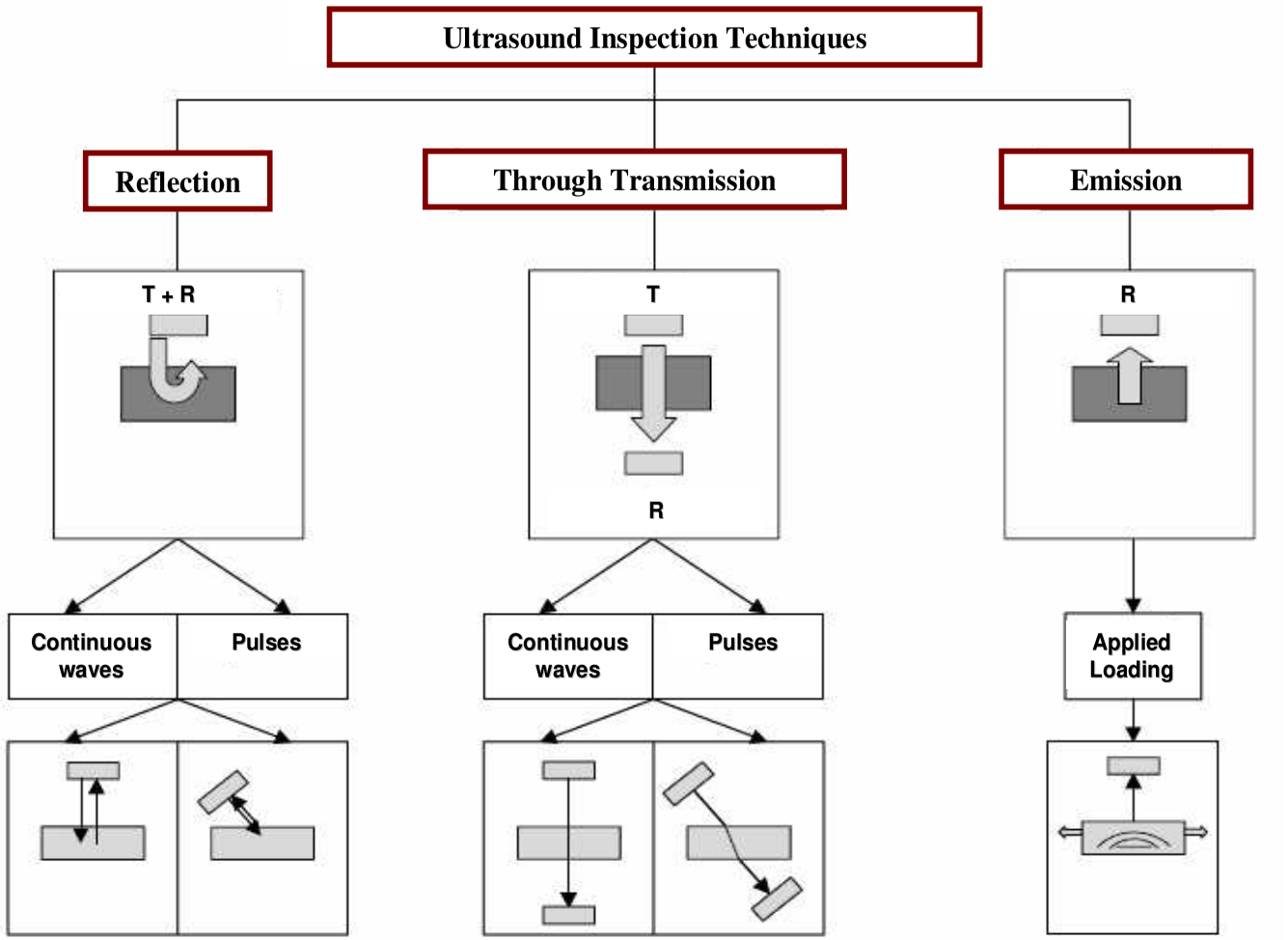

Figure 5.7. Ultrasound inspection techniques and modes of operation

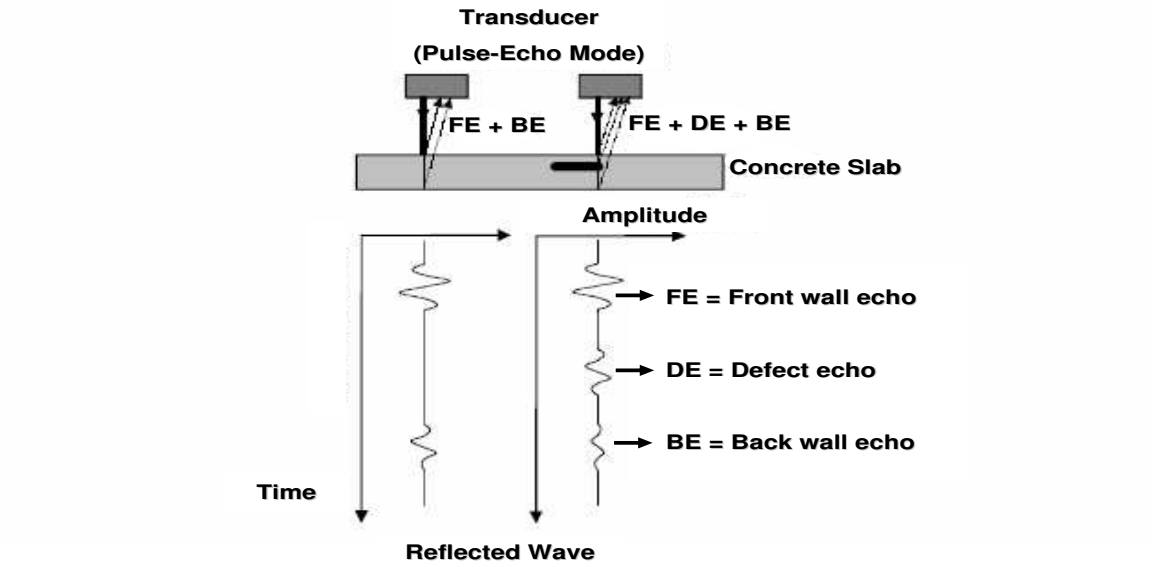

Figure 5.8. Schematic of reflection technique in pulse-echo mode

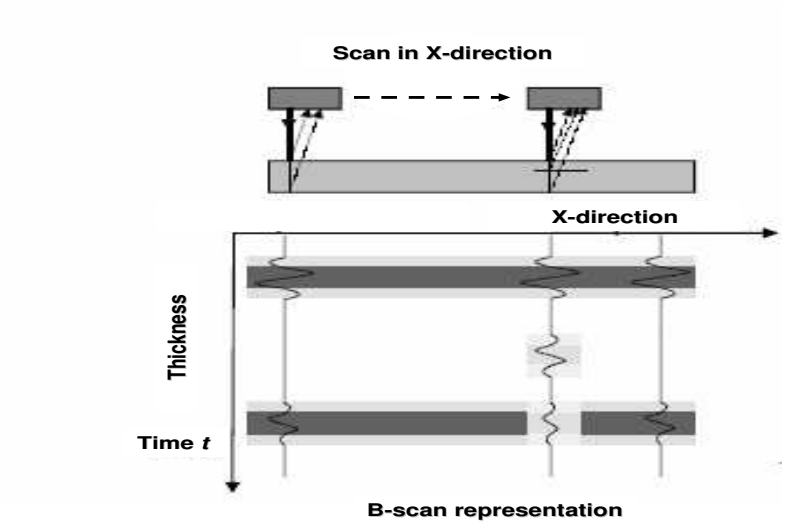

Figure 5.9. B-scan representation.

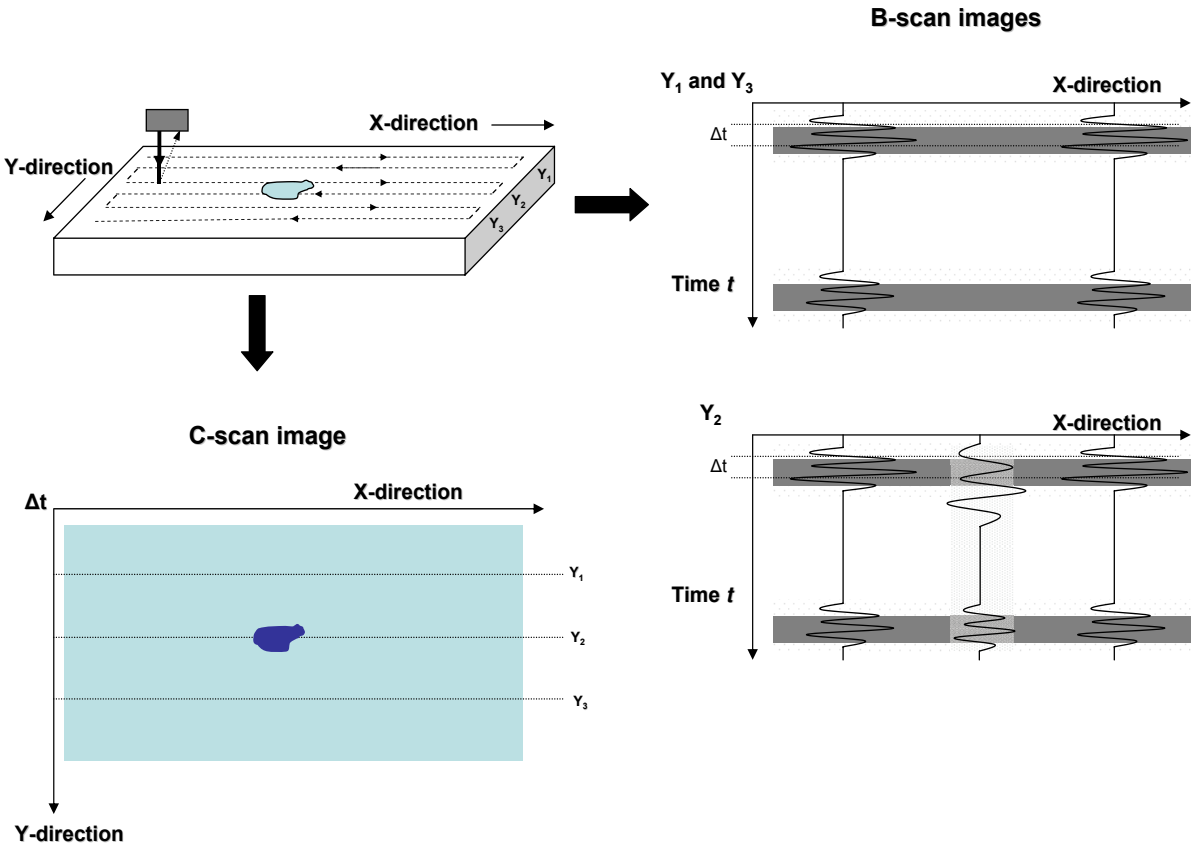

Figure 5.10. Process of generating a C-scan image. The region of interest is scanned and either a B-scan (right)or A-scans are mapped by gating a particular time range. The change in amplitude with a time range Δt is displayed in a C-scan image for all points scanned in the x-y plane.

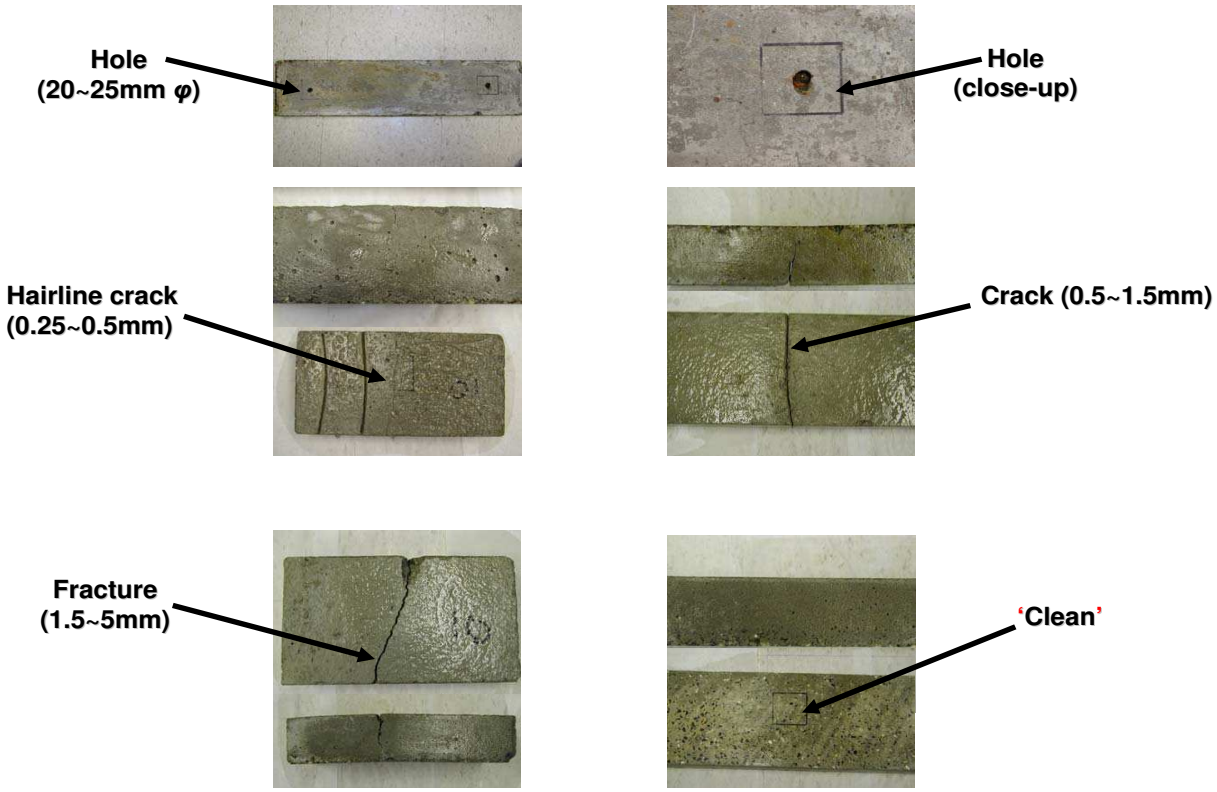

Figure 5.11. Concrete slabs with defects used for experimental data collection. All concrete slabs are 460 mm x 150 mm x 60 mm.

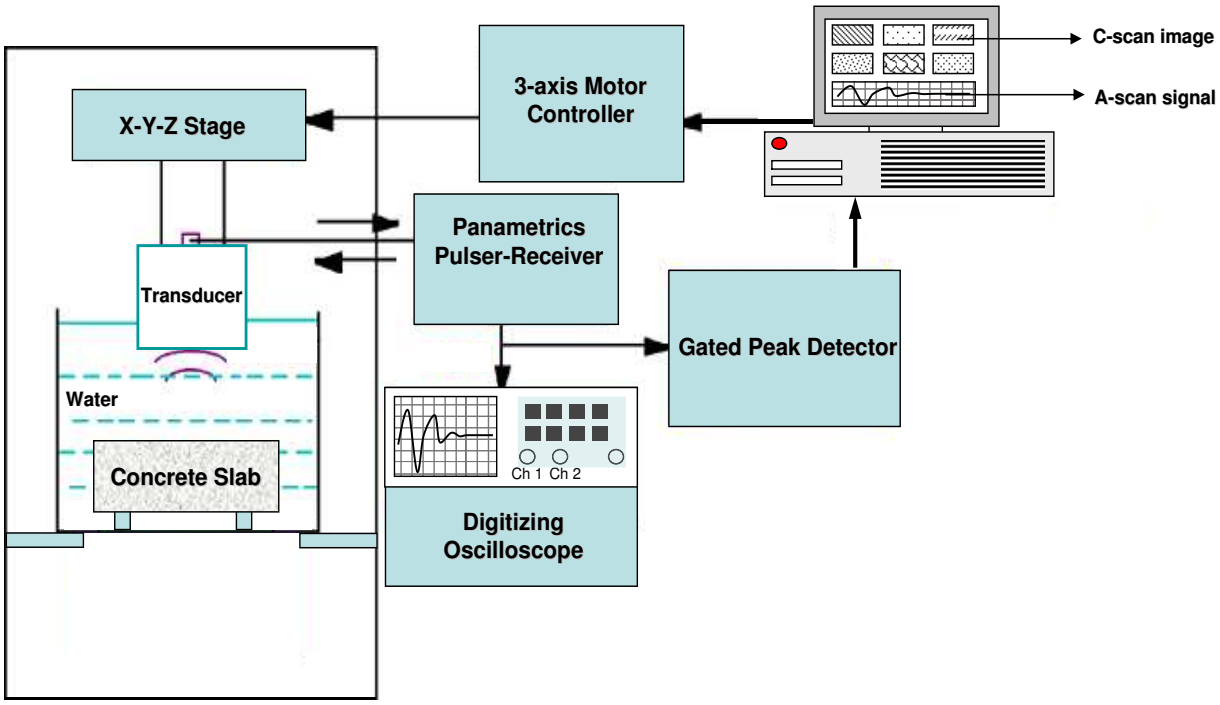

Figure 5.12. Block diagram of experimental setup

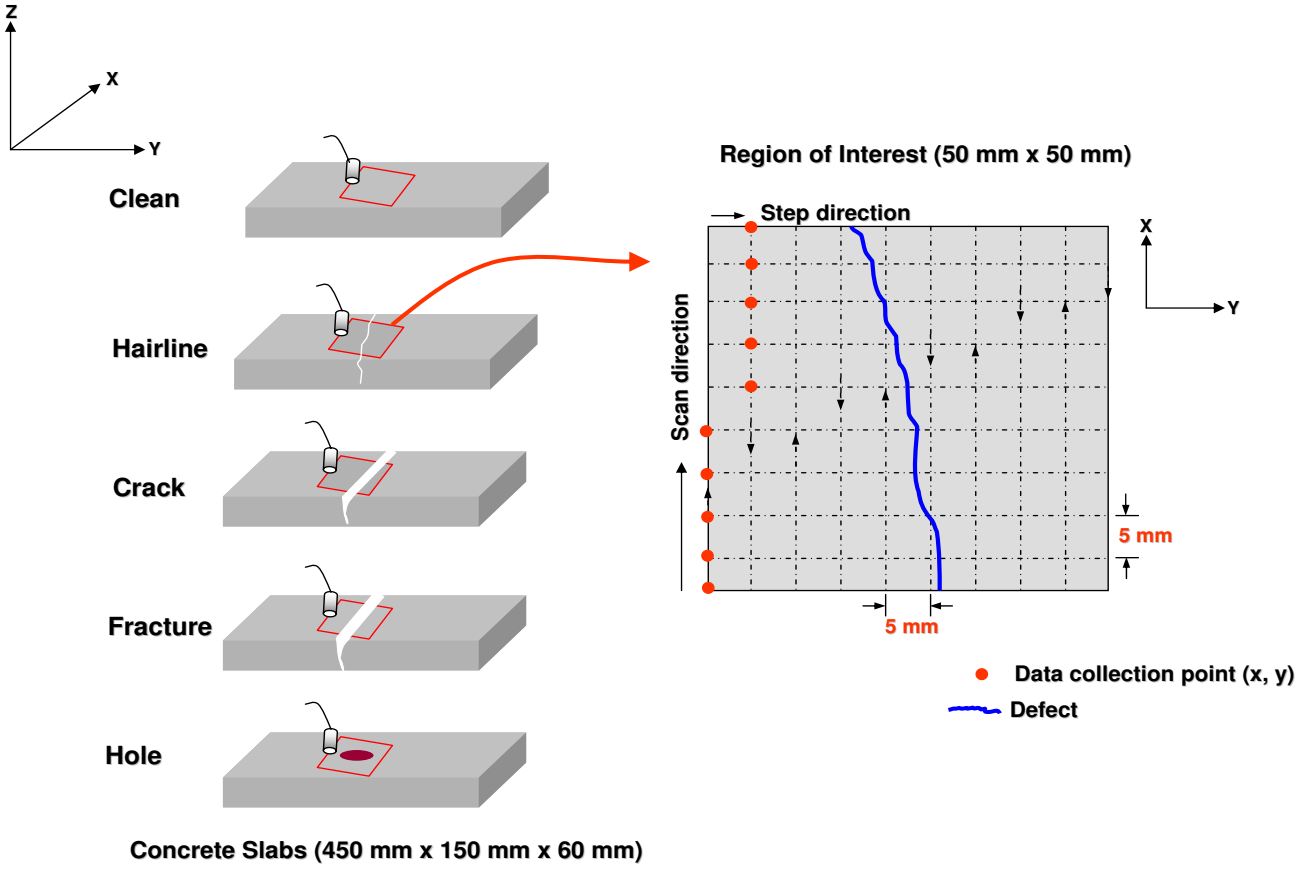

Figure 5.13. Experimental data collection scheme

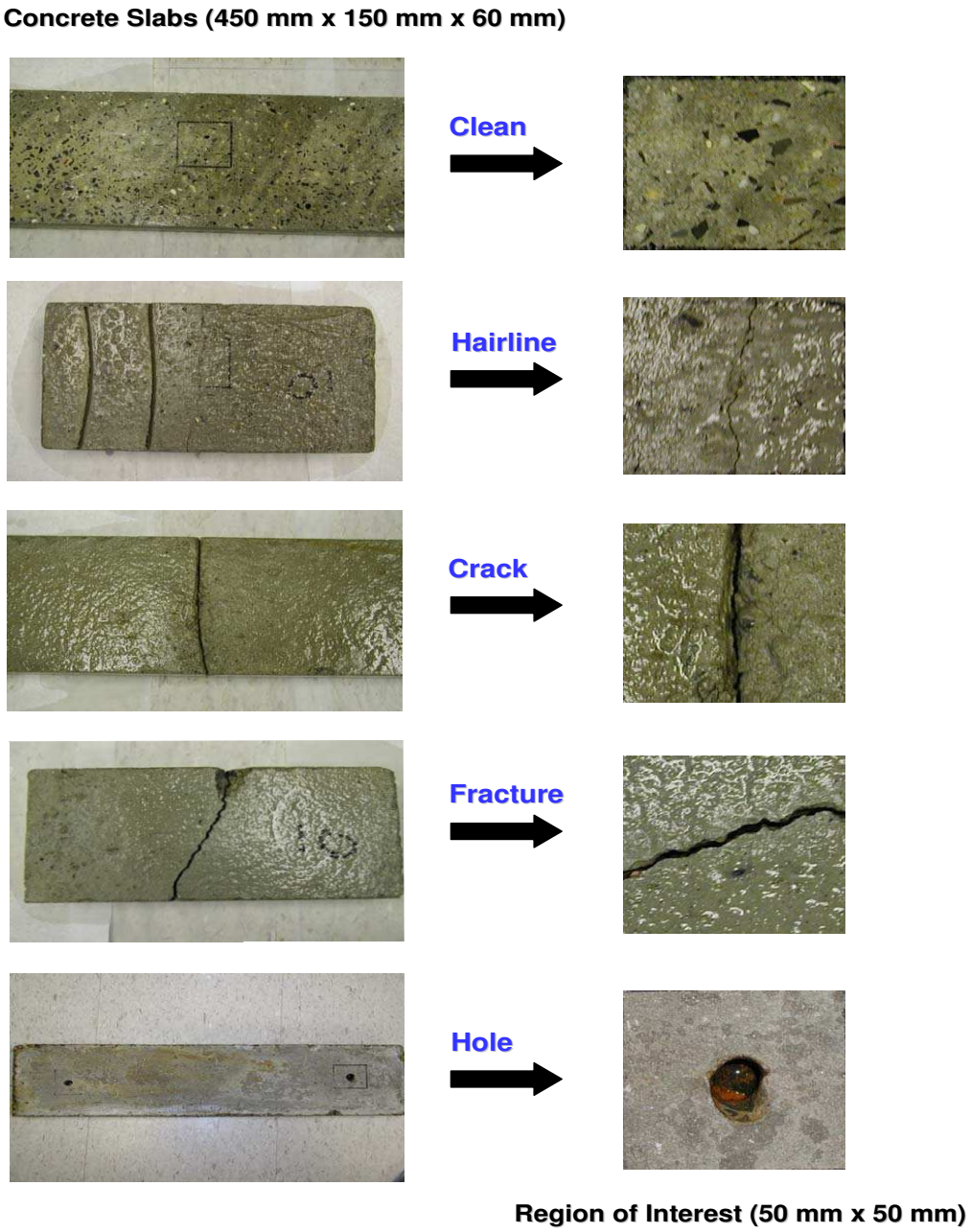

Figure 5.14. Close up view of Region of Interest (ROI) for all concrete samples

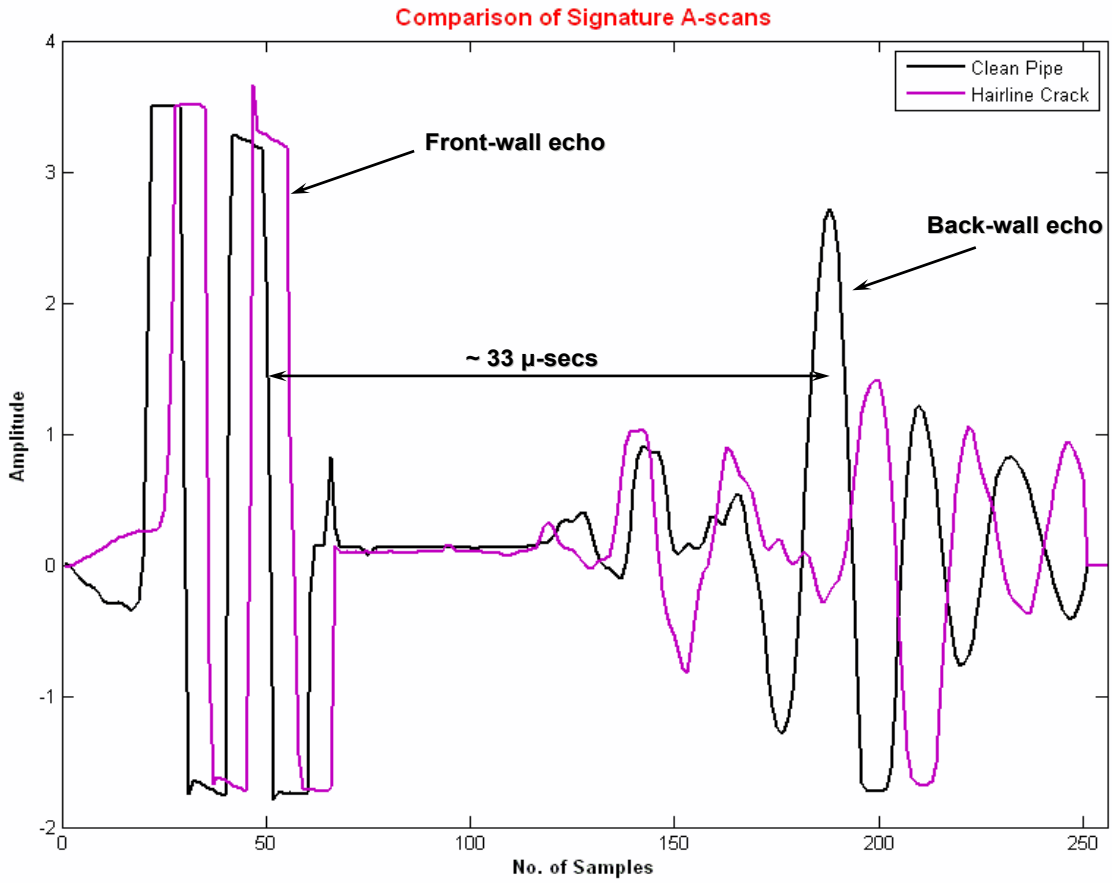

Figure 5.15. Comparison of A-scan signatures - Clean vs Hairline

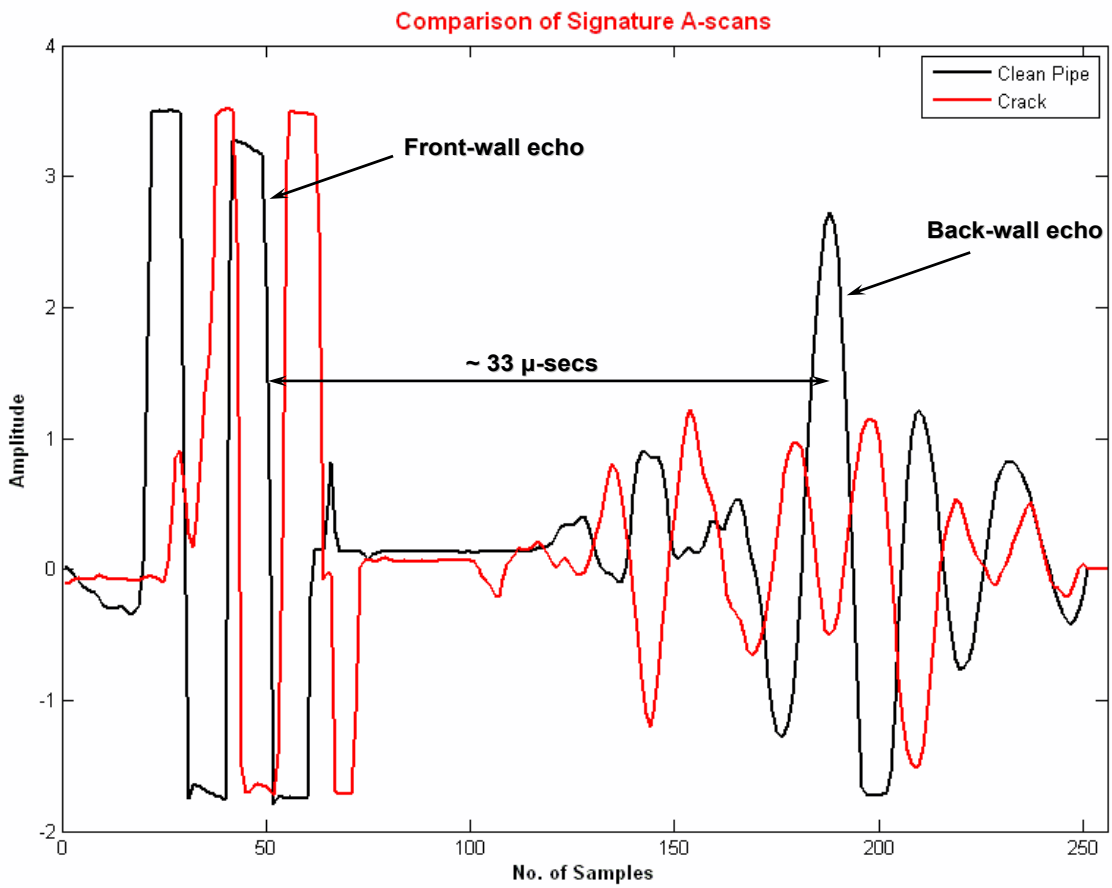

Figure 5.16. Comparison of A-scan signatures - Clean vs Crack

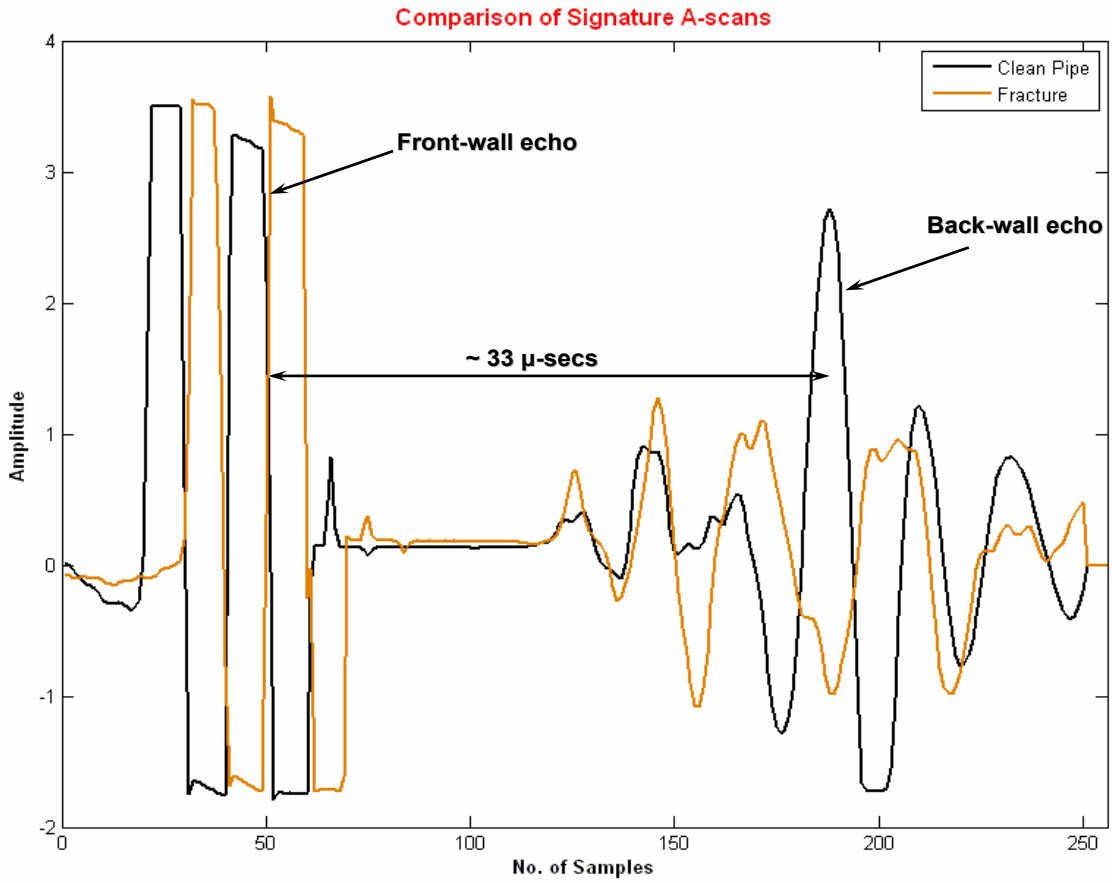

Figure 5.17. Comparison of A-scan signatures - Clean vs Fracture

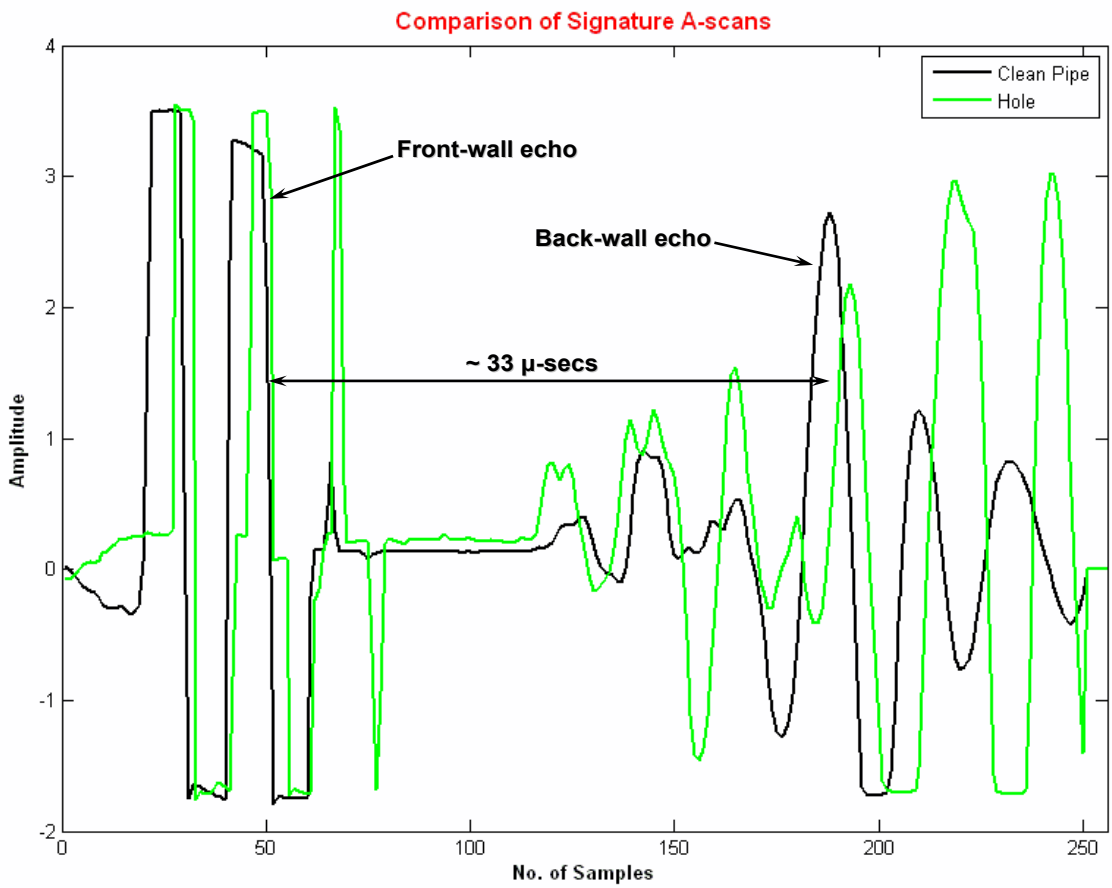

Figure 5.18. Comparison of A-scan signatures - Clean vs Hole

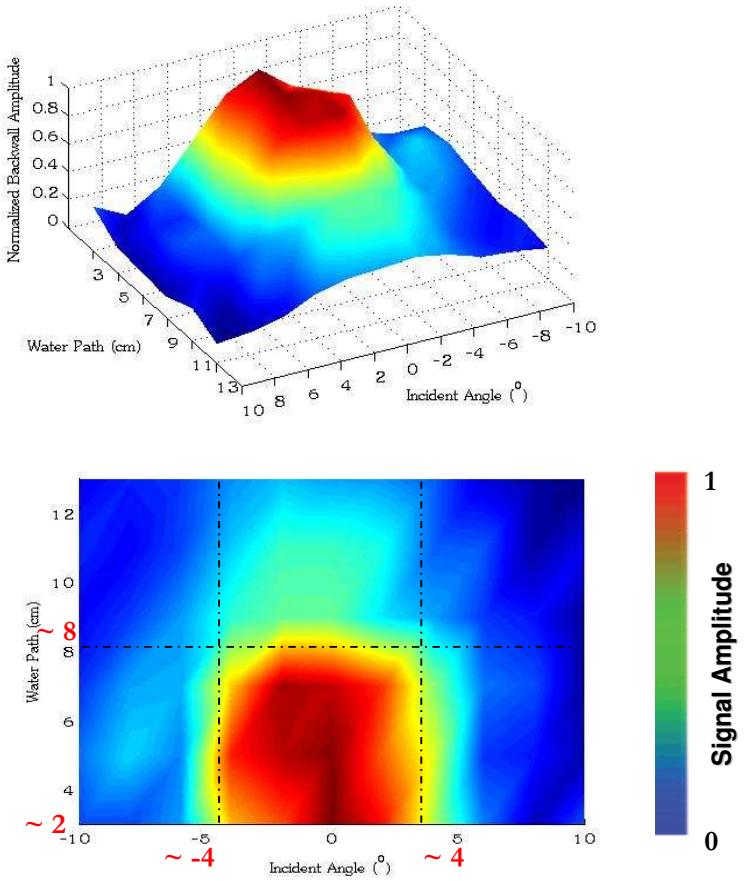

Figure 5.19. Plot of back-wall signal amplitude as a function of angle sensitivity and liftoff distance

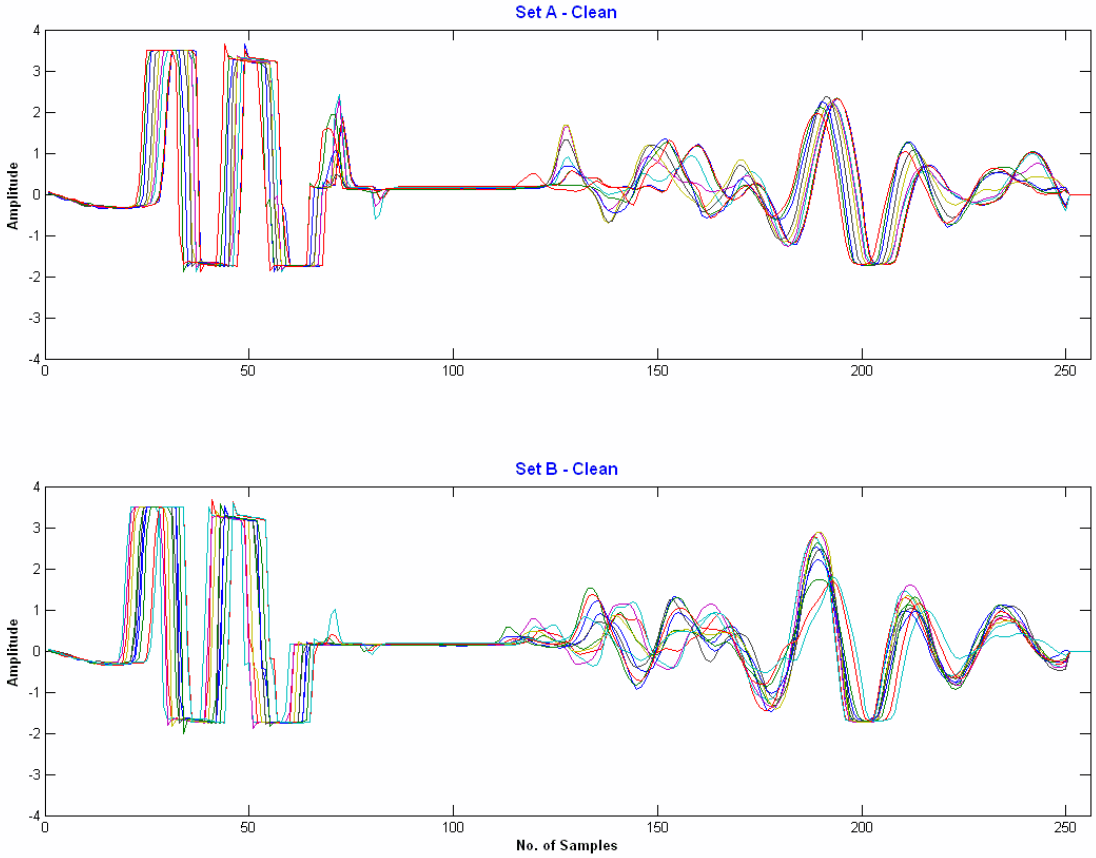

Figure 5.20. Comparison of Set A and Set B A-scans for Clean sample

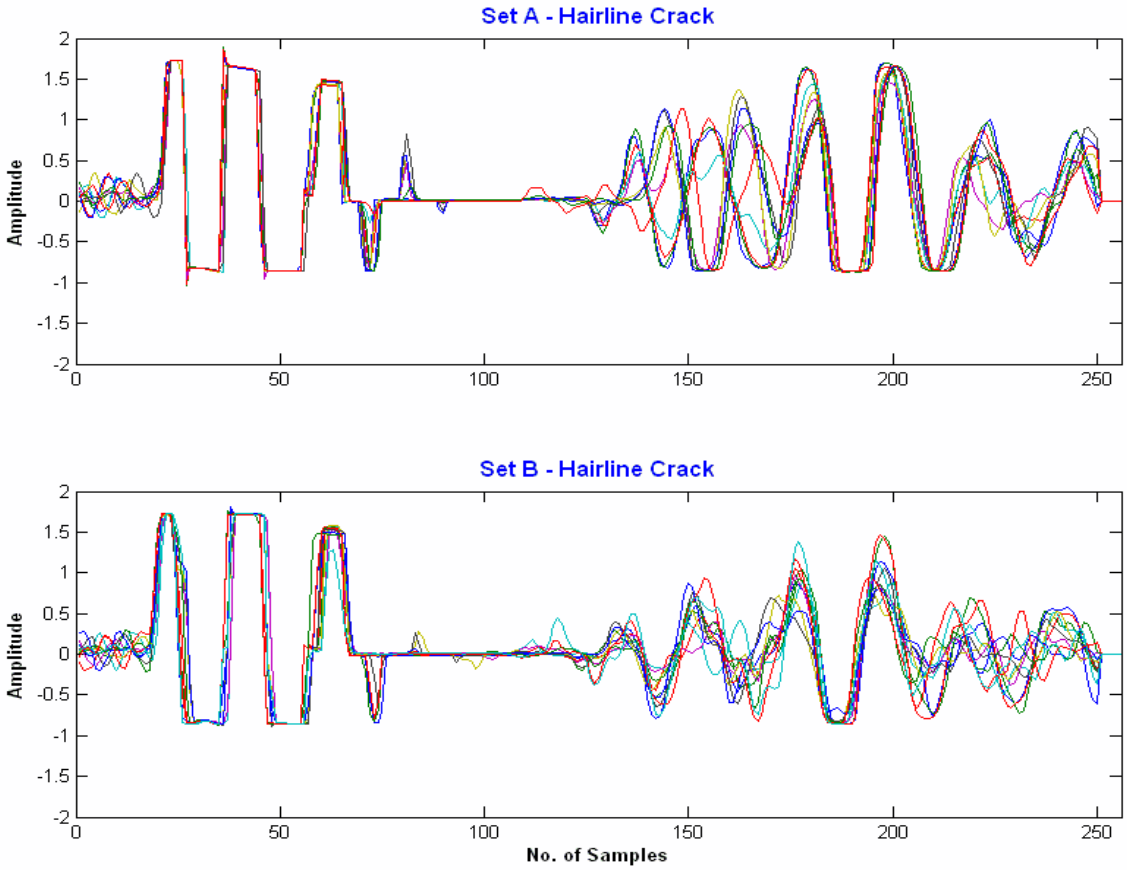

Figure 5.21. Comparison of Set A and Set B A-scans for Hairline Crack sample

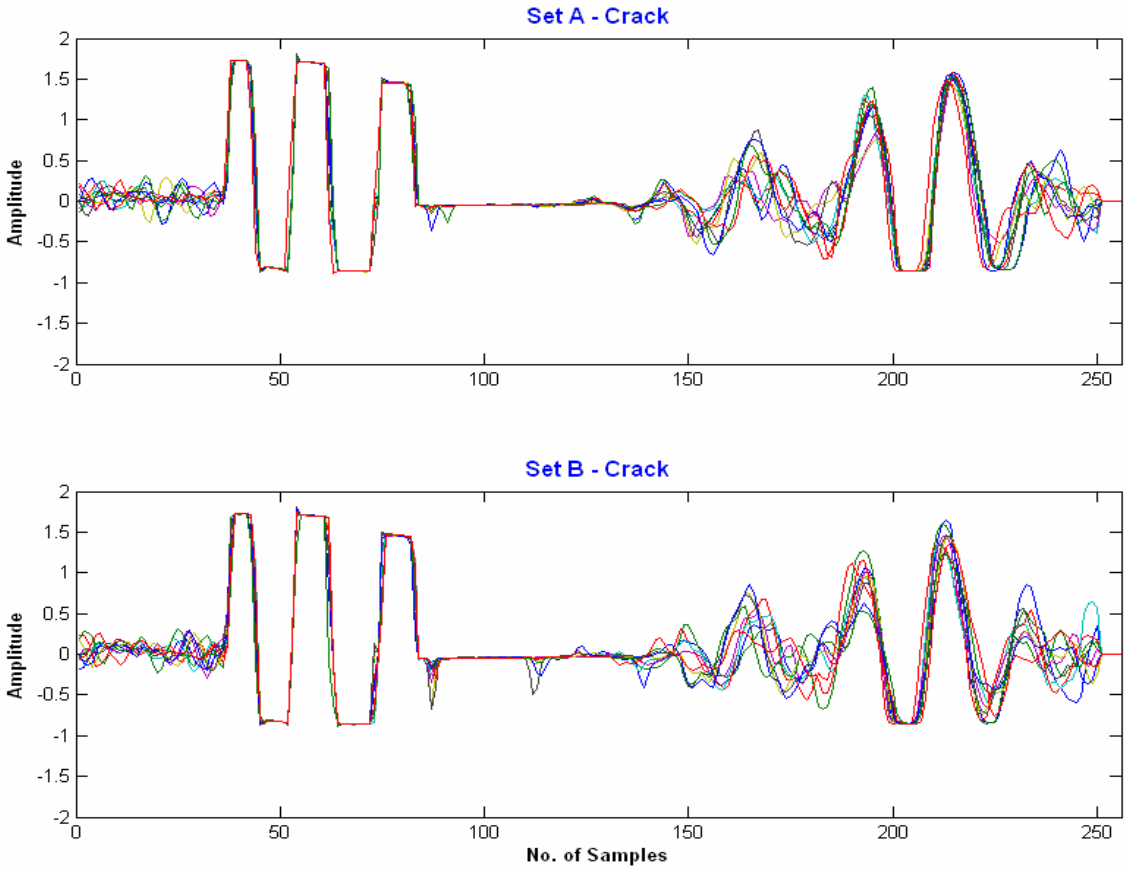

Figure 5.22. Comparison of Set A and Set B A-scans for Crack sample

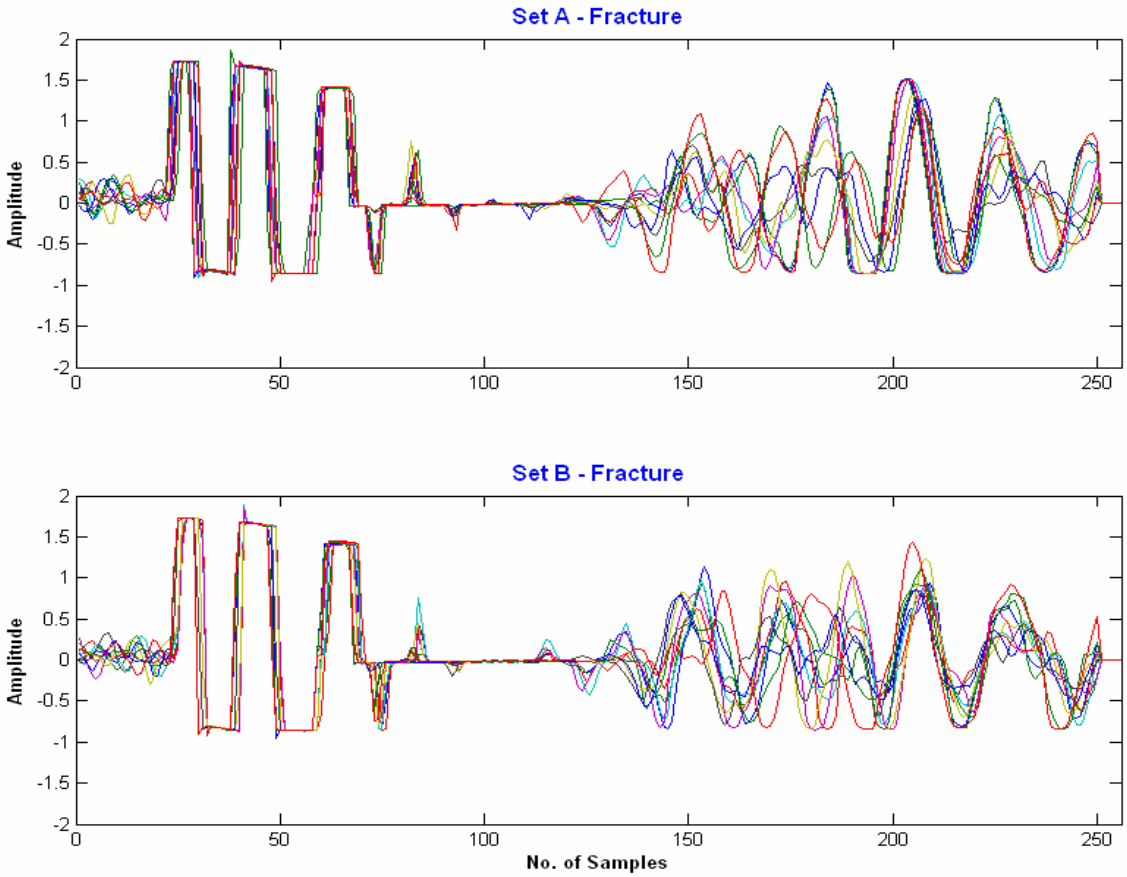

Figure 5.23. Comparison of Set A and Set B A-scans for Fracture sample

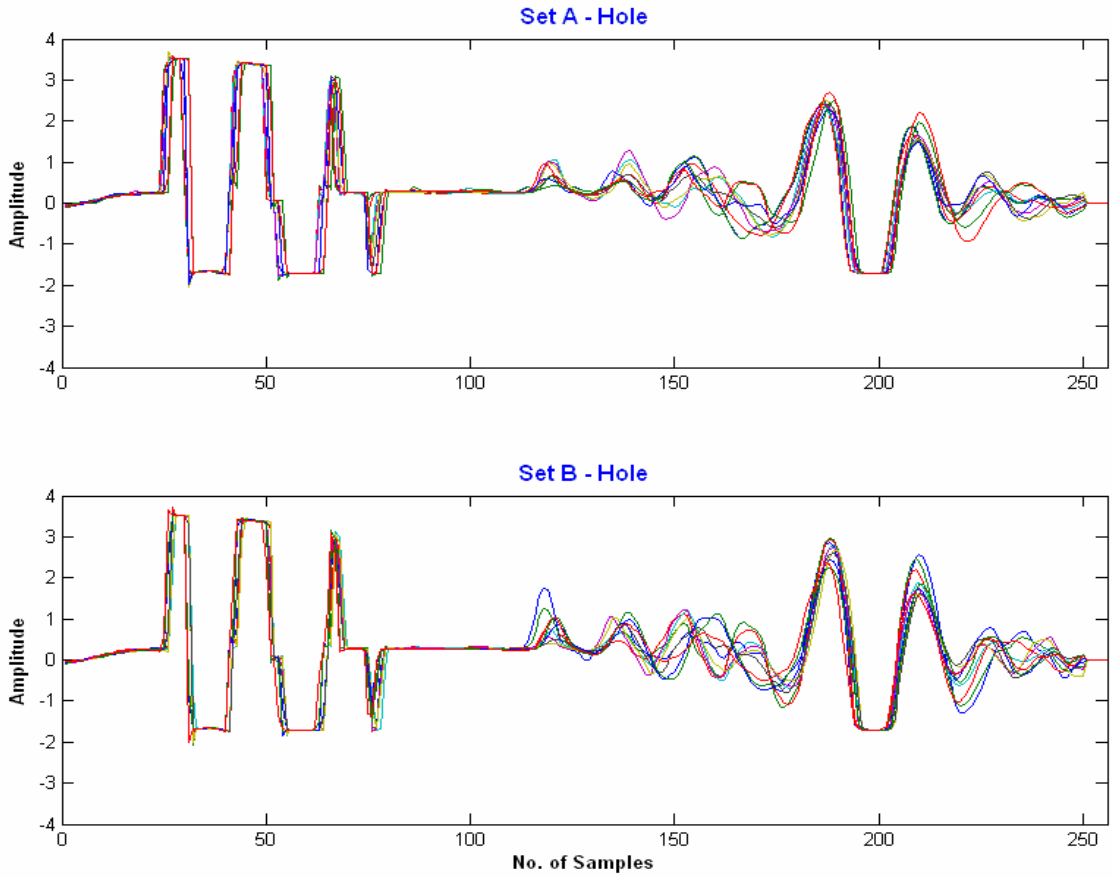

Figure 5.24. Comparison of Set A and Set B A-scans for Hole sample

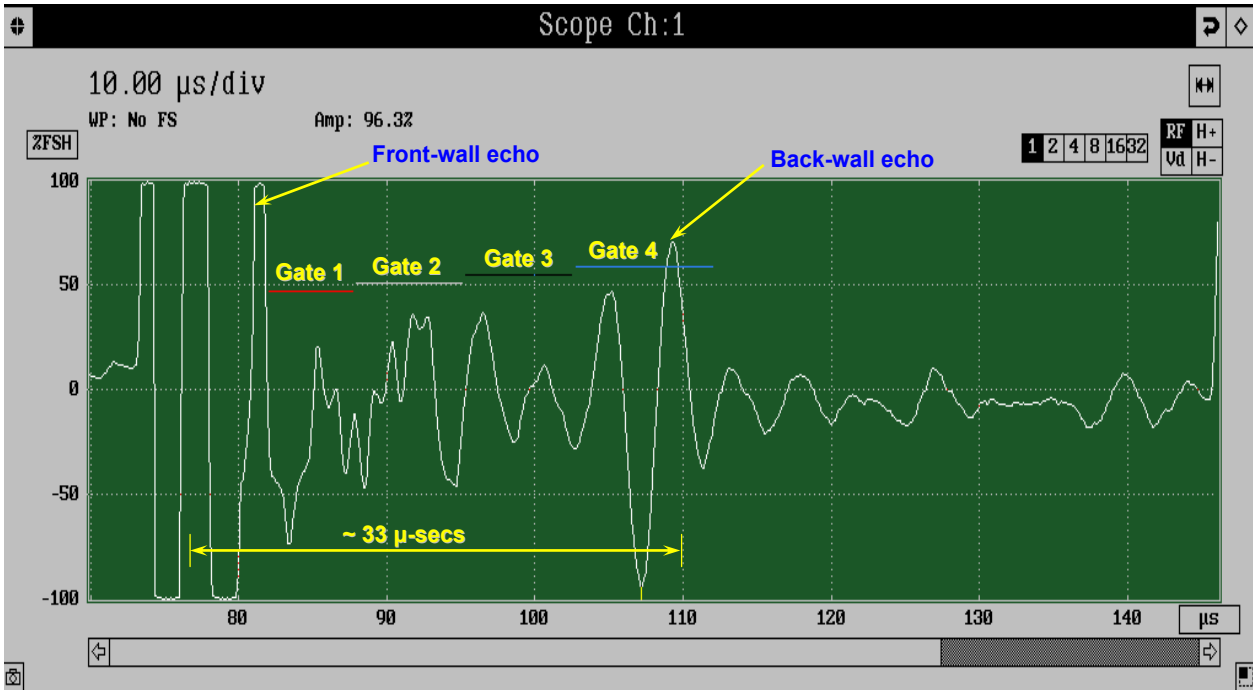

Figure 5.25. A-scan time trace with time window (gate) locations for C-scan imaging

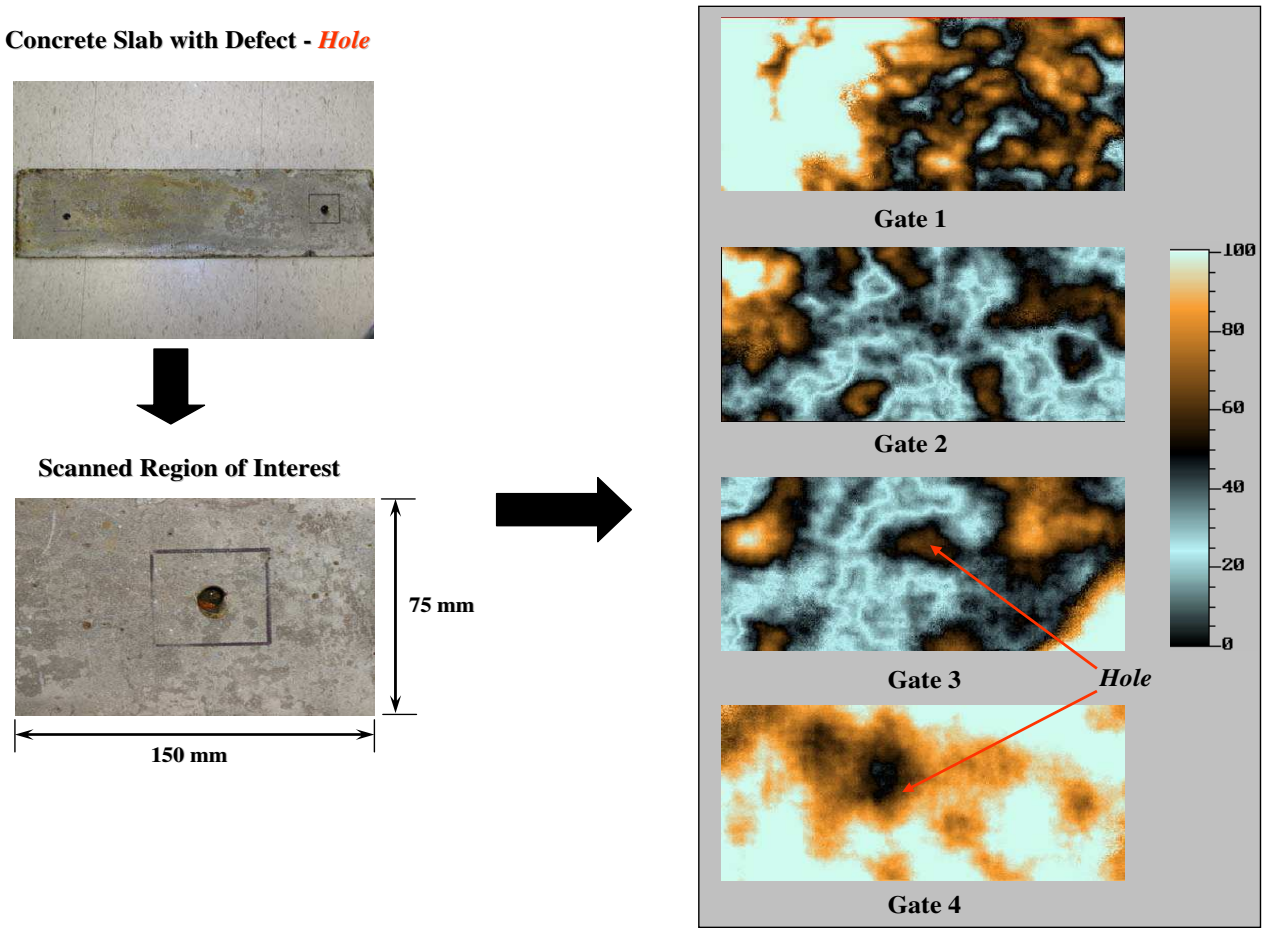

Figure 5.26. C-scan image slices - Hole defect

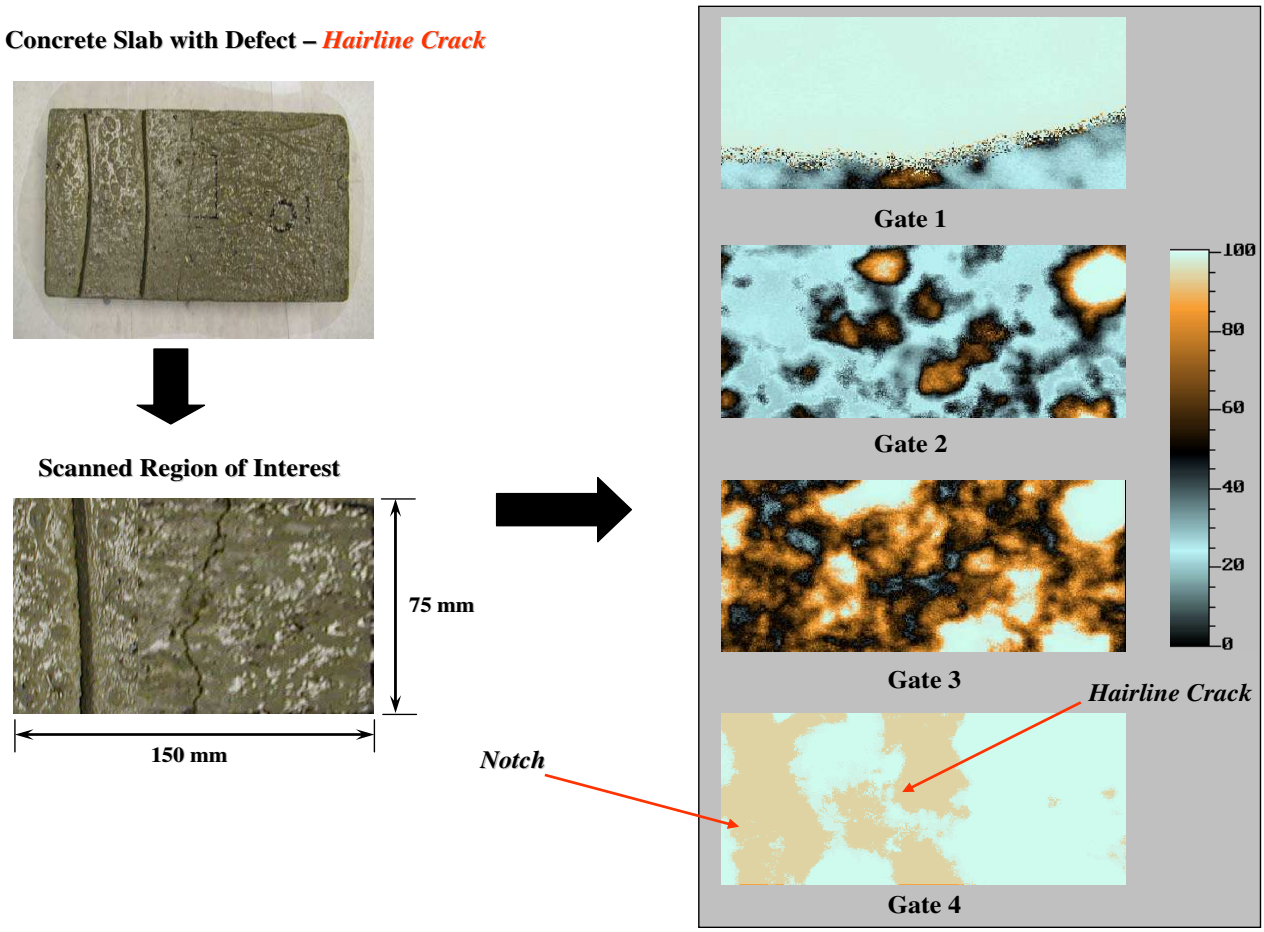

Figure 5.27. C-scan image slices - Hairline defect

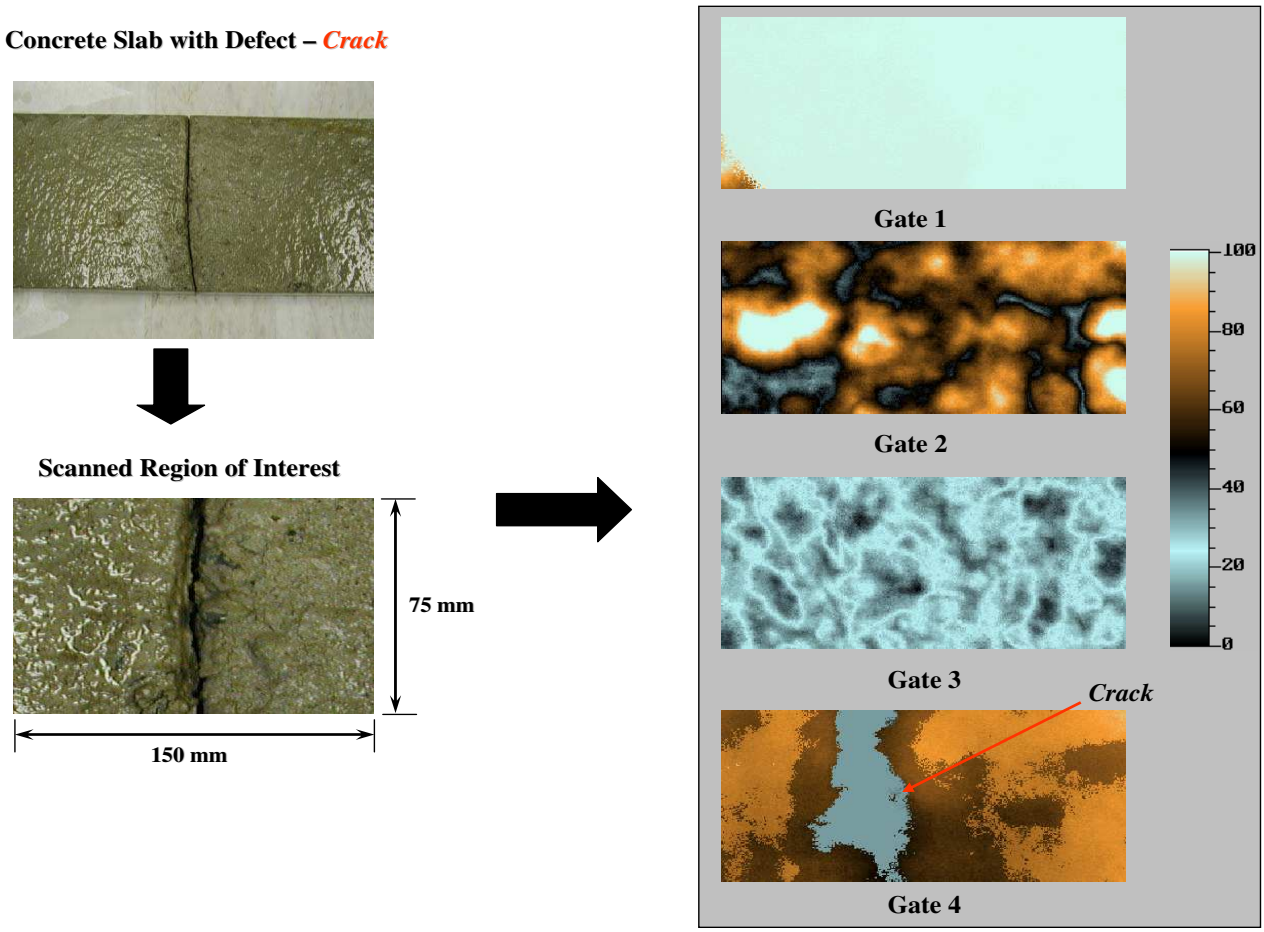

Figure 5.28. C-scan image slices - Crack defect

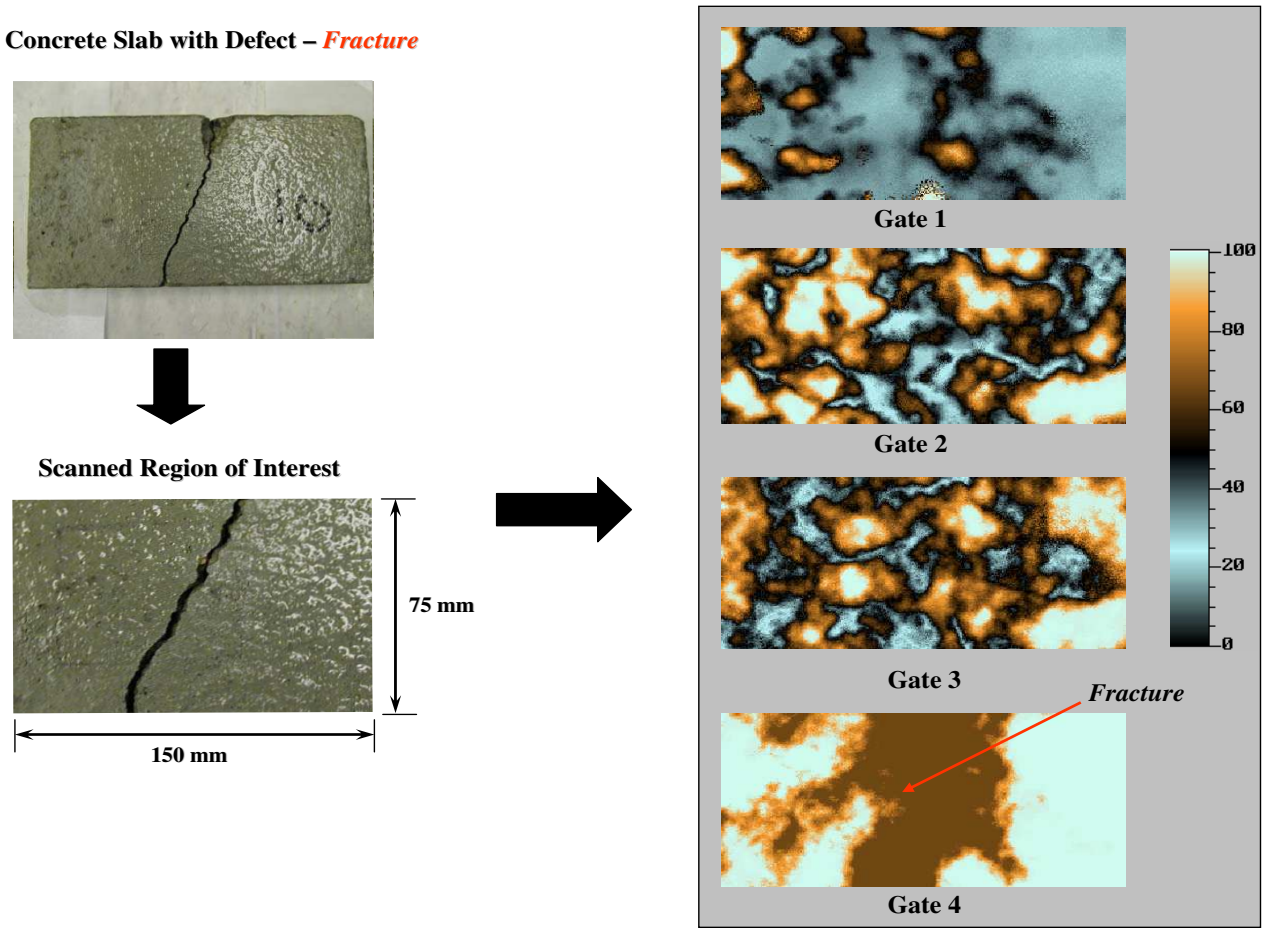

Figure 5.29. C-scan image slices - Fracture defect

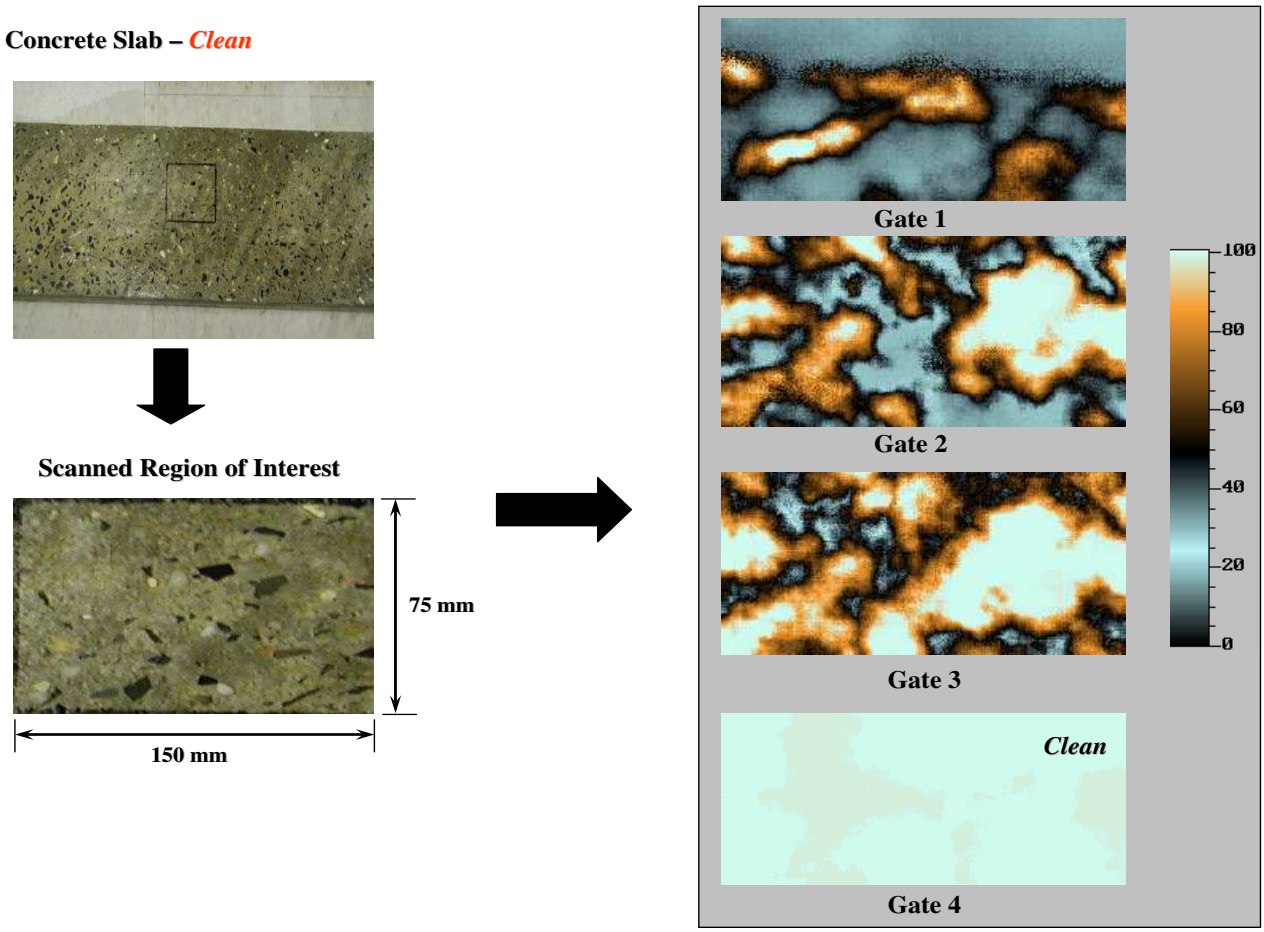

Figure 5.30. C-scan image slices - Clean sample

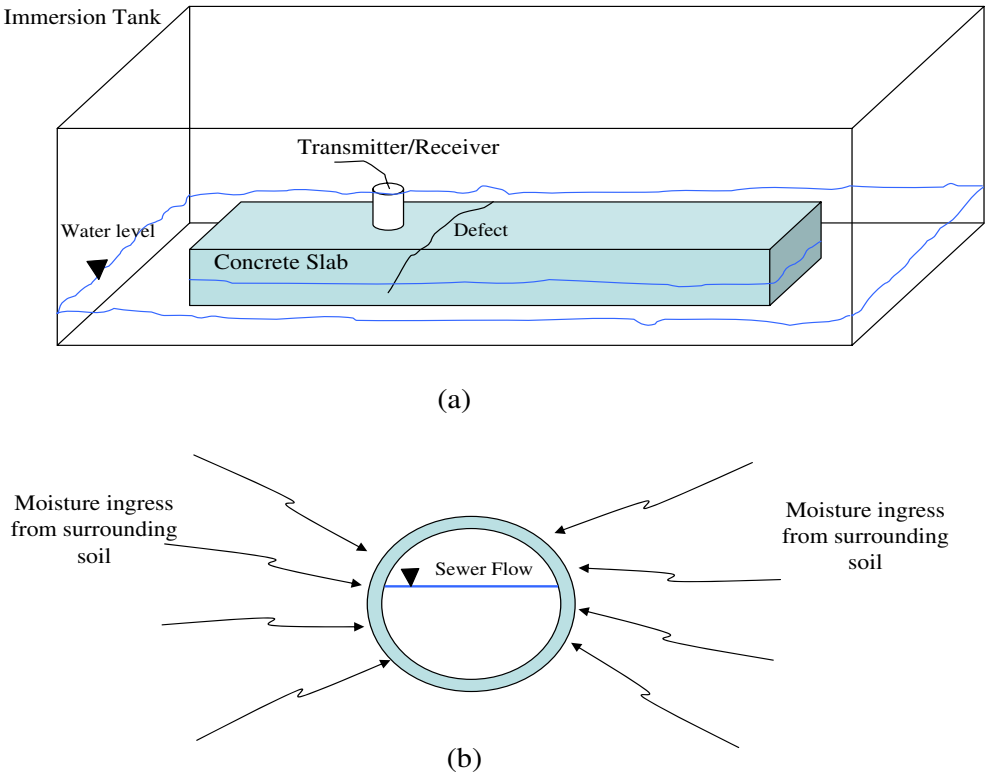

Figure 5.31. Pipe saturation experiments

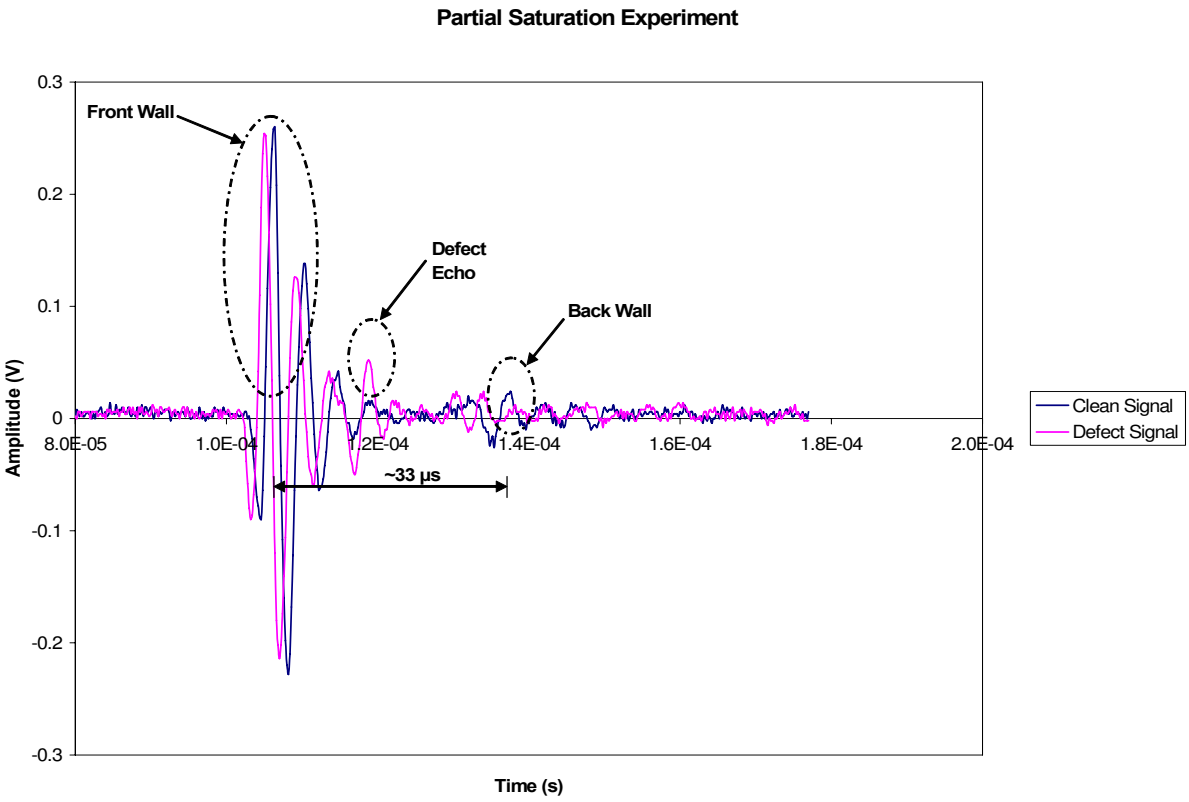

Figure 5.32. Signals from partially saturated concrete slab

Chapter 6

Feature Extraction And Classification of Ultrasonic Signals

6.1 Introduction

Predictive modeling is at the heart of supervised machine learning. It refers to a branch of computer science interested in reproducing human "learning" capabilities with computer programs. Machine learning research has mostly focused on finding relationships in data and analyzing the processes for extracting such relations, rather than building truly intelligent systems (Guyon et al., 2004). Machine learning problems occur when a task is defined by a series of cases or examples rather than by predefined rules. Such problems are found in a wide variety of application domains, ranging from engineering applications in robotics and pattern recognition (speech, handwriting, face, anomaly recognition), to Internet applications (text categorization) and medical applications (diagnosis, prognosis, drug discovery). Given a number of "training" examples (also called data points, samples, patterns or observations) associated with desired outcomes, the machine learning process consists of finding the relationship between the patterns and the outcomes using solely the training examples (Jain et al., 2000). This shares a lot with human learning where humans are given examples of what is correct and what is not and have to infer which rule underlies the decision. Thus, a machine learning system "learns" the relationship between the input (training data points) and the pattern

(or class) to which it belongs. It is then called upon to predict the pattern of a "new" input (test data) based on its learning of the problem inference rules. The performance on test data is called "generalization". To perform this task, one must build a predictive model or predictor, which is typically a function with adjustable parameters called a "learning machine". The training examples are used to select an optimum set of parameters. The higher the generalization of the predictive model, the better its performance. Thus, selection of features of the input data used for prediction plays a key role in machine learning generalization (Duda et al., 2000).

Machine learning systems perform two main functions, *feature extraction* and *classification*. Over the last past few decades, extensive research has taken place in the development of efficient and reliable methods for the selection of features in the design of machine learning systems, where features constitute inputs to the classifiers (Mukherjee and Pal, 2005). The quality of performance of this design depends upon the relevance, discriminatory information and ease of computation of various features. Another important issue in classification is the choice of an appropriate classifier. Some classical classifiers are Fisher's linear discriminant and K-Nearest Neighbors (K-NN). Recently, state-of-the-art classifiers like neural networks, neuro-fuzzy classifiers, tree classifiers and Support Vector Machines (SVM) are finding widespread applications. Many researchers in the civil infrastructure area have paid a great deal of attention to automated pavement cracking classification (Cheng and Miyogim, 1998, Cheng et al., 1999). Chou et al (1995) employed a fuzzy filtering image enhancement and fuzzy thresholding approach based on the maximum fuzzy entropies to generate features that were used to train a neural network (Chou et al., 1995). Automated real-time pavement distress detection using fuzzy logic and neural networks was studied using fuzzy homogeneity for image enhancement and feature extraction (Cheng, 1996). This methodology demonstrated the potential of using neural networks for classification and quantification of cracking on pavement although it requires further improvement of the image segmentation process for this particular application. However, in practice, most of the above approaches have been only partially successful and have been shown to produce high false-alarm rates, probably because of an inadequate image feature

segmentation approach. Shin and Kil (1997) used a combination of statistical classifiers and expert systems to develop an automated road-distress identification and classification system based on subimage and object processing. They used a combination of the multivariate Gaussian and probabilistic neural network classifiers, depending on the actual class-conditional feature distribution of the subimage pixels (Kil and Shin, 1997).Again, they had a high false alarm rate of 79%.

In buried concrete pipe defect analysis, the main objective is to identify and classify regions of the pipe as "clean" or "defective". Further classification of defects into various sub-classes like hole, fracture, crack and hairline crack is possible based on the type of information available. Sinha (2000) has shown that defects in buried pipe can be accurately classified into cracks, holes, laterals, joints and pipe collapse by type, severity and extent of distress based on CCTV inspection images of the internal surface of the pipe (Sinha, 2000). In this study, time series signals from the region of interest are considered instead of 2-D images for defect detection and classification. Thus, a multi-layer perceptron (MLP) neural network classifier that uses discriminatory features computed by clustering the discrete wavelet transform (DWT) coefficients of the input time series signal is proposed. The proposed approach uses wavelet analysis to decompose the signal into its useful information components and then employs an unsupervised clustering scheme to extract feature vectors that represent the class of the signal. The MLP classifier classifies the signal into its appropriate class based on extracted features of interest. The overall scheme is shown in figure 6.1. Final classification of the region of interest is done by fusing the classifier response and *apriori* knowledge about the problem characteristics through a post processing step. This step is necessary as the inspection system is envisioned as a two step approach.

6.2 Feature Extraction

Feature extraction is an important stage for any pattern recognition task especially for concrete pipe defect classification, since defects in concrete are highly variable and it is difficult to find reliable and robust features in the signal domain. Ultrasound signals contain reflections from discontinuities which manifest in the A-scans

as abrupt time localized changes resulting in time varying spectral characteristics. The Fourier transform (FT), which converts time series signals into the frequency domain, has been commonly applied to the signal processing of ultrasound signals for various problems (Smith, 1997). However, the time axis information in signals is lost by the FT. Consequently, the conventional Fourier decomposition technique is not an appropriate tool for analyzing these signals. The discrete wavelet transform is a multiresolution analysis technique used to obtain the time-frequency representation of a signal. These representations are used to analyze time localized signals with time-varying spectra, where conventional Fourier transform analysis methods prove to be inadequate. These limitations led to the development of wavelet analysis by Mallat (1989), Daubechies (1992), Chui (1992), and Meyer (1993) (Mallat, 1989, Daubechies, 1992, Chui, 1992, Meyer, 1993). Subsequently, it was applied to solve problems in signal processing for nondestructive testing and medical imaging (Lefebvre and Lasaygues, 1994, Abbate et al., 1997, Unser et al., 2005). The following sections briefly introduce wavelet transforms and the proposed clustered discrete wavelet transform (DWT) based feature extraction technique. Furthermore, two other DWT based feature extraction techniques are also discussed for comparison purposes.

6.2.1 Clustered Discrete Wavelet Transform Based Feature Extraction

In this section, the theoretical basis for wavelet analysis and the clustering approach is briefly discussed. Then, the proposed approach combining both, to extract features from a set or representative A-scan signals for defect classification is presented.

6.2.1.1 Discrete Wavelet Transform

The wavelet transform is like a filter that extracts frequency components from the signal without losing time axis information. The continuous wavelet transform is defined as:

$$W_x^{\psi}(\tau, s) = \frac{1}{\sqrt{|s|}} \int x(t)\psi^* \left(\frac{t-\tau}{s}\right) dt \tag{6.1}$$

where the transformed signal $W_x^{\psi}(\tau, s)$ is a function of two variables, translation τ, and scale s. $\psi(t)$ is a transformation function called the mother wavelet and $\psi^*(.)$ is the complex conjugate of $\psi(t)$. By scaling and translating the mother wavelet, components similar to that of the mother wavelet at a particular scale and time can be obtained from the signal. Thus, the wavelet transform represents the correlation between the signal *x(t)* and the scaled versions of a prototype function, i.e. the mother wavelet function. The scaling of the mother wavelet involves contraction and dilation of the signal and translation involves shifting the wavelet function along the time axis. One of the properties of this transform is that it is covariant under dilations. In other words, variations in the time domain of a signal are appropriately represented in the wavelet transform domain. This property of the transform makes it a very valuable tool for analysis of non-stationary signals (like ultrasound acoustic A-scan signals) because it is capable of analyzing hierarchical structures. It is like a mathematical microscope with properties that are independent of magnification. Calculating wavelet coefficients at every possible scale generates a lot of data. It turns out, that if scales and translations are chosen based on powers of two – so-called dyadic scales and translations, the analysis is much more efficient and just as accurate with fewer computation time and data generation. Such an analysis is possible through the discrete wavelet transform (DWT).

The discrete wavelet transform (DWT) is a fast algorithm that is used to obtain the wavelet transform of a discrete time signal. For a discrete time signal represented by 2^n samples, the DWT may be considered to simply pair up input values, storing the difference and passing the sum. This process is repeated recursively, pairing up the sums to provide the next scale: finally resulting in 2^n - 1 differences and one final sum. The discrete transform can be performed in O(n) operations. Moreover, the transform captures not only some notion of the frequency content of the input, by examining it at different scales, but also captures temporal content, i.e. the times at which these frequencies occur. These two properties make the discrete wavelet transform (DWT), an alternative to the conventional fast fourier transform (FFT). An efficient way to implement this scheme using filters was developed in 1988 by Mallat. The Mallat algorithm is in fact a classical scheme known

in the signal processing community as a two-channel subband coder (Strang and Nyugen, 1996). An extensive discussion on discrete wavelet transform and the theory of multiresolution analysis is presented in Strang and Nguyen (1996), Chui (1992), Mallat (1989), and Daubechies (1992) (Strang and Nyugen, 1996, Chui, 1992, Mallat, 1989, Daubechies, 1992). In this study, the DWT implementation is done using the subband coding technique and hence will be described in greater detail.

The DWT of a signal 'x[n]' is calculated by passing it through a series of filters. First the samples are passed through a low pass filter with impulse response 'g[n]' resulting in a convolution of the two:

$$y[n] = (x * g)[n] = \sum_{k=-\infty}^{\infty} x[k] \cdot g[n-k] \tag{6.2}$$

The signal is also decomposed simultaneously using a high-pass filter 'h[n]'. The outputs giving the detail coefficients (from the high-pass filter) and approximation coefficients (from the low-pass). It is important that the two filters be related to each other and so they are known as a quadrature mirror filter. However, since half the frequencies of the signal have now been removed, half the samples can be discarded according to Nyquist's rule (Smith, 1997). The filter outputs are then downsampled by 2:

$$y_{\text{low}}[n] = \sum_{k=-\infty}^{\infty} x[k] \cdot h[2 \cdot n - k] \tag{6.3}$$

$$y_{\text{high}}[n] = \sum_{k=-\infty}^{\infty} x[k] \cdot g[2 \cdot n - k] \tag{6.4}$$

where $y_{\text{low}}[n]$ and $y_{\text{high}}[n]$ are the outputs of the highpass and lowpass filters. This decomposition in effect halves the time resolution and doubles the frequency resolution as the frequency band of the signal now spans only half the previous frequency band. The above procedure is repeated for subsequent decompositions of the low-pass filtered signals. The highpass filtered signals constitute the DWT coefficients also known as "detail" coefficients (cD_1, cD_2,.....cD_M). Similarly, at every level, the filtering and downsampling results in half the number of samples spanning half

the frequency band leading to reduced time and improved frequency resolutions. The subband coding scheme for computation of DWT coefficients is illustrated in figure 6.2. 'x[n]' is the original A-scan signal to be decomposed, and 'h[n]' and 'g[n]' represent discrete wavelet lowpass and highpass filters respectively. The bandwidth of the resulting signal at every level is indicated by f as shown in figure 6.2. This procedure in effect provides better time resolution at higher frequencies and better frequency resolution at lower frequencies. Ultrasonic signals are nonstationary in nature and hence, subband coding provides an effective way of obtaining time-frequency representation that is not possible in fourier transforms.The DWT coefficients at different levels are concatenated starting with the coarsest coefficients (last level). As for example, a time series signal with 256 sample points will have 128 samples (or detail coefficients) at the first level (highest resolution), 64 samples at the second level, 32 at the third level, and so on. This algorithm requires that the signal be sampled such that the discrete samples are multiples of a power of two.

6.2.1.2 Clustering Procedure

Recursive application of equations 6.3 and 6.4 lead to a decomposition of signal x[n] into a matrix of sequences cD_1, cD_2,.....cD_M, cA_M as shown in figure 6.3. The index 'm' of a sequence cA_m or cD_m is the scale (or level of decomposition) and the coefficients cA_{mn} and cD_{mn} are called approximation and detail coefficients respectively. They contain the same amount of information as x[n] and have the property:

$$\|x[n]\|^2 = \|cA_M\|^2 + \sum_{m=1}^{M} \|d_m\|^2 \tag{6.5}$$

The computed coefficients in these sequences form the wavelet decomposition of the measured signal x[n]. As a preparation step to feature extraction from this discrete wavelet coefficient matrix, the coefficients are grouped into clusters in an unsupervised mode. These clusters are formed by using a set of representative signals (for e.g., A-scan signatures from all defect samples) also known as 'training' data set used to train the classifier. This clustering procedure divides the discrete wavelet coefficient matrix shown in figure 6.3 into disjoint clusters C_1, C_2, ..., C_c for each of which a single robust feature F_i (i = 1,2, ..., c) can be computed. The

feature vector so obtained serves as an input pattern to the multi-layer perceptron (MLP) neural network classifier.

The clustering method uses a set of 'S' training data signals that represent the entire spectrum of possible defect classes to determine the boundaries of the clusters in an unsupervised mode (Pittner and Kamarthi, 1999). First, the discrete wavelet transform is computed for all 'S' training data signals. The wavelet coefficients contained in the sequences cD_1, cD_2,.....cD_M, cA_M are arranged into a matrix for each individual signal in the training data set as shown in figure 6.3. Each discrete wavelet coefficient matrix is denoted by $A = [a_{ij}]$, i = 1, 2, ..., M + 1; j = 1, 2, ..., (n + N - 1)/2 for even 'n'; and j = 1, 2, ..., (n + N)/2 for odd 'n'. N is some odd natural number. The shaded portion of A is filled with zero-valued elements. The formation of clusters from wavelet coefficients is guided by the implicit assumption that the regions of A containing large-size wavelet coefficients allow better discriminability of the original signals than other regions of B. More details on the mathematical basis of this clustering scheme can be found in Pittner and Kamarthi (1999).

Let the matrix $\tilde{A} := (\|a_{ij}\|)$, constructed from the wavelet coefficients of the S^{th} training data signal, be indexed by $\tilde{A}_s$ where s = 1, 2, ..., S. For any defined matrix P, its sample mean and standard deviation can be denoted by $\mu(P)$ and $\sigma(P)$ respectively. Let I be an identity matrix of the same size as $\tilde{A}$. Let V be an operator that reduces the matrix P by its last row. Then, it so happens that the elements of a new matrix:

$$B = (b_{ij}) := \frac{1}{\sigma\left(V\left(\sum_{s=1}^{S}\tilde{A}_s\right)\right)}\left(\sum_{s=1}^{S}\tilde{A}_s - \mu\left(V\left(\sum_{s=1}^{S}\tilde{A}_s\right)\right)\cdot I\right) \tag{6.6}$$

reflects the size of the absolute values of a "typical wavelet decomposition" of the S selected signals that are treated as training data signals for all defect classes. In other words, the size of the matrix B equals the size of each matrix $\tilde{A}_s$.

The elements at the same position in different matrices $\tilde{A}_s$ can be considered as samples from independent random variables (Pittner and Kamarthi, 1999). This follows from the fact that these wavelet coefficients were computed for A-scan signals measured at different time instances while scanning the ROI. If $\gamma \geq e^2$ (e is the Euler number) be a constant and L be the number of computed wavelet detail coefficients, a threshold of the form Th := $\sqrt{2(\ln L - \ln \gamma)}$ can be applied to the elements of matrix B so that it yields a binary matrix

$$B_2 := (\Theta\,(b_{ij} - Th)) \tag{6.7}$$

where $\Theta(x) = 1$ for x$\geq$0 and $\Theta(x) = 0$ for x$<$0, is a Heavyside function. The 1s in the matrix B_2 occur at the same positions where the largest wavelet coefficients occur in the matrices A_s.

The clusters C_1, C_2, ..., C_c are determined as rowvectors in B_2 such that each cluster contains a 1 situated near the midpoint of the cluster. Clusters do not overlap across subsequent scales. If an entire row of the matrix B_2 does not contain any 1s, it is treated as a cluster by itself. Upon completion of the division of matrix B_2 into disjoint clusters, the entire pattern is used as a mask and superimposed on matrix A. By using this cluster pattern mask, regions of A containing important signal information that are characterized by larger wavelet coefficients, are further decomposed into a larger number of clusters than the regions of A containing less relevant information.

For this study, a discrete wavelet transform with 5 level decomposition is applied to the S^{th} training signal $x_s[n]$ with 256 samples. The mother wavelet function used was 'symlet' with eight vanishing moments (sym8) (Daubechies, 1992). This yields A_s with 5 rows of detailed coefficients and one row of approximation coefficients corresponding to the fifth level output of the lowpass filter. As mentioned above, the first row corresponding to level one decomposition has 128 coefficients spanning half the frequency band of the sampled signal. Similarly the second, third, fourth and fifth row will have 64, 32, 16, and 8 detail coefficients respectively. The last row has 8 approximation coefficients. However, the rest of the

elements in matrix A_s are filled with zeros so that the dimension of A_s is maintained at 6 x 128. Table 6.1 shows a sample wavelet coefficient matrix after the clustering operation. In this table, scale 4 contains four clusters, while scale 3 contains two clusters. This means that signal frequencies corresponding to scale 4 carry more useful information than frequencies corresponding to scale 3. There are fourteen clusters C_1, C_2, ..., C_{14} in matrix A corresponding to 5 levels of discrete wavelet decomposition of the original A-scan signal, that will constitute the parameters for this feature extraction method.

The feature extraction method is summarized as follows. From the procedure described above, clusters C_1, C_2, ..., C_c are determined from a set of training data signals. The input feature vectors to a defect classification system can be computed from test data signals through a two step procedure. In the first step, the discrete wavelet transform with 5 level decomposition is applied to an A-scan signal to obtain the matrix A of wavelet coefficients. This matrix is then divided into clusters C_1, C_2, ..., C_{14} according to the process described before. Every rowvector that is formed by the elements of a particular cluster C_i in the matrix A is denoted by r_i for i = 1, 2, ..., c. The second step consists of simply determining every component F_i of the feature vector (F_1, F_2, ..., F_c) by computing the energy of each cluster

$$F_i := \|r_i\|_2 = \sqrt{\sum_{w \in C_i} w^2} \tag{6.8}$$

through its corresponding vector r_i. In other words, each feature F_i is determined as the square root of the energy of the wavelet coefficients in the corresponding cluster C_i. The number of features 'c' in the feature vector extracted for a test signal 's' is equal to the number of clusters determined by the procedure above.

The proposed feature extraction technique is demonstrated on a test set of 2100 A-scan signals belonging to 4 main and 2 subclasses of defects. This method is then compared with two other feature extraction procedures based on the discrete wavelet transforms described in the following sections.

6.2.2 Subset and Compressed Discrete Wavelet Transform Based Feature Extraction

In the subset feature extraction technique, a small subset of discrete wavelet coefficients computed by decomposing the signal x[n] into its approximate and detail coefficients at five levels, is chosen to serve as feature vectors. The choice of the subset is made based on *apriori* knowledge about the central frequency of interest for the problem at hand (Hatanaka et al., 2005). The decomposition scheme and corresponding frequency ranges are shown in figure 6.4. Figure 6.5 shows a sample defect A-scan and its subsequent decomposed signals with corresponding frequency ranges. The signal at the top of the figure is the pre-processed A-scan signal *S(t)*. S is decomposed at 5 levels using the discrete wavelet transform to yield detail signals d_1–d_5 and approximation signal a_5. From previous discussions, it is known that coefficients of signal d_1 belong to the highest frequency component of the signal and d_2 coefficients are half the frequency component of d_1. In discrete terms, the 5 level decomposition of the signal *S(t)*can be written as:

$$S(t) = a_5(t) + \sum_{n=1}^{5} d_n(t) \tag{6.9}$$

If the sampling frequency of the data is f_s, d_n has the frequency components between $f_s/2^{n+1}$ and $f_s/2^n$. All data collection was done by a panametrics transducer with a central frequency of 250 kHz. The time series A-scan signals were sampled at 5 MHz. Hence, d_1, d_2, and d_3 have frequency components of 1.25 2.5 MHz, 0.625 1.25 MHz, and 312 625 kHz respectively. The frequency of interest for this problem, , 250 kHz, lies in decomposition level d_4 as seen from figure 6.5. There are some frequency components at the farther end of level 5, d_5, that may help locate the flaw echo characteristics in this particular application. The choice of these two levels is made based on the reasoning that most of the signal energy will be present in these frequency bands whereas other levels will mainly consist of noise. Thus, a subset of detail coefficients from decomposition levels 4 and 5 are chosen as feature vectors to serve as inputs to the classifier.

The DWT also provides very effective signal compression and data reduction

scheme (Polikar et al., 1998). From *apriori* information about the central frequency of the generated ultrasound signal, it can be known that the energies of signals will be concentrated in a certain frequency band. All other frequencies are represented by very low amplitudes in the wavelet transform domain and hence can be discarded without loss of information. Figure 6.6(a) and (b) show a typical 250 kHz ultrasonic crack signal sampled at 5 MHz and its DWT respectively. The last 128 samples constituting level 1 detail coefficients (samples 129 through 256) characterize the signal in the $\pi/2$–π frequency band corresponding to frequency range of 1.25 to 2.5 MHz (see figure 6.4). These samples do not carry much information, because the signal does not have any spectral components in this frequency range. Level 2 detail coefficients (samples 65 through 128) characterize the signal in the $\pi/4$–$\pi/2$ frequency band corresponding to frequencies 0.625 to 1.25 MHz. The main energy of the signal appears in the level 4 detail coefficients (samples 17 to 32), which characterize the signal in the $\pi/16$–$\pi/8$ range, corresponding to frequency range of 156 kHz to 312 kHz. It is almost evident that the 256 sample long signal can be represented by the first 128 coefficients of the discrete wavelet transform with little loss of information as contribution from the last 128 coefficients is negligible. From the discussion above, it can be inferred that DWT provides significant data reduction or compression, thereby reducing the computational burden. Therefore level 1 detail coefficients are discarded without any loss of information. The signal information is thus compressed and remaining 128 coefficients are then built into a feature vector for input to a classifier.

6.3 Classification

Pattern recognition (PR) can be generally defined as the allocation of objects to classes so that individual objects in one class are as similar as possible to each other and as different as possible from objects in the other classes. Considered as a pattern recognition problem, there have been numerous techniques investigated for classification. Clearly, the more *a priori* information that is known about the problem domain, the more the classification algorithm can be made to reflect the actual situation. For example, if the *a priori* probabilities and the state conditional densities of all classes are known, then Bayes decision theory produces optimal re-

sults in the sense that it minimizes the expected misclassification rate. However, in many PR problems, the classification of an input pattern is based on data where the respective sample sizes of each class are small and possibly not representative of the actual probability distributions, even if they are known.

A number of supervised and unsupervised pattern recognition algorithms have been employed for the classification of multidimensional signals. The K-means clustering algorithm is one of the most widely used techniques for partitioning the feature space. More recently, neural networks have proved to be very effective in signal classification, due to their ability to generate arbitrarily complex decision boundaries. Neural network models have an advantage over the statistical methods that they are distributed free and no prior knowledge about the statistical distributions of classes in the data is needed in order to apply these methods for classification. On the other hand, neural network models can be very complex computationally and need many training samples to be applied successfully, and their iterative training procedures usually are slow to converge. Additionally, neural network models have more difficulty than statistical methods in classifying patterns that are not identical to one or more of the training patterns. The performance of neural network models in classification is therefore more dependent on having representative training samples, whereas the statistical approaches need to have an appropriate model of each class. A variety of neural network architectures and learning algorithms have been developed over the years, including the hopfield, multilayer perceptron (MLP), radial basis functions, Kohonen, and adaptive resonance networks (Haykin, 1994). For classification of signals that are separated by complex decision boundaries in the feature space, the MLP networks have gained widespread acceptance and have become the network of choice due to their simple yet powerful learning algorithm (Bishop, 1995, Polikar et al., 1998).

The scope of this research is to implement a simple neural network classifier to classify A-scan signals acquired from the concrete sample ROI into several defect classes. A MLP neural network is chosen for this particular application owing to its proven ability in signal classification problems. In this study, the performance of the MLP classifier is also empirically compared with a simple linear statistical

classifier such as the Linear Discriminant Analysis (LDA). Set A data was used for the evaluation of both classifiers. The objective of both classifiers was to classify A-scan signals as belonging to one of the seven classes, namely,

1. Clean (CP)
2. Hairline Crack originating from outer diameter (HCOD)
3. Hairline Crack originating from inner diameter (HCID)
4. Crack originating from outer diameter (CROD)
5. Crack originating from inner diameter (CRID)
6. Fracture (FR)
7. Hole

Two data sets were generated, one to train and the other to test the classifiers. The performance of each classifier is quantified in terms of the accuracy of classification.

6.3.1 Proposed Multilayer Perceptron (MLP) Neural Network Classifier

Multilayer perceptrons (MLPs) are feedforward neural networks trained with the standard backpropagation algorithm (Haykin, 1994). They are supervised networks, so they require a desired response to be trained. They learn to transform input data into a desired response and thus are widely used for pattern classification. They have been shown to approximate the performance of optimal statistical classifiers in difficult problems. MLP networks are general-purpose, flexible, nonlinear models consisting of a number of units organized into multiple layers. The complexity of the MLP network can be changed by varying the number of layers and the number of units in each layer. Given enough hidden units and enough data, it has been shown that MLPs can approximate virtually any function to any desired accuracy. In other words, MLPs are universal approximators. MLPs are valuable tools in problems when one has little or no knowledge about the form of

the relationship between input feature vectors and their corresponding outputs.

The multi-layer perceptron neural network model consists of a network of processing elements or nodes arranged in layers. Typically it requires three or more layers of processing nodes: an input layer which accepts the input feature vectors used in the classification procedure, one or more hidden layers, and an output layer with one node per class (see figure 6.7). The principle of the network is that when data from an input pattern is presented at the input layer, the network nodes perform calculations in the successive layers until an output value is computed at each of the output nodes. This output signal should indicate which is the appropriate class for the input data, i.e. it should have a high output value on the correct class node and a low output value on all the rest.

Every processing node in one particular layer is usually connected to every node in the layer above and below. The connections carry weights which encapsulate the behaviour of the network and are adjusted during training. The operation of the network consists of two stages. The "forward pass" and the "backward pass" or "back-propagation". In the "forward pass" an input feature vector is presented to the network and the output of the input layer nodes is precisely the components of the input pattern. For successive layers the input to each node is then the sum of the scalar products of the incoming vector components with their respective weights. Mathematically, the input to a node j is given by

$$input_j = \sum_i w_{ji} out_i \tag{6.10}$$

where w_{ji} is the weight connecting node i to node j and out_i is the output from node i. The output of a node j is

$$out_j = f(input_j) \tag{6.11}$$

which is then sent to all nodes in the following layer. This continues through all the layers of the network until the output layer is reached and the output vector is computed. The input layer nodes do not perform any of the above calculations.

They simply take the corresponding value from the input pattern vector. The function f denotes the activation function of each node. A sigmoid activation function is frequently used

$$f(x) = \frac{1}{1 + e^{-x}} \tag{6.12}$$

The multi-layer feed-forward neural network is trained by supervised learning using the iterative back-propagation algorithm. The back-propagation algorithm is a gradient descent optimization procedure that minimizes the mean square error between the network's output and the desired output for all input patterns. In the learning phase a set of input patterns, called the training set, are presented at the input layer as feature vectors, together with their corresponding desired output pattern which usually represents the classification for the input pattern. Beginning with small random weights, for each input pattern the network is required to adjust the weights attached to the connections so that the difference between the network's output and the desired output for that input pattern is decreased. Based on this difference the error terms or δ terms for each node in the output layer are computed. The weights between the output layer and the layer above (hidden layer) are then adjusted by the generalized delta rule (Rumelhart et al., 1988). The training set is presented iteratively to the network until a stable set of weights is achieved and the error function is reduced to an acceptable level. To measure the generalization ability of the multi-layer feed-forward neural network it is common to have a set of data to train the network and a separate set to assess the performance of the network during or after the training is complete. Once the neural network has been trained, the weights are saved to be used in the classification phase.

The architecture of the MLP used in this study is similar to the one shown in figure 6.7. F_i is the input feature vector, where i = 1, 2, ..., n; $HID1_j$, j = 1, 2, ..., n1 are output values of the first hidden layer nodes, $HID2_k$, k = 1, 2, ..., n12 are output values of the second hidden layer nodes, and OUT_l, l = 1, 2, ..., n3 are the values at the output nodes. The input feature vector $F = F_1, F_2, ..., F_n$ is fed to the input layer of the network that simply passes on the values to the first hidden layer. The values of the hidden layer nodes and the output nodes are

computed as follows:

$$HID1_j = f\left(u_{0j} + \sum_{i=1}^{n} u_{ij} \cdot F_i\right) \qquad j = 1, 2, .., n1 \tag{6.13}$$

$$HID2_k = f\left(v_{0k} + \sum_{j=1}^{n1} v_{jk} \cdot H1_j\right) \qquad k = 1, 2, .., n2 \tag{6.14}$$

$$OUT_l = f\left(w_{0l} + \sum_{k=1}^{n2} w_{kl} \cdot H2_k\right) \qquad l = 1, 2, .., n3 \tag{6.15}$$

The activation function f in above equations is the sigmoid function of equation 6.12. The index '0' used in equations (13), (14) and (15) indicate the extra bias node with a constant value of 1 introduced to serve as a threshold level. The convergence or training time of the network can be reduced significantly by choosing an appropriate learning rate, η which controls the rate at which the weights are adjusted in the gradient descent algorithm. As there is no set criteria for the selection of learning rate, it can also be chosen adaptively. The learning rate is constantly changed according to the change in the error from one iteration to another. If the new error is greater than a predefined ratio α (1.04 in this case) times the previous error, the new weights, output values, and errors are discarded, and the learning rate is decreased by a predefined factor β (typically 0.7). The learning then continues with the previous weights, error values, and node values. If the new error is less than the predefined ratio times the previous error, the learning rate is increased by a predefined factor ξ (typically 1.05) (Hagan et al., 1996).

The MLP described above is used to classify A-scan signals into seven classes, namely, clean, hairline crack from outer diameter, hairline crack from inner diameter, crack from outer diameter, crack from inner diameter, fracture and hole. The training database consisted of 555 A-scan signals from all seven classes. All A-scan signals were mapped to the feature domain using the proposed feature extraction method and two other methods thus generating three different training databases. Three different MLP networks were designed and trained using these training data. The classifier was then tested with a test data set of approximately 820 A-scan signals. The MLP parameters used for all the three networks are summarized in

Table 6.2.

6.3.2 Statistical Classifier for Performance Comparison

Statistical classification is a statistical procedure in which individual items are placed into groups based on quantitative information on one or more characteristics inherent in the items (referred to as traits, variables, characters, etc) and based on a training set of previously labeled items. Formally, the problem can be stated as follows: given training data $\{(x_1, y_1), \ldots, (x_n, y_n)\}$ produce a classifier $h : \mathcal{X} \to \mathcal{Y}$ which maps an object $x \in \mathcal{X}$ to its classification label $y \in \mathcal{Y}$.

Linear Discriminant Analysis (LDA) is a statistical classification technique used for classifying a set of observations into predefined classes. The purpose is to determine the class of an observation based on a set of variables known as predictors or input variables. The model is built based on a set of observations for which the classes are known. This set of observations is sometimes referred to as the training set. Based on the training set , this statistical technique constructs a set of linear functions of the predictors, known as discriminant functions, such that

$$f = a_1x_1 + a_2x_2 + \cdots + a_nx_n + c; \tag{6.16}$$

where the a's are discriminant coefficients, the x's are the input variables or predictors and c is a constant. These discriminant functions are used to predict the class of a new observation with unknown class. For a k-class problem k discriminant functions are constructed. Given a new observation, all the k discriminant functions are evaluated and the observation is assigned to class i if the i_{th} discriminant function has the highest value. The *total error of classification* (TEC) is used as a performance evaluation rule on a random sample of training data. The objective in designing a classifier is to ensure that the proportion of misclassifications are kept to the minimum. This is done by minimizing the TEC. Thus, TEC can be stated as the probability that the classification rule under consideration will misclassify an object. The classification rule is to assign an observation to a class with highest conditional probability . This is called Bayes Rule which also minimizes the TEC.

If there are g classes, the Bayes' rule is to assign the observation to group i where

$$P(i|x) > P(j|x), \forall j \neq i \tag{6.17}$$

Given a set of observations x, the objective is to know the probability $P(i|x)$ that an observation belongs to class i. In practice, the probability $P(i|x)$ is difficult to obtain but the quantity $P(x|i)$, the probability of getting a particular set of observations x given that the observations belong to class i, is relatively easier to compute. Fortunately, there is a relationship between these two conditional probabilities known as the Bayes Theorem which states that:

$$P(i|x) = \frac{P(x|i) \cdot P(i)}{\sum_{\forall j} P(x|j) \cdot P(j)} \tag{6.18}$$

Prior probability *P(i)* is the probability of class i without making any observations. It is either assumed that the prior probability is equal for all classes or based on the number of observations in each class. However, it is impractical to use the Bayes rule directly because of the fact that a lot of data is needed to get the relative frequencies of each classes for each observation. An alternative is to assume the distribution and compute the probability theoretically. If it is assumed that each class has multivariate normal distribution and all classes have the same covariance matrix, the result is the Linear Discriminant Analysis equation

$$f_i = \mu_i C^{-1} x_k^T - \frac{1}{2} \mu_i C^{-1} \mu_i^T + \ln(P_i) \tag{6.19}$$

where f_i is the discriminant function for class i, μ_i is mean of features in class i, C is the global covariance matrix, x_k is the input feature vector for a particular observation k, and *P(i)* is prior probability of class i. The classification rule is to assign observation k to class i that has maximum f_i. Note that equation 6.19 is a more specific form of the general equation in 6.16. Detailed theoretical derivation of equation 6.19 can be found in Duda et al (2000) (Duda et al., 2000).

To evaluate the performance of the proposed MLP neural network classifier, the LDA statistical classifier described above is used to classify A-scan signals into seven classes, namely, clean, hairline crack from outer diameter, hairline crack from

inner diameter, crack from outer diameter, crack from inner diameter, fracture and hole. The same training database consisting of 555 A-scan signals from all seven classes were mapped to the feature domain using the proposed feature extraction method. The classifier was then tested with the same test data set used for the MLP classifier to facilitate performance comparison.

6.4 Experimental Results and Discussion

The performance of the proposed A-scan signal feature extraction and classification scheme was tested on a test data set consisting of A-scan signals collected from concrete samples on a 50 mm x 50 mm ROI. The test data set consisted of A-scan signals from five concrete slabs (1 clean + 4 defects) oriented at 0, 45, and 90 degrees. In real world applications, defects could be oriented in any direction in the pipe geometry. As the overall classification accuracy should be independent of the orientation, it was intended to train and test the classifier at these three representative orientations. Various tests were performed to evaluate the overall approach in general, and the choice of feature extraction techniques and classifiers in particular.

Three feature extraction methods have been implemented to generate feature vectors from raw A-scan signals for classifying the ROI. To allow for comparison between the three methods, results are presented to show the difference in the magnitude of classification accuracy with respect to expert classification. The confusion matrix is way of comparing the output of a classifier against an expert classification. Table 6.3 shows classification results for the proposed multilayer perceptron (MLP) neural network classifier using the proposed clustered DWT feature extraction method. These results are for 0 degree orientation of defects. Results for 45 and 90 degree orientation are included in tables 6.4 and 6.5. Table 6.6 shows the overall classification results for the proposed classifier with different feature extraction methods. The classification accuracy from each feature extraction method and class is calculated in terms of the confusion matrix as shown in table 6.3. It can be observed that the proposed clustered DWT feature extraction technique provides consistent classification results. Classification percentages for

all classes are consistently above 80% except for the Fracture class. The other two methods perform very well in certain classes but show poor performance in some classes. The subset DWT method is generally better than the compressed DWT method in terms of consistency. The compressed DWT method performs very poorly in obvious classes like Hole and Crack. Overall, the clustered DWT method provides a better classification rate across classes although its performance in the fracture class has scope for improvement. This feature extraction method has been selected as the best performing scheme to generate input feature vectors for classification. Next, results of the proposed multilayer perceptron classifier are compared with the output from a statistical classifier.

Table 6.7 shows a comparison of classification accuracies of the MLP and LDA classifiers. Clearly, the LDA classifier is unable to identify signals belonging to hairline, crack and fracture classes. The MLP classifier performs much better than the statistical LDA classifier owing to its ability to learn from data. One of the inherent limitations of the LDA classifier is its inability to handle singularity in the feature vectors. Also, it implicitly assumes a multivariate gaussian distribution of the input data and uses class mean 'μ' as a discriminating factor. A-scan signals from defects like crack and hairline crack can have subtle variances in their echo amplitude that can be used to discriminate between the two classes. However, this is not possible using the LDA. Also, there is no mechanism to re-distribute the error from training data so that 'learning' occurs. Therefore, the MLP classifier is recognized as an ideal tool for this application as it has the ability to repetitively learn from an increasing database of varied patterns.

6.5 Post Processing for Depth Perception

The scope of this research study is to propose a methodology to inspect buried concrete pipes. The inspection system is envisioned as a two step approach. In the first step, which is called the reconnaissance mode, the ultrasound transducer is used to scan a ROI and acquire A-scan data. The ROI A-scan signals are passed through the classifier and identified as belonging to defect or clean class. If the scanned ROI belongs to a defect of interest, the second step of the approach is

to characterize the ROI with a C-scan imaging process for depth perception as described in Chapter 5. In other words, the second step involving C-scan imaging will only be '*triggered*' when a defect of interest is detected. From a field application perspective, a reliable decision as to whether the reconnaissance mode of operation has detected the presence of a defect in the ROI needs to be taken to trigger the characterization mode which is costly and time consuming. Frequent false alarms will render the system invaluable to the user community.

In context of the above requirement, it must be noted that output from the proposed MLP classifier cannot be entirely interpreted in isolation from the visual context of the problem. Consider an actual ROI from the concrete sample with a fracture defect as shown in Figure 6.8. A grid is superimposed on the ROI image to show the points at which A-scan signals were collected. The red dots on the grid belong to those signals that were classified as belonging to fracture class. Maroon and green colored dots are signals that were classified as hairline crack originating from inner diameter and crack originating from outer diameter. All other signals in the ROI were classified as belonging to the clean class. By relying solely on the confusion matrix results, it may lead one to believe that the MLP classifier is not performing well in case of fracture class signals (see table 6.3). But, when interpreted in terms of the visual context as shown in figure 6.8, it is evident that those signals that were either exactly on the defect or nearer to it were mostly classified as fracture signals whereas those at the fringes of the defect were either classified as hairline or crack. This result can be explained from the point of view of ultrasound acoustics. As mentioned in Chapter 5, a plane wave ultrasonic transducer with a central frequency of 250 kHz was used for data collection on the ROI. The transducer generates pulses of ultrasonic wave that leave its face and change in shape with time as it travels through the medium. The beam shape varies with direction depending on the relative size of the transducer to wavelength of ultrasound in the medium. With a simple calculation, it is found that the width of the beam as it reaches the front surface of the sample at the near field is 22 mm. Thus, although it seems as if the A-scan signal is an accurate representation of the wave that leaves the center of the transducer and hits the sample at a particular spot on the sample, it is not the case. The A-scan signal amplitudes are influenced

by the spread of the ultrasound beam over an area rather than a spot. This means that the ultrasound signal amplitude is effected by a defect from far distances due to its spread and will reflect the information as a change in amplitude and echo characteristic that may be classified as a less or more severe defect. Hence, the signal at grid point number 32, 33, 46 and 47 are classified as non-fracture defect (see figure 6.8) although they are very near to the actual defect. Figure 6.9 shows the raw A-scan signal from all these locations and the preprocessed signal used for feature extraction. It can be seen that the A-scans have different amplitude and echo characteristics although they come from the same vicinity. The feature extraction algorithm picks up these differences in amplitude and echo characteristics and the classification algorithm tries to match it with known defect signatures. Thus, an intelligent post processing step that brings in *apriori* knowledge about the geometry of defects is required before deciding the final class of the ROI. This will ensure better reliability of the proposed system due to reduced false calls for C-scanning operation. The assumptions, arguments in support of assumptions, and proposed post processing algorithm are presented in the following sections.

6.5.1 Assumptions

Based on *apriori* knowledge, it is known that larger defects have a higher probability of being detected. The hierarchy of defects considered as per their severity is:

1. Hole
2. Fracture
3. Crack
4. Hairline

Experiments on the proposed classifier have shown that its performance in detecting larger defects is good. From a defect geometry perspective, if a defect is present in the ROI, signal points classified as defects will follow a geometric (shape) trend

that can be represented by a second order polynomial. Finally, triggering to C-scan image acquisition mode will only occur when there is a hole, fracture or crack defect. It will *not* trigger for clean and hairline crack cases.

6.5.2 Proposed Post Processing Algorithm

It can be inferred based on the type of transducers used in the inspection process and the relative dimension of defect that the ability of the ultrasound wave to see larger defects is better than smaller ones. Hence, while scanning a ROI where fracture or hole defect is present, there is a very high probability that it will detect a considerable number of signals as belonging to that class. If a defect is present, for a given point classified as defect, neighboring points will be classified as either belonging to one defect class or the other. A neighborhood search will either retain a defect point or eliminate it as noise. The remaining signal points can then be 'analyzed' for geometric trends based on known defect characteristics. From a large number of experiments conducted on the proposed classifier, it is clear that if a fracture is present, it will classify greater than 10% of the ROI signals as fracture. This is a significant *apriori* knowledge that can be used to assign the final class of an ROI scan in the case of a conflict. The approach can easily be summarized in a decision tree that will assign the ROI to a final class based on which C-scan imaging can be triggered. Figures 6.10 and 6.11 show the decision tree and associated pseudo code for each node of the decision tree.

As majority of the scanned pipe will belong to clean class, it is very critical to decide if a given ROI is clean or a defect. The classifier performance statistics and a geometry-based evaluation approach are combined to classify the ROI at the top of the decision tree. The classifier performs very well when the ROI is clean. However, in reality, there may be scattered noise in the ROI that may be picked up as defect class signals and exceed the threshold of 95% set for classifying it as a clean ROI. In such situations, a two step procedure is used to determine if the signals classified as defect actually indicate the presence of a defect against random noise. As shown in the pseudo code in figure 6.11, a k-nearest neighbor(NN) search is performed for signals in each defect class and those points that have neighbors

belonging to the same class are retained, whereas others are eliminated from the defect signal pool as noise. This is repeated for all defect classes and the total remaining signals are computed to find out if the 95% clean class threshold has been met. If the criteria is met, the ROI is classified as belonging to the clean class. If the percentage of defect signals is still below the upper bound threshold, a second order polynomial is fit to the remaining defect signal points on the grid and its goodness of fit (R^2) is calculated. If the signals classified as defect on the grid belong to a defect, they will be grouped such that they describe the shape of the defect. In such situations, a non-linear regression analysis of the data can yield insights into the 'trends' in signals points. If the (R^2) value is high enough (good fit), it indicates that the probability of remaining defect points being random noise is low and hence the ROI must be classified as defect ROI. The threshold value for (R^2) is decided based on 25,000 simulations done on combinations of defect signals within the ROI that are randomly generated as scattered noise versus known patterns of defect signals from truth data.

The two step procedure can be understood by means of an example situation as shown in figure 6.12. Figure 6.12a is the output of the classifier when a ROI scan data was provided as input. There are 30 defect signals in the ROI indicating that the post processing algorithm will have to perform the two step procedure described above. In figure 6.12b, a 16-nearest neighborhood window centered around every signal looks for signal points similar to its class. If none are found, the signal point on which the window is centered is treated as noise and eliminated from the defect signal pool. So, two signal points belonging to the crack class are eliminated by this rule. In figures 6.12c-d, the same procedure is repeated for hairline crack and crack class signals. As all the signals lie within the defined neighborhood, none of them are eliminated. At the end of this first step, there are 28 defect signal points left and the threshold value of 95% clean signals is not met (see figure 6.12e). Hence, a second step involving fitting a second degree polynomial to the remaining defect signal points is carried out yielding an (R^2) value of 0.571 as shown in figure 6.12f. It must be noted that the probability of getting an (R^2) value of 0.571 with 28 defect signals randomly scattered in the ROI is very low. An experiment was conducted to prove this hypothesis. Twenty five thousand combinations of 28

signal points were randomly generated and fitted with a second order polynomial. A histogram of their (R^2) values is shown in figure 6.13. It was found that 90% of the 25,000 random combinations of 28 signals had a (R^2) value of less than 0.173. This means that, a value of 0.571 (from the fracture ROI example) has a very high probability of resulting from a good fit of the signal points having a definite geometric pattern. Thus, this two step procedure has the ability to finally take a decision whether the ROI under question must be classified as clean (no C-scan triggering) or defect(further steps before C-scan triggering). As mentioned above, majority of the inspected pipe section will belong to clean class that requires no C-scan imaging. This post processing step ensures with a high confidence level that the C-scan will not be triggered frequently thus minimizing false alarms that could prove costly.

6.6 Summary

In this chapter, a multilayer perceptron neural network classifier for classification of A-scan signals from a region of interest into clean and defect classes was proposed. A feature extraction scheme based on discrete wavelet transform and unsupervised clustering to extract signal features for classification by the MLP classifier was also proposed and evaluated. 'S' representative A-scan signals from all classes are decomposed into their discrete wavelet coefficients using the famous subband coding approach and then clusters of coefficients are formed by the unsupervised clustering approach. These clusters are then converted into feature vectors by taking the energy of each cluster as a single feature. This feature vectors then serves as input to the multilayer perceptron classifier which is trained on a training data set consisting of 555 A-scan signals and tested on various region of interest A-scan signals. Two other feature extraction schemes were evaluated against the proposed clustered DWT feature extraction method. The proposed method provided features that could discriminate the defect classes consistently in comparison to subset DWT and compressed DWT methods. The MLP classifier was compared to a statistical classifier, Linear Discriminant Analysis (LDA), to show that the MLP classifier is superior in its ability to 'learn' from training patterns.

A post processing scheme to interpret the classifier outputs and finally classify the ROI into an appropriate class taking into consideration some *apriori* knowledge of the problem was developed. The proposed post processing scheme is composed of several steps that combines the statistics from the classification matrix as well as a two step procedure based on k-nearest neighbor and non-linear regression. Finally, the inspection system is proposed as a two step approach consisting of the reconnaissance mode and characterization mode. In the reconnaissance mode, the ultrasound transducer is used to scan a ROI and acquire A-scan data. The ROI A-scan signals are passed through the classifier and identified as belonging to defect or clean class. If the scanned ROI belongs to a defect of interest, the second step of the approach is to characterize the ROI with a C-scan imaging process for depth perception. The proposed post processing scheme provides a high confidence that C-scan imaging will only be '*triggered*' when a defect of interest is detected. From a field application perspective, a reliable decision as to whether the reconnaissance mode of operation has detected the presence of a defect in the ROI needs to be taken to trigger the characterization mode which is costly and time consuming. The feature extraction, classification and post processing schemes proposed in this chapter provide a sound proof-of-concept for developing this inspection system into a field applicable tool.

Table 6.1. An Example of the Clustering Scheme of Coefficients Computed with the Discrete Wavelet Transform

Scale m	Wavelet Coefficients of S^{th} signal	No. of Clusters
1	$\{cD_{1(1)}, cD_{1(2)}, ..., cD_{1(128)}\}$	1
2	$\{cD_{2(1)}, cD_{2(2)}, ..., cD_{2(128)}\}$	1
3	$\{cD_{3(1)}, cD_{3(2)}, ..., cD_{3(13)}\}\{cD_{3(14)}, cD_{3(15)}, ..., cD_{3(128)}\}$	2
4	$\{cD_{4(1)}, cD_{4(2)}, ..., cD_{4(5)}\}\{cD_{4(6)}, cD_{4(7)}, ..., cD_{4(14)}\}$ $\{cD_{4(15)}, cD_{4(16)}, cD_{4(17)}\}\{cD_{4(18)}, cD_{4(19)}, ..., cD_{4(128)}\}$	4
5	$\{cD_{5(1)}, cD_{5(2)}, cD_{5(3)}\}\{cD_{5(4)}, cD_{5(5)}, ..., cD_{5(8)}\}$ $\{cD_{5(9)}, cD_{5(10)}, ..., cD_{5(128)}\}$	3
5	$\{cA_{5(1)}, cA_{5(2)}, cA_{5(3)}\}\{cA_{5(4)}, cA_{5(5)}, cA_{5(6)}\}$ $\{cA_{5(7)}, cA_{5(8)}, ..., cA_{5(128)}\}$	3

Table 6.2. MLP parameters for three feature extraction schemes.

Parameters	MLP I	MLP II	MLP III
No. of Feature Vectors	14	24	128
Error goal	0.001	0.001	0.001
Initial learning rate	0.05	0.05	0.05
α	1.04	1.04	1.04
β	0.7	0.7	0.7
ξ	1.05	1.05	1.05
Momentum term	0.95	0.95	0.95
Number of input nodes	14	24	128
Number of hidden layers	2	2	2
Number of first hidden layer nodes	32	34	34
Number of second hidden layer nodes	15	14	14
Number of output nodes	7	7	7
Activation function	sigmoid	sigmoid	sigmoid

Table 6.3. Confusion matrix for the proposed multilayer perceptron (MLP) classifier using the proposed clustered DWT feature extraction method

	Clean	Hairline (I.D.)	Hairline (O.D.)	Crack (I.D.)	Crack (O.D.)	Fracture	Hole	Total Signals ROI
Clean	99	0	1	0	0	0	0	100
Hairline-I.D.	19	9	0	1	1	0	0	30
Hairline-O.D.	18	6	0	3	3	0	0	30
Crack-I.D.	0	0	0	27	3	0	0	30
Crack-O.D.	0	0	0	1	29	0	0	30
Fracture	1	11	0	0	7	11	0	30
Hole	5	0	0	0	0	0	20	25
Total								**275**

Table 6.4. Confusion matrix for the proposed multilayer perceptron (MLP) classifier using the proposed clustered DWT feature extraction method when defects are oriented at 45°

	Clean	Hairline (I.D.)	Hairline (O.D.)	Crack (I.D.)	Crack (O.D.)	Fracture	Hole	Total Signals ROI
Clean	99	0	1	0	0	0	0	100
Hairline-I.D.	20	6	0	0	3	1	0	30
Hairline-O.D.	25	5	0	0	0	0	0	30
Crack-I.D.	0	0	1	21	4	0	1	27
Crack-O.D.	0	0	0	11	16	0	0	27
Fracture	3	8	0	1	10	8	0	30
Hole	5	0	0	0	0	0	20	25
Total								**269**

Table 6.5. Confusion matrix for the proposed multilayer perceptron (MLP) classifier using the proposed clustered DWT feature extraction method when defects are oriented at 90°

	Clean	Hairline (I.D.)	Hairline (O.D.)	Crack (I.D.)	Crack (O.D.)	Fracture	Hole	Total Signals ROI
Clean	99	1	0	0	0	0	0	100
Hairline-I.D.	19	6	0	4	0	0	1	30
Hairline-O.D.	10	17	0	1	2	0	0	30
Crack-I.D.	0	0	0	29	1	0	0	30
Crack-O.D.	0	0	0	3	27	0	0	30
Fracture	5	10	0	2	1	12	0	30
Hole	5	0	0	0	0	0	20	25
Total								**275**

Table 6.6. Classification accuracy comparison of proposed MLP classifier with different feature extraction methods

	Classification Accuracy (%)						
	Clean	Hairline (I.D.)	Hairline (O.D.)	Crack (I.D.)	Crack (O.D.)	Fracture	Hole
Clustered DWT	99	81.8	0	90	96.7	40	100
Subset DWT	99	0	0	100	11.1	77.8	94.4
Compressed DWT	100	69	3.5	100	7	58.6	51.7

Table 6.7. Classification accuracies of proposed MLP classifier and LDA

	Classification Accuracy (%)						
	Clean	Hairline (I.D.)	Hairline (O.D.)	Crack (I.D.)	Crack (O.D.)	Fracture	Hole
MLP	99	81.8	0	90	96.7	40	100
LDA	96	0	0	0	0	0	100

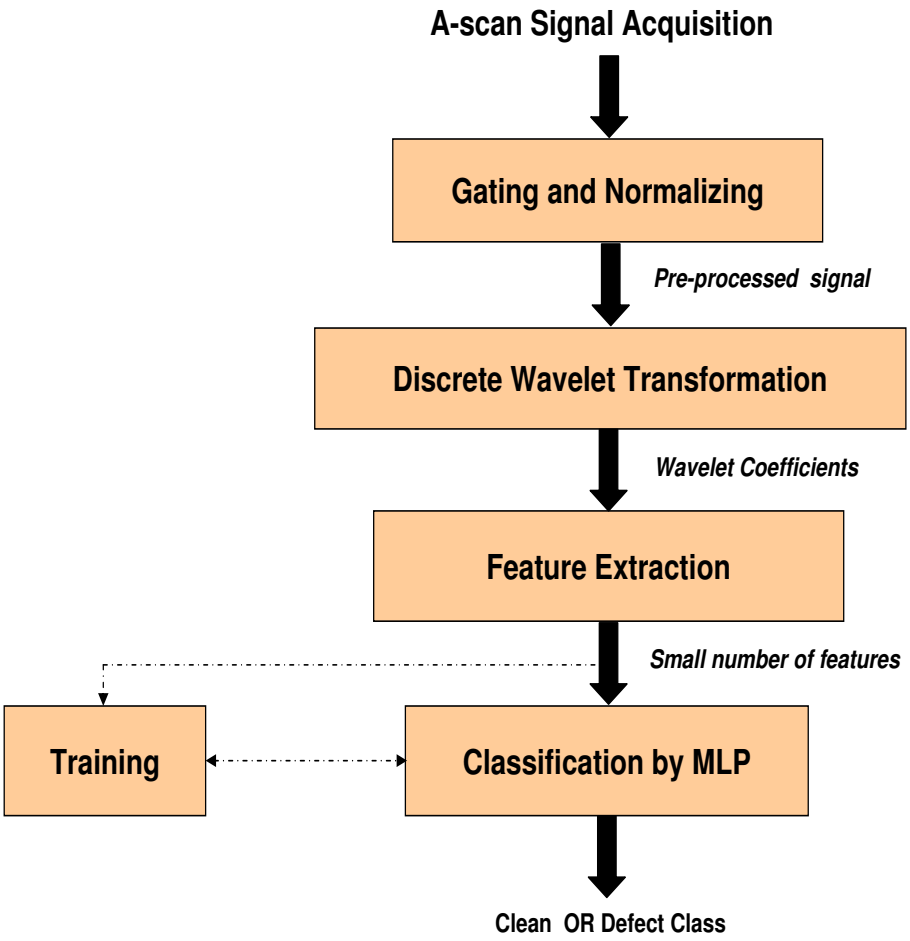

Figure 6.1. Overall approach for ultrasonic signal processing and classification

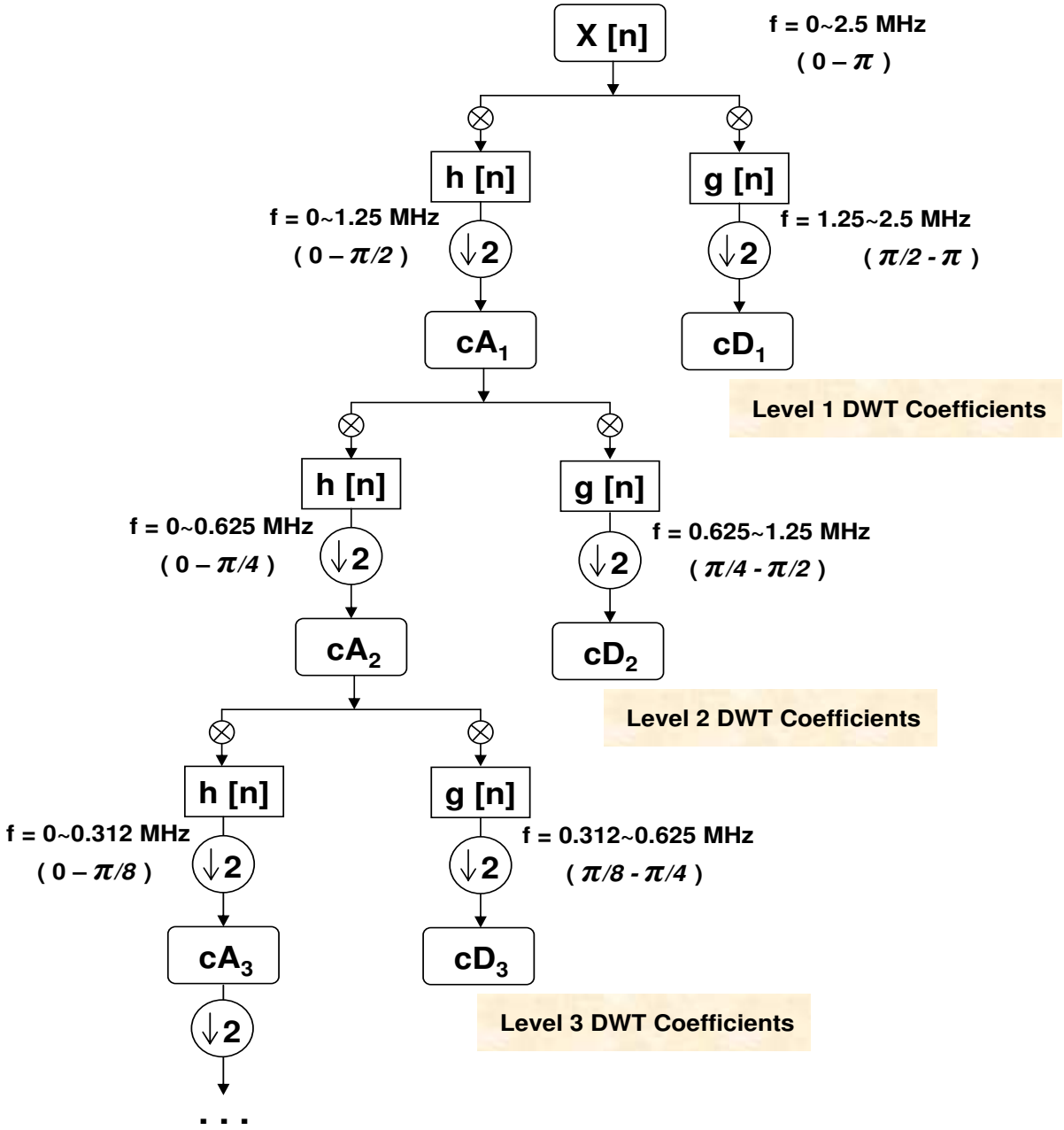

Figure 6.2. Discrete Wavelet Transform decomposition by subband coding scheme.

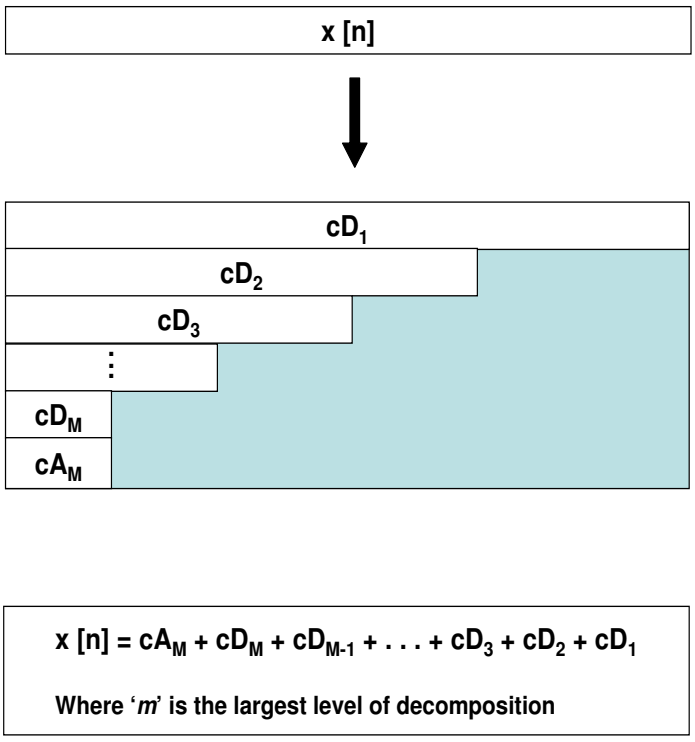

Figure 6.3. DWT coefficient matrix for a signal x[n].

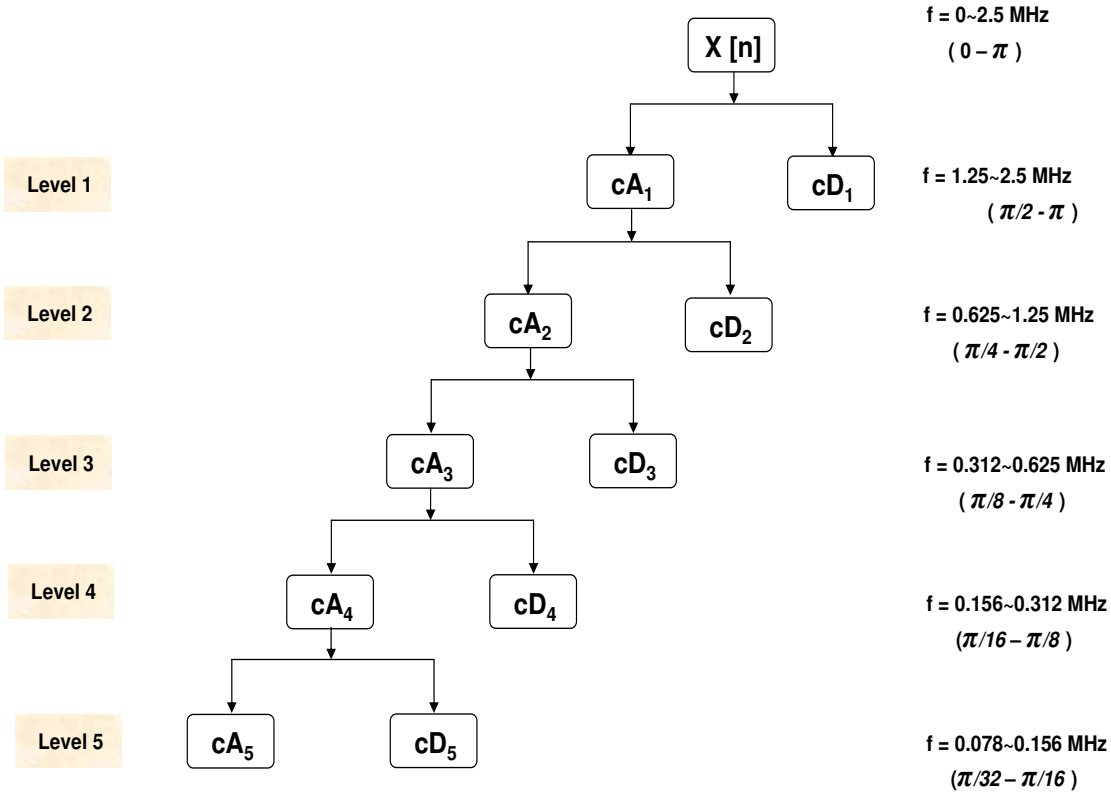

Figure 6.4. Decomposition scheme showing frequency range at each level.

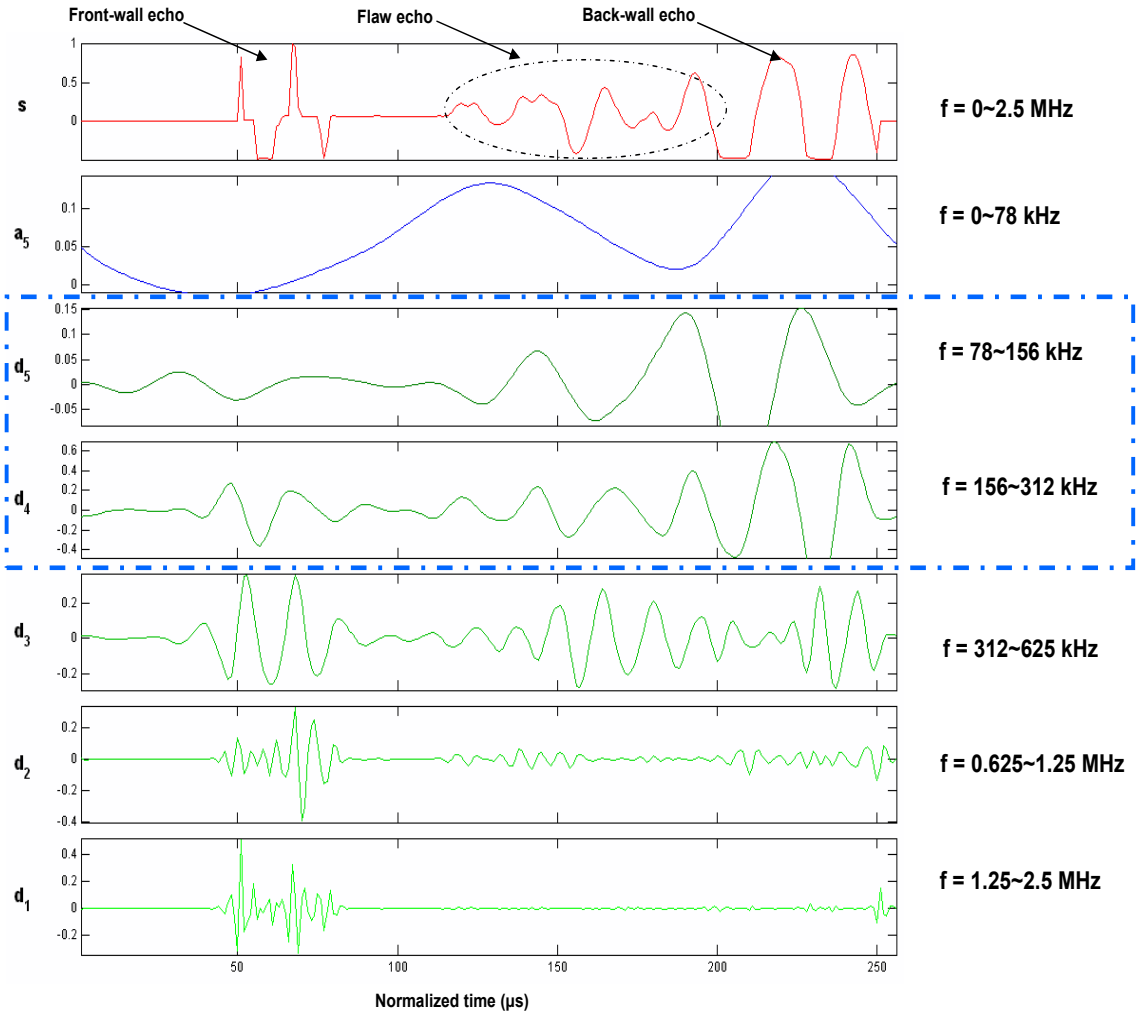

Figure 6.5. Example of a defect A-scan signal being decomposed into its detail and approximate signals.

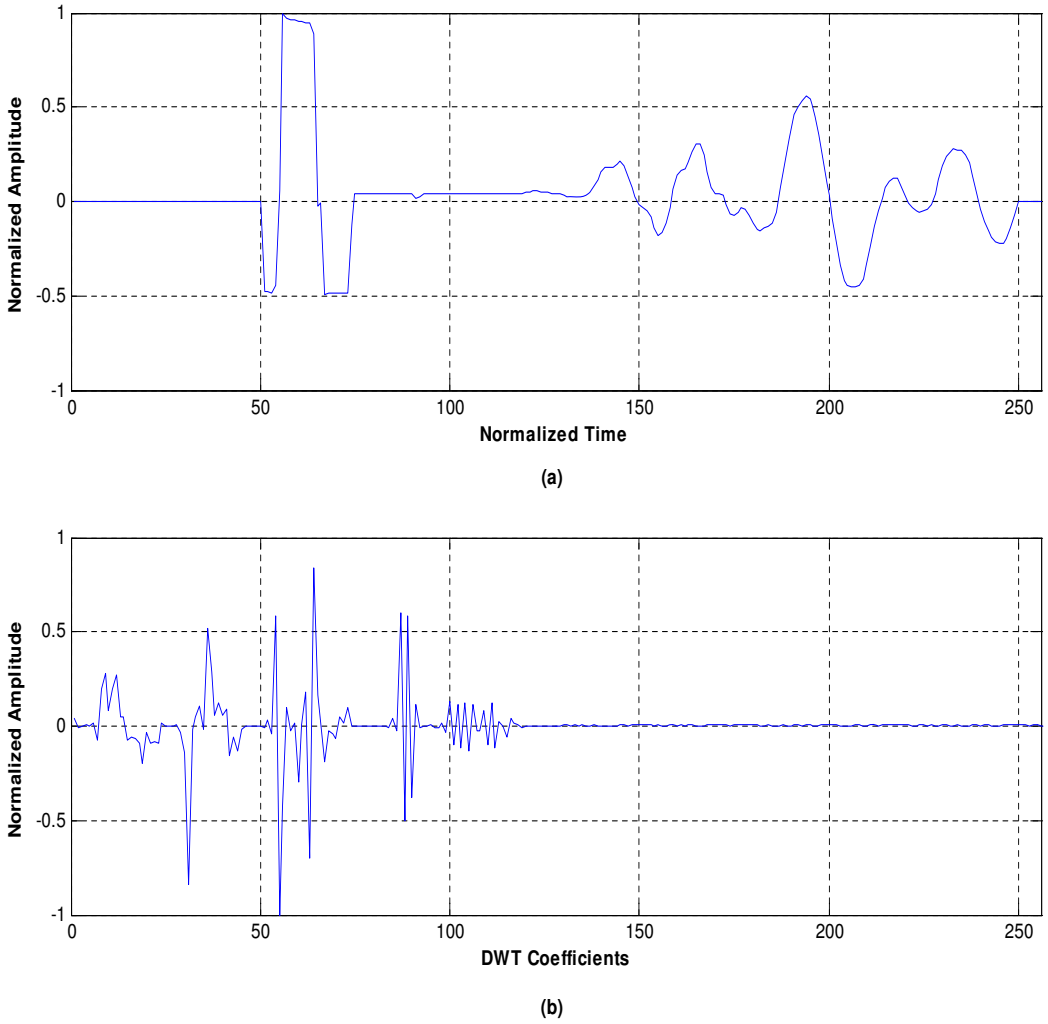

Figure 6.6. A typical crack signal (a) and its DWT (b).

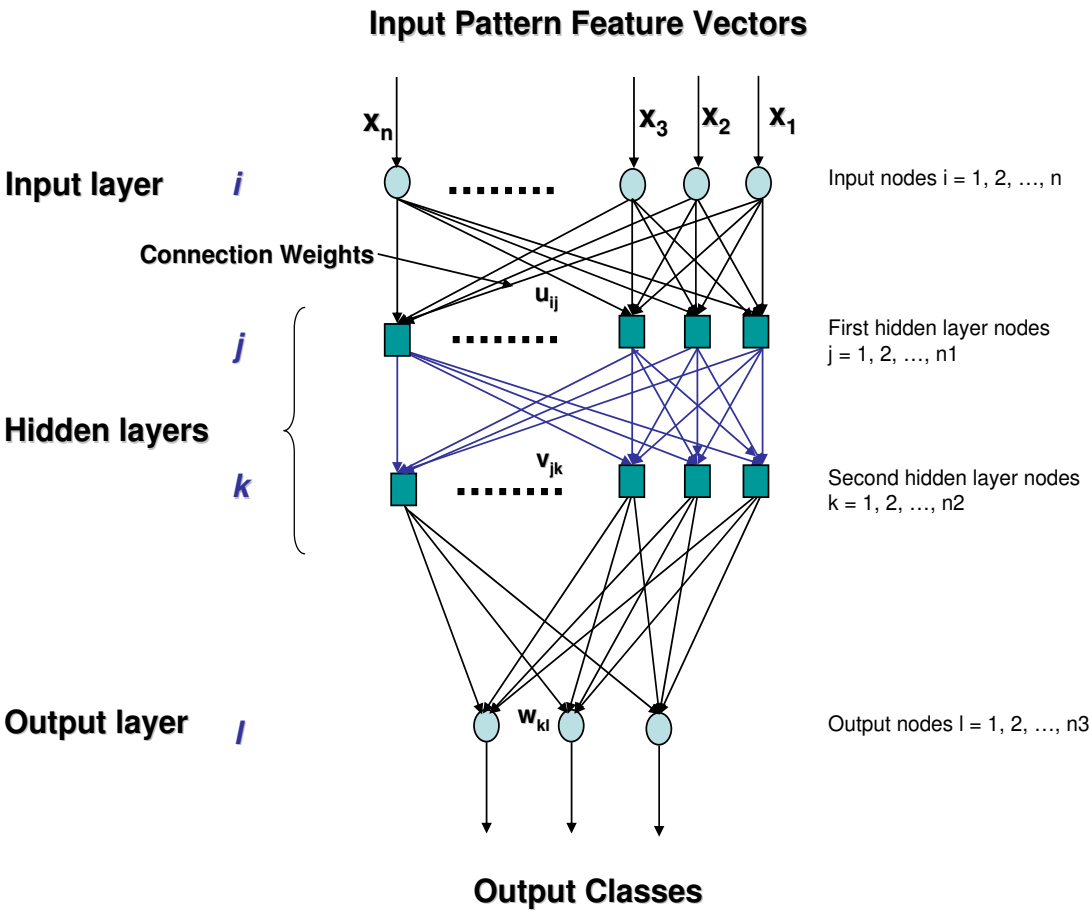

Figure 6.7. Multilayer perceptron architecture.

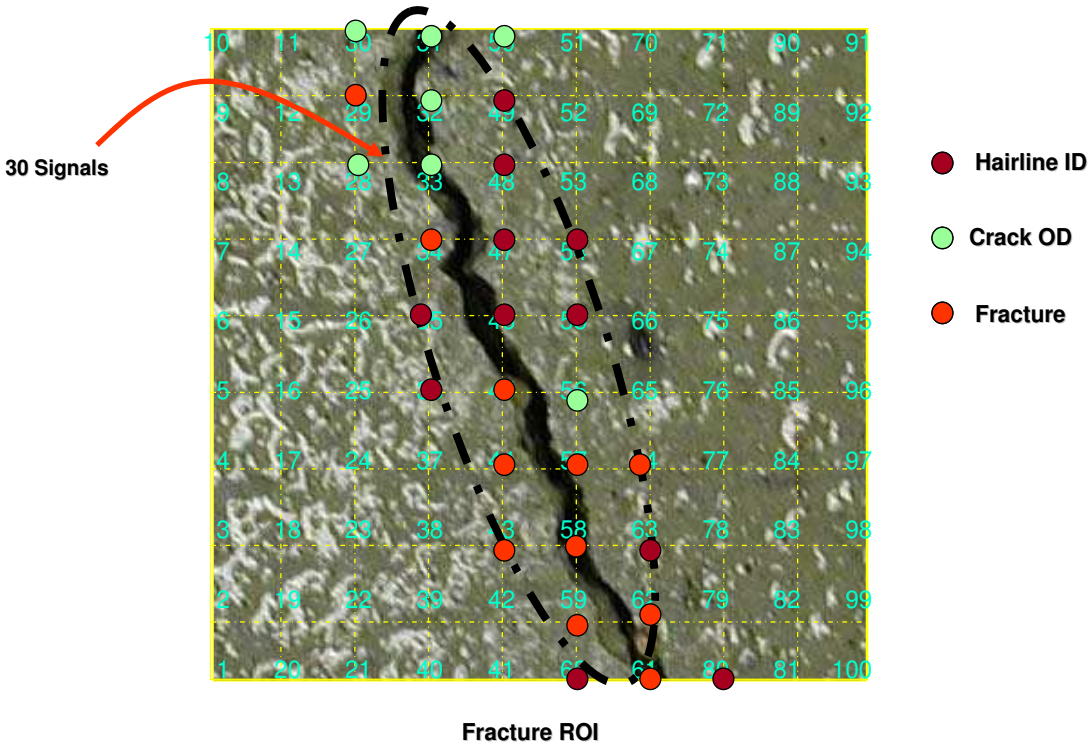

Figure 6.8. Visual representation of classifier output for fracture ROI.

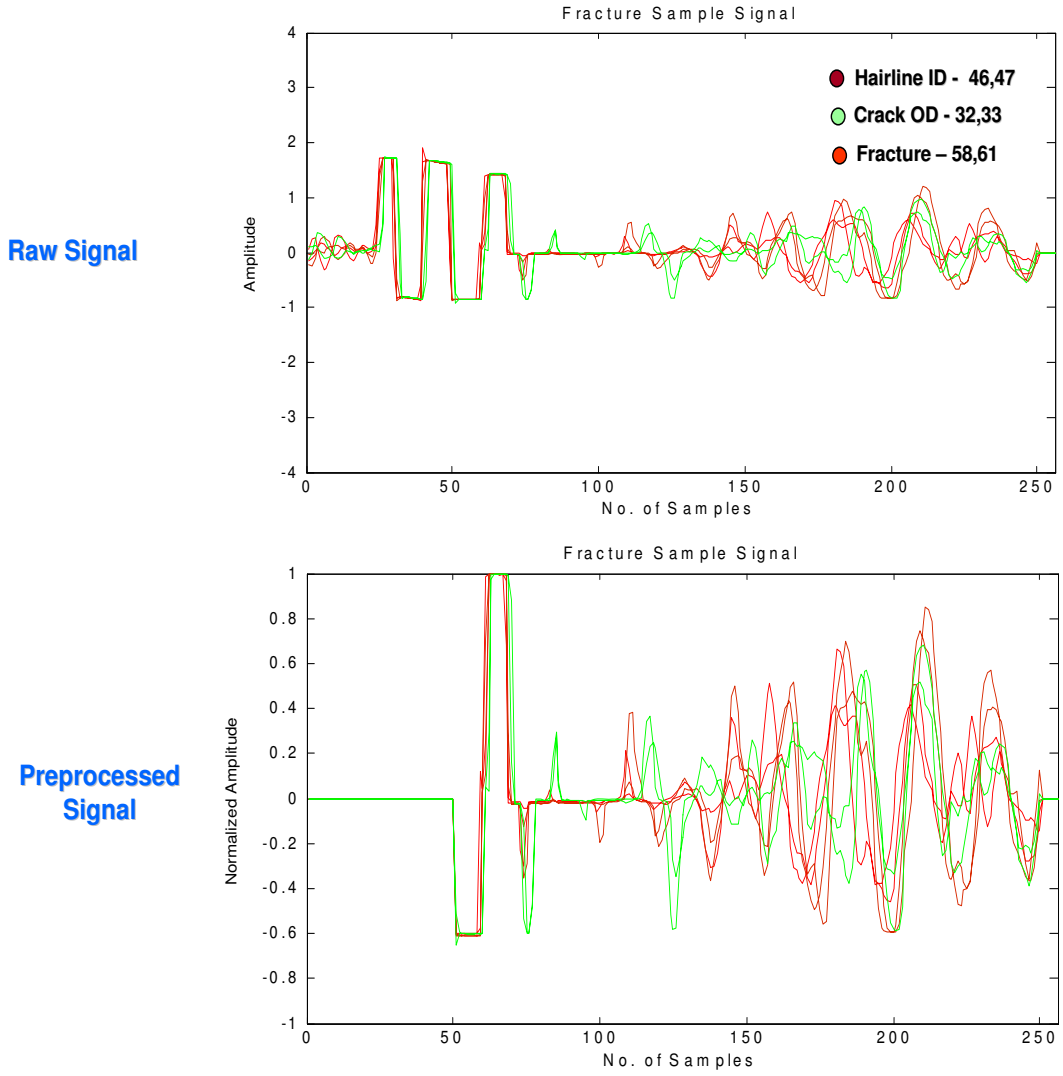

Figure 6.9. Raw and pre processed A-scan signals used for feature extraction and classification.

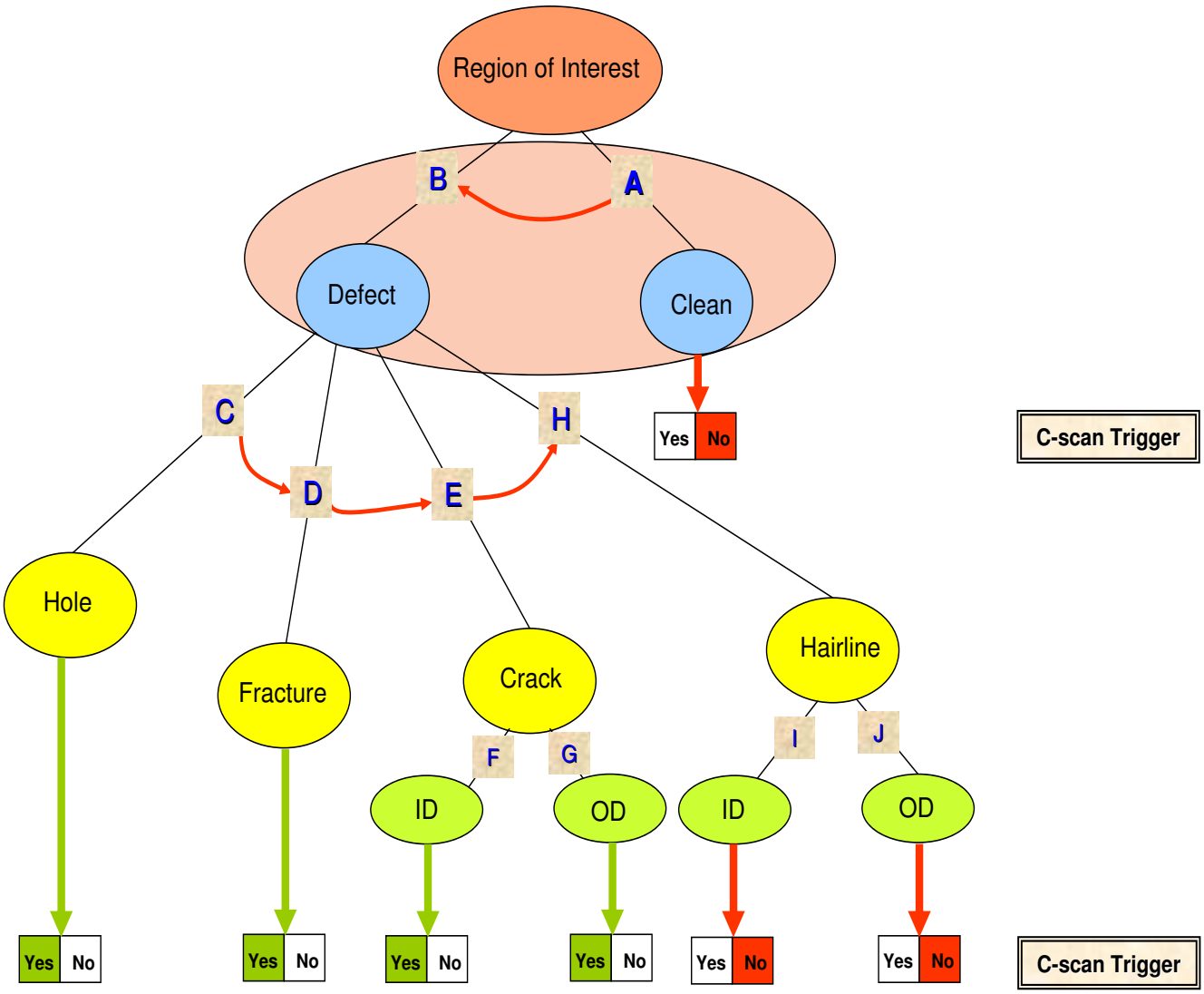

Figure 6.10. Decision tree for post processing of classification results.

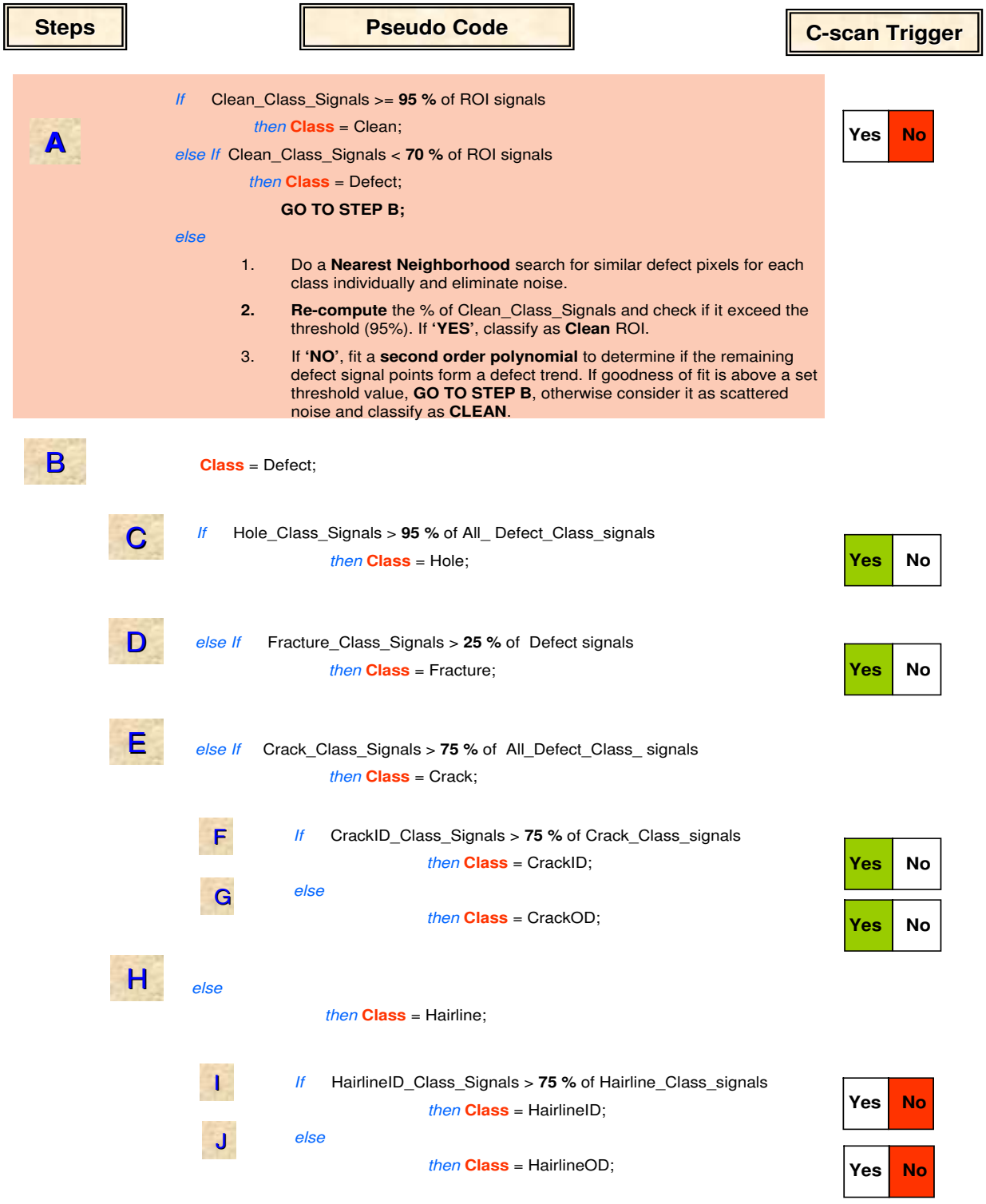

Figure 6.11. Pseudo code for post processing algorithm.

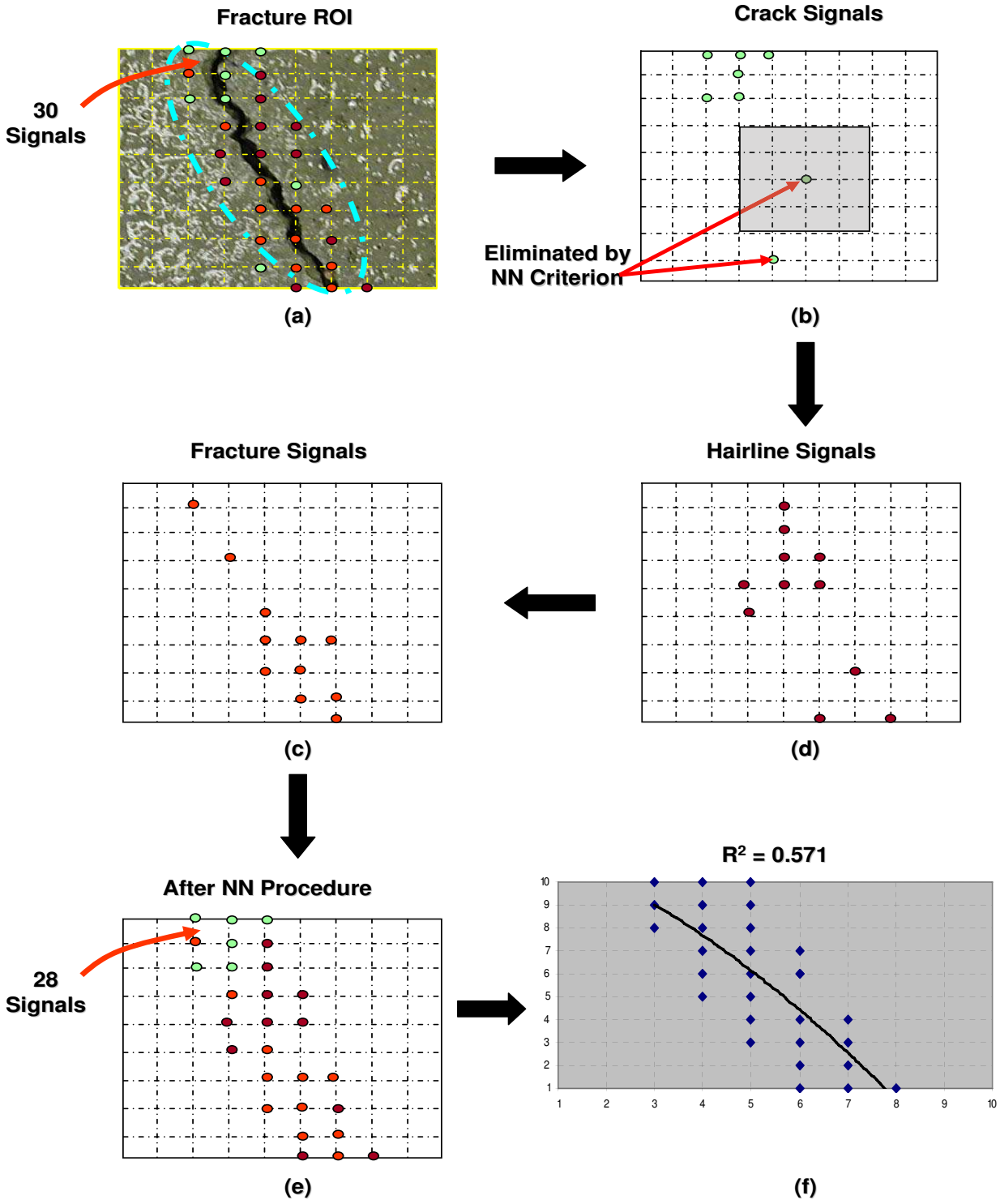

Figure 6.12. Example of fracture ROI to demonstrate nearest neighbor and second order polynomial fitting procedure.

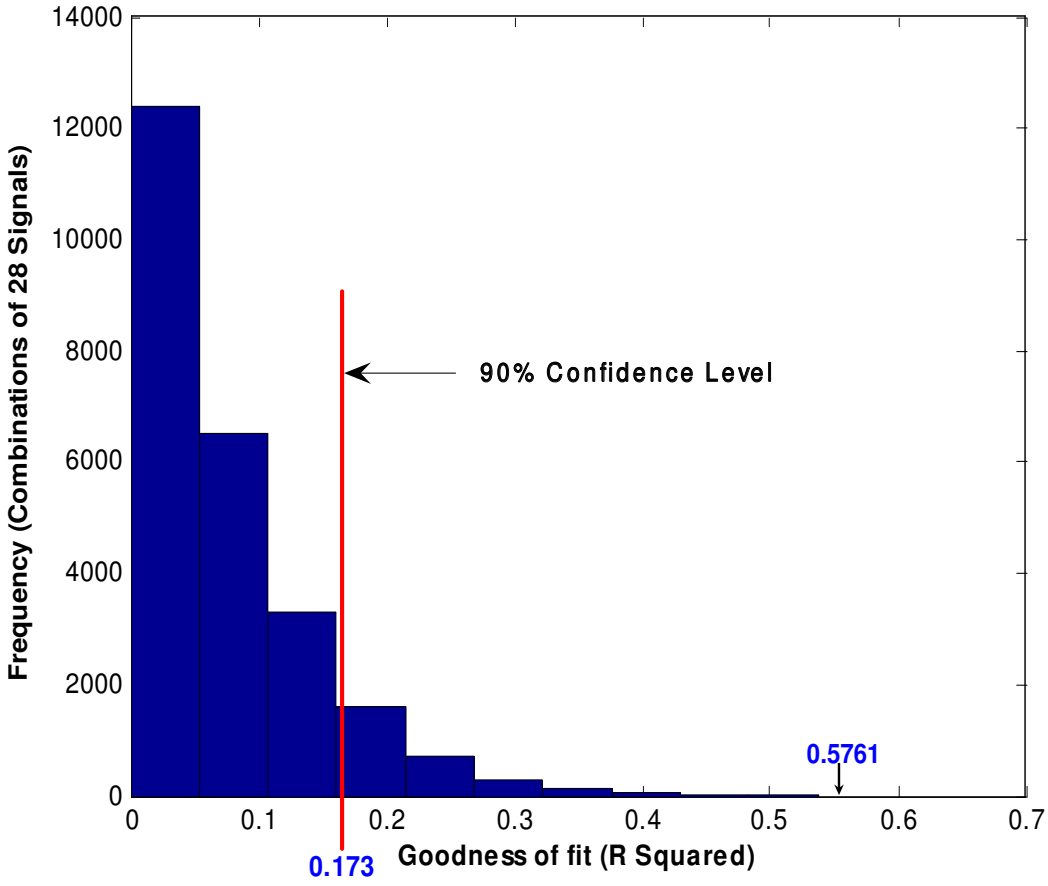

Figure 6.13. Histogram of R^2 values for 25,000 random combinations of 28 defect signals.

Chapter 7

Prototype Development

7.1 Introduction

Various ultrasound-based inspection techniques that may be employed to acquire depth perception data for defects in buried concrete pipes were explored. Ultrasound immersion inspection that uses water as a couplant is widely used in the industry owing to its adaptability to automation and hence chosen for this research. Experiments were conducted on several concrete samples with defects of interest to the water/waster water pipe community. A-scan and C-scan data representations were generated to make interpretations about the presence of defects and track them through the slab thickness. Signal processing algorithms were designed and implemented to process the A-scan data and determine the need for further characterization by means of high resolution C-scan. All these accomplishments were in the domain of providing a proof-of-concept for developing a comprehensive pipe inspection tool. However, a natural progression of this research is in demonstrating that this technique can be implemented in the field with further research and development in robotic technology and delivery mechanisms. This chapter briefly presents the concept, implementation, and results from a water bubbler system that emulates the immersion environment in real-world scenario on an actual concrete pipe specimen with a defect.

7.2 Prototype Inspection Design

The most common ultrasonic scanning systems involve the use of an immersion tank as shown in previous chapters. The ultrasonic transducer and the specimen are immersed under water so that consistent coupling is maintained by the water path as the transducer or specimen is moved within the tank by means of a controller . In the case of inspecting a sewer pipe buried in the ground, it is impractical to remove the pipe section and bring it to the laboratory for immersion inspection. A system where inspection can be done from within the pipe by a pipe robot is required. For this to happen, the immersion environment must be emulated within the pipe. This is possible by means of a water bubbler system. In this system, the ultrasound travels through a column of forced water which is scanned about the surface with a robotic system. The water column is made possible by a closed chamber that is attached to the transducer with water inlets. Water is pumped into the chamber at a constant rate so that a fixed water column is made available for the ultrasound energy to travel from the transducer face to the surface under test.

A typical design of a water bubbler system is as shown in figure 7.1. The focused transducer beam is enclosed in a chamber filled with water forming a column and constant contact with the test material. The ultrasonic beam travels through water couplant in pulse echo mode and is received by the same unit. As water escapes from a thin opening (1∼2mm), it creates a film over which the sliding shoe attached to the bubbler enables the unit to move in the horizontal plane rendering a raster scan pattern. Water collection systems are also commercially available to create closed loop continuous operation of the bubbler.

7.3 Experimental Setup & Data Collection

An Ultran Laboratories system setup was used in conjunction with a focused Ultran transducer having a center frequency of approximately 350 kHz . A block diagram of the set-up is shown in figure 7.2. In this phase, a concrete pipe quadrant (instead of a slab) was saturated for 24 hrs before being placed on a pedestal. The Ultran transducer with the bubbler assembly was attached to an automated

computer-controlled x-y-z stage and was excited by a Panametrics Pulser-Receiver to generate ultrasonic waves. The bubbler assembly had an inlet for pumping water into the chamber to maintain a constant water column for contact between the transducers face and pipe surface. In order to maintain a closed loop system, the entire setup was placed in an immersion tank filled with water to an extent such that it did not submerge the pipe specimen. The water in the tank was pumped into the bubbler chamber using a general purpose garden pump with a capacity of 25 gallons/min. To maintain a constant water column while scanning the pipe, a soft styrofoam was used as a sliding shoe. The advantage of using a soft styrofoam is that it has the ability to take shape of the pipe curvature while scanning thus preventing the water to rapidly escape from the bubbler chamber. Moreover, the styrofoam allows the bubbler assembly to slide over the thin film of water on a rather rough surface of concrete pipe. The transducer consisting of transmitter and receiver was housed in the same assembly resembling a single unit transmitter-cum-receiver in pulse-echo mode. The ultrasonic wave was reflected by the specimen and returned to the transducer, which also acted as a receiver. Figure 7.3 shows an actual setup for the water bubbler system discussed above.

7.4 Results

The main aim in this phase is to demonstrate that the ultrasound inspection technique developed in Chapter 5 is feasible from a practical standpoint. The A-scan and C-scan data that were collected in the ideal laboratory condition need to be reproduced using the prototype water bubbler system as shown in figure 7.3. Moreover, the sample under investigation here is a pipe quadrant instead of a representative concrete slab. Hence, the data collected in this phase consists of a series of A-scans collected in a region of interest (ROI) on the curved surface of a pipe specimen. The same ROI was later automatically scanned in a raster pattern to generate a C-scan image.

Figure 7.4 shows two representative A-scans taken from the clean portion and defect portion of the concrete pipe quadrant while it is being scanned by the water bubbler system. In figure 7.4a, a strong front-wall and back-wall echo separated

$\sim$33μs apart indicates the following: 1) The water bubbler system is successfully able to maintain a water column that allows for coupling of the ultrasonic energy from the transducer to the concrete surface without the need to submerge it, and 2) the coupling is good enough to allow sufficient energy to penetrate 60mm thick concrete and return back to the transducer. However, when the transducer is positioned on the defect, a significant loss in back-wall amplitude and gain in echo activity in between the front-wall and back-wall is observed as expected (see figure 7.4b). It was observed that the A-scan signal trace consistently followed the same behavior as the bubbler system was scanned across a ROI on the pipe quadrant. Figure 7.5 shows C-scan images of a 10mm x 200mm ROI on the pipe quadrant. The C-scan images were generated by monitoring the back-wall echo only using a single gate. Two images at different resolutions (1mm-figure 7.5b, and 0.5mm-figure 7.5c) were generated to determine if it was possible to gain additional insight at a higher resolution. Obviously, the time taken to generate a C-scan at 0.5mm resolution is much higher as compared to 1mm resolution. However, it can be seen from figures 7.5b-c that no additional information is available at a considerably higher time cost. Figure 7.5b demonstrates the ability of the bubbler technique to not only acquire C-scan data but also detect the presence of rebars in the concrete pipe material. This is an added advantage when considering that large diameter pipes are heavily reinforced. Moreover, with further research, a relationship between the degree of corrosion in reinforcements to the strength of signals reflected from the concrete-rebar interface can be established based on C-scan image modeling. The signal processing algorithm developed in this research study was applied to 2000 A-scan signals generated by using the water bubbler system in the ROI. As expected, because of the characteristics of signal being similar to the ones generated by the laboratory setup, it was able to detect the presence of defect with a reasonable accuracy.

7.5 Field Implementation

A water bubbler system that emulates the ultrasound immersion technique in a real-world scenario has been demonstrated. A-scan and C-scan data were successfully acquired using an automated scanning setup on an actual concrete pipe

quadrant to illustrate the practical applicability of this technique. At this juncture, it is important to consider issues related to its adoption in the field.

This technique can be adopted in the field by developing an ultrasonic inspection attachment that can be incorporated onto a sewer robot. The attachment head will have the ability to radially extend out from the robot so that it can transmit and receive signals in close proximity to the test area in question. It will also have a position sensor coupled to it so that proper alignment with test surface is always ensured. The field inspection tool may include the following items:

- A self-propelled (wheeled or tracked) digital robotic assembly with CCTV capability,
- An ultrasonic inspection attachment to detect anomalies on the pipe surface,
- On-board pulser-receiver,
- A custom housing for the transducer and the bubbler attachment,
- An umbilical chord carrying water to the bubbler at a constant flow-rate,
- Control architecture to correctly position the attachment within the pipe and scan, and
- All necessary software to read the signal from the attachment and download required information to the laptop.

A mockup of the proposed solution is shown in Figure 7.6. It must be noted that various issues such as instrumentation and methodology for delivering, receiving and processing ultrasonic signals while in the field is out of the scope of this research study. The technology and expertise for adopting an ultrasound-based inspection methodology into a field-application device falls in the domain of robotics and instrumentation research. Clearly, this is not the focus of the present study. However, work presented in this chapter intends to serve as a buffer for transition of the inspection technique from bench top to actual field implementation with continued research and development from the inspection industry. Current inspection systems use optical cameras that are clearly limited in that they cannot

interrogate below the surface through the pipe wall all the way to the back wall. This limitation does not exist for ultrasonic waves. Moreover, ultrasonic waves have the potential to interrogate surrounding soil condition enveloping the buried pipe.

The ultrasonic inspection technique developed in this research has been tested on a bench-top on various concrete slabs. These studies led to the design of a prototype water bubbler system that was tested on an actual concrete pipe quadrant. The next step in the development process would be to design the attachment described above and test it on a commercial sewer robot in the field.

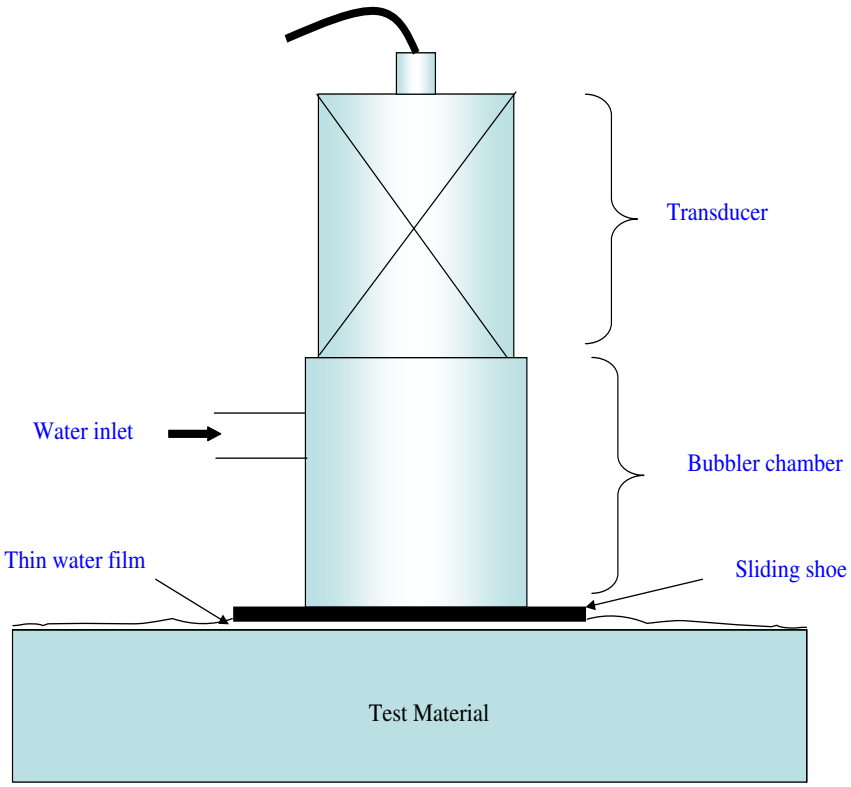

Figure 7.1. Schematic diagram of a bubbler system.

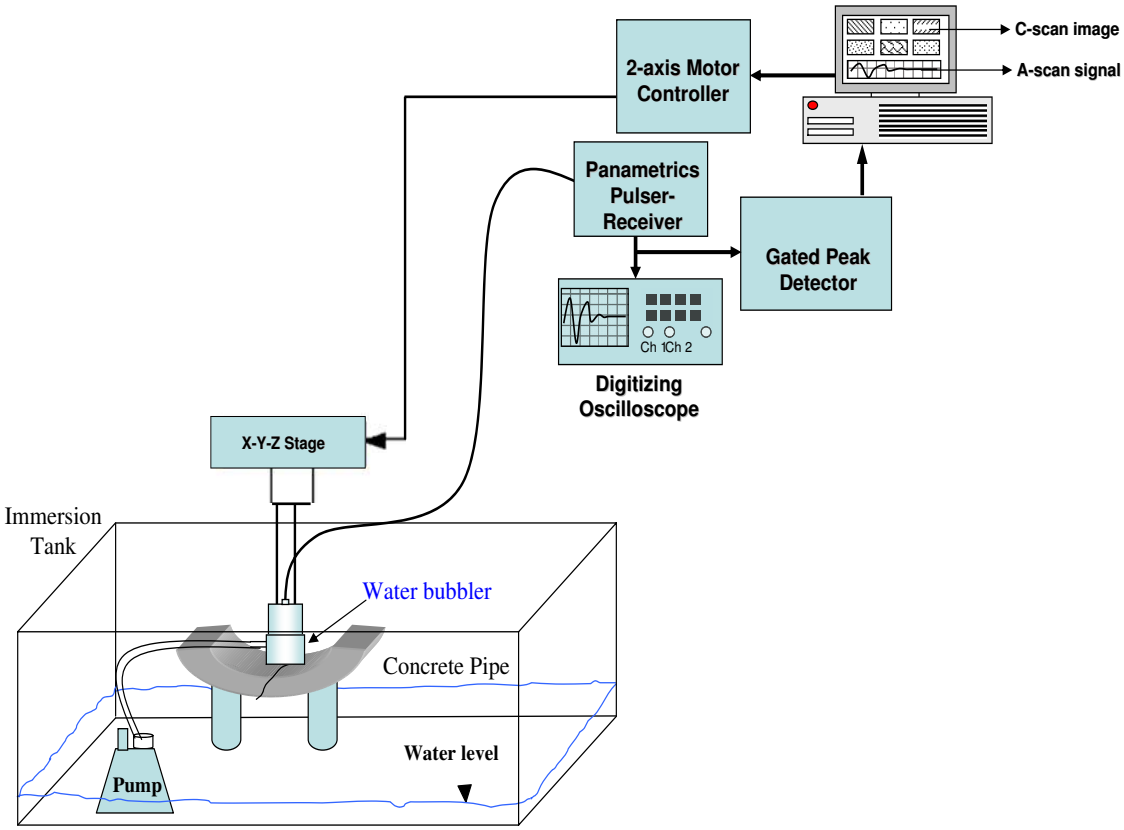

Figure 7.2. Schematic diagram of experimental setup for a water bubbler system.

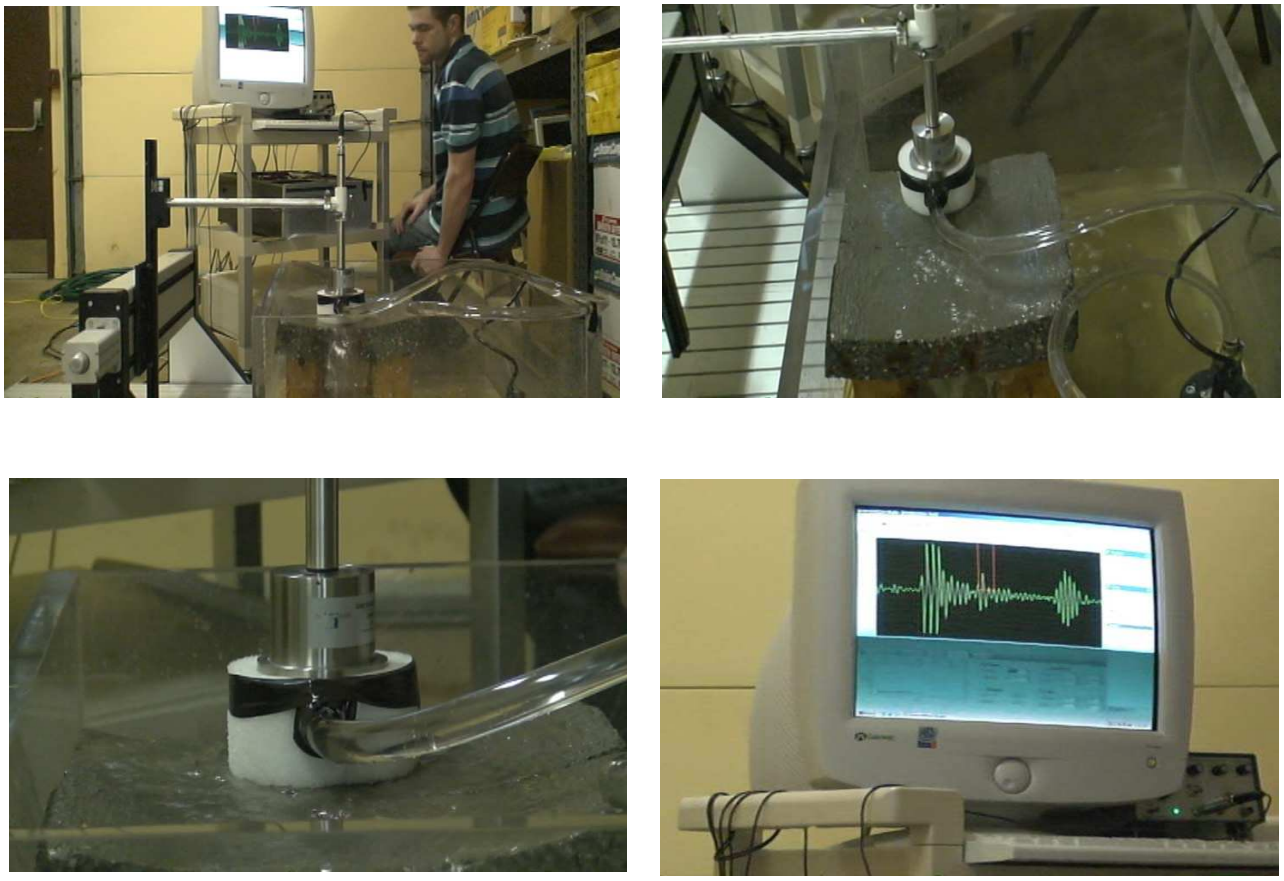

Figure 7.3. Experimental setup of an actual water bubbler system.

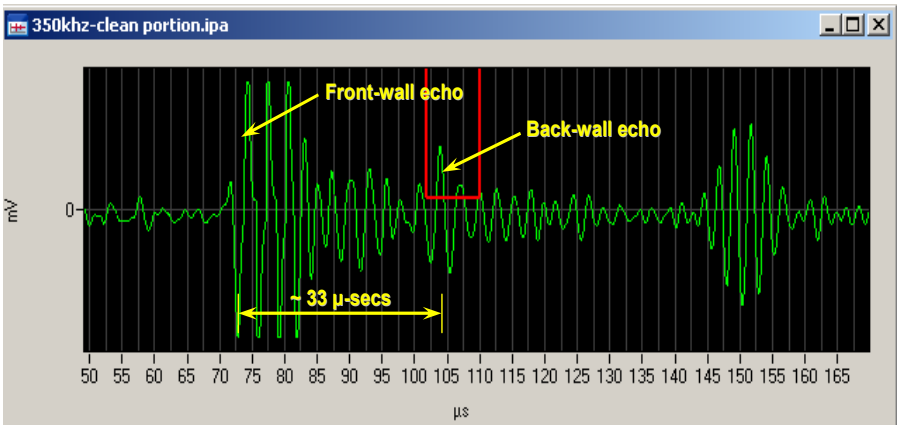

(a)

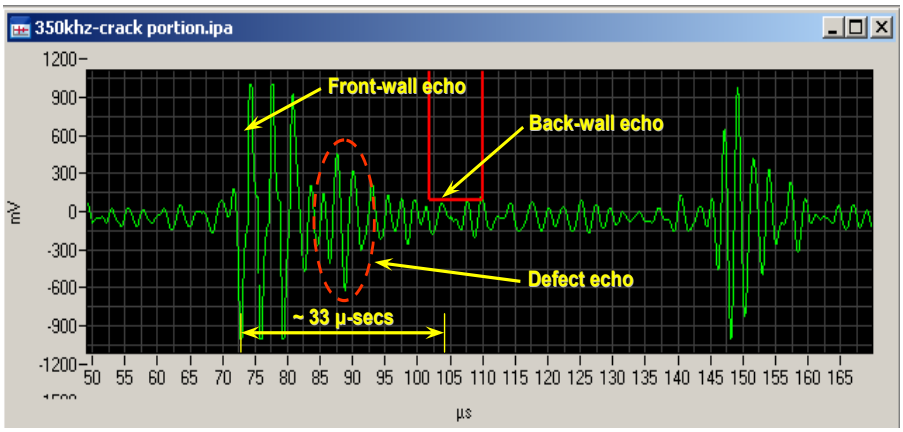

(b)

Figure 7.4. A-scan signals from (a) clean portion and (b) crack portion of the pipe quadrant.

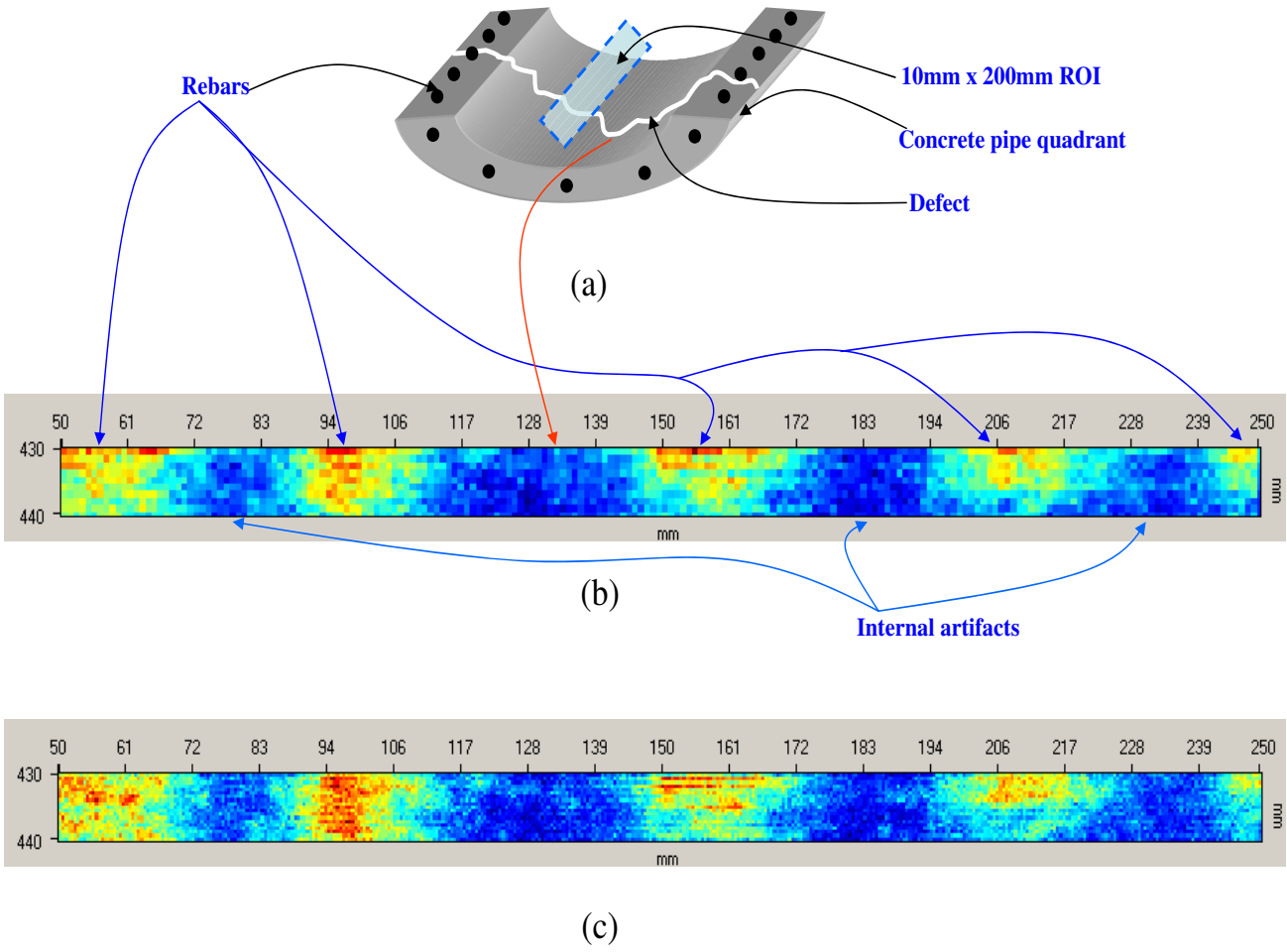

Figure 7.5. C-scan images. (a) schematic of pipe specimen and ROI (b) 1mm resolution C-scan, and (c) 0.5mm resolution C-scan.

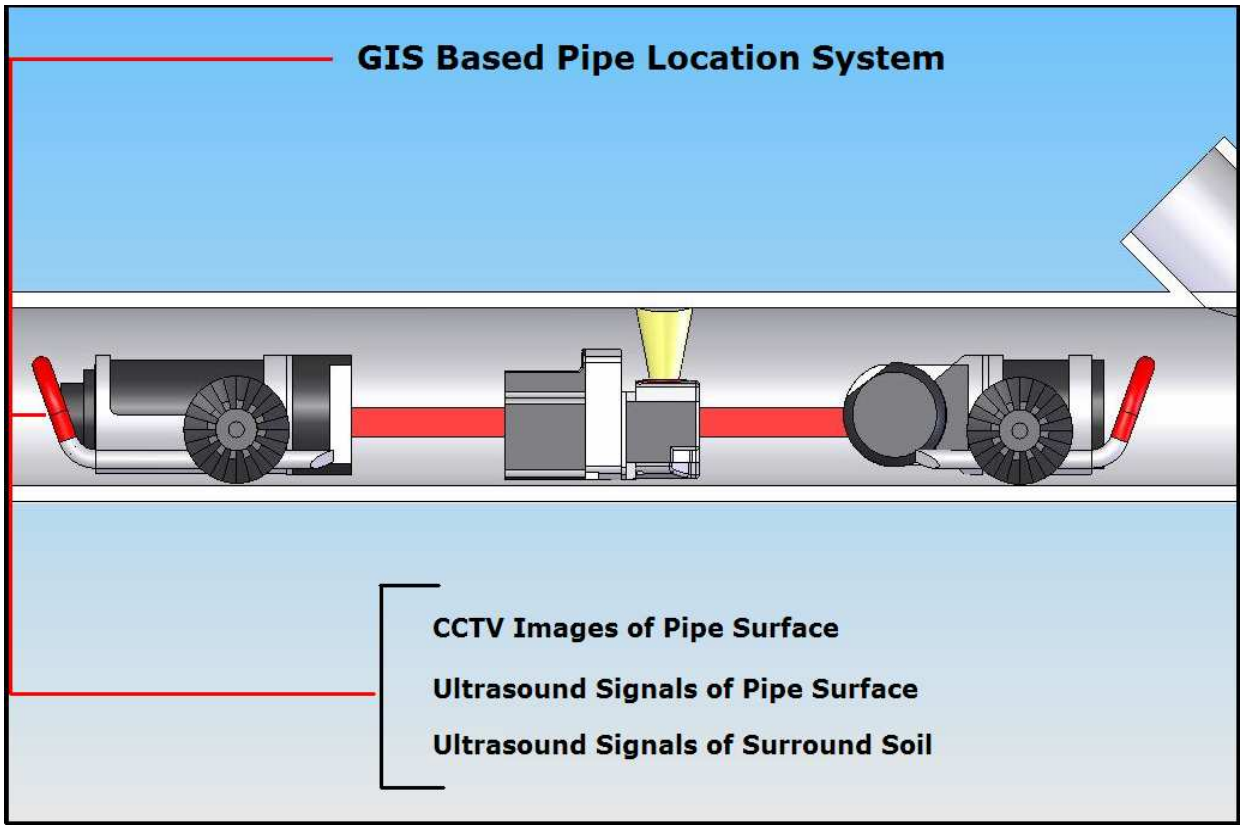

Figure 7.6. Proposed system for automated inspection of buried concrete pipe. *Sketchup courtesy of* ***RedZone Robotics***.

Chapter 8

Conclusions

This chapter reviews the contribution of this thesis, lists directions for future research and provides concluding remarks.

8.1 Contributions

The main objective of this thesis was to develop an automated buried concrete pipe inspection system based on scanned images obtained from SSET camera and signal/image data from an ultrasound transducer. The focus of this thesis has been on developing proof-of-concept of an intelligent automated ultrasound inspection system that can inspect concrete pipes and provide depth perception. Novel applications of image processing and segmentation techniques to improve detection of cracks under varying background, pipe color and complicated defect patterns from CCTV images were developed. However, the main concentration of this thesis has been in developing an ultrasound acoustics-based methodology to first determine the presence of defect and then acquire depth information about the defect for characterization purposes. The contributions of this thesis can be summarized under four main topics as follows:

1. **CCTV Image Processing & Segmentation**
    - Proposed two contrast enhancement schemes

- A simple, robust and efficient crack detection algorithm was developed and evaluated
- Approach can be fully automated and results show that the algorithm is effective for segmenting CCTV images

2. **Development of Ultrasound-based Inspection System**

- Various ultrasound-based inspection techniques were evaluated for suitability with concrete pipe inspection
- Guided wave and impact echo were experimentally examined and discarded due to their limitations
- Proposed an ultrasound-immersion based inspection method that needs only one-sided access and can be fully automated
- Experimental results, in A-scan signal and C-scan image format prove the suitability of this technique for depth perception

3. **Development of Feature Extraction & Classification Schemes**

- Three feature extraction schemes were proposed and evaluated against classifier response for selection
- The proposed clustered discrete wavelet transform feature extraction method was developed and implemented on A-scan signals
- A multilayer perceptron neural network classifier that uses features from the above method is developed
- A statistical classifier, LDA, is implemented to compare performance with proposed MLP classifier

4. **Development of Inspection Approach**

- Overall contribution is in developing a framework for the inspection system
- The system is proposed as a two step approach consisting of reconnaissance and characterization mode

- Each of the steps in the inspection approach is studied in detail and developed keeping practical applicability in mind
- A prototype water bubbler system is designed and implemented to demonstrate practical applicability of the technique

8.2 Future Directions

This research aimed at providing a proof-of-concept of an automated ultrasound-based inspection system for buried concrete pipes. This study has been successful in showing that the proposed methodology can detect defects in representative concrete pipe specimens. However, there are many interesting directions for continued research and testing to take the proof-of-concept presented in this study to the field where its application will significantly impact the buried asset management community. A few areas that need to be investigated based on the results of this study are outlined and discussed for future research:

- **Image Processing:** In this study, a CCTV image preprocessing and segmentation algorithm was presented for detecting cracks in color images with varying crack, background and color patterns. For complex situations, further development of this algorithm in terms of recovering the crack structure with bifurcations is required. Moreover, all CCTV images were transformed into the grayscale domain before performing any processing to reduce the computational time. Processing in the color image domain can provide significant improvement in crack detection owing to the fact that color is a powerful descriptor as it can augment object identification and classification approaches. Research in segmenting color images for crack detection will definitely help in building a reliable image based defect detection system.

- **Ultrasound Inspection:** The ultrasound inspection methodology presented in Chapter 5 was based on laboratory tests on representative concrete samples and aimed at providing a proof-of-concept. The defects generated in the laboratory tests are not sufficient to entirely capture the field scenario. Extensive testing of the methodology on different samples with a variety of defect patterns is needed. Also, the transducer used in this study was a plane

wave transducer. As mentioned in Chapter 6, although it appears as if the A-scan signal is an accurate representation of the wave that leaves the center of the transducer and hits the sample at a particular spot, it is not the case. The A-scan signal amplitudes are influenced by the spread of the ultrasound beam over an area rather than a spot. This means that the ultrasound signal amplitude is effected by a defect from far distances due to its spread and will reflect the information as a change in amplitude and echo characteristic that may be classified as a less or more severe defect. Using a focussed transducer with a narrow beam spot can avoid this overlap and is a promising avenue for future research and improvement of the proposed methodology. Also, C-scan image resolution can be increased with a focussed transducer in pulse-echo mode. Moreover, several other possibilities for pipe inspection that were out of the scope of this research exist. 1) *Pressurized Air Bag Ultrasound Transducer* : The acoustic impedance of a media is known to be equivalent to the product of density and sound velocity within the media. It follows that an increase in pressure causes a significant increase in the gas (air) density. The density change in the gaseous media increases its acoustic impedance. With increase in the acoustic impedance of air, the mismatch of impedances between interfaces becomes less in magnitude. This translates into improved ultrasonic energy transmission from the transducer to the test material via the gaseous media. By increasing the pressure, theoretically, the possibility of recording and distinguishing and signal is higher (Halter, 2001). Hence, an inspection technique consisting of a pressured air bag that can transmit ultrasound energy from the transducer to the pipe surface can be explored. 2) *Water Wheel Transducer*: A device that couples ultrasonic energy to a test object through the rolling contact area of a wheel (flexible tire) containing a liquid (oil/water) and one or more transducers is called a wheel transducer. The transducer is attached to the axle of the wheel. They are applied in pulse echo and through transmission technique. Since the tire material shows high attenuation they are mostly used in low frequency applications. The main driving advantage of this contact wheel transducer is that it works to overcome problems with couplant contamination as well as eliminating the practicality of immersion systems. The "tyre" or delay material

is constructed of hydrophilic polymers which have acoustic properties that lend themselves ideally to the implementation of ultrasonics. Applications include thickness measurement, composite inspection, delamination detection and general flaw detection. The only disadvantage of this approach is that the achievable signal to noise ratio is worse than that of regular transducers due to its construction which can not prevent some spurious echoes.

- **Feature Extraction & Classification:** Feature extraction is an important stage for any pattern recognition task especially for concrete pipe defect classification, since defects in concrete are highly variable and it is difficult to find reliable and robust features in the signal domain. Extensive research on the development of efficient and reliable methods for the selection and extraction of features for pattern classification problems is ongoing. In this thesis, the defect features from A-scan signals have been selected based on the the energy of their discrete wavelet transform coefficients. One useful extension of this thesis would be to perform a thorough feature evaluation and extraction optimization in order to provide an optimal set of features for classification. A simple multilayer perceptron (MLP) neural network classifier was proposed for classifying A-scan signals into several defect classes. The aim of this study was to provide a framework for feature extraction and classification. There exists enough scope for improving the design of the MLP classifier in terms of the optimum number of hidden layers, neurons per hidden layer and activation function. The MLP neural network seemed to perform very well in cases where the signal patterns were distinct but lowered its performance when the signal patterns were fuzzy. Introducing the concept of fuzzy logic and combining it with the power of neural network computation can enhance the performance of the classifier. The term "Neuro-fuzzy" refers to hybrids of artificial neural networks and fuzzy logic. Neuro-fuzzy hybridization results in a hybrid intelligent system that synergizes these two techniques by combining the human-like reasoning style of fuzzy systems with the learning and connectionist structure of neural networks. Hence designing a neuro-fuzzy classifier will be a good extension of the present work. The C-scan images have been used primarily to acquire depth perception and further characterization of the defect if triggered by the

post processing algorithm. Developing a C-scan image based classification system would also constitute a useful extension of this work.

- **Prototype Development:** The techniques for assessing buried concrete pipe that were developed in this research, both hardware and software need to be forged together into a prototype package that will then be evaluated in the field. The prototype development will require further refinement of the ultrasound transducer and allied hardware from a practical delivery point of view. Presently, a robotic vehicle on crawlers is used to carry optical and/or laser sensors on board for inspection in the field. An attachment that can carry the proposed ultrasound transducer needs to be designed so that extensive field evaluations can be performed to validate the proof-of-concept provided in this study.

8.3 Concluding Remarks

The motivation for this thesis lay in the daunting task faced by municipal asset managers in knowing the present condition of their assets. Most municipal systems in North America are inspected visually and defect classification is done manually by an operator. Although the human eye is extremely effective at defect detection and classification, it is unreasonable to achieve high efficiency in assessing pipe defects in thousand of miles of pipeline due to fatigue and subjectivity. Thus, simply trying to assess the condition of a buried sewer pipeline when it runs in thousands of miles is a daunting task. The aim of this thesis was to propose an automated pipeline inspection system that could not only provide better defect detection from CCTV images, but also provide depth perception of defects beyond the surface level. In continuation of this objective, an automated ultrasound-based inspection system was proposed to detect defects in buried concrete pipes. The inspection system was proposed as a two step approach. The first step is used as a reconnaissance mode in which the ultrasound transducer is used to scan a region of interest. A signal interpretation and classification scheme coupled with a post processing algorithm classifies the region of interest into a clean or defect region. If the scanned region of interest belongs to a defect, the second step of the

approach is to characterize the region of interest with a C-scan imaging process for depth perception. The feature extraction, classification and post processing schemes proposed in this thesis provide a sound proof-of-concept for developing this inspection system into a field applicable tool. Such a tool can aid asset managers to quickly evaluate the status of their buried infrastructure, ultimately leading to a sustainable asset management system.

Bibliography

Abbate, A., Koay, J., Frankel, J., Schroeder, S. C., and Das, P. (1997). "Signal detection and noise suppression using a wavelet transform signal processor: application to ultrasonic flaw detection." *IEEE Trans. on Ultra. Ferro. and Freq. Control*, 44(1), 14–26.

Agin, G. J. (1980). "Computer Vision Systems for Industrial Inspection and Assembly." *J. of Computer Vision*, 11–20.

American National Standards Institute, N. Y. (1995a). *American Society for Testing and Materials, ASTM C 597-83-Concrete and Aggregates.*

American National Standards Institute, N. Y. (1995b). *American Society for Testing and Materials, ASTM D 638-95-Tensile Properties of Plastics.*

American National Standards Institute, N. Y. (2002). *American Society for Testing and Materials, ASTM C 76-02-Standard Specification for Reinforced Concrete Culvert, Storm Drain, and Sewer Pipe.*

Association, P. C. P. "www.paconcretepipe.com. [Online Document].

Aydin, T., Yemez, Y., Anarim, E., and Sankur, B. (1996). "Multidirectional and Multiscale Edge detection via M-band wavelet Transform." *IEEE Trans. on Image Processing*, 5, 1370–1377.

Ballard, D. H. and Brown, C. M. (1982). *Computer Vision.* Prentice-Hall, Englewood Cliffs, New Jersey.

Bassim, M. N. and Houssny-Emam, M. (1983). *Time and Frequency Analysis of Acoustic Emission Signals.* Acoustic Emission, Gordon and Breach Scientific Publishers.

Besl, P. J., Delp, E. J., and Jain, R. (1985). "Automatic Visual Solder Joint Inspection." *IEEE J. Robot. Automation*, 1, 42–56.

Birks, A. and Green, R. (1991). *Nondestructive Testing Handbook,2nd ed., Vol. 7.* American Society for Nondestructive Testing, Columbus, Ohio, USA.

Bishop, C. M. (1995). *Neural Networks for Patern Recognition.* Oxford University press.

Blitz, J. and Simpson, G. (1996). *Ultrasonic Methods of Non-destructive Testing.* Chapman & Hall London.

Boltz, E. S., Fortunko, C. M., Hamstad, M. A., and Reneken, M. C. (1995). *Review of Progress in Quantitative Nondestructive Evaluation.* Plenum Press New York.

Brown, L. G. (1992). "A survey of image registration techniques." *ACM Comput. Surv.*, 24(4), 352–376.

Bungey, J. H. and Millard, S. G. (1996). *Testing of Concrete in Structures, 3rd edition.* Blackie Academic and Professional, London.

Canny, J. (1986). "A Computational Approach To Edge Detection." *IEEE Trans. Pattern Anal. Machine Intell.*, 8, 679–698.

Carino, N. J. (1984). "Laboratory study of flaw detection in concrete by the pulse-echo method." *In Situ/Nondestructive Testing of Concrete, Malhotra, V.M., Ed.*, American Concrete Institute, ACI SP-82, 557.

Carino, N. J., Sansalone, M., and Hsu, N. N. (1986). "A point source-point receiver technique for flaw detection in concrete." *J. of American Concrete Institute*, 83(2), 199.

Cartz, L. (1995). *Nondestructive Testing.* ASM International, OH.

Cawley, R., Lowe, M. J. S., Alleyne, D. N., Pavlakovic, B., and Wilcox, P. (2002). "Practical long range guided wave testing: applications for pipes and rail." *Material EvaluationAmerican Society for Nondestructive Testing*, 61(1), 66–74.

Chang, Y. L. and Li, X. (1995). "Fast Image Region Growing." *Image and Vision Computing*, 13, 559–571.

Cheng, H. D. (1996). "Automated Real-Time Pavement Distress Detection Using Fuzzy Logic and Neural Networks." *SPIE Proc. on Nondestructive Evaluation of Bridges and Highways*, 140–151.

Cheng, H. D., Chen, J. R., Glazier, C., and Hu, Y. G. (1999). "Novel Approach to Pavement Cracking Detection Based on Fuzzy Set Theory." *Journal of Computing in Civil Engineering*, 13(4), 270–280.

Cheng, H. D. and Miyogim, M. (1998). "Novel System for Automatic Pavement Distress Detection." *Journal of Computing in Civil Engineering*, 12(3), 145–152.

Chin, R. T. and Harlow, C. A. (1982). " Automated Visual Inspection: A Survey." *IEEE Trans. Pattern Anal. and Mach. Intell.*, 4, 557–573.

Chou, J. C., O'Neil, W. A., and Cheng, H. D. (1995). "Pavement Distress Evalution Using Fuzzy Logic and Moment Invariants." *Trans. Res. Record,Transportation Research Board, Washington, D.C.*, 1505, 39–46.

Chow, C. K. and Kaneko, T. (1972). "Automatic Boundary Detection of the Left Ventricle from Cineangiograms." *Computers in Biomedical Research*, 5, 388–410.

Chui, C. K. (1992). *Introduction to Wavelets*. SIAM: Philadelphia.

Daubechies, I. (1992). *Ten Lectures on Wavelets*. SIAM: Philadelphia.

Davies, T. G. and Mamlouk, M. S. (1985). "Theoretical Response of Multilayer pavement System to Dynamic Non-Destructive Testing." *Transp. Res. Rec.,Transp. Res. Board, Washington, D.C.*, 1022, 1–7.

Davis, H. E., Troxell, G. E., and Hauck, G. F. W. (1982). *The Testing of Engineering Materials*. McGraw-Hill, Inc, Toronto.

Demigny, D., Lorca, F. G., and Kessal, L. (1995). "Evaluation of Edge Detectors Performances with a Discrete Expression of Canny's Criteria." *Proc. Intl. Comf. On Image Processing, IEEE, Los Alamitos, CA*, 169–172.

Djordjevic, B. B., Berndt, T., Ehrlich, M., Baldwin, K., Palmer, D., and Holmes, S. (1998). "Advances in NDE for On-line Fiber Placement Process." *Proc. SAMPE98, Anaheim, CA*.

Djordjevic, B. B. and Green, R. E., J. (1994). "Non-Contact Ultrasonic Techniques for Process Control of Composite Fabrication." *Proc. NDE Applied to Composite Processing,St. Louis, MO, NTIAC*.

Duda, R. O. and Hart, P. E. (1973). *Pattern Classification and Scene Analysis*. John Wiley and Sons, New York.

Duda, R. O., Hart, P. E., and Stork, D. G. (2000). *Pattern Classification, 2nd ed.* Wiley Interscience.

Fieguth, P. W. and Sinha, S. K. (1999). "Automated Analysis and Dectection of Cracks in Underground Pipes." *Proc. Intl. Conf. Image Processing (ICIP)*, 395–399.

Gauch, J. and Hsia, C.-W. (1992). "A Comparison of Three Color Image Segmentation Algorithms in Four Color Spaces." *Proc. of the SPIE, Bellingham, WA*, 1818, 1168–1181.

Geman, D. and Jedynak, B. (1996). "An Active Testing Model for Tracking Roads in Satellite Images." *IEEE Trans. Pattern Anal. Machine Intell.*, 18, 1–14.

Gevers, T. and Smeulders, A. W. M. (1996). " A comparative study of several color models for color image invariant retrieval." *Proc First International Workshop on Image Databases and Multimedia Search, Amsterdam, Holland*, 17–26.

Giardina, C. R. and Dougherty, E. R. (1988). *Morphological Methods in Image and Signal Processing.* Prentice-Hall, Englewood Cliffs, NJ.

Gokhale, S. R., Abraham, D. M., and Iseley, T. (1997). "Intelligent Sewer Condition Evaluation Technologies - An analysis of three promising options." *North American NO-DIG 1997 Conference*, North American Society for Trenchless Technology, 253–265.

Gonzalez, R. C. and Woods, R. E. (2002). *Digital Image Processing.* Pearson Education, Singapore., second edition edition.

Grandia, W. A. and Fortunko, C. M. (1995). "NDE Applications of Air-Coupled Ultrasonic Transducers." *Proc. IEEE Ultrasonics Symposium*, 1, 697–709.

Grimson, W. E. L. and Lozano-Perez, T. (1987). "Localizing Overlapping Parts by Searching the Interpretation Tree." *IEEE Trans. Pattern Anal. Mach. Intell.*, 9(4), 469–482.

Guyon, I., Gunn, S., Nikravesh, M., and Zadeh, L., E. (2004). *Feature Extraction, Foundations and Applications.* Series Studies in Fuzziness and Soft Computing, Physica-Verlag, Springer.

Haas, C. and Hendrickson, C. (1990). "Computer-Based Model of Pavement Surfaces." *Transp. Res. Rec.,Transp. Res. Board, Washington, D.C.*, 1260, 149–157.

Hagan, M., Demuth, H. B., and Beale, M. H. (1996). *Neural Network Design.* Boston, MA: PWS Publishing.

Halmshaw, R. (1991). *Non-Destructive Testing, 2nd Edition.* Edward Arnold Publishers, UK.

Halter, R. (2001). "Development of an ultrasonic sensing technique for target location in a multi-phase high-impedance mismatched layered configuration. Master's thesis, The Pennsylvania State University.

Haralick, R. M. and Shapiro, L. G. (2000). *Computer and Robot Vision, 1st Ed.* Addison-Wesley, Reading, MA.

Hatanaka, H., Kawano, Y., Ido, N., Hato, M., and Tagami, M. (2005). "Ultrasonic testing with advanced signal processing for concrete structures." *Nondestructive Testing and Evaluation*, 20(2), 115–124.

Hayashi, T. and Rose, J. L. (2003). "Guided wave simulation and visualization by a Semi-Analytical Finite Element Method." *Material EvaluationAmerican Society for Nondestructive Testing*, 61(1), 75–79.

Haykin, S. (1994). *Neural Networks, A Comprehensive Foundation.* New York: Macmillan College Publishing Co.

Heath, M., Sarkar, S., Sanocki, T., and Bowyer, K. W. (1997). "A Robust Visual Method for Assessing the Relative Performance of Edge-Detection Algorithms." *IEEE Trans. Pattern Anal. Machine Intell.*, 19(12), 1338–1359.

Hellwich, O., Mayer, H., and Winkler, G. (1992). "Detection of Lines in Synthetic Aperture Radar (SAR) Scenes." *Proc. Intl. Archives Photogrammetry Remote Sensing (ISPRS)*, 31, 312–320.

Hibino, Y., Nomura, T., Ohta, S., and Yoshida, N. (1994). "Laser Scanner for Tunnel Inspections." *J. of Intl. Water Power and Dam Const.*, 6, 17–28.

Hillger, W. and Neisecke, J. (1993). "Quality control of mineral building materials by means of the novel ultrasonic pulse-echo technique." *Betonwerk+Fertigteil-Technik*, 59(6).

Hoff, W. and Ahuja, N. (1989). "Surface from stereo: Integrating feature matching, disparity estimation, and contour detection." *IEEE Trans. Pattern Anal. Machine Intell.*, 11.

Iseley, T. (1999). "Development of A New Sewer Scanning technology." *No-Dig America*, North American Society for Trenchless Technology.

Jain, A. K. (1989). *Fundamentals of Digital Image Processing.* Prentice-Hall Inc., Englewood Cliffs, New Jersey.

Jain, A. K., Duin, R. P. W., and Mao, J. (2000). "Statistical Pattern Recognition: A Review." *IEEE Pattern Analysis and Machine Intelligence*, 22(1), 4–37.

Jones, R. (1949). "The non-destructive testing of concrete." *Magazine of Concrete Research*, (1827), 67–78.

Joynson, R. E., McCary, R. O., Oliver, D. W., Silverstein-Hendengren, K. H., and Thumhart, L. L. (1986). "Eddy Current Imaging of Surface Breaking Structures." *IEEE Transactions on Magnetics*, 22, 11–24.

Jung, Y.-C., Na, W.-B., Kundu, T., and Ehsani, M. R. (2000). "Damage detection in concrete using lamb waves." *in Nondestructive Evaluation of Highways, Utilities, and Pipelines IV, Proc. of SPIE*, 3995, 448–458.

Kanal, L. and Chandrasekaran, B. (1971). "On Dimensionality and Sample Size in Statistical Pattern Recognition." *Pattern Recognition*, 3, 225–234.

Kass, M., Witkin, A., and Terzopoulos, D. (1988). "Snakes: Active Contour Models." *Intl. J. Computer Vision*, 1(4), 321–331.

Kil, D. H. and Shin, F. B. (1997). "Automatic road-distress classification and identification using a combination of hierarchical classifiers and exper stystems - subimage and object processing." *Proc. of Int. Conf. on Image Processing 1997*, 2, 414–417.

Kittler, J. and Illingworth, J. (1985). "On Threshold Selection Using Clustering Criteria." *IEEE Trans. on Systems, Man and Cybern.*, 15(51), 652–655.

Koutsopoulos, H. N., Sanhouri, I. E., and Downey, A. B. (1993). "Analysis of Segmentation Algorithms For Pavement Distress Images." *ASCE J. Transportation Engineering*, 119(6), 868–888.

Krstulovic, O. N., Woods, R. D., and Al Shayea, N. (1996). "Nondestructive Testing of Concrete Structures Using the Rayleigh Wave Dispersion Method." *ACI Mat. J.*, 93, 75–86.

Langley, P. (1995). *Elements of Machine Learning*. Morgan Kaufman.

Law, T., Itoh, H., and Seki, H. (1996). "Image Filtering, Edge Detection, and Edge Tracing Using Fuzzy Reasoning." *IEEE Trans. Pattern Anal. Machine Intell.*, 18, 481–491.

Lefebvre, J. P. and Lasaygues, P. (1994). "Wavelet analysis for ultrasonic crack detection and modelization." *Proc. of IEEE Ultrasonics Symposium*, 2, 1143–1146.

Lengagne, R., Fua, P., and Monga, O. (1996). "Using crest lines to guide surface reconstruction from stereo." *Proc. Conf. Pattern Recognition*.

Lin, Y. and Su, W. (1996). "Use of stress waves for determining the depth of surface-breaking cracks in concrete structures." *ACI Materials Journal*, 93, 494–505.

Liu, H. C. and Srinath, M. D. (1990). "Partial shape classification using contour matching in distance transformation." *IEEE Trans. Pattern Anal. Machine Intell.*, 12, 1072–1079.

Malhotra, V. M. and Carino, N. J., E. (2004). *Handbook of Nondestructive Testing of Concrete, 2nd Ed.* CRC Press,ASTM International, PA.

Mallat, S. (1989). "A theory for multiresolution signal decomposition: the wavelet representation." *IEEE Pattern Analysis and Machine Intelligence*, 11, 674–693.

Maragos, P. and Schafer, R. W. (1990). "Morphological Systems for Multidimensional Signal Processing." *Proc. Of IEEE*, 78(4), 690–710.

McDonnell, M. J. (1981). " Box Filtering Techniques." *Computer Graphics and Image Processing*, 17(3), 42–56.

Merlet, N. and Zerubia, J. (1996). "New Prospects in Line Detection by Dynamic Programming." *IEEE Trans. Pattern Anal. Machine Intell.*, 8, 426–431.

Meyer, Y. (1993). *Wavelets: Algorithms and Applications.* SIAM: Philadelphia.

Michie, D., Spiegelhalter, D. J., and Taylor, C. C. (1994). *Machine Learning, Neural and Statistical Classification.* Ellis Horwood Publications.

Mitchell, T. (1997). *Elements of Machine Learning.* McGraw Hill Publications.

Mitra, S. K. and Strobel, N. (1995). "Quadratic Filters for Image Contrast Enhancement." *Proc. of the Twenty-Eighth Asilomar Conference on Signals, Systems and Computers*, 1, 208–212.

Mohajeri, M. H. and Manning, P. J. (1991). "ARIA: An operating System of Pavement Distress Diagnosis by Image Processing." *Trans. Res. Record*, 1311, 120–130.

Mukherjee, D. P. and Pal, S. (2005). "Advances in Pattern Recognition." *Pattern Recognition Letters*, 26(4), 395–398.

Na, W.-B., Kundu, T., and Ehsani, M. R. (2002). "Ultrasonic guided waves for steel bar concrete interface testing." *Materials Evaluation*, 97, 437–444.

Na, W.-B., Kundu, T., and Ehsani, M. R. (2003). "A comparison of steel/concrete and glass fiber reinforced polymers/concrete interface testing by guided waves." *Materials Evaluation*, 97, 155–161.

Newman, T. S. and Jain, A. K. (1995). " Survey of Automated Visual Inspection." *Computer Vision Image Understanding*, 61(2), 231–262.

Olsen, L. O. (1993). "Nondestructive tesing role in repair and rehabilitation of Concrete Structures." *in Innovation repair techniques of concrete structures, Proc. of ASCE National Convention Dallas, Texas.*

Otsu, N. (1979). "A Threshold Selection Method from Gray-Scale Histogram." *IEEE Trans. Syst., Man Cybernetics*, 9(1), 62–66.

Pal, N. R. and Pal, S. K. (1987). "Segmentation Based on Contrast Homogeneity Measure and Region Size." *IEEE Trans. on Systems, Man and Cybern.*, 17(5), 857–868.

Pittner, S. and Kamarthi, S. V. (1999). "Feature Extraction from Wavelet Coefficients for Pattern Recognition Tasks." *IEEE Pattern Analysis and Machine Intelligence*, 21(1), 83–88.

Polikar, R., Udpa, L., Udpa, S., and Taylor, T. (1998). "Frequency Invariant Classification of Ultrasonic Weld Inspection Signals." *IEEE Trans. on Ultra. Ferro. and Freq. Control*, 45(3), 614–625.

Popovics, S. (2005). "Effects of uneven moisture distribution on the strength of and wave velocity in concrete." *Ultrasonics*, 43, 429–434.

Popovics, S. and Popovics, J. S. (1992). "A critique of the pulse velocity method for testing conrete." *Proc. of Nondestructive Testing of Concrete Elements of Structures*, 94–103.

Pratt, W. K. (1978). *Digital Image Processing.* Wiley, New York.

Priese, L. and Rehrmann, V. (1993). "On Hierarchical Color Segmentation and Application." *Proc. in Computer Vision and Pattern Recognition, Los Alamitos, CA*, 633–634.

Ramamoorthy, S. K., Kane, Y., and Turner, J. A. (2004). "Ultrasound diffusion for crack depth determination in concrete." *Journal Acoust. Soc. America*, 115(2), 523–529.

Ramesh, V. and Haralick, R. M. (1994). "An Integrated Gradient Edge Detector: Theory and Performance valuation." *Proc. of ARPA Image Understanding Workshop, Monterey, CA*, 689–702.

Ratha, N. K., Karu, K., Chen, S., and Jain, A. K. (1996). "A real-time matching system for large fingerprint databases." *IEEE Trans. Pattern Anal. Machine Intell.*, 18, 799–812.

Redwood, M. (1960). *Mechanical waveguides; the propagation of acoustic and ultrasonic waves in fluids and solids with boundaries.* Pergamon Press, New York.

Rose, J. L. (1999). *Ultrasonic Waves in Solid Media.* Cambridge, New York.

Rose, J. L. (2000). "Guided Wave Nuances for Ultrasonic Nondestructive Evaluation." *IEEE Trans. on Ultrasonics, Ferroelectrics, and Freq. Control*, 47(3), 575–583.

Rosenfeld, A. and Kak, A. C. (1982). *Digital Picture Processing, 2nd edition.* Academic Press, New York.

Rumelhart, D. E., Hinton, G. E., and Williams, R. J. (1988). *Learning internal representations by error propagation,in Parallel Distributed Processing. Explorations in the Microstructures of Cognition, Vol. 1: Foundations (D. E. Rumelhart, J. L. McClelland, and the PDP Research Group, eds.).* Cambridge, Massachusetts: MIT Press.

Sanchez, R. T., Balibrea, L. M. T., Alcantud, J. A. L., and Asensi, G. D. (1994). " Automatic Vision Inspection System For The Analysis And Detection Of Breakages And Defects of Satsuma Slices." *Proc. IEEE Inlt. Conf. on Humans, Information and Technology*, 1, 853–858.

Sansalone, M. and Carino, N. J. (1986). *Impact-echo: a method for flaw detection in concrete using transient stress waves.* National Bureau of Standards, ntis pb 87 104444as edition.

Sansalone, M., Lin, J., and Streett, W. B. (1998). "Determining the depth of of surface-opening cracks using impact-generated stress waves and time-of-flight technique." *ACI Materials Journal*, 95, 168–177.

Sansalone, M. and Streett, W. (1997). *Impact-Echo: Nondestructive Testing of Concrete and Masonry.* Bullbrier Press, Jersey Shore, PA.

Schettini, R. (1993). "A Segmentation Algorithm for Color Images." *Pattern Recognition Letters*, 14, 499–506.

Schickert, M. (2005). "Progress in Ultrasonic Imaging of Concrete." *Materials and Structures, Special issue on Concrete Science and Engineering*, 38(283), 807–815.

Schickert, M., Krause, M., and Muller, W. (2003). "Ultrasonic Imaging of Concrete Elements Using Reconstruction by Synthetic Aperture Focusing Technique." *Journal of Materials in Civil Engineering*, 15, 235–246.

Schickert, M., Tummler, and Buhling, L. (2006). "Rapid Scanning Approaches for Ultrasonic Imaging of Concrete." *Proc. of ECNDT 2006, Poster Session*, (P20).

Serra, J. (1982). *Image Analysis and Mathematical Morphology.* London, U.K.: Academic.

Simone, G., Morabito, F. C., Polikar, R., Ramuhalli, P., Udpa, L., and Udpa, S. (2001-2002). "Feature extraction techniques for ultrasonic signal classification." *Intl. J. of App. Electro. and Mech.*, 15, 291–294.

Sinha, S. K. (2000). "Automated Underground Pipe Inspection Using a Unified Image Processing and Artificial Intelligence Methodology," PhD thesis, University of Waterloo, Canada.

Sinha, S. K. and Fieguth, P. W. (2001). "Assessment, Rehabilitation and Maintenance of Buried Pipes." *Proc., ASCE International Pipeline Conference, San Diego, California.*

Sinha, S. K., Karray, F., and Fieguth, P. W. (1999). "Underground Pipe Crack Detection Using Image Analysis and Neuro-Fuzzy Algorithm." *Proc., 1999 IEEE International Conference on Intelligent Control/Intelligent Systems and Semiotics*, North American Society for Trenchless Technology, 399–404.

Skingley, J. and Rye, A. J. (1987). "The Hough Transform Applied to Images for Thin Line Detection." *Pattern Recognition Letters*, 6, 61–67.

Smith, S. W. (1997). *The Scientist and Engineer's Guide to Digital Signal Processing.* California Technical Publishing, San Diego.

Song, W. J., Popovics, J. S., Aldrin, J. C., and Shah, S. (2003). "Measurement of surface wave transmission coefficient across surface-breaking cracks and notches in concrete." *Journal of Acoustical Society of America*, 113(2), 717–725.

Steinbach, J. and Vey, E. (1975). "Caisson evaluation by stress wave propagation method." *Journal of the Geotechnical Engineering Division, ASCE*, 101((GT4)), 361.

Stewart, T. L. (1993). "Operating Experience Using a Computer Model for Pipeline Leak Detection." *J. of Pipelines*, 3, 233–237.

Strang, G. and Nyugen, T. (1996). *Wavelets and Filter Banks.* Wellesley-Cambridge Press.

Technical Report (WIN) (2001). *Water Infrastructure Network (WIN) Agency Report.*

Technical Report (WIN) (2002). *Water Infrastructure Network (WIN) Agency Report.*

Unser, M., Aldroubi, A., and Laine, A. (2005). *Wavelets Are Enhancing Medical Imaging, in Medical Imaging.* Thomson Gale (Greenhaven Press), MI.

Van Cauwelaert, F. J., Alexander, D. R., White, T. D., and Barker, W. R. (1989). "Multilayer Elastic Program for Backcalculating Layer Moduli in Pavement Evaluation." *Non-destructive Testing of Pavements and Backcalculation of Moduli, ASTM STP 1026, ASTM*, 171–188.

Vincent, L. (1987). "Morphological Grayscale Reconstruction in Image Analysis: Applications and Efficient Algorithms." *IEEE Trans .Image Processing*, 2(2), 176–201.

Vrabel, M. J. (1996). "Edge Detection with Recurrent Neural Network." *Proc. of Application and Science of Artificial Neural Networks II, SPIE, Bellingham, WA*, 2760.

Walker, R. S. and Harris, R. L. (1991). "Noncontact Pavement Crack Detection Systems." *Trans. Res. Record*, 1311, 149–157.

Wei-Du, L. (1992). "Frequency sprectrum analysis of ultrasonic testing signal in concrete." *Proc. of Nondestructive Testing of Concrete Elements of Structures.*

Weszka, J. S. and Rosenfeld, A. (1979). "Histogram Modification for Threshold Selection." *IEEE Trans. on Systems, Man and Cybern.*, 9(1), 38–52.

Wiedemann, C. (1987). "External Evaluation of Road Networks." *ISPRS Archives*, 34(3/W8), 93–98.

Wirahadikusumah, R., Abraham, D. M., and Iseley, T. (2001). "Challenging Issues in Modeling Deterioration in Combined Sewers." *ASCE J. of Infra. Syst.*, 7(2), 77–84.

Wu, T. T., Fang, J. J., and Liu, P.-L. (1995). "Detection of the depth of a surface-breaking crack using transient elastic waves." *Journal Acoust. Soc. America*, 97, 1678–1686.

Zana, F. and Klein, J. C. (2001). "Segmentation of vessel-like patterns using mathematical morphology and curvature evaluation." *IEEE Trans. Image Processing*, 10(7), 1010–1019.

Vita

Shivprakash Iyer

Education

B.E. (Civil Engineering), Aug 2000, S.V.N.I.T., Surat, India.

M.S. (Civil Engineering), Aug 2002, The Pennsylvania State University.

Ph.D. (Civil Engineering), May 2007, The Pennsylvania State University.

Work Experience

Graduate Research Assistant, Dept. of Civil & Env. Engr., The Pennsylvania State University, University Park, PA, 2005 – 2007.

Graduate Teaching Assistant, Dept. of Civil & Env. Engr., The Pennsylvania State University, University Park, PA, 2003 – 2005.

Instructor, Dept. of Civil & Env. Engr., The Pennsylvania State University, University Park, PA, Summer and Fall 2004, Summer 2005.

Selected Publications

Iyer, S., Pedrick, M. K., Sinha, S. K., and Tittmann, B. R., "An Automated Inspection System for Buried Wastewater Concrete Pipes, Part I - Ultrasound Sensing for Defect Detection," *submitted* to Automation in Construction, Elsevier Publications, February 2007.

Iyer, S., Sinha, S. K., Pedrick, M. K., and Tittmann, B. R., "An Automated Inspection System for Buried Wastewater Concrete Pipes, Part II - Automated Ultrasonic Signal Classification," *submitted* to Automation in Construction, Elsevier Publications, February 2007.

Iyer, S., and Sinha, S. K., "Segmentation of Pipe Images for Crack Detection in Buried Sewers," Computer Aided Civil and Infrastructure Engineering, Blackwell Publishers, Volume 21, 2006, pp. 395-410.

Iyer, S., and Sinha, S. K., "A Robust Approach For Automatic Detection & Segmentation of Cracks in Underground Pipeline Images," Image & Vision Computing, Elsevier Publications, Volume 23, No. 10, September 2005, pp. 921-933.